Trinity College Dublin
Coláiste na Tríonóide, Baile Átha Cliath
The University of Dublin

Chemical biology studies on human and mouse secondary bile acids

A thesis submitted to the University of Dublin for the degree of

Doctor of Philosophy

By

Yin Lu, B.Sc, M.Sc

Based on the research carried out under the supervision of

Professor. John F. Gilmer, PhD

School of Pharmacy and Pharmaceutical Sciences

Trinity College Dublin

2022

Declaration

I guarantee that this final thesis that I submit to Trinity College Dublin is a result of my own research work and it has not been submitted as an exercise for a degree at this or any university. I declare that it is entirely my own work over past four years from September 2016 to 2021 and has no plagiarism. I agree that Trinity college library can access to this thesis.

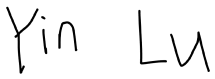

Yin Lu

January 2022

Abstract

Bile acids are important regulators of multiple homeostatic mechanisms integrating cell proliferation, metabolism and inflammation. The overall objective of this thesis was to use chemical biology tools to understand problems in bile acid research including metabolism and mechanism of cytotoxicity and FXR activation with the purpose of informing development of new therapeutic agents.

Chapters 1 and 2 review the general background of bile acids, including their classification, functions and biosynthesis in the liver and intestine. Chapter 2 goes on to describe investigations into synthesis of so-called isobile acids by epimerization of the 3α-hydroxyl group. We carried out biological evaluations on their cytotoxicity *in vivo* and found that isobile acids cause less cell death than their alpha isomer counterparts in general. Their effect on FXR activation in both reporter assay and coactivator assay was assessed.

In Chapter 3 is described a novel and highly efficient process towards the synthesis of muribile acids (MCAs), a group of bile acids found in mice, that are of interest because of the position of the mouse in the study of bile acid function and metabolism and because selected bile acids may have therapeutic potential. We examined the ability of muribile acids to prevent cell death and identified ω-muricholic acid (ωMCA) with potential cytoprotective properties. The impact of ωMCA on DCA and tunicamycin-induced ER stress gene expression was assessed and the favourable cytoprotective and ER stress-reducing properties of ωMCA were identified.

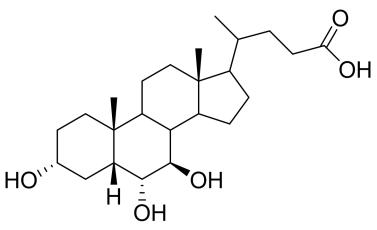

ω-MCA

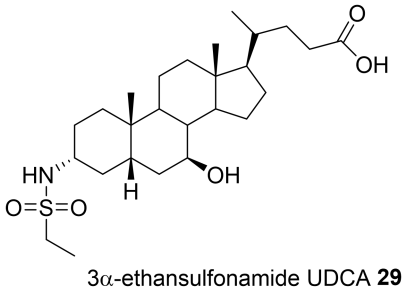

3α-ethansulfonamide UDCA **29**

In Chapter 4 is described the synthesis and characterization of a panel of 3-sulfonamide-24-amides derived from UDCA based on SAR around potent cytotoxicity exhibited by 3-azido-24-amides and 3α-ethansulfonamide UDCA **29** (a cytotoxic compound causing entire cell death in the Caco-2 cell line) from previous studies from our lab. Toxicity was characterized in liver and colonic epithelial cells, showing some differences in sensitivity. 24-Amidation, which had been successful in generating highly toxic 3-azido analogues did not enhance further the toxicity of the 3α-sulfonamide series. It was shown that in the toxic sulfonamide series, 24-carboxylate was not necessary for activity since it could be replaced with primary alcohol or primary amide without loss in activity. Further studies on toxicity effects of 3α-trifluoromethyl derivatives were also carried out.

In Chapter 5 is described a strategy for the design of bile acid carrier-based cytotoxic drugs by enhancing uptake of a cytotoxic payload. Bile acid analogues of chlorbambucil were designed and analysed in relation to their effect on cell viability and on their uptake and breakdown under cell proliferation assay conditions. It was shown that conjugation to bile acids can enhance uptake and increase cytotoxicity.

A summary of the major findings drawn from the experimental data are articulated here. Firstly, isobile acids have less cytotoxicity activity compared with their 3α counterparts and this can be applied in the cancer treatment by altering the bile acid pool. Besides, muribile acids, especially ω-MCA is found to prevent cell death caused by toxic bile acids.

Acknowledgements

First of all, I would like to express my great gratitude and special appreciation to my supervisor, Professor. John Gilmer, who has been an influential mentor for me. Thanks him for providing me this valuable opportunity to work on the bile acid project and I would like to thank him for always giving me patient guidance in my English and research and allowing me to grow as a pharmaceutical research scientist. He is like a father to me in these five years. I feel so lucky and honorable to work for him and would like to carry out the future work in this incredible research team.

Many thanks to all those who have ever helped me in my research along the way. Thanks to Dr. John O' Brien for help with NMR, Brian Talbot for help with LC-MS and HPLC, Gary Hessman for HR-MS, Rhona Prendergast for her help in the demonstration, Ray Keaveny, Conan Murphy, Derek Harford and Marcus Phelan for help with solvent and chemical order. Thanks to Anne-Marie Byrne in the TTMI for helping me with FXR and relevant biology work. Thank you Jun Wang for the guidance in bile acid synthesis in my initial year. Huge thanks to Gerard Colleran for the help going through my thesis. A special thanks to Maria Pigott for her help and care throughout my PhD life.

To all the TCD pharmacy postgrads, in particular Anjali, Nadhim, Eavan, Su, Johannes, Jinfan, Michael, Luiza, Sara, Karl, Shizhe, Emer, Alina and Mohammed, thank you all for the friendship and it is my pleasure to meet you here. I would like to send heartfelt thanks to all fellow members of the 'Gilmer group' for the unforgettable moments inside and outside the lab and I am fortunate enough to have the opportunity to work in this cracking place. I have to thank Miriam for being of constant help and her kindness made the day-to-day work much easier. Mark provided many interesting conversations about daily life. Kate always came up with some smart ideas when we encountered problems inside or outside the lab. James was always the right person to ask when encountering any problem.

Besides, I would like to take this opportunity to express sincere thanks to Tao Zhang for his help and encouragement in my entire PhD life. He is reported to be a great lecturer in pharmaceutical science. Also, I owe my deep gratitude to Brian Murray, a fantastic lecturer in organic chemistry and an expert in NMR field, who provided timely support and guidance to me.

Most importantly, I would like to thank my mum and dad for supporting me spiritually throughout my life, and I know that is huge sacrifice for them. Thanks for their understanding and patience especially when I was struggled.

Last but not least, I would like to take this opportunity to express my sincere appreciation to healthcare, Garda and those frontline workers fighting the coronavirus pandemic all over the world. Thank you for all your contribution to make the world better. 2020 has been a tough year, but I'm grateful for that. Hopefully 2021 will be better.

Associated Publications

Publications

Zaufel A, van de Wiel SMW, **Yin L**, Fauler G, Chien D, Dong X, Gilmer JF, Truong JK, Dawson P, van de Graaf SFJ, Fickert P, Moustafa T. Secondary (iso)BAs cooperate with endogenous ligands to activate FXR under physiological and pathological conditions. Biochimica et Biophysica Acta. Molecular Basis of Disease. 2021; **1867**(8): 166153.

Oral Presentations

'Isobile acids, their toxicity and effect on activation of FXR'. **Yin Lu**. Trinity Biomedical Science Institute Research Symposium. September 2019. Trinity College Dublin, Ireland.

Poster Presentations

‘Isobile acids, their toxicity and effect on activation of FXR'. **Yin Lu**, Sandra Van de Wiel, Tarek Moustafa, and John Gilmer. GP2A medicinal chemistry conference. August 2019. University of Nottingham, UK.

Abbreviations

4-DMAP	4-(Dimethylamino) pyridine
6-EMCA	6a-ethyl-23(S)-methyl-cholic acid
ABC	ATP-binding cassette
Abs	Absorbance
Ac_2O	Acetic anhydride
AcCl	Acetyl chloride
AD	Alzheimer's disease
AF-1	Ligand-independent transactivation function-1
AF-2	Ligand-dependent transactivation fuction-2
ALS	Amyotrophic lateral sclerosis
aq.	Aqueous
ATCC	American type culture collection
BA	Bile acid
BAAT	Bile acid-CoA amino acid N-acetyltransferase
BACS	Bile acid-CoA synthetase
BAS	Bile acid sensor
Bax	Bcl-2-associated X protein
BSEP	Bile salt export pump
BSH	Bile salt hydrolases
CA	Cholic acid
cAMP	Cyclic adenosine monophosphate
CCF2-AM	CCF2-acetoxymethylated
CCF4-AM	CCF4-acetoxymethylated
CDCA	Chenodeoxycholic acid
CMC	Critical micellization concentration
CRC	Colorectal cancer
CsF	Cesium fluoride
CYP27A	Sterol 27-hydroxylase

CYP7A1	Cholesterol 7α-hydroxylase
CYP8A1	Sterol 12α-hydroxylase
d	Day(s)
d	Doublet
DBD	DNA binding domain
DCA	Deoxycholic acid
DCM	Dichloromethane
DMEM	Dulbecco's Modified Eagle's Medium
DMF	*N,N*'-Dimethylformamide
DMSO	Dimethyl sulfoxide
DNA	Deoxyribonucleic acid
EC_{50}	Half maximal effective concentration
EDC	N-(3-Dimethylaminopropyl)-N'-ethylcarbodiimide
EGFR	Epidermal growth factor receptor
Eq.	Equivalence
ER	Endoplasmic reticulum
ERK	Extracellular signal regulated-kinase
Et_3N	Triethylamine
ETC	Electron transport chain
EtOAc	Ethyl acetate
EtOH	Ethanol
FADD	Fas-associated protein with death domain
FBS	Fetal bovine serum
FDA	Food and Drug Administration
FGF-15	Fibroblast growth factor 15
FGF-19	Fibroblast growth factor 19
FGFR-4	Fibroblast growth factor receptor 4
FRET	Fluorescence resonance energy transfer
FXR	Farnesoid X receptor
FXREs	Farnesoid X receptor response elements

FXRα	Farnesoid X receptor α
FXRβ	Farnesoid X receptor β
GLP-1	Glucagon-like peptide 1
GPCR	G-Protein coupled receptors
GR	Glucocorticoid receptor
h	Hour(s)
H_2	Hydrogen gas
H12	Helix 12
HCA	Hyocholic acid
HCl	Hydrochloric acid
HCC	Hepatocellular carcinoma
HDCA	Hyodeoxycholic acid
HMBC	Heteronuclear multiple bond correlation
HOBt	Hydroxybenzotriazole
HRMS	High-resolution mass spectrometry
HSA	Hydrophobic surface area
HSA	Human serum albumin
HSDHs	Hydroxysteroid dehydrogenases
Hz	Hertz, SI unit
IBABP	Intestinal bile acid binding protein
IBD	Inflammatory bowel disease
IR	Infrared Spectroscopy
LBD	Ligand binding domain
LCA	Lithocholic acid
$LiAlH_4$	Lithium aluminium hydride
LiOH	Lithium hydroxide
Li(s-Bu_3BH)	Lithium triethylborohydride
Log P	Partition coefficient
LRH-1	Liver receptor homolog-1
L-Selectride	Lithium-selectride

LTSB	Lithium trisiamylborohydride
JNK	Jun N-terminal kinase
KBr	Potassium Bromide
KOH	Potassium hydroxide
M	Multiplet
MAPK	Mitogen-activated protein kinase
MCA	Muricholic acid
MDA	Malondialdehyde
MDR	Multidrug resistance protein
MeOH	Methanol
Mg	Milligramme
$MgSO_4$	Magnesium sulfate
ml	milliliter
mM	millimolar
MOE	Molecular operating environment
MPT	Mitochondria permeability transition
MPTP	Mitochondrial permeability transition pore
MTT	3-(4, 5-dimethylthiazol-2-yl)-2, 5-diphenyltetrazolium bromide
MS	Mass spectrum
MW	Molecular weight
N_2	Nitrogen gas
Na	Sodium
NaOH	Sodium hydroxide
$NaHCO_3$	Sodium bicarbonate
NEAA	Non-essential amino acids
NF-kB	Nuclear factor kappa-light-chain-enhancer of activated B cells
nm	Nanometre
nM	Nanomolar
$NaBH_4$	Sodium borohydride
NAFLD	Non-alcoholic fatty liver diseas

NASH	Non-alcoholic steatohepatitis
NaN_3	Sodium azide
NBS	N-Bromosuccinimide
NMR	Nuclear Magnetic Resonance
NOE	Nuclear Overhauser Effect
NTCP	Na^+/taurocholate cotransporting polypeptide
OATP	Organic anion transporting polypeptide
OCA	Obeticholic acid
PBC	Primary biliary cholangitis
PBS	Phosphate buffered saline
PCC	Pyridinium chlorochromate
PCR	Polymerase chain reaction
Pd/C	Palladium on activated carbon
Pen/strep	Penicillin-Streptomycin
PKA	Protein kinase A
PPh_3	Triphenylphosphine
ppm	Parts per million
PXR	Pregnane X receptor
R_f	Retention Factor
RFTLC	Reverse phase thin layer chromatography
RIPA	Radioimmunoprecipitation assay
RT	Room temperature
RNA	Ribonucleic acid
ROS	Reactive oxygen species
RP-TLC	Reverse phase thin layer chromatography
RXR	Retinoid X receptor
s	Singlet
SAR	Structure-activity relationship
SEM	Standard error of the mean
SHP	Small heterodimer partner

TBAF	Tetrabutylammonium fluoride
TFA	Trifluoroacetic acid
TGR5	G-protein-coupled bile acid receptor-1
THF	Tetrahydrofuran
TM	Tunicamycin
TMS	Tetramethylsilane
TNF	Tumor necrosis factor
TLC	Thin layer chromatography
TNF	Tumor necrosis factor
TRAIL	Tumor necrosis factor related apoptosis inducing ligand
UDCA	Ursodeoxycholic acid
UPR	Unfolded protein response
U2OS	Human Bone Osteosarcoma Epithelial Cells
VDR	Vitamin D receptor

Table of contents

Preamble

This PhD thesis is in the field of medicinal chemistry, and it relates to synthetic studies on the bile acid 3α-sulfonamide UDCA and its analogues, isobile acids and muribile acids and the further biological evaluation on their cytotoxicty towards Huh-7 and Caco-2 cell line. The agonist or antagonist effects on a specific bile acid nuclear receptor called FXR also forms a significant element of this study. The outcome of the research may contribute to future treatments of relevance to medical conditions including obesity, diabetes, liver injury, inflammation, cardiovascular diseases, liver and colorectal cancer.

Chapter 1. Introduction and thesis overview

1.1 Bile acid overview

The first description of bile acids was made in 1848 when cholic acid (CA) was discovered in ox gall [1]. Subsequent research stretching back to the early 1900s has resulted in identification of many other bile acids.

The bile acid family include a group of molecular species of steroids with specific physical, chemical and biological characteristics. They are the final product of cholesterol catabolism in animals and are biosynthesized in the pericentral hepatocytes of the liver. Cholesterol is the precursor of steroid hormones and is essential for building and maintaining cellular membranes. Around 500 mg of cholesterol is converted into bile acids daily in the adult human liver. Bile acids, together with cholesterol and phospholipids comprise the main components of bile. Bile acids metabolized in the liver pass into the small intestine, where the majority is reabsorbed at the terminal ileum by passive diffusion or active transport, and returned to the liver via the hepatic portal vein. The liver extracts bile acids and reconjugates before distributing back into the bile, ready for a new circulation. This process happens 4–12 times daily especially during a typical high-fat meal and this continuous cycle of secretion, absorption, and secretion is termed the *enterohepatic circulation*. This highly efficient circulation occurs through the liver, intestine, biliary tree and the portal blood and recycles approximately 95% of the bile acids in the pool [2][3], conserving original bile acids and thus avoiding the synthesis of new bile acids. The 5% that is lost in the feces are compensated by de novo synthesis in the liver from cholesterol [2]. Besides, enterohepatic circulation of bile acids provides a negative feedback mechanism to maintain bile acid homeostasis. Bile acid biosynthesis is strictly regulated to ensure that adequate amounts of cholesterol are catabolized to maintain homeostasis. Absorption of bile acids from the intestine contributes to the accumulation of a significant mass of bile acid, termed the bile acid pool, which is about 2–3 g in adults. Bile acids are the major solutes in bile, constituting around 80% of the

organic compound. These endogenous metabolites have various roles and functions. Traditionally, they have been viewed as solubilizing agents (also termed biological soap) in the intestinal lumen, facilitating the absorption of fats and dietary lipids by emulsifying them in the gut after a meal. This can prevent the formation of gallstones [4]. Besides, bile acids are powerful detergents in the intestines and help the digestion and absorption of fatty acids, fat-soluble vitamins and other fatty products [5]. In addition to these, bile acids can change the mobility of the membrane and alter protein activity. Excess bile acids can lead to cytolysis and necrosis through the emulsification of cellular membranes particularly in digestive epithelia.

Biosynthesis of bile acid from cholesterol is a quite complex and multi-enzyme process. A full complement requires the involvement of approximately 17 different enzymes, many of which are preferentially expressed in the liver. This activity is tightly regulated by nuclear hormone receptors and other transcription factors. The insoluble and uncharged cholesterol molecule can be converted into an ionized and water-soluble compound (see Figure 1.1). This process mainly involves initiation (C7-hydroxylation of sterol precursors), modification of the cholesterol ring structures, oxidation and side chain shortening to generate a carboxylic acid group. Before excretion from the hepatocyte, bile acids are able to conjugate via amide linkage with glycine or taurine in humans to form glyco-bile acids and tauro-bile acids, respectively.

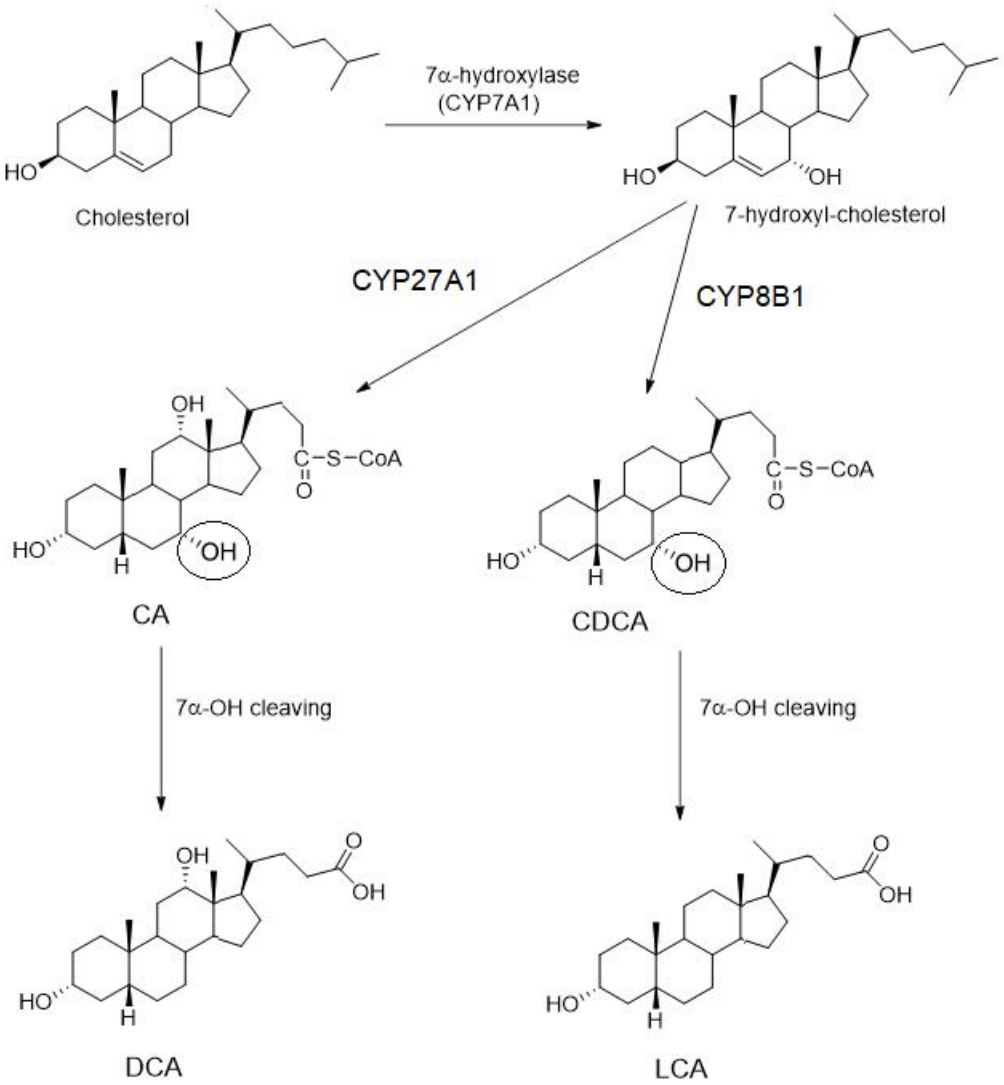

Figure 1.1- The classic pathway for the conversion of cholesterol into the primary bile acids and the subsequent synthesis of secondary bile acids. The C7-OH group is highlighted with the shaded circle in this diagram and the cleavage of this group is important for the generation of secondary bile acids.

The 7α-hydroxylase enzyme, CYP7A1, contributes to the process of primary bile acids synthesis. The 7-OH group of primary bile acids can be removed by microflora producing the secondary bile acids, like deoxycholic acid (DCA) and lithocholic acid (LCA). This part will be explained in detail in Chapter 2.

Bile acids can be classified into two different types, *primary* and *secondary*. Primary bile acids are those synthesized directly in the liver (for example CDCA and cholic acid) whereas secondary bile acids are produced from enzymatic

action of the bacterial flora in the colon.

Bile acids consist of a group of molecules with similar but not identical chemical structure, approximately 20 Å long and with an average radius of 3.5 Å. Bile acids from different species differ mainly in three respects: side chain structure, the distribution of the number, position and stereochemistry of hydroxyl groups in the steroid nucleus and stereochemistry of the A/B ring fusion.

Based on their difference in the side chain functional group, bile acids can be classified into C_{24}, C_{27} bile acids and C_{27} bile alcohols. The structures of these different types of bile acids are depicted in Table 1.1. Among these bile acid molecules, C_{24} (with a C_5 side chain) and C_{27} (with a C_8 side chain) bile acids are quite common. In higher vertebrates, C_{24} bile acids constitute a major part of bile [6]. C_{27} bile alcohols are quite rare in nature. C_{27} bile alcohols are mainly found in fish species and there are conjugated by esterification of the C_{27} hydroxyl group with sulfate rather than taurine or glycine. Thus, the following text will deal for the most part with C_{24} bile acids.

Table 1.1- Brief classification into different types of bile acids

Bile acids	Occurrence	Structure
C_{24} bile acids	In all vertebrate classes eg. reptiles, birds, bony fish, and mammals	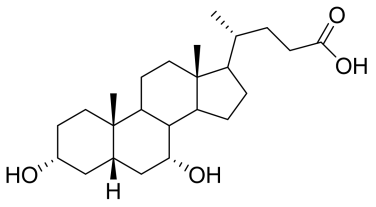 C_{24} bile acids
C_{27} bile acids	In a number of early evolving vertebrates, birds and some amphibians	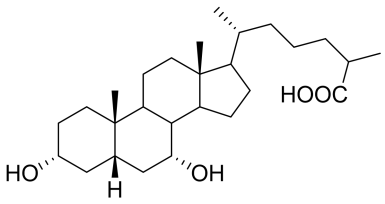 C_{27} bile acids

C_{27} bile alcohol	In the early evolving fish and amphibians eg. Greenland shark, elephant	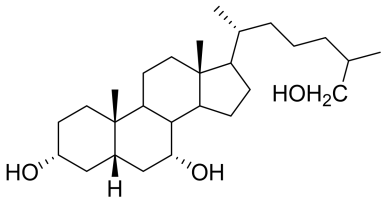 C_{27} bile alcohols

1.1.1 Basic structure of bile acids

Bile acids are amphiphilic molecules composed by 24 carbon atoms and a short and flexible acidic aliphatic side chain. The steroidal core of bile acids consists of three six-membered rings (A, B and C) and one five-membered ring (D) [7] usually with a *cis*-fused configuration between the A and B ring (5β-H). Due to the function of the steroid 5β-reductase (aldo-keto reductase), most of the bile acids are 5β-reduced. In lower vertebrates, some of bile acids exhibit an A/B trans-fusion.

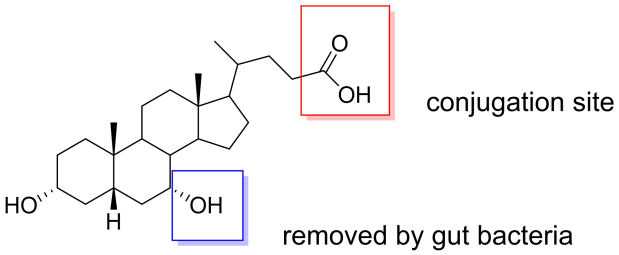

Figure 1.2- The basic structure of bile acids. The hydroxyl group at C-7' can be removed by anaerobic bacteria in the colon. The C-24' position is the conjugation position, and it can be conjugated with glycine or taurine.

The activities of each bile acid are different based on the position, number and stereochemistry of the hydroxyl groups, as well as the conjugation of amino acids, such as taurine or glycine [8]. Six common bile acids have been found in the bile of different mammalian species (see Table 1.2). These natural bile acids exhibit different biological activities *in vivo* and *in vitro* and this is highly dependent on the nature of their chemical structures. In addition to hyodeoxycholic acid (HDCA), all these bile acids have been widely investigated

in this thesis. Among these bile acids, CDCA and CA are the most abundant bile acids in human bile and the main organic bile acids produced in the liver [8].

Table 1.2- Overview of six common bile acids in nature.

Bile acids	Position of hydroxyl groups	Structure	Species
Cholic acid (CA)	3α, 7α, 12α	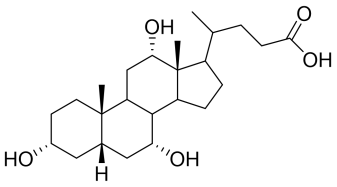	bear, cat, mouse, pig, rabbit, human
Deoxycholic acid (DCA)	3α, 12α	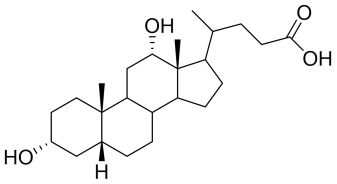	cat, rabbit, human
Chenodeoxycholic acid (CDCA)	3α, 7α	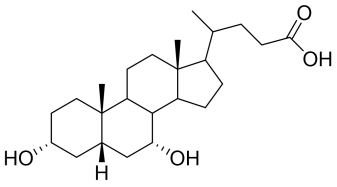	bear, pig, human
Ursodeoxycholic acid(UDCA)	3α, 7β	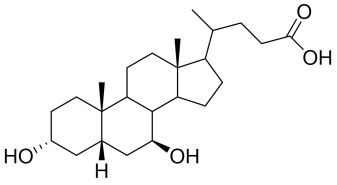	bear
Hyodeoxycholic acid (HDCA)	3α, 6α	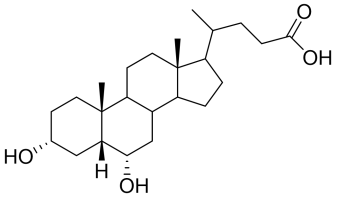	rat, pig, human
Lithocholic acid (LCA)	3α	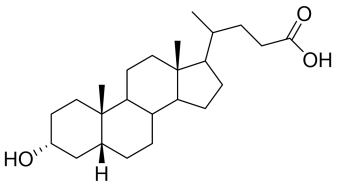	first isolated from a gallstone taken from a calf

Bile acids may also be classified according to their physicochemical properties

as hydrophobic including LCA, DCA, and CDCA and hydrophilic including CA and UDCA. Moreover, because of their beneficial as well as toxic effects, they can be divided into three board groups: beneficial bile acids (UDCA and CA), beneficial and toxic bile acids (CDCA and DCA), and toxic bile acids (LCA). It is worth noting that the beneficial effects are observed with bile acids which are more hydrophilic, while the toxic effects are seen with bile acids that are more hydrophobic.

1.1.2 The structure-activity relationship of the bile acids

The biological activity of a bile acid is closely associated with its chemical properties such as the number and orientation of hydroxyl groups or its conjugation as these parameters affect its hydrophobicity, an important predictor of toxicity.

First of all, the hydrophilic index of bile acids is not only proportional to the number of hydroxyl groups but also influenced by their position on both sides of the steroid ring. Most of the biliary bile acids and bile alcohols are amphipathic with a polar face and a non-polar face. For the C_{24} conjugated bile acids, they all have a hydrophobic side and a hydrophilic side with the exception of the naturally occurring UDCA (3α, 7β). Bile acids with hydroxyl groups positioned on both sides of the steroid ring (α and β orientation) are less hydrophobic than their counterparts with the same number of hydroxyl groups in only α orientation. An important example is the lower hydrophobicity of UDCA compared with CDCA (3α, 7α). Less hydrophobicity is usually associated with less toxicity, and for example UDCA promotes hepatic bile acid efflux and bile flow and is anti-apoptotic. An increased level of hydrophilic bile acids also influences micelle formation and intestinal lipid absorption. Bile acids become small aggregates or micelles when their concentrations are above critical micellar concentration (CMC). This is of central importance for their physiological function.

Hepatic conjugation also exerts an important influence on the biological properties of bile acids since it decreases the pK_a. Unconjugated bile acids have a pK_a of 5, whereas the conjugation with amino acids further lowers pK_a to approximately 4 for glycine conjugates and less than 2 for the taurine conjugates. Conjugated bile acids therefore are slightly stronger acids with lower pK_a values and conjugation contributes to increased hydrophilicity, enhanced solubility and decreased cytotoxicity. Bile is the principal route for bile acid excretion. Solubility of the bile acids in intestinal tract improves when amidation with glycine or taurine and this conjugation process greatly improves their physicochemical properties so that they pass through the cellular membrane without the help of a transporter.

All bile acids, no matter conjugated or not, that cannot be absorbed in human body are eventually eliminated from the body. The degradation of bile acids results from gut bacteria as bile acids are major carbon source for them.

1.1.3 Physiological functions of bile acids

Bile acids are the main component of bile, the exocrine secretion of the liver. Bile is formed in the canalicular space between hepatocytes. It provides a route for excretion of many endogenous solutes and also assists in digestion of fat by introducing bile acids to the duodenum. Whereas we now perceive bile acid as endogenous metabolites with various functions, they were initially considered mainly as digestive molecules which help in the emulsion and absorption of fats and liposoluble vitamins [9]. Recent studies have suggested the involvement of bile acids in various functions.

One of the principal effects of bile acid production is the elimination of cholesterol. Cholesterol can be converted into bile acid enabling clearance to the intestinal lumen from hepatocyte, finally leading to elimination via the fecal route. Bile acid digestion function relates to solubilizing dietary lipids and their digestion products including phospholipids, and fatty acids coming from the

enzymatic breakdown of triglycerides in the small intestinal. Bile acids are actively transported into the biliary canaliculi between hepatocytes which then stimulates canalicular bile flow by generating an osmotic pressure. They promote the transfer of phospholipids from the canalicular membrane into bile and induce biliary phospholipid secretion resulting in the formation of bile acid-phospholipid micelles (see Figure 1.3). The presence of phospholipid diminishes the overall cytotoxicity of bile, therefore preventing injury to the biliary epithelium, at least in those species whose bile acids are hydrophobic. The existence of bile acids in the small intestine promotes the solubilization of insoluble fatty acids, like vitamins A, D, E, K, which is required for their absorption. Bile acids also promote intestinal calcium absorption [10] and regulate pancreatic enzyme secretion [11]. Furthermore, they have an antimicrobial effect in the small intestine, inhibiting bacterial overgrowth in the bowel caused by biliary diversion or bile duct ligation in animals [12].

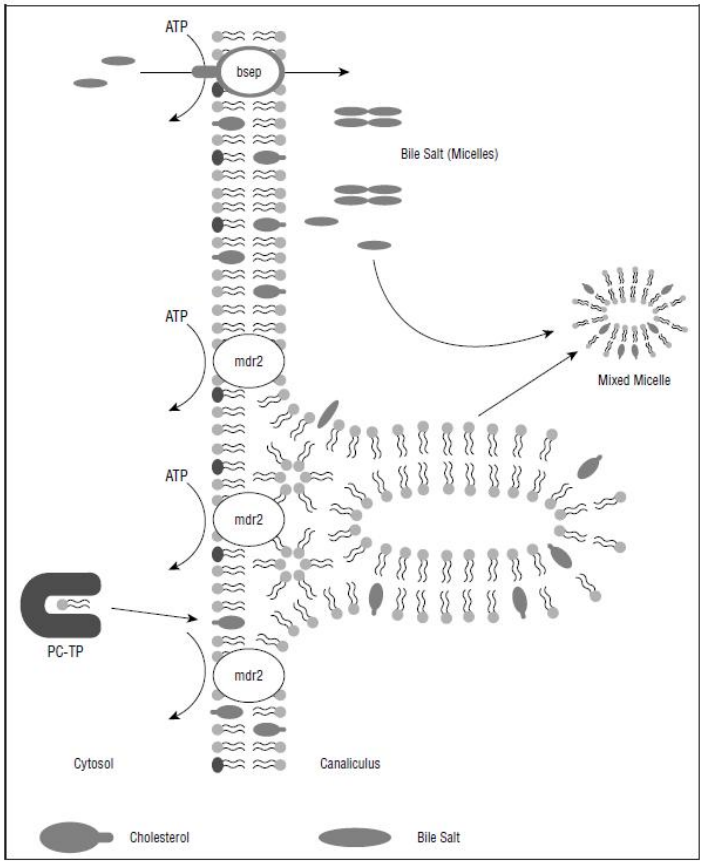

Figure 1.3- Bile acid transportation at the canalicular membrane [27].

At the same time, the negative feedback regulation of bile acid level and cholesterol biosynthesis is very important which is in accordance with the reported activation of Farnesoid X receptor (FXR) in liver and intestine and this will be described in Chapter 2. Bile acids in the hepatocyte play a signaling role [13]. Bile acid synthesis is regulated through a number of feedback loops regulated by FXR, increasing when levels are low and decreasing when levels are high.

Bile acids have been reported to control obesity and prevent the development of insulin resistance by affecting glucose homeostasis. Many studies of physiological functions in the brain have been reported as well [14A]. UDCA and TUDCA (the taurine conjugate of UDCA) prevent the accumulation of amyloid β peptides in Alzheimer's disease [14B] and protect against mitochondrial damage in Parkinson's disease [14C], which relates to GR activation.

1.1.4 Bile acid toxicity

Until the late 1980s the role of bile acid in causing liver injury in human was only suspected based on the toxicity of whole bile and bile salts. As has been mentioned above, bile acids are facially amphipathic because they have both hydrophilic side (represented by the hydroxyl groups, the amide carbonyl, and the ionized acidic groups of either glycine or taurine) and hydrophobic side (represented by the steroid backbone of the molecule). Bile acids can interfere with fatty acid uptake and are potentially hepatotoxic, which in many cases is the main cause of bile acid induced damage when accumulating in the liver and other organs [15]. Persistent increases of hydrophobic bile acids enables the detachment of the phospholipids and proteins of the cell membranes in abnormal high concentration so that the cell membrane can be damaged, ultimately causing cell death. Hence high amount of hydrophobic bile acids in

humans can promote liver injury and finally lead to liver failure [16] and is pertinent in cancer development. Bile acids can induce cell death in a wide range of mammalian cell types and can cause apoptosis in the liver and intestine.

Bile acid cytotoxicity is strongly influenced by structure. The *intrinsic toxicity* is firmly linked to the hydrophobicity of the bile acids. The hydrophobicity of the bile acids is inversely related to the number of hydroxyl groups. Hence, intrinsic toxicity of the bile acids increases with reduction in the number of hydroxyl groups. For example, LCA with only one OH group is the most toxic, whereas other highly hydrophobic compounds, DCA and CDCA with two hydroxyl groups and CA with three hydroxyl groups, show decreasing hydrophobicity and toxicity. UDCA, although a dihydroxy bile acid, is considered non-toxic by comparison.

Unconjugated bile acids are relatively cytotoxic to cells *in vivo* as they are membrane permeable, and they can readily accumulate to pathological levels within cell and in cell membranes. The concentration at which bile acids causes cytotoxicity is close to their CMC values. CDCA and DCA have a lower CMC than other bile acids so they are more cytotoxic under a certain concentration and exhibit great extracellular toxicity.

Bile acid exposure can increase the level of superoxide within cells. In addition, they can inhibit the synthesis of ATP and increase the permeability of calcium ions. Excessive calcium ions can activate the proteolytic enzymes and enable the degradation of RNA, DNA and proteins.

Chronic exposure to hydrophobic bile acids promotes local inflammation, metabolic disorders and ultimately, tumor development. Primary prevention strategies, such as changing dietary habits and lifestyle and reducing exposure to environmental toxins, can modulate gut microbiota and reduce risk of diseases. These observations give new impetus to therapeutic efforts to reduce

elevated hydrophobic bile acid level and decrease overall toxicity by using beneficial bile acids to manipulate the bile acid pool. The hydrophilic bile acid, UDCA, is a good candidate on which to base efforts in this area.

1.2 UDCA

UDCA is an approved drug (e.g. Ursofalk®) that constitutes approximately 3% of the total bile acid pool in humans [17]. As its name suggests, it is naturally obtained from the dry gallbladder bile of the Chinese bears [18], like *Ursus thibetanus* and it is the major component of bile acid pool in bear bile. It has proved to be quite efficient in treating many liver and digestive diseases in Chinese Traditional Medicine for hundreds of years from the time of the Tang Dynasty (618-907 AD) [19]. Indeed, the Chinese drug 'yutan', a powder preparation taken from the bile of adult bears, can be used to alleviate hepatobiliary disorders.

Orally administrated UDCA is taken up from the portal blood in humans during the first passage, and then conjugates glycine and to a lesser extent, taurine. Conjugated UDCA is absorbed mainly in the distal ileum, where it completes with endogeneous bile acids for active transportation and undergoes extensive enterohepatic circulation. Unabsorbed conjugated UDCA enters into colon and is then deconjugated and converted into LCA by intestinal microbiota.

UDCA is a natural bile acid with no measurable toxicity at physiological levels or side effects and it can be delivered orally to patients. It has distinct therapeutic properties, in contrast to the relative toxicity of other more hydrophobic acids and it is now well documented to be both cytoprotective and anti-inflammatory. The first paper on the therapeutic effect of UDCA in patients with liver disorders was published in Japan in 1961 [20]. UDCA is now widely used in clinics, with a potential role in cholesterol regulation and as a therapeutic drug for the treatment of cholestatic liver diseases. It can significantly reduce cholesterol saturation in the bile [21] and increase bile flow.

More importantly, in the 1970s, UDCA emerged as a treatment for patients suffering from primary biliary cholangitis (PBC) [22]. UDCA is also used to treat primary sclerosing cholangitis (PSC), another cholestatic disease in which it shows only marginal efficacy. It is used because there are no other therapeutic options available. Furthermore, UDCA has a potential role as a neuroprotectant in Huntington's disease and TUDCA exhibits neuro-protective effects *in vitro* that may be relevant to Alzheimer's disease and amyotrophic lateral sclerosis (ALS, also known as Motor Neuron Disease). UDCA is approved for treatment of ALS by the South Korean FDA.

Despite these beneficial properties and related applications, UDCA has potential toxicity, which relates to its interference with drug detoxification. For example it is metabolized to LCA, which can cause cholestatic liver injury, liver cell failure and death [23, 24]. Indeed, UDCA has been reported to influence normal liver cell functions due to its toxicity profile. [25] The usage of UDCA is controlled as it can lead at high dose to a range of side effects like immune suppression, fever, hepatitis, pruritus, severe diarrhoea, and interstitial lung disease [26A, 26B].

1.2.1 Chemical features of UDCA

UDCA (3α, 7β-dihydroxy-5β-cholan-24-oic acid) is a physiologically hydrophilic dihydroxy bile acid similar in overall shape to other mammalian bile acids. The pK_a of UDCA is 5.1 [28]. In humans, UDCA is a secondary bile acid formed by bacterial 7β-epimerization of primary bile acid CDCA in the gut by intestinal bacteria. The main difference between these is that UDCA has a unique C-7β hydrogen orientation that confers on it a much higher hydrophilicity than CDCA. From the structural formulae shown in Figure 1.4, it is understood that UDCA is A/B cis and B/C trans.

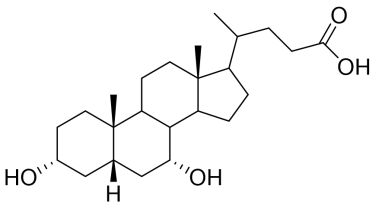

CDCA

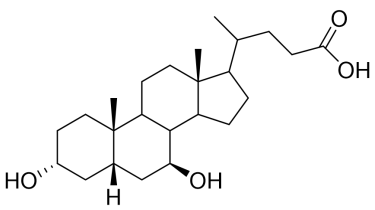

UDCA

Figure 1.4- Structure of UDCA and CDCA. They both have a four-ring structure but the main difference between them is the different orientation of the hydroxyl group at C-7' position, which explains the difference of the hydrophobicity and membrane-damaging properties of these two bile acids. The 7β orientation UDCA shows higher hydrophilicity than the 7α-orientation CDCA and this is why UDCA is much weaker than CDCA in interacting with and disturbing lipid membranes.

1.2.2 Mechanisms of action of UDCA

UDCA is used to effectively dissolve gallstones by solubilizing cholesterol in bile. Besides this, UDCA's actions in cholestatic liver diseases are attributed to its ability to protect liver cells from the kinds of toxic insults that could be relevant to other important disease states. This is a very important and unusual property; very few substances are able to similarly affect liver cell viability and tissue protection in a clinically acceptable way. The biochemical and molecular mechanism underlying UDCA and its effects on cellular survival has only been demonstrated over the last decades.

UDCA exerts beneficial effects in treating liver disorders through a diverse, complementary array of effects. These are summarised below.

(a) UDCA protects cholangiocyte and hepatocyte against cytotoxicity of other toxic endogenous bile acids

The liver absorbs and transports bile acids from two main types of epithelial cells, the cholangiocyte and hepatocyte. Bile acid synthesis and transportation in the intestinal lumen determine bile formation and they are used for degradation of cholesterol. However many bile acids are toxic, especially the hydrophobic bile acids, CDCA and DCA. They bind to proteins that exist

between the double lipid layers of epithelial cells of hepatocyte, which may influence cellular structures and functions. In cholestasis the excretory pathway from the hepatocytes becomes blocked, and toxic hydrophobic bile acids retained in the liver cause liver injury, fibrosis and death [29]. Bile acids are believed to influence overall cytotoxicity through the emulsification effects on the cellular membranes. Retention of hydrophobic bile acids in chronic cholestasis triggers cholangiocyte proliferation [30].

UDCA competes with other hydrophobic bile acids for absorption in the terminal ileum thereby decreasing the proportion of the more toxic CDCA and DCA. This effect is sometimes referred to as shifting the bile acid pool to more polar character. Enrichment of UDCA makes bile more hydrophilic and less damaging by replacing more toxic endogenous bile acids [31, 32]. In addition, the incorporation of UDCA into the non-polar domain of the lipid bilayer stabilizes the membrane structure. UDCA plays an important role in inhibiting cholangiocyte growth and secretion.

(b) UDCA directly protects of hepatocytes against bile acid-induced apoptosis

Bile acids induce cellular apoptosis at concentration as low as 25 μM and this is mainly because they can lead to cell death through independent death receptor pathways especially Fas receptor (this apoptosis pathway is illustrated in Chapter 4). Bile acid-induced apoptosis on hepatocytes can be inhibited by UDCA. UDCA seems to up-regulate canalicular transport, reducing the amount of bile acids in the hepatocyte. Besides, it has been reported that UDCA can block apoptosis by interrupting the classic apoptosis pathway involving inhibition of mitochondrial membrane permeability transition [33]. Apart from inhibiting cellular apoptosis, UDCA has been shown to activate survival pathways including the intracellular mitogen-activated protein kinase (MAPK)

signaling pathway, a pathway mediating signal transduction from cell surface to the nucleus, through activating epidermal growth factor receptor (EGFR) [29, 34]. Activated MAPK, in turn, phosphorylates and activates transcription factors leading to expression of target genes. This UDCA/MAPK/EGFR pathway reduces bile acid mediated cytotoxicity by preventing mitochondrial dysfunction, an organelle playing the role of amplifying apoptotic signaling pathways. Anti-apoptotic effects of UDCA have been found in both rat liver and human hepatocytes [35, 36].

(c) UDCA stimulates endogenous secretion of bile to alleviate cholestasis

The accumulation of hydrophobic bile acids and other toxic biliary constituents, caused by the damage of bile formation in many forms of cholestasis, leads to cell injury in the liver [37]. An effective method to alleviate cholestasis caused by toxic bile acids is to promote their secretion from the hepatocyte. UDCA has been demonstrated to provoke endogenous secretion of bile and alleviate cholestasis induced by toxic hydrophobic bile acids [38]. UDCA leads to biliary secretion of bile acids in patients with cholestasis and reduces the level of endogenous bile acids [39]. The number and activity of carrier proteins on the cellular membrane determines the secretory capacity of hepatocytes. UDCA stimulates the expression of transporter proteins, like bile salt export pump (BSEP) and the efflux transport proteins, like canalicular multidrug resistance associated protein 2 (Mrp2) [40] for bile acids across the canalicular membrane of the hepatocyte. This accounts for an increased overall elimination for those potentially toxic biliary compounds [41, 42]. Besides, UDCA might compete for intracellular transporters that promote the uptake of retained bile acids into organelles. A typical example is that UDCA exhibits its protective mechanism by repressing the expression of ASBT, an important transporter for bile acid uptake, in liver disorders.

Moreover, UDCA stimulates biliary secretion of bile acids via a variety of intracellular signaling pathways like MAPK signaling pathways in mammalian cells. MAPK pathways are mainly composed by ERK and JNK, which contain similar kinases. MAPK mediates diverse cellular functions including cellular apoptosis, proliferation, and differentiation. Activation of MAPK pathways appears to produce beneficial effects in cholestasis and may mediate the cholestatic effects of bile acids. Choleretic as well as cholestatic bile acids activate ERK1/2 while only cholestatic bile acids activate JNK.

To conclude, the ability to replace hydrophobic bile acid and cause a significant shift in the composition of the bile acid pool towards hydrophilicity accounts for the beneficial properties of UDCA in treating liver disorders.

1.3 Cholestatic liver diseases and cancer

1.3.1 Cholestatic liver diseases

Cholestasis is a pathological condition where normal bile flow from liver is impaired, causing intrahepatic accumulation of bile acids. Cholestasis results from genetic defects in canalicular transporters, mechanical obstruction of the intrahepatic and extrahepatic bile duct by gallstones, and factors related to bacterial infection, drugs, genetic disorders and pregnancy. Inherited defects in bile acid synthesis are also a trigger for certain cholestatic liver diseases in adults [43]. When the bile is obstructed, bile flow rate decreases and bacteria present in the bile begin to grow and proliferate [44], causing cholangitis. Some cases of cholangitis are mild and happen slowly with time. This is called chronic cholangitis. Some conditions are serious and even life-threatening and these are called acute cholangitis. The symptoms of serious cholangitis can include high fever, vomit, nausea and low blood pressure. Primary biliary cirrhosis (PBC) and Primary sclerosing cholangitis (PSC) are two important types of chronic cholestatic liver disease that have low prevalence.

PSC is a chronic disease of the bile duct, first described by Hoffman in 1867 [45].

It is an innate liver disease caused by chronic liver inflammation and progressive destruction of the bile ducts. An estimated 1 in 10,000 people is diagnosed with PSC which is more prevalent in men. The underlying cause is unknown, but genetic susceptibility may play a role. This disease is slowly progressive and patients may feel well for 10–15 years before they have obvious symptoms. However it finally results in a high risk of liver failure, tumors in the liver or bile duct. PSC has a strong association with inflammatory bowel disease (IBD), type I diabetes and a higher risk of developing colorectal cancer. The signs of disease progress include itching, obvious weight loss, yellow discoloration of the skin and eyes and pain in the upper right part of the abdomen. PSC is diagnosed via blood test and cholangiogram, an X-ray image of bile duct. Liver transplantation is the only effective cure and there are no effective medical therapies available [46].

PBC is another chronic disease slowly impairing the intrahepatic bile ducts in the liver and is considered as an autoimmune disease of the liver. It affects the bile duct epithelium and leads to the destruction of small bile ducts and liver tissue by the immune system causing hepatocyte damage and subsequent fibrosis, scaring and cirrhosis. PBC is not a common disease, affecting up to 1 in 3 to 4 thousand people. The majority of sufferers are middle-age women. Typical symptoms are fatigue, severe itching and upper abdominal discomfort but nearly half of the patients have no clinical symptoms at initial presentation. Diagnosis of PBC is through a combination of serum liver tests and the presence of anti-mitochondrial antibodies [47].

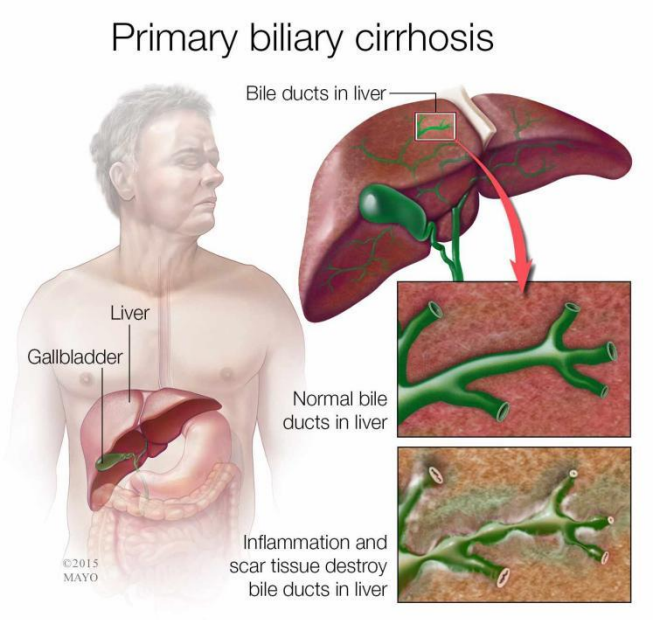

Figure 1.5- A comparison of normal bile ducts and damaged bile ducts in liver. The diagram is from the Primary Biliary Cholangitis section on the Transplant liver in India website [48]. Inflammation and scar tissue cause damage to bile duct in liver. Bile and other substances cannot be eliminated from liver, which are harmful to the liver.

Hydrophobic bile acid induced injury of hepatocyte membranes is the main trigger for PBC and PSC [49A][49B]. For a healthy individual, around 10% of the total bile acids that has not been cleared in the liver reaches the systemic circulation to the kidney and then reabsorbed by epithelial cells in the kidney and finally returns to the liver. Bile acids are virtually absent in the urine. But for patients with PBC and PSC, bile acids become easily detectable as urinary excretion of toxic bile acids occurs to clear those bile acids accumulating in the liver. High concentration of hydrophobic bile acids is especially cytotoxic and causes liver inflammation by activating NF-kB-mediated pro-inflammatory cytokine production and induce many liver disorders, and this is mainly because these toxic bile acids damage the basolateral membrane and cell organelle membranes. This is particularly serious in the outside layer of the canalicular membrane as bile acids are very concentrated in bile.

Early diagnosis is of great importance to those patients mainly because some of these diseases can be managed if detected in the early stages. There is no

effective cure for PBC at the time being, but some medical interventions are available to help slow down disease progression including use of UDCA, OCA and liver transplant [50].

Maintaining bile acid homeostasis is critical for protection against liver injury. Bile acid therapy in the treatment of multiple liver disorders involves bile acid replacement in deficiency states or bile acid displacement by UDCA. It is worth mentioning that UDCA is reported to exhibit anti-inflammatory effects in various liver disorders [51, 52] by regulation the expression of tumor necrosis factor (TNFα) and other inflammatory cytokines [53]. Administration of UDCA decreases hepatocyte injury caused by retained toxic bile acids. UDCA improves cholestasis by altering signaling pathways that regulate the expression of various transporters, for example, it stimulates the expression of the export pump at the hepatocyte membrane involved in the detoxification process [54]. Besides, UDCA promotes the biliary excretion of bile acids under the situation of impaired bile secretion and current research suggest that UDCA therapy has shown favorable effects in the treatment of PSC [55], particularly given its excellent safety profile and its low cost compared with other drug candidates. UDCA has also been approved by the FDA for treating PBC [56], slowing down progression of liver fibrosis in the early stage [57]. Studies found that UDCA enhances natural killer activities in patients with PBC [58]. The daily dose for the treatment of PBC depends on the body weight of patients, with 13.5 mg UDCA recommended per kg of body weight [59]. It has been reported that treatment of UDCA in patients with PBC for up to six years significantly prolongs survival rates [60]. While it is the only approved therapy it is ineffective in a significant minority of patients who progress to liver transplant.

1.3.2 Bile acids and cancer

Cancer is a family of disorders marked by common features such as uncontrolled or dysregulated cell growth. Cancer is the second most common

cause of death among all human diseases after cardiovascular disease. It is estimated that around 19.3 million people are diagnosed with cancer globally and almost ten million cancer deaths occurred in 2020 [61]. At least 90% of cancer cases occur due to environmental factors or unhealthy lifestyles. Common environmental factors include tobacco (25%–30%), obesity [62] (30%–35%), infection, solar-radiation and environmental pollution. Individuals with certain inherited genetic factors are more likely to be diagnosed with specific forms of cancer.

Bile acids were first proposed as carcinogens in the 1940s [63] but the toxicity and cancerogenic effects of certain bile acids have only been established in recent decades. Bile acids can act as carcinogens when there is repeated exposure to high levels. Bile acids have been added into the list of tumor promoting agents and play a major role in carcinogenesis of some tissues for example liver, colon and gastrointestinal tract. Pathways potentially linking bile acids to tumor development mainly involves DNA damage, apoptosis [64], genetic instability [65]. Abnormally high concentrations of serum bile acids induce hepatocyte DNA damage and cause cell death and inflammation, thereby accelerating cancer development [66]. Increased incidence of cancer in the liver, colon, stomach, small intestine, pancreas, breast and gastrointestinal relate closely to high concentration of hydrophobic bile acids and the association of bile acid with liver cancer has already been proven in both human and animal studies.

A large amount of secondary bile acids, DCA and LCA, in the colon may contribute to damage to colonic epithelial cells, induce reactive oxygen species (ROS) generation and apoptosis at physiologically relevant concentrations and promote colorectal cancer (CRC, cancer developed from the colon or rectum). The epidermal growth factor receptor (EGFR) pathway may be important for bile acid action linked to CRC progression as over activation of this pathway in tumor cells leads to tumor cell proliferation and survival [67]. Emerging evidence

shows CDCA may be mutagenic as well [68]. Exposure to high level of CDCA facilitates the inflammation and development of Hepatocellular carcinoma (HCC) [69] by significantly increasing the mutation rate of tumor suppressor genes and oncogenes. The consumption of a high-fat diet contributes to a large amount of 7α-dehydroxylating bacteria in the intestine and higher fecal concentration of DCA, which also promotes carcinogenesis. This indicates a potential link between diet and cancer mediated by a microbiota-derived bile acid. These hydrophobic acids induce DNA damage and cell aging in hepatocytes, with initiation of inflammation and tumor-inducing pathways potentially causing liver cancer [70]. Changes in expression at the mRNA level of many genes by hydrophobic acids leads to apoptosis and early carcinogenesis [71].

Therapeutic potential of novel bile acids

Targeting bile acids may be an effective strategy for cancer, especially for CRC prevention and treatment [72]. The conversion of DCA into another epimer, isoDCA, may have therapeutic potential in the treatment of CRC which will be explained in detail in Chapter 2. A series of studies indicate FXR signaling is a potential target for blocking the bile acid contribution to CRC progression. Chapter 4 will describe investigations into the potential of certain bile acids as anti-tumor agents by modulating the same pathways which induce toxicity, i.e. apoptosis [73, 74]. Patients with CRC and liver cancer, on average, have experienced high levels of bile acid exposure, while existing evidence shows that therapy with UDCA protects against the development of chemically induced CRC in animal studies [75]. UDCA exhibits a chemoprevention effect against CRC [33, 76] via multiple mechanisms including inhibition of CRC cell proliferation [34]. Thus, synthesizing UDCA derivatives to evaluate their apoptotic activity is a very promising method for CRC chemoprevention and treatment.

Chapter 2. Nuclear receptors FXR and isobile acids

2.1 Introduction

Over the past two decades it has emerged that bile acids regulate aspects of metabolism including their own formation, the synthesis of lipids and glucose as well as aspects of inflammation. Many of these effects are mediated by a receptor that recognizes bile acids in the cells lining the gut and in the liver. Activation of this nuclear receptor causes hormonal signaling affecting key aspects of metabolism. The receptor is termed FXR and this area is one of the most intensely investigated in modern medicine. The FXR receptor however does not explain the full range of bile acid effects including the most important clinical effect of a particular bile acid. This chapter is concerned with the synthesis and biological evaluation of five human bile acids (CDCA, UDCA, DCA, LCA and CA) and their corresponding 3β-epimers. (The chemical structures are shown in Figure 2.1).

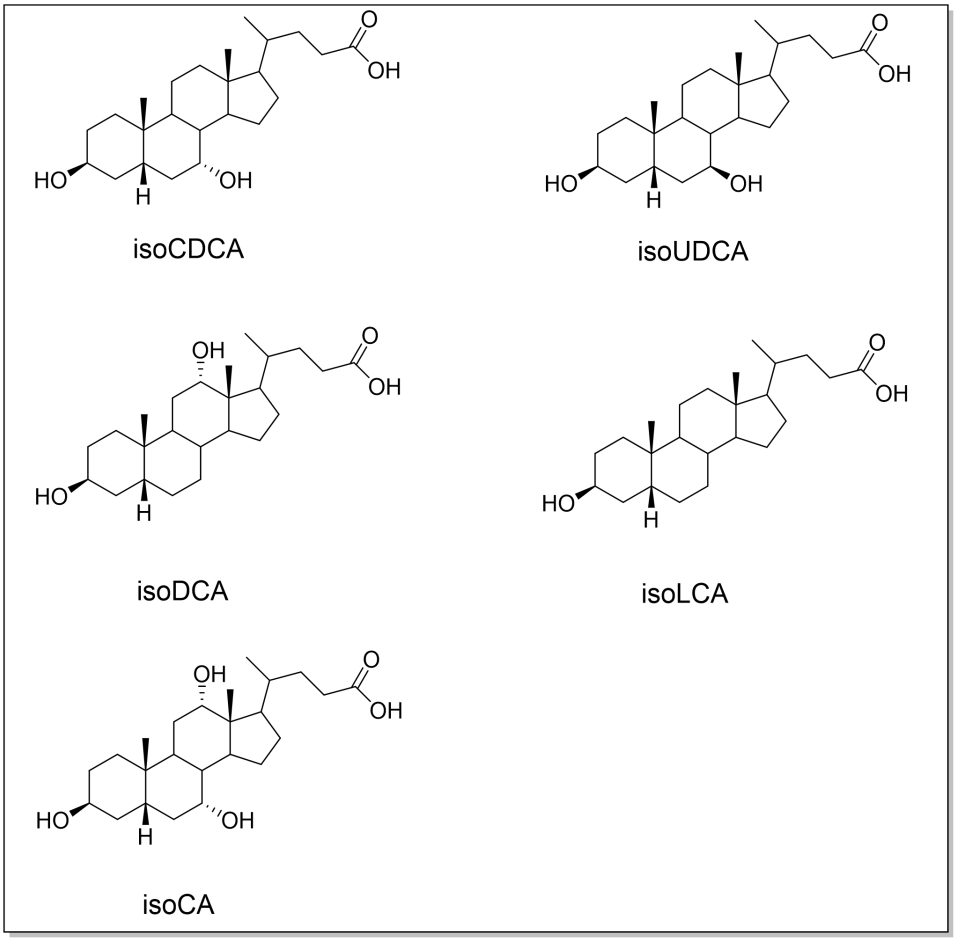

Figure 2.1- Five different types of isobile acids. They are 3β epimers of the normal occurring bile acids.

Isobile acids, the 3β-OH stereoisomers of the normally occurring bile acids, are commonly found in the feces, urine, serum and blood of human individuals and other animals, contributing around 15–20% of all bile acids [77], however, there are no detectable isobile acids in bile because after reabsorption and transport to the liver these molecules undergo re-epimerization to their 3α-stereoisomers [78]. Isobile acids are the isomerization of 3α-OH presenting on the C3 of the cholestane nucleus and they are generated during enterohepatic circulation. The level of isobile acids can exceed 300 μM in the human gut [79]. So far, the isobile acids are known to be produced by *Ruminococcus gnavus*, an abundant commensal, mainly founded in human intestines. IsoDCA and isoLCA are the most abundant isobile acids. IsoUDCA has been investigated for the treatment of PBC as an alternative to UDCA. Isobile acids are presumably less efficient than 3α- bile acids in solubilizing dietary lipids.

2.1.1 Overview of bile acids synthesis in the human liver

In the past three decades, the pathways of bile acid synthesis have been defined and the genes encoding the biosynthetic enzymes of these pathways have been identified. Bile acids are synthesized from cholesterol in the liver, the only organ that has all 14 enzymes required for de novo synthesis of two primary bile acids. This occurs through a series of sterol ring hydroxylations, side chain oxidation steps and final reduction of 3-oxo into the alpha stereochemical configuration. This process is complex multi-enzyme and multi-organelle defined as two main metabolic pathways, known as neutral pathway (classic pathway where biosynthesis begins with hydroxylation at C-7 on the steroid nucleus) and acidic pathway (alternative pathway where hydroxylation begins at C-27, the terminal methylene group of the side chain). The neutral pathway accounts for the 90% of the primary bile acids production

in the human liver [80]. This route is composed by a series of reactions catalyzed by enzymes localized at the cytosol, peroxisomes and mitochondria. In the ER of hepatocytes, cholesterol is metabolized into 7α-hydroxycholesterol by cholesterol 7α-hydroxylase (CYP7A1) [81]. CYP7A1, known as bile acid synthesis cytochrome P450 A1 and expressed only in the hepatocyte, is the enzyme involved in the catabolism of cholesterol and it regulates the biosynthesis from cholesterol. CYP7A1 is the first and main rate-limiting enzyme in the neutral pathway for bile acid synthesis. Afterwards, the 7α-hydroxycholesterol is converted to 7α-hydroxy-4-cholesten-3-one (C4, the common precursor for synthesis of CA and CDCA) by a hydroxyl steroid dehydrogenase and further into CA by branching enzyme sterol 12α-hydroxylase (known as CYP8A1, another highly regulated microsomal enzyme) and into CDCA (rat, human and hamster) by mitochondrial sterol 27-hydroxylase (CYP27A1). CA and CDCA are the end products of cholesterol degradation. The level of sterol 12α-hydroxylase in the liver determines the relative amounts of these two primary bile acids.

Cholesterol 7α-hydroxylase deficient species produce bile acids from the alternative biosynthetic pathway, called the acidic pathway (named because of the formation of acidic intermediate metabolites). In the acidic pathway, only CDCA is generated. This is initiated mainly by mitochondrial sterol 27-hydroxylase (CYP27A1, is found in most tissues and macrophages) and followed by hydroxylation at C-12’ position (CYP8B1, expressed at high level in the liver and at lower levels in the kidney and brain). Transport of cholesterol into mitochondria for 27-hydroxylation by CYP27A1 is the rate-limiting stage for the alternative pathway [82]. CYP27A1 and CYP8B1 are commonly expressed in extrahepatic tissues, for example, macrophages, adrenal glands and other tissues. Mitochondrial CYP27A1 catalyzes sterol side chain oxidation and subsequent cleavage of a three-carbon unit and this contributes to the formation of a C24 cholestenoic acid, the backbone of most bile acids.

Although both CYP27A1 and CYP7B1 are ubiquitously expressed in many tissues, the conversion to bile acids from steroids must take place in the liver as only the liver has all the required enzymes to accomplish the bile acid biosynthesis.

The contribution of the alternative pathway to overall bile acid biosynthesis depends on the species. In human this pathway is responsible for the generation of oxidized cholesterol molecules that can be subsequently converted to CDCA but this pathway only contributes to 10% of CDCA production in the liver during routine physiological conditions [83], but it is quite important in the amount of bile acid synthesis in the patients with liver disorders [84]. The alternative pathway plays a critical role in anti-inflammation and lipogenesis. The inner mitochondrial membranes are the main reaction site for this pathway.

The neutral pathway and acidic pathway may not occur at the same rate in all hepatocytes, but these two bile acid synthesis pathways compensate each other to produce bile acids and determine the overall bile acid pool size and bile acids composition. The balance of two bile acid synthesis pathways is critical to generate a sufficient bile acid pool size and proper bile acid composition in humans.

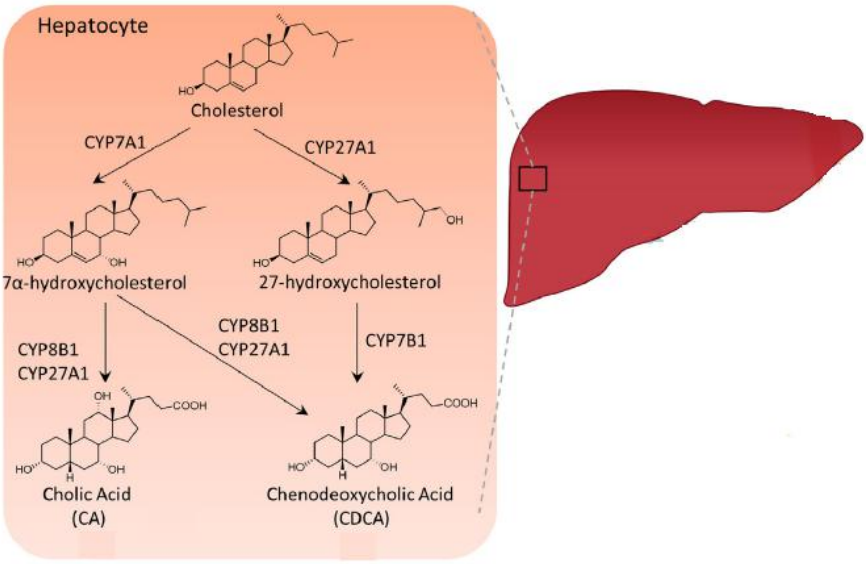

Figure 2.2- Summary of the biosynthesis of primary bile acids from cholesterol in the human liver [85]. Only key intermediates are shown here in what is a complex multistep metabolic process in each case.

Several other minor routes have been discovered, which have relevance in some species. Very recently, a third synthesis pathway was discovered, called the neuronal pathway, initiated by cholesterol 24-hydroxylase (CYP46A1) in the brain and 24-hydroxycholesterol 7α-hydroxylase (CYP39A1) in the liver. The contribution of this pathway to overall bile acid synthesis is minor and the end product of this minor pathway is CDCA only.

2.1.2 Synthesis of secondary human bile acids

The diversity of the bile acid pool is further expanded by the actions of the gut microbiota in the intestine (a community comprising 500–1000 distinct bacterial species) during the enterohepatic circulation, which converts primary bile acids into secondary bile acids by performing a series of enzymatic reactions. The relationships between gut microbiota and bile acids have been recognized for a long time. In human liver, the newly synthesized primary bile acids undergo amidation i.e., conjugated with amino acids glycine or taurine at C-24 carboxyl group via bile acid-CoA synthetase (BACS) localized at the ER and bile acid-CoA amino acid N-acetyltransferase (BAAT) enzyme located in localized in peroxisomes and cytosol. The majority of bile acids are conjugated with glycine, the minority with taurine in humans: the ratio of glycine to taurine conjugation is approximately 3:1 under physiological conditions [86]. Conjugation of bile acids alters their physicochemical properties and their metabolism by increasing their ionization and solubility at physiological pH (conjugation decreases the bile acid pK_a and convert it to a much stronger acid) [87], makes them impermeable to cell membrane (negative charge on the side chain of conjugated bile acids and size of the molecule prevents passive absorption across the epithelial cells of the biliary tract and small intestine) and persist in bile and intestine in high concentration. This amino acid conjugation

decreases overall toxicity of the bile acid pool. The conjugated bile acids, TCA and TCDCA, are stored in the gallbladder and then secreted into bile ducts after each meal and transported into the human small intestine, where they are deconjugated by microbial bile salt hydrolases (BSHs, abundantly expressed in the human gut and expressed in a broad spectrum of bacteria) activity. Deconjugation helps improve the bacterial colonization of the gastrointestinal tract. These enzymes function as a gateway reaction in bile acid metabolism and they are expressed mainly by *Bacteroides*, *Clostridium*, *Lactobacillus* and *Bifidobacteria*. The deconjugated primary bile acids, CA and CDCA, are further metabolized in the large intestine by the gut bacteria into secondary bile acids DCA and LCA, respectively, through the activity of 7α-dehydroxylase [85, 88] in bacteria flora. These bile acids then passively diffuse through the colonic mucosa. Dehydroxylation at position C-7 is the most important bacterial bile acid biotransformation in the human colon and it is involved in disease of the GI tract including colon cancer [89]. In the known bacterial species that have 7-dehydroxylation activity, it is encoded by the bile acid-inducible (bai) gene. This conversion is confined to free bile acids and removal of glycine or taurine is a prerequisite for 7α-dehydroxylation [90]. The deconjugation and 7α-dehydroxylation of bile acids increase their overall pK_a and hydrophobicity, enabling them to across the colonic epithelium more easily by passive absorption. DCA, CDCA and CA are reabsorbed in the intestine and transported back to liver for detoxification and then recycling. Only 5–10% of these bile acids are lost in feces (about 0.2–0.6 g per day) and they are replenished by the bile acids synthesized via *de novo* synthesis by the liver in order to maintain a constant bile acid pool under physiological conditions.

Once transported back to the liver, the secondary bile acids can be further converted to UDCA via the 7β-HSDH, which represents only a marginal bile acid species and this process involves the participation of multiple enzymes. These synthesis and metabolic pathways produce more than 18 different bile

acid compounds, which maintains a multifunctional bile acid pool and ensures multiple signaling activities in the human body.

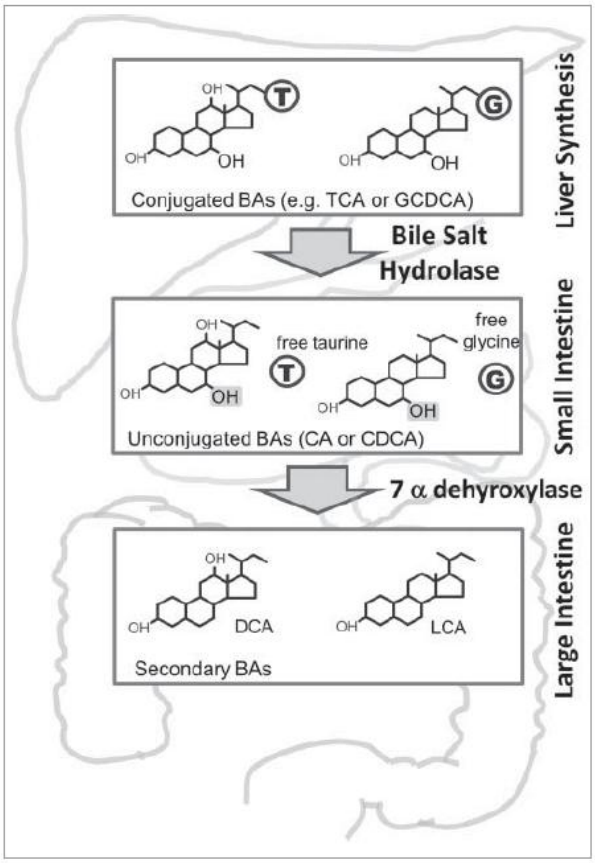

Figure 2.4- The formation of secondary bile acids in the human intestine from primary bile acids [88] **via 7-dehydroxylation.** Dehydroxylation at C-7' is a complex and multienzyme process. The primary bile acids are conjugated to taurine or glycine molecules. Then they are deconjugated by bacterial BSH and further metabolised by bacterial 7α-dehydroxylase. Secondary bile acids are absorbed from the intestine and taken up by the liver, thereby bile contains both primary and secondary bile acids.

DCA is reabsorbed into the colon and then reconjugated and secreted into blood (occupying 20–25% of the overall bile acid pool). The pathway for LCA is slightly different as it is a highly toxic bile acid. It is efficiently amidated and then undergoes one or more detoxification steps during its transport through the hepatocyte. A small amount of LCA circulates back to the liver and can then undergo sulfation at the 3-hydroxy position (sulfation detoxifies the extremely hydrophobic bile acids in human [91]), N-acylamidated and rapidly

excreted in the bile again, contributing to the enterohepatic circulation of bile acids [92], and ultimately secreted into urine. However, the majority of LCA is excreted into the feces.

Bacterial 7α-dehydroxylase converts CA into DCA and CDCA into LCA by removal of 7α-OH group on ring B. DCA and CDCA is termed as 7-deoxy bile acids. These secondary bile acids in human then pass into the portal vein and reach the liver, where they join newly produced primary bile acids. They are reconjugated to glycine or taurine in the canaliculi of the liver, and are then stored in the gallbladder.

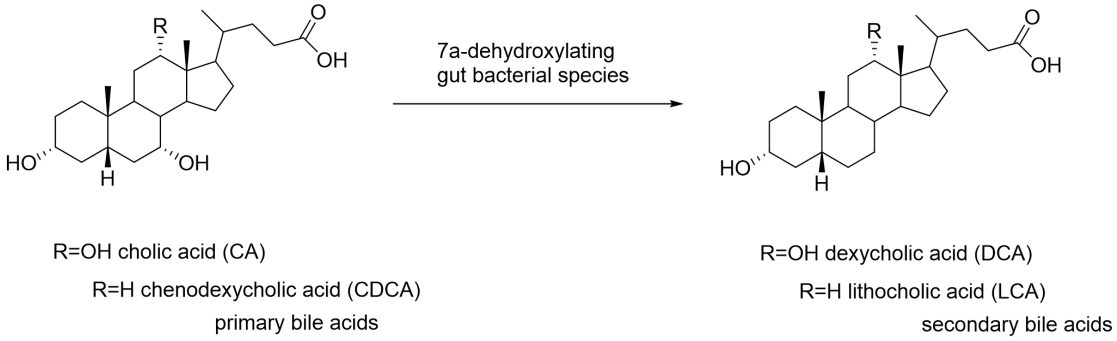

Figure 2.5- Chemical transformation of primary bile acids into secondary bile acids involving the removal of 7α-hydroxyl group [79].

To sum up, the classic bile acid synthesis pathway in human is the predominant pathway for synthesis of a bile acid pool composed of around 30% each of CA, CDCA and DCA.

2.1.3 Biological synthesis of isobile acids and colonic mechanism of bile acids

Microbial metabolism not only produces bile acids with 3-OH group in alpha configuration, but a variety of keto/oxo intermediates and stereoisomers with C-3 in beta configuration [93]. Isobile acids (3β-OH bile acids) are generated from the 3α- bile acids *in vivo* by epimerization of the 3α-hydroxyl group. The biosynthetic pathway for conversion of primary bile acids and secondary bile

acids into their 3β isomers involves the consecutive activity of 3α- and 3β-hydroxysteroid dehydrogenases (HSDHs) in the cytoplasm of two bacterial species, *Eggerthella lenta* and *Clostridium perfringens* [94].

HSDHs are NAD(P)(H)-dependent enzymes with stereospecificty for steroid and bile acid hydroxyl groups and they have been discovered in several protein families, including short-chain reductase and aldo-keto reductase superfamily [95]. They mainly catalyze the dehydrogenation of hydroxysteroids and act as reversible switches regulating the physicochemical properties of bile acids [79, 96].

Epimerization of bile acid hydroxyl groups carried out by the HSDHs is a reversible conversion in stereochemistry from the α to the β configuration, through the generation of a stable keto bile acid intermediate (Figure 2.7). The mechanism of the biotransformation includes the bacterial oxidation of the 3α-OH into its 3-oxo derivative by 3α-HSDHs (*CDD59474*) and followed by reduction of the 3-oxo compounds by the 3β-HSDHs (*CDD59473*).

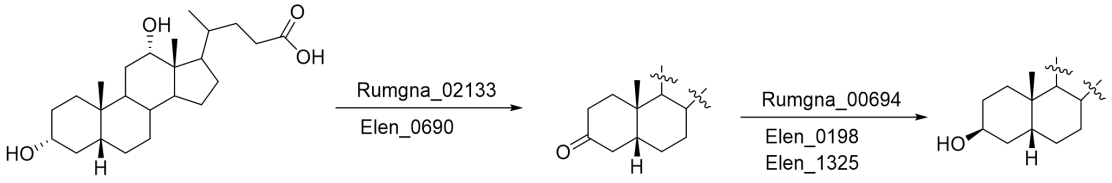

Figure 2.7- The biosynthetic pathway in conversion of normal occurring bile acids into isobile acids [88]**.** This pathway involves the oxidation of 3α-OH into 3-oxo (intermediates in the epimerization of bile acids at C-3 [97]) by 3α-HSDHs and the reduction of 3-oxo into 3β-OH by 3β-HSDHs. These two bacterial HSDHs constitute novel enzymes in the isobile acids pathway.

To conclude, there are three main metabolic processes affecting bile acids during the enterohepatic circulation for most species [98, 99]: reconjugation followed by deconjugation in the hepatocyte, dehydroxylation at C-7, and oxidation at C-3 or C-7 followed by reduction to corresponding α or β hydroxy group. The microbial transformation of bile acids plays an essential role in their metabolism [100].

What could be the advantages of using isobile acids over 3α-epimers?

The conversion of normal bile acids into their 3β epimers is likely to have biological consequences which were partly the subject of this thesis project. For example, isobile acids may play as a role of detoxicant, which means that conversion into isobile acids may cause less detergent effect and toxicity towards the cells. They shift bile acid pool from hydrophobic and toxic to hydrophilic and health-promoting. The secondary bile acid DCA causes cell membrane damage at high concentration (5–10 mM). DCA inhibits colonic cell proliferation and decreases tumor suppressor activation in the cell cycle. Bacterial conversion to isoDCA is predicted to decrease its detergent properties by disrupting the hydrophobic/hydrophilic (amphiphatic) facial nature of the molecule. DCA is known as causative agent in colon cancer [101, 102] through an indirect mechanism involving the induction of oxidative stress and generation of ROS. Indeed, isoDCA is speculated to oppose or reduce DCA's toxicity to colorectal epithelial and bacterial cells. Hence, its detergent properties are greatly diminished at physiological concentrations and so for example isoDCA (12mM) has a higher CMC than DCA (5 mM). IsoLCA and isoCDCA are also present in considerable amount in the colon and their amount even increases during bile acid therapy [103]. One of the objectives of our work was to explore the relative toxicity of a panel of bile acids and their 3-epimers.

Secondly, isobile acids may have a positive effect on increasing cell membrane integrity. DCA, itself the natural bile acid, damages membrane integrity at the concentration of 200–400 μM causing nonspecific signaling leading to oxidative DNA damage and apoptosis. The epimeric isoDCA is expected to lead to less cell membrane damage compared with DCA but this has not been properly characterized before this work. Other effects on the microflora can be envisaged to flow from the epimerization of the bile acids. For example, conversion of DCA into isoDCA benefits the growth of abundant

genus *Bacteroides* [104], which is found in the human intestine and helps in breaking down food and produce nutrients and energy in human body.

Lastly, our collaborators in Graz and Amsterdam are interested in signaling properties of isobile acids through the bile acid receptors and this interacts with the normal bile acids. We proposed to develop synthetic methods for the isobile acids to allow us to supply the collaborator labs with adequate study quantities and then to work with them on analysis of the results of studies *in vitro* and *in vivo*. This will be described later in this thesis. By understanding the interactions between isobile acids and the human bile acid receptors it might be possible to predict their contribution to health and disease.

2.1.4 Bile acid receptors in health and diseases

In the past two decades it has emerged that bile acids play important functions as versatile signaling molecules involved in the regulation of various cellular activities in mammalian physiology and that for example they can regulate lipid, glucose and energy metabolism. Bile acids have been demonstrated to activate several cell signaling pathways involved in the regulation of bile acid metabolism, optimizing nutrient absorption and metabolism. One of the most typical example is that bile acids can bind and activate several nuclear receptors, Farnesoid-X-Receptor (known as FXR), Vitamin D Receptor (VDR) [105], Constitutive Androstrane Receptor (CAR), and Pregnane X Receptor (PXR) [106]. Bile acids also active cell surface receptors including GPCRs such as G-Protein-Coupled Bile Acid Receptor-1 (Gpbar-1 and Mbar, known commonly as TGR5). Although bile acids are able to activate many signaling pathways, two major bile acid regulated receptors, FXR and TGR5, receive the most attention in the scientific literature [107]. These two signaling pathways are highly expressed in the gastrointestinal tract and their mechanisms will be explained in detail in the following content in this chapter. Each bile acid is able to interact with more than one receptor but with different levels of activity and

selectivity. This complexity is one of the reasons that the biochemistry of bile acids continues to receive so much attention. Primary bile acids, CA and CDCA, are the most potent physiological ligands for FXR while secondary bile acids, LCA and DCA and their taurine conjugates, are more effective agonists of TGR5 [108]. The activation of these two receptors contributes to the specific signaling pathways, which collectively regulates many physiological functions in lipid and glucose metabolism [109]. FXR and TGR-5 agonists and antagonists are prospective approaches in treating many common metabolic and hepatic diseases [110] like PBC and non-alcoholic steatohepatitis (NASH, a chronic liver disease with inflammation and fibrosis) [111] and the receptors have potential as diagnostic markers. These bile acid receptors play important roles in lipid, carbohydrate, liver, bone and renal metabolism [112]. The discovery of the FXR and TGR5 has opened up new horizons in drug discovery and drug development.

The FXR- an overview

Nuclear receptors are ligand-activated transcriptional factors in regulating multiple key physiological activities including homeostasis, metabolism and cell death. They are also important in every aspect of development, physiology and diseases in humans. In the 1990s, when receptors had been identified for many known nuclear hormones, scientists were looking for the type of molecule involved in regulation of the mevalonate pathway. This is an important metabolic pathway in higher eukaryotes and involves the synthesis of cholesterol, bile acids, lipoproteins and steroid hormones [113, 114]. A farnesol derivative, which is the last precursor in activating the mevalonate pathway, was shown to activate an orphan receptor that was therefore termed, farnesoid X receptor (FXR). It was firstly discovered from a rat liver cDNA library in 1995 [115]. FXR, is an intracellular nuclear bile acid receptor encoded by the NR1H4 gene in humans and it is one of 48 nuclear transcription factors identified so far,

which are involved in diverse biological processes, including cell growth, differentiation and metabolism. FXR is localized in the nucleus. This makes it different to the majority of nuclear receptors which reside mostly in the cytosol and traffic to the nucleus only under the influence of their ligand hormone. It is expressed in high quantity in several gastrointestinal and intestinal organs like liver, intestine, kidney and adrenals [116]. FXR regulates liver inflammation and regeneration. It maintains liver triglyceride homeostasis and protection against fatty liver injury in nonalcoholic fatty liver disease (NAFLD) [117].

Physiological functions of FXR

The main physiological role of FXR is to function as a biological sensor for bile acids, regulating their biosynthesis, conjugation, transport and detoxification in the liver and intestine [109]. It maintains bile acid homeostasis [118] by controlling its level within a physiological range in order to prevent bile acid accumulation and cellular damage. As has been described already, FXR activation inhibits bile acid biosynthesis in liver by down-regulating some key enzymes involved in bile acid synthesis, for example, CYP7A1.

The impact of FXR on bile acid synthesis has been well defined, however, its role in bile acid transport is not fully understood. FXR has an established profile in the regulation of enterohepatic circulation of bile acids. The enterohepatic circulation is considered the way that evolution developed to recycle valuable functional molecules/drugs. FXR modulates the expression of major bile acid transporter proteins involved in whole enterohepatic circulation and these bile acid transporters are important components in mediating bile acid efflux and minimizing the deleterious effects of bile acid accumulation. FXR activation in the liver contributes to increased conjugation of bile acid followed by the excretion of bile acids from the hepatocyte into bile, thereby facilitating bile flow. Furthermore, FXR activation in the intestine enhances the reabsorption of bile acid back into liver.

The function of FXR in this enterohepatic circulation mainly involves the regulation of various transporter proteins on the membrane of liver and intestine. FXR regulates bile acid conjugation by inducing BACS and BAAT gene transcription. At the same time, FXR reduces bile acid uptake primarily by hepatocytes by suppressing the expression of Na^+-taurocholate cotransporting polypeptide (NTCP, *SLC10A1,* mediating the uptake of conjugated bile acids) [119], a transporter that facilitates bile acid across the sinusoidal membrane of the hepatocyte from the portal blood and to a lesser extent by sodium independent organic anion transporter OATPs (OATP1, *SLCO1A1* and OATP4, *SLCO1B2*) present on the sinusoidal membrane of hepatocytes. In addition, FXR promotes basolateral bile acid excretion into bile canaliculi by inducing the expression of ATP-binding cassette (ABC proteins) in the membrane of hepatocytes, known as bile salt export pump [120, 121] (BSEP, *ABCB11*, an transporter helping bile acids export across the canalicular membrane considered as the driving force for bile formation), multidrug resistance protein, MDR2 (in mice, involved in biliary excretion of phospholipids) and MDR3 (*ABCB4*, in human), multidrug resistance-associated protein 2 (MRP2, *ABCC2*, mediates canalicular excretion of conjugated organic anions) and multidrug export pump 1a (MDR1A, *ABCB1A*). These ABC proteins transport bile acids to the bile from liver cells and finally down-regulate the bile acid level in the hepatocytes. The regulation of these ABC proteins is to reduce bile acid accumulation in the liver and consequent liver injury. Activation of FXR leads to the upregulation of intestinal bile acid binding protein (IBABP, first FXR target gene identified in the gastrointestinal system), which affects the transport of bile acids in intestinal epithelial cells. FXR also activates an ileal bile acid binding protein called apical sodium-dependent bile salt transporter (ASBT, *SLC10A2*) [122] located in the distal segment of the small intestine, facilitating the reabsorption of conjugated bile acids in the brush border membrane and uptake of bile acids into the terminal ileum. FXR induces the organic solute transporter (OSTα/β,

SLC51A/SLC51B) gene transcription [123–125]. OSTα/β is the major bile acid efflux transporter in the intestine [125] essential for intestinal bile acid export across the basolateral membrane from enterocytes and it provides alternative excretion routes for bile acids into the systemic circulation. FXR stimulates the hepatic OSTα/β expression in patients with PBC and OSTα/β acts as an adaptive response to cholestasis to excrete bile acids from hepatocytes. Additionally, activation of FXR induces the expression of MPR2 on the basolateral surface of renal tubular cells increasing the overall elimination of toxic bile acids from the body [126, 127].

FXR plays a vital role in enterohepatic circulation of bile acids by regulating bile acid synthesis, biliary bile acid secretion, intestinal bile acid reabsorption and hepatic uptake of bile acids into hepatocytes [128–130]. All these ensure a constant bile acid level and prevents accumulation of bile acids in enterocytes and liver, colon diseases caused by build-up of toxic bile acids.

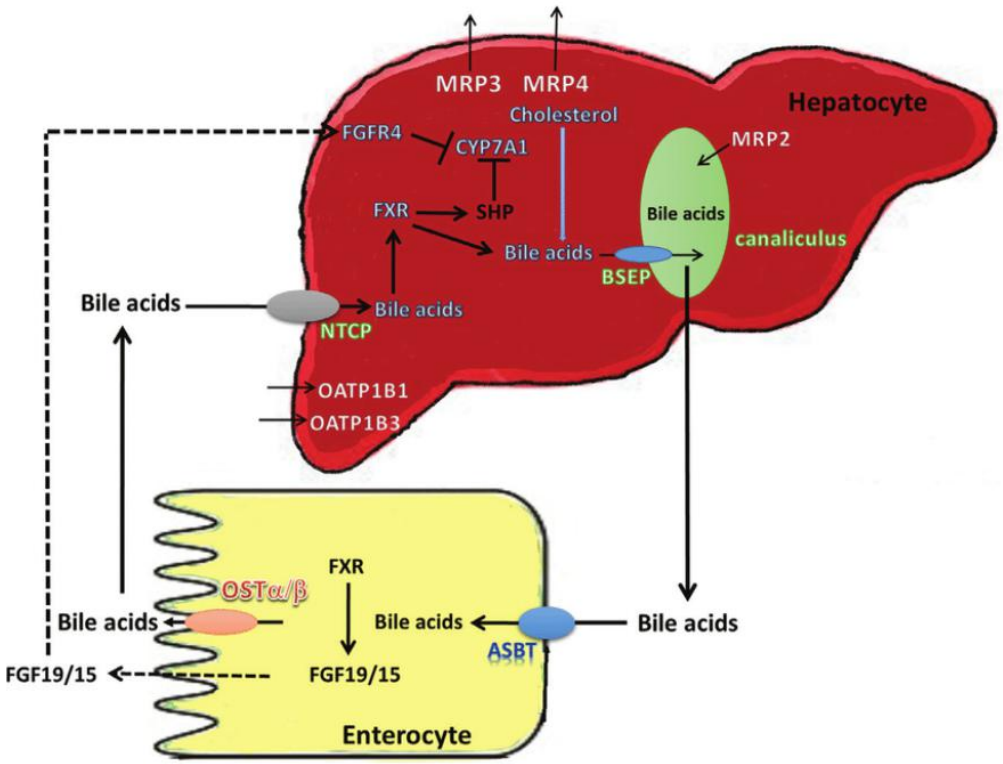

Figure 2.8- A schematic illustration of the effect of bile acid and FXR in the enterohepatic circulation [318]. Bile acids activate hepatic and intestinal

FXR to regulate genes important for bile acid metabolism. This circulation involves the participation of two main hepatocyte transporters and two main ileal enterocyte transporters. Ileal uptake of conjugated bile acids aids by a sodium dependent transporter, ASBT while exiting from the ileal enterocyte requires organic solute transporter, OSTα/β. In the hepatocyte, uptake of conjugated bile acids is mediated by sodium-dependent, NTCP, the apical transporter shares homology with ASBT, and sodium-independent transporters, a large family of OATP molecules (OATP1 and OATP4) present on the basolateral membrane. The driving force for the elimination of conjugated bile acids into the bile from the hepatocyte is, BSEP, an ATP-energized efflux transporter in the canalicular membrane. In addition to these, a large amount of transporter proteins involved in the whole enterohepatic cycling. These bile acid transporters are the vital components in the circulation, maintaining bile acid homeostasis and also minimizing faecal and urinary loss of bile acids. Deficiency in FXR regulation of enterohepatic circulation of bile acids may cause many hepatic disorders.

FXR regulates gene expression involved in the regulation of a network of metabolic pathways including lipid [131], glucose, and triglyceride metabolism [87]. The activation of FXR signaling is found to reduce inflammation in diabetes [132, 133] and fibrosis as well (Figure 2.9). Bile acids and FXR are therapeutic targets for the treatment of obesity, diabetes, lipogenesis, fatty liver diseases, cholestatic liver diseases and many other metabolic disorders. However, FXR activation leads to increases in low-density lipoprotein (LDL), which is predictive of cardiovascular risk. This may be an important limit on the therapeutic usefulness of FXR agonists. Despite this issue FXR is regarded as an attractive target for new drug discovery especially in liver protection and modulation of metabolism.

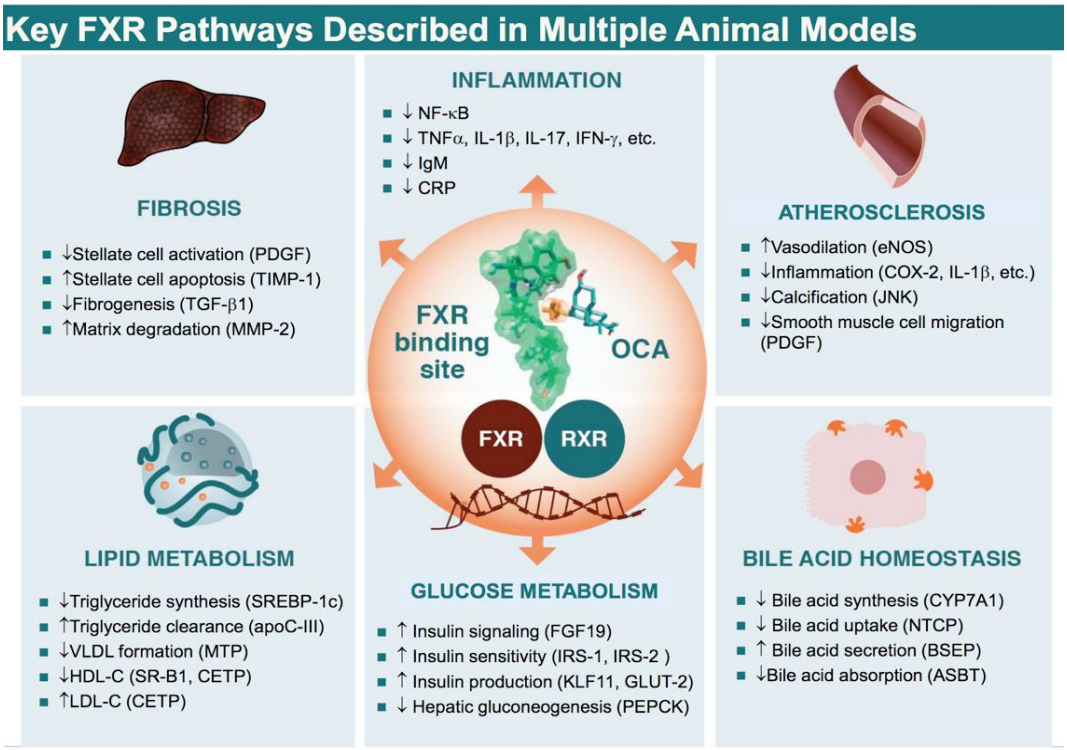

Figure 2.9- Multiple effects of FXR in animals [134]. FXR regulates multiple gene expression involved in bile acid, glucose and lipid homeostasis and helps reduce inflammation and hepatic fibrosis. FXR agonist OCA has many clinical applications.

FXR and colon/liver cancer

Many important physiological functions of FXR have been identified and some of these have already been described. An abundance of evidence suggests that FXR may be a useful target in the prevention of colon carcinogenesis [135]. Colon cancer is the third most common cancer causing 700,000 deaths worldwide in 2012 [136]. Colon cancer is link to a high level of fat intake and consumption of high-fat food itself is linked to increasing levels of bile acids in the colonic lumen. Following a high-fat, high-sugar, Western-style diet, abnormal high levels of bile acids might be found in the intestine [137, 138]. Patients with higher concentrations of secondary bile acids, DCA and LCA, are more frequently diagnosed with colon cancer [139]. FXR regulates the bile acid concentration within a physiological range, preventing cell cytotoxicity caused by excessive bile acid in ileal enterocytes and in hepatocytes. It has been demonstrated that decreasing FXR activation in the intestine leads to

increasing tumor size and numbers. Increasing level of FXR expression activates expression of tumor suppress gene, therefore be effective in colon and liver cancer treatment [140].

FXR activation has been demonstrated to promote liver repair/regeneration [141] and liver regrowth [142] in response to the increased bile acid stress as it prevents excessive inflammation and bile acid induced liver toxicity after partial hepatectomy or liver injury [143–148] and directly suppressing liver cancer cell proliferation [148, 149]. FXR protects the liver from cancer development and it leads to hepatoprotection and HCC suppression at multiple levels [150] including repressing ROS generation and preventing hepatocyte apoptosis. Besides, elimination of FXR generates high bile acid level, leading to inflammation and an increase in colon cell proliferation and colorectal tumor formation. This points to the protective role of FXR on colon cancer [151, 152].

FXR structure

The FXR protein consists of several functional domains (Figure 2.10). One is the N-terminal DNA binding domain (DBD). It is composed of around 70 amino acids and it contains two zinc finger motifs for DNA binding. Zinc fingers allow the nuclear receptor to bind to DNA elements, known as hormone response elements composed of the sequence AGGTCA [153]. DBD is a highly conserved DNA binding domain and it directs nuclear receptors to specific DNA sequence. Another side is the moderately conserved ligand binding domain (LBD) that is a very complex encoding domain for ligand binding and receptor dimerization [122]. It consists of 250 amino acids and it has a dimerization motif for binding to other nuclear receptors. Generally, FXR binds to corepressors and is inactive in the absence of a ligand, while ligand binding enables coactivators to displace corepressors. The two main domains are connected by flexible hinge region which contains the nuclear localization signal.

A ligand-independent transactivation function-1 (AF-1 sequence) and

ligand-regulated transactivation function-2 (AF-2 sequence, helix 12), are located in the N-terminal and C-terminal domain, respectively. AF-1 has many post-translational modification sites and AF-2 is important for recruitment of transcriptional coactivators.

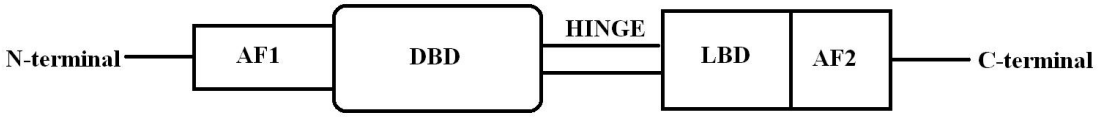

Figure 2.10- The structure of FXR. It includes an NH_2-terminal binding domain and a COOH-terminal binding domain. Each domain contains a transactivation function domain [154].

Until now, two FXR genes known as FXRα and FXRβ are found in mammals. FXRβ is a separate gene in some rodents such as rodents, mice, rabbits and dogs but it is a non-expressed pseudogene in humans [155] and does not function as a bile acid receptor [156]. Its physiological function remains to be established. FXRα is dominantly expressed in the liver and also in kidney and gut. FXRα encodes four FXR isoforms (FXRα1, FXRα2, FXRα3 and FXRα4) because of diverse promoters and alternative splicing in the human or mouse gene. Notably, they differ in their tissue distribution and different FXR isoforms regulate the expression of different target genes *in vitro*. FXRα1 and FXRα2, are mainly expressed in human liver and moderately in ileum and adrenal gland. It has been reported that they can regulate human bile salt export pump (BSEP) [157]. FXRα3 and FXRα4 are abundantly expressed in ileum, moderately in kidney and at low levels in the duodenum and jejunum. It is worth stressing that the term 'FXR' used in this thesis refers to its FXRα isoform.

The main effect of FXR activation is the suppression of bile acid synthesis genes. FXR activation inhibits CYP7A1 gene expression through the hepatic small heterodimer partner (SHP) protein in liver cells. SHP is an atypical

nuclear receptor as it is devoid of DNA binding domain (DBD) but it has high sequence homology [85]. It is a common transcriptional repressor of nuclear receptors and mediates bile acid homeostasis and preventing cholestatic injury. The promoter for SHP gene involves an FXR response element composed of inverted repeats separated by a single base pair. SHP forms a non-functional complex with liver receptor homolog-1 (LRH-1, NR5A2) and up-regulating SHP levels lead to the binding and inhibition of LRH-1 and subsequent decreasing CYP7A1 gene expression as LRH-1 is required for the transcription of CYP7A1 [158–160]. In the absence of LRH-1 activity, the synthesis of bile acids declines.

SHP also blocks the DNA binding activity of several other nuclear receptors via direct protein-protein interactions. One of these nuclear receptor target is hepatocyte nuclear factor 4 (HNF4α, *NR2A1*), a third transcription factor, to inhibit the expression of CYP7A1 [161, 162]. CYP7A1 gene have a binding site for HNF4α. HNF4α is a key regulator of bile acid biosynthesis and conjugation [163] (by inducing the genes encoding BACS and BAAT in the hepatocyte) and contributes to the feedback inhibition of CYP7A1 expression by bile acids. HNF4α is essential for maintaining normal CYP7A1 expression [164] and deficiency of HNF4α leads to significant reduced expression of CYP7A1 [165] and increased bile acid synthesis [166].

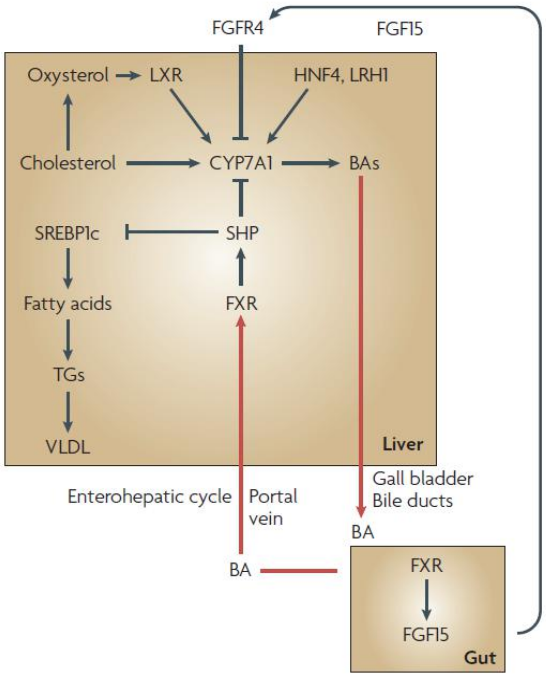

Figure 2.11- Mechanism of regulation of lipid and bile acid homeostasis by bile acids [167]. Bile acid mediated CYP7A1 expression is through several different pathways, (i) hepatic FXR/SHP pathway: bile acid activated FXR induces SHP, which represses HNF4α transcription of CYP7A1 and CYP8B1 gene transcription in hepatocyte; (ii) intestinal FXR/FGF19/FGFR4 pathway: FXR induces FGF-19 in human and FGF-15 in mouse, which is secreted into portal circulation to activate FGFR-4 in hepatocyte via the portal vein. FGFR4 signaling stimulates JNK and ERK1/2 pathways of MAPK signaling to repress CYP7A1 gene transcription. (iii) FXR independent signaling pathways: Conjugated bile acids activate Protein kinase C, which activate the MAPK pathways to inhibit CYP7A1 gene expression.

Given the large number of animal studies conducted, FXR/SHP is not the only pathway involved in bile acid negative feedback regulation [168]. Bile acid synthesis is upregulated and bile acids pool size is increased in FXR deficient mice [169] but bile acid synthesis is still inhibited in SHP deficient mice. Most studies on the feedback inhibition involved in bile acid homeostasis focused only on liver but with little attention paid to the intestine. FXR in the intestine has been proven to contribute significantly to repress bile acid synthesis in the liver [170, 171]. Nevertheless, many reports suggest bile acids can regulate their own biosynthesis via another negative feedback mechanism, FXR/FGF19/FGFR-4 pathway, generally defined as alternative

SHP-1-independent pathway (endocrine pathway) in the regulation of bile acid biosynthesis. In the ileum, FXR activation leads to the upregulation of FGF-19 (fibroblast growth factor 19, synthesized by the ileum epithelial cells) in primary human hepatocytes and FGF-15 (fibroblast growth factor 15, released by the ileal enterocyte) in mouse intestine [172]. FGF-15/19 circulates back to the liver from ileum, functions as a signaling hormone and binds to the hepatic FGFR-4 tyrosine kinase, at the plasma membrane of hepatocytes and other epithelial cells, via the portal vein. The interaction with hepatocyte FGFR-4 requires the assistance of partner membrane-bound glycosiade β-Klotho, a membrane-bound glycosidase and its level is significantly high in the liver. This complex then leads to activation of extracellular JNK1/2 of the MAPK pathway (a second SHP-independent pathway) and subsequent inhibition of both ASBT and CYP7A1 mRNA expression in primary hepatocytes [79, 173–178], and thereby decrease bile acid synthesis [177–179]. Over-expression of a human FGFR-4 represses CYP7A1 gene expression indicating the important role of FGFR-4 signaling in mediating bile acid feedback inhibition. This FXR/FGF19/FGFR-4 pathway may be an important physiological pathway in the regulation of bile acid synthesis. Moreover, FGF-19 relates with the inhibition of hepatic glucose production [180] and lipogenesis [181] and promotion of glycogen synthesis [182].

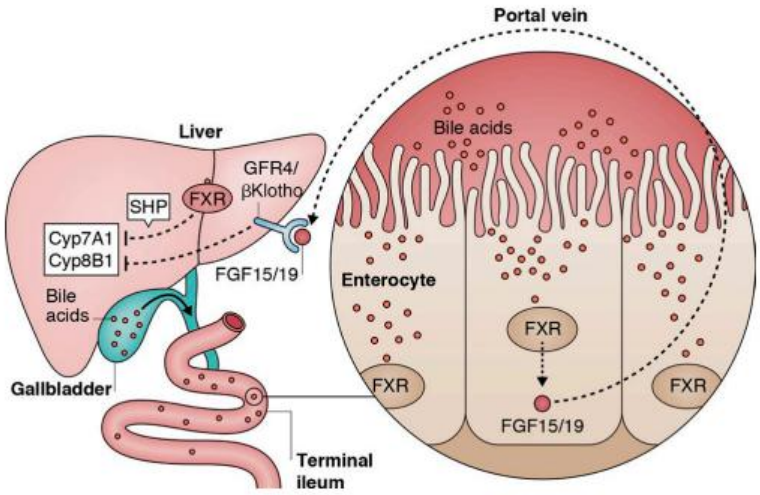

Figure 2.12- Regulation of bile acid synthesis by repression of CYP7A1 gene expression by FXR signaling [183]. This involves the activation of SHP

in liver and release of FGF15/19 in the gut and following binding to FGFR-4, which leads to the reduction of CYP7A1 expression.

FXR/FGF19/FGFR-4 pathway cooperates with SHP to regulate bile acid synthesis [174]. It is likely that the major physiological mechanism for feedback regulation of bile acid synthesis is through bile acid activation of intestinal FXR/FGF-19 signaling to activate hepatic FGFR-4 pathway. When bile acid concentration increases during liver cholestasis, the FXR/SHP pathway can be activated to repress bile acid synthesis. However, the mechanism remains to be further clarified.

In the autocrine pathway, a third pathway, FXR activation by conjugate bile acids activates the MAPK/ERK1/2 pathway to inhibit CYP7A1 transcription. Activation of ERK1/2 by bile acids has been proved to mediate beneficial effects of bile acids and may be involved in cytoprotection from bile acid-induced apoptosis [184] and stimulation of bile formation [185]. This pathway may be an adaptive response to protect liver cells from cholestatic injury. In addition to these, many other signaling pathways exist and they protect against bile acid toxicity during liver diseases by regulating CYP7A1 expression corporately.

In addition to bile acids, hormones and exogenous compounds may affect bile acid synthesis. These include insulin [186] and thyroid hormones [187] by targeting CYP7A1 protein. Insulin down-regulates CYP7A1 enzyme in different animal species and thyroid hormones induce CYP7A1 gene transcription in rats. This is well related to the structure of CYP7A1 and it has been reported that bile acids reduce CYP7A1 mRNA stability via the bile acid response elements located in the 3'-untranslated region [188, 189], which are extremely long and have a short half-life.

To summarize, CYP7A1 contributes to the production of bile acids from cholesterol. Bile acids influence their own production through the FXR. Therefore bile acids have the potential to regulate their own levels through

feedback inhibition via enterohepatic circulation to repress CYP7A1 [190] activities and expression. In addition to CYP7A1, FXR inhibits CYP8B1 and CYP27A1 transcription by complicated mechanisms as well.

Bile acids activate Farnesoid X receptor (FXR) in the ileal enterocytes and hepatocytes. Once activated, FXR translocates to the cell nucleus and forms a FXR-RXR (retinoid X receptor) heterodimer complex. The dimer complex binds to the FXR response element (FXRE), transducing signals and regulating multiple gene expression, involved in bile acid, lipid, glucose and amino acid metabolism. In addition to these, the dimer complex contributes to allosteric conformational changes on the binding site of FXR, which can lead to the dissociation of corepressor and increase the transcriptional effect of FXR by promoting the coactivator binding [191] in an AF-2 dependent way.

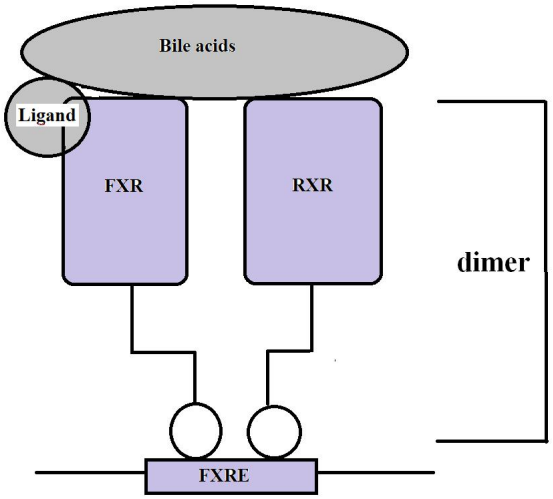

Figure 2.13- FXR regulates multiple genes expression in DNA when activated by BAs [116]. FXR binds with RXR as a heterodimer complex to FXR response elements on DNA (FXREs).

FXR agonists

Based on the great importance of FXR, FXR agonists have been developed and some of them are currently tested in clinical trials for many liver diseases. FXR ligands bind to the C-terminal ligand binding domain (LBD) of the receptor.

Figure 2.14 below shows the different binding modes of FXR ligands to the LBD of FXR receptor. Both bile acid ligands and synthetic ligands bind to the FXR.

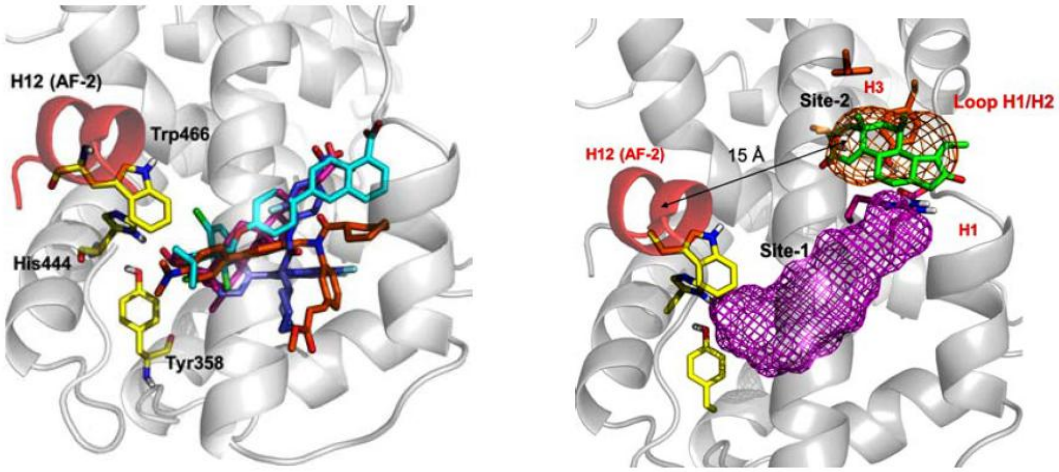

Figure 2.14- Different binding modes of ligands to the LBD of FXR [192]. The left diagram shows the binding of FXR agonist, OCA and synthetic ligands GSK8062 (cyan carbon sticks), fexaramine (orange carbon sticks) and benzimidazole derivative (purple carbon sticks) and the right diagram shows the binding of FXR antagonist, guggulsterone.

FXR can be activated by both free and conjugated bile acids. The bile acid pool of an organism is usually composed of twenty or more different members varying in their ability to activate FXR. Among all the normal existing bile acids, only hydrophobic CDCA is found to bind and significantly activate FXR at physiological concentrations. CDCA is highly effective at suppressing CYP7A1 gene expression and activating FXR function, followed by LCA, DCA and CA. They can also activate FXR, but to a lesser extent than CDCA. Hydrophilic bile acids, such as UDCA and other muricholic acids (MCA), are weak FXR agonists [1116, 193–194]. One of the potential outcomes of this project is a reclassification of the secondary bile acids and their 3-epimers as agonists, inverse agonists or antagonists. Differences in their potency of FXR activation is further complicated by ability of gaining into cells with the aid of appropriate transporters [195] or the relative affinities of the various bile acids for the nuclear receptor.

CDCA has already been recognized as a potent endogenous FXR ligand and acts as an important signaling molecule to regulate bile acid level via the activation of FXR [196–198]. Based on the structure of CDCA, a potent high efficacy FXR agonist was discovered soon after the classification of FXR as a bile acid receptor. 6α-Ethyl-CDCA (6α-ethyl, 23(R)-methyl CDCA, INT-747, obeticholic acid, OCA), developed by Intercept Pharmaceuticals Inc [199, 200], is a semi-synthetic first-in-class FXR agonist and has been shown to have around 100-fold higher agonist effect than CDCA. It is an amiphipathic compound and these physicochemical properties contribute to its recognition by the FXR. The higher affinity to the FXR is because its 6α-ethyl group locates in the hydrophobic cavity, which is not fully filled by bile acids. This provides 6α-ethyl CDCA with additional molecular recognition by FXR [202].

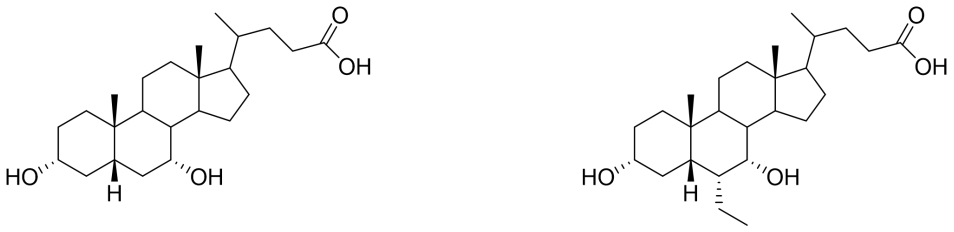

CDCA **6-ECDCA (INT-747)**

Figure 2.15- The effective bile acid ligands for FXR. Left is CDCA and right one is synthesized 6α-ethyl-CDCA (INT-747). INT-747 is more lipophilic than its corresponding natural analogue.

OCA is the first steroidal FXR agonist to be approved as a medicine [203]. So far, it has been approved to treat cholestasis in subjects with PBC [202, 204] approved by the FDA and is in the later stages of clinical development for NAFLD [205] and NASH [206]. It protects the liver against the retention of bile acids and subsequent necrosis and cirrhosis by stimulating bile acid conjugation and secretion from hepatocyte. It has been shown to be safe and the results of Phase II human clinical studies have shown that this compound exerts benefit. OCA improves insulin sensitivity and potentially can be used therefore to treat

patients with type 2 diabetes [205]. It reduces inflammation and fibrosis [207] and its administration was shown to decrease alkaline phosphate levels in patients in a double-blind, placebo-controlled clinical trial. As such OCA was approved on the basis of a marker of disease rather than a clinical endpoint. OCA is the most advanced clinical candidate of a new generation of bile acid based metabolic modulators. This suggests that minor structural modifications could significantly affect their therapeutic effects by interacting with FXR. Although this compound is of great benefit, its use is associated with some side effects. The major limitation of OCA is the high incidence of pruritus and itching happens to around 80% patients with PBC receiving OCA treatment [208–210]. Besides, it leads to increased serum LDL cholesterol and decreased HDL cholesterol [211]. The severity of its side effect restricts the use of OCA in cholestasis and prevents its use in the Phase III and IV PBC patients.

GW4064, an isoxazole derivative, was the first reported synthetic non-steroidal FXR agonist identified by high-throughput screening and combinatorial chemistry [212]. Its EC_{50} is around 90 nM and it exhibits greater efficacy than CDCA. It plays a role as the typical FXR non-steroidal reference compound. It can protect against cholestatic liver damage [213] and cholesterol gallstone diseases [214] and reduce CRC cell proliferation by reducing EGFR pathway activation. GW4064 inhibits CYP7A1 mRNA expression in human hepatocyte and reduces inflammation by inhibiting the transcriptional activity of pro-inflammatory transcriptional nuclear factor (NF-kB) [215] in hepatic and intestinal cells. However, its poor pharmacokinetic property and bioavailability restricts its therapeutic application and precludes its use in clinical trials.

Based on the chemical structure of GW4064, some other synthetic FXR ligands were evaluated, for example, Px-104 [216], cilofexor (GS-9674 derived from GW4064, improves cholestasis and liver injury), imatinib and fexaramine [217]. However, these synthetic non-steroidal FXR ligands all have the disadvantages of poor bioavailability and toxic effect, which restrict their

clinical utility [218, 219].

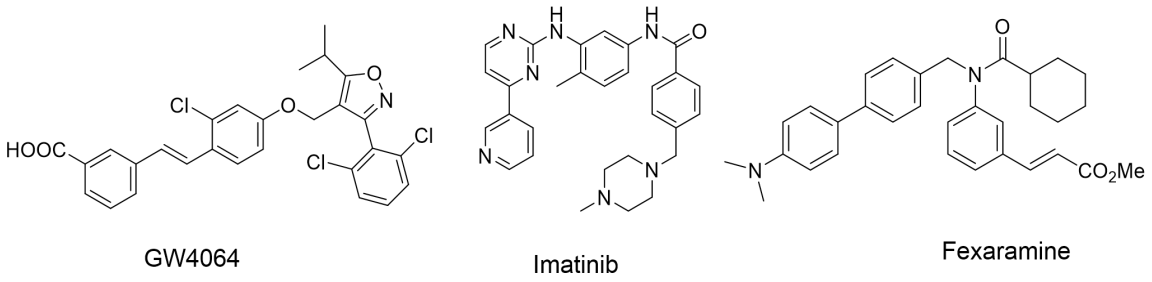

Figure 2.16- Examples of non-steroidal FXR ligands, GW4064 and other synthetic FXR ligands. Imatinib, an approved drug (Gleevec ®), possesses high therapeutic relevance in the treatment of chronic myeloid leukemia. Fexaramine is a promising new class of FXR agonist, exerting strong anti-obesity effect by improved insulin sensitivity.

Although CDCA is a potent FXR ligand, its 7β-epimer, UDCA, does not activate FXR. This is because of the β-oriented hydroxyl group at C-7, altering the optimal balance between the hydrophobic area and hydrophilic region. We now know a lot of the structure activity requirements to activate FXR [220]. Firstly, bile alcohol synthesized from CDCA and CA, activates FXR also. Secondly, 7β-hydroxyl group diminishes their ability in activating FXR. Thirdly, taurine and glycine conjugation has minimal effect on FXR activation [221]. Moreover, introduction of bulky alkyl substitute on 3β or 7β diminishes their ability in FXR activation because of the effect of steric hindrance. Increasing the length of side chain leads to diminished activity.

FXR activation has many interesting therapeutic applications. FXR agonists regulate bile acid, lipid and glucose homeostasis and have anti-inflammatory effects. The most important application is that they can protect the liver against the hepatotoxic accumulation of bile acids that is seen in cholestatic liver disease. FXR activation could also be beneficial to decrease levels of liver and serum triglyceride. Agonists that selectively target intestinal FXR is useful for the treatment of obesity associated diseases [156] and type 2 diabetes. Furthermore, bile acid-mediated FXR activation has shown to be

enteroprotective and leads to the prevention of bacterial overgrowth and epithelial deterioration [222].

FXR antagonists

Activation of FXR leads to complex responses and potentially undesirable side effects, for example, it leads to reduced triglyceride levels in hypertriglyceridemic patients which results in decreased HDL level and accumulation of cholesterol in the body, finally inhibition of bile acid synthesis. In contrast to FXR agonists, FXR antagonists stimulate the conversion of cholesterol into bile acid by increasing CYP7A1 activity and thus promote cholesterol metabolism and reduce the level of total cholesterol. From this point, FXR antagonists might be developed as drug candidates [223] and they may be useful as therapeutic agents for hyperlipidemia and cholestatic disease as well as atherosclerotic heart diseases. Most recent researches indicate that FXR antagonism may have therapeutic effect for the treatment of NAFLD [111].

FXR antagonists bind to the LBD of the nuclear receptor but do not activate it as they do not stabilize AF-2 domain of LBD. Their binding to the FXR prevents transcription, by causing a different positioning of H12 to sterically hinder binding of coactivators. Moreover, by occupying the FXR site, antagonists inhibit receptor activation by agonists. FXR antagonists are normally more sterically hindered and bulkier than FXR agonists. The overall effect of FXR antagonist administration is reduction of FXR signaling and reduced expression of FXR target genes. FXR antagonists are divided into two different types based on their functions, which they can either destabilize the receptor-coactivator complex or stabilize the receptor-corepressor complex [224].

The sterol guggulsterone is the first FXR antagonist reported in the literature based on preliminary pharmacological results [203]. It is the active component

extracted from Indian gugal tree (*Commiphora mukul* [225–227]), a traditional herb widely used in medicine to treat obesity and lipid disorders. It is sold in western countries as a food supplement for decreasing cholesterol levels and preventing the accumulation of cholesterol in the liver. As can be seen from its chemical structure (Figure 2.17), it has two isomers (E and Z). Neither isomer has FXR activity, while they can interfere with CDCA activity. The putative beneficial effect of guggulsterone was attributed to its FXR antagonizing activities and it can repress the FXR activation by CDCA *in vitro*. Surprisingly, it is found to increase endogenous BSEP expression with up to 4- or 5- fold compared with FXR agonists like CDCA and GW4064 [228]. The mechanism of antagonist action of guggulsterone is not clear currently and possibly it does not bind FXR on the LBD. It lacks specificity for FXR but it triggers the activation of other nuclear receptor like PXR. Some studies suggest that guggulsterone inhibits CYP7A1 transcription by activating PXR [229]. PXR interacts with HNF4α and blocks HNF4 interaction with PGC-1α, a transcriptional coactivator regulating the genes involved in energy metabolism, resulting in inhibiting CYP7A1 transcription. However, the use of guggulsterone is very limited because it is non-specific and has very low potency (IC_{50}=12–25 μM) [230].

A sulfated sterol from marine ophiuroids, is also a potent and selective FXR antagonist and it has distinctive structural features. It contains two sulfate groups on C-3’ and C-21’ position and the longer and bulkier side chain with an OH-group at C-26’ position (Figure 2.17). Also, it has rare A/B cis ring junction and negative charge on the side chain. These structural characteristics are linked to its activity as FXR antagonist [231]. This sulfated sterol prevents the recruitment of the transcriptional coactivator complex essential for gene transcription.

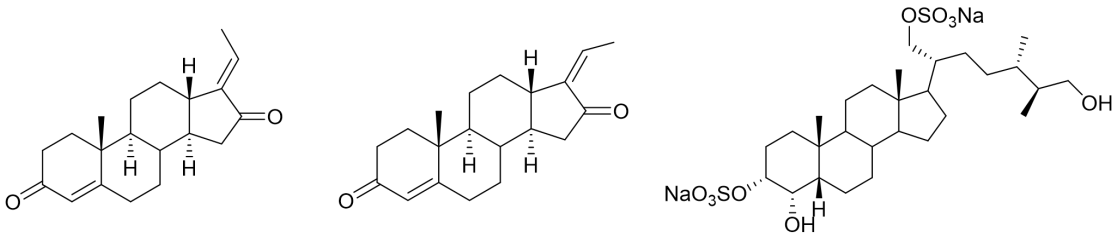

Figure 2.17- The FXR antagonists, two isomers of guggulsterone and sulfated sterol from marine ophiuroids.

Many other FXR antagonists derived from natural products have been found after the identification of guggulsterone. A typical example is stigmasterol acetate, a water-soluble semisynthetic derivative of the main components of soy-derived lipids, stigmasterol. It shows a dose-dependent FXR antagonist effect suppressing CDCA mediated expression of FXR target genes.

TGR5 receptor

The discovery of FXR as the bile acid receptor has significantly facilitated our understanding of bile acid regulation. However, bile acids are also ligands for TGR5 [232, 233]. This is a member of novel transmembrane G-protein coupled receptor (GPCR) family, originally considered an orphan GPCR. TGR5 is the known GPCR for bile acids characterized in 2003. TGR5 is encoded by a single exon gene and on chromosome position 2q35 in humans [234] and a region on mouse chromosome 1c3. TGR5 is widely distributed in different organs and cells with varying degree of expression. It is highly expressed in gallbladder epithelium and lower in liver, intestine and central nervous system [235–238].

A number of synthetic non bile acids agonists have been found for the TGR5 receptor for multiple synthetic agonists [239]. TGR5 is now regarded as a potential drug target for the treatment of many metabolic disorders, such as type 2 diabetes [240], fatty liver disease and also obesity and its activation has effect on inflammation and liver cancer. TGR5 is a key receptor for mediating the effects of bile acids in regulating insulin signaling and energy homeostasis.

The structure of TGR5 gene is composed by 993 base pairs and seven transmembrane domains, three extracellular loops and three intracellular loops (for signal transduction). It has flexible N-terminal and C-terminal [241]. (See Figure 2.18)

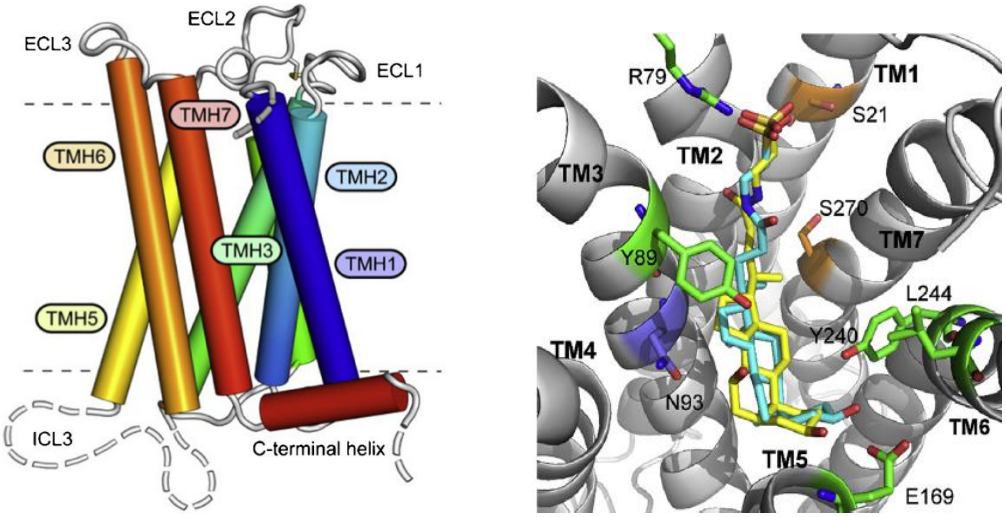

Figure 2.18- The structure of TGR5 receptor [241] and binding modes of ligands to the TGR5 [242].

TGR5 is important in cell signaling pathway. When binding to the ligands in the extracellular space, TGR5 transduces the signal in the extracellular space inside by activating multiple effector pathways. Bile acid binding to TGR5 leads to the activation of the adenyl cyclase cyclic AMP (cAMP) signaling pathways [243]. cAMP is a secondary messenger of intracellular signal transduction for hormones which cannot pass through cell membrane. Activation of cAMP triggers activation of protein kinase A (PKA) and target gene expression [241]. This leads to further signaling and cell response and results in alleviation of obesity and hepatic steatosis [244]. In liver and intestine, TGR5/cAMP signaling represses inflammation by inhibiting nuclear factor NF-κB mediated inflammatory cytokine production [245]. Besides, this reduces bile acid-induced ROS and protects liver against bile acid-induced injury. In metabolic tissues like brown adipose tissues in muscle, cAMP activation by bile acids contributes to the activation of a thyroid hormone-activating enzyme called type 2

iodothyronine deiodinase 2 (D2) and hence increases the production of thyroid hormone T_3, leading to stimulation of energy metabolism and improving glucose tolerance. Furthermore, bile acids boost mitochondria activities and oxidative phosphorylation in human skeletal cells via activation of D2, which relates to a remarkable insulin sensitization [246].

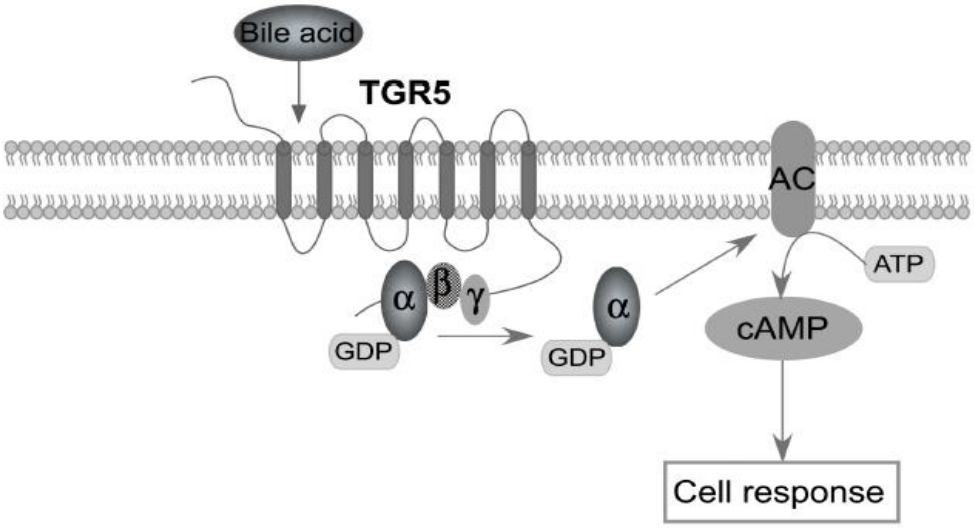

Figure 2.19- The mechanism of TGR5 signaling pathway [247]. The activation of the TGR5 receptor contributes to downstream signaling via cAMP induction. cAMP accumulation is key to the function of TGR5.

FXR and TGR5 dual agonist

Targeting both bile acid receptors could be beneficial in distinct clinical application, and could provide therapeutic effects in the treatment of metabolic diseases such as obesity and Type 2 diabetes. Dual agonists are attractive candidates as a novel therapeutic option in a range of metabolic and liver diseases [216].

A FXR and TGR5 dual agonist derived from human primary bile acid CDCA, called INT-767 (6a-ethyl-3α,7α,23-trihydroxy-24-nor-5β-cholan-23-sulfate sodium salt, Intercept Pharmaceuticals), has been developed. It is a three-fold more potent FXR agonist than OCA. It stimulates intestinal FXR expression and intracellular Ca^{2+} and cAMP activation to induce GLP-1 secretion and improve lipid and glucose metabolism. INT-767 contributes to insulin signaling

and reduces fatty acid synthesis [248]. It has the potential to demonstrate greater efficacy in repressing inflammation and organ damage because of fibrosis and it has raised interest as therapeutic agent for treatment of diabetes, NAFLD and NASH [249–252], two highly prevalent conditions in western countries. Phase 1 clinical development of INT-767 has completed and further clinical trials for the treatment of NASH are on the way.

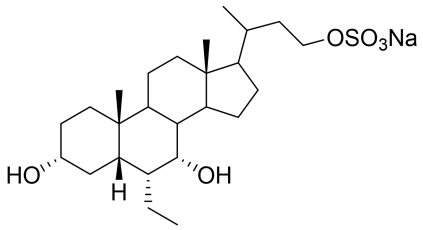

INT-767

Figure 2.22- The structure of FXR/TGR5 dual agonist, INT-767.

This review provides an extensive overview on FXR and TGR5 ligands identified from natural compounds to medicinal chemistry optimization on their endogeneous counterparts. These ligands mainly focus on steroidal scaffolds, including hormones, sharing the structural features with natural bile acids. Bile acid activation of FXR and TGR5 displays the importance of bile acids as signaling molecules with critical paracrine and endocrine functions [253]. They can modulate the immune responses [254] in macrophages, intestine, and hepatocytes and constitute a potent defence mechanism by suppressing NF-κB-mediated proinflammatory cytokine production. Besides, FXR and TGR5 regulate bile acid, lipid, glucose and energy metabolism in the liver and intestine.

Regulation of bile acid signaling pathways mediated by FXR and TGR5 could be considered as novel and attractive targets for drug development. Although a variety of synthetic or natural ligands have been identified already, the discovery of more potent and selective compounds for FXR and TGR5 is ongoing. Several new FXR ligands have been identified and are currently

under clinical trials. The research for TGR5 ligands remains active and some of them will go through the clinical trials process in the near future.

2.1.5 Aims and objectives of present work

The main aim of the work described in this chapter is to describe new synthetic approaches for producing isobile acids to help in the characterization of their effect on cellular toxicity and on bile acid receptor activation. It can be hypothesised that isobile acids can influence FXR responses to endogenous primary bile acids because of their presence in the bowel. We describe work focused on synthetic approaches to isobile acids from 3α-bile acids, and then study in intestinal cell lines for toxicity, lipophilicity and FXR reporter assays for the effect on FXR receptor of the normally occurring bile acids (CDCA, UDCA, DCA, LCA and CA) compared with their synthesized 3β isomers.

In the biological experiments, we investigated their effect on intestinal cell viability, and then we tried to find whether these compounds are able to activate FXR according to FXR reporter assay and recruitment assay. The compounds have been studied for their lipophilicity using experimental approaches and relationship explored between log P value and effect on intestinal cell viability.

2.2 Design and synthesis of different isobile acids

2.2.1 Synthetic discussions

The steroidal ring A contains a hydroxyl group in the C-3’ position with alpha orientation. In the work described here, we have focused on the synthesis of the 3-beta OH isomers of five different bile acids (DCA, CDCA, LCA, UDCA and CA) through reduction of the corresponding 3-oxo derivatives.

CA is taken as a typical example to show the general strategic approach shown in Scheme 2.1. The synthetic route uses the introduction of the acetyl

groups to hydroxyl groups except at position C-3' followed by conversion the 3α-hydroxyl into 3-ketone with PCC. Then the 3β-hydroxyl is obtained via the reduction of keto group. The reducing agents investigated included $NaBH_4$ and L-selectride solution. Finally the synthetic approach includes a necessary deprotection step. Most of the bile acid synthesis follow this approach except LCA which has one hydroxyl group, at C-3' position.

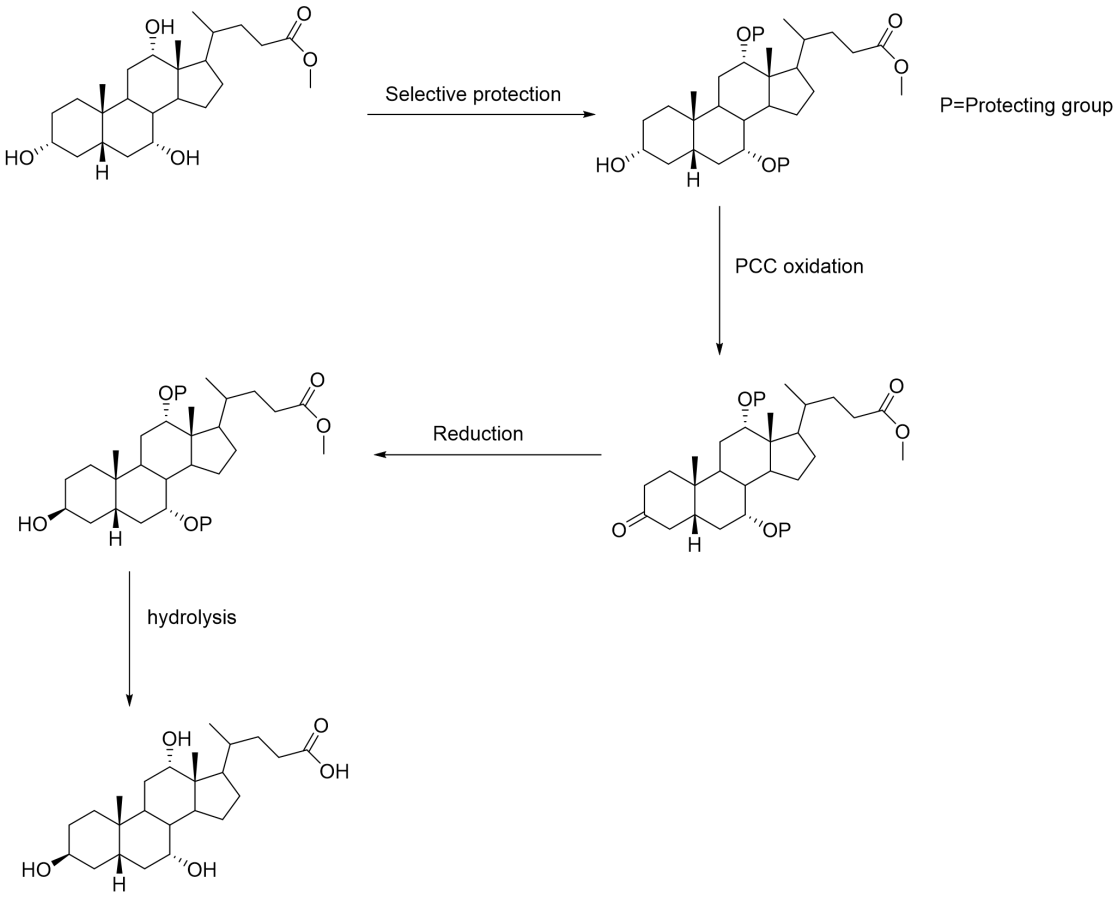

Scheme 2.1- The synthetic route for the synthesis of isoCA.

2.2.2 Protection of bile acids

The first step in the synthetic approach was the selective protection of the 24-carboxylic acid followed by the protection of the secondary hydroxyl groups at position C-3', C-7' and C-12' as appropriate. The synthesis of methyl ester **39** was carried out in MeOH by adding acid catalyst at reflux. After leaving overnight, TLC showed 100% conversion to product. The TLC plate was

developed in hexane: EtOAc= 1:4 with vanillin solution used for detection. After the completion of the reaction, the methyl ester was obtained as white solid in high yield (94%). (Scheme 2.2)

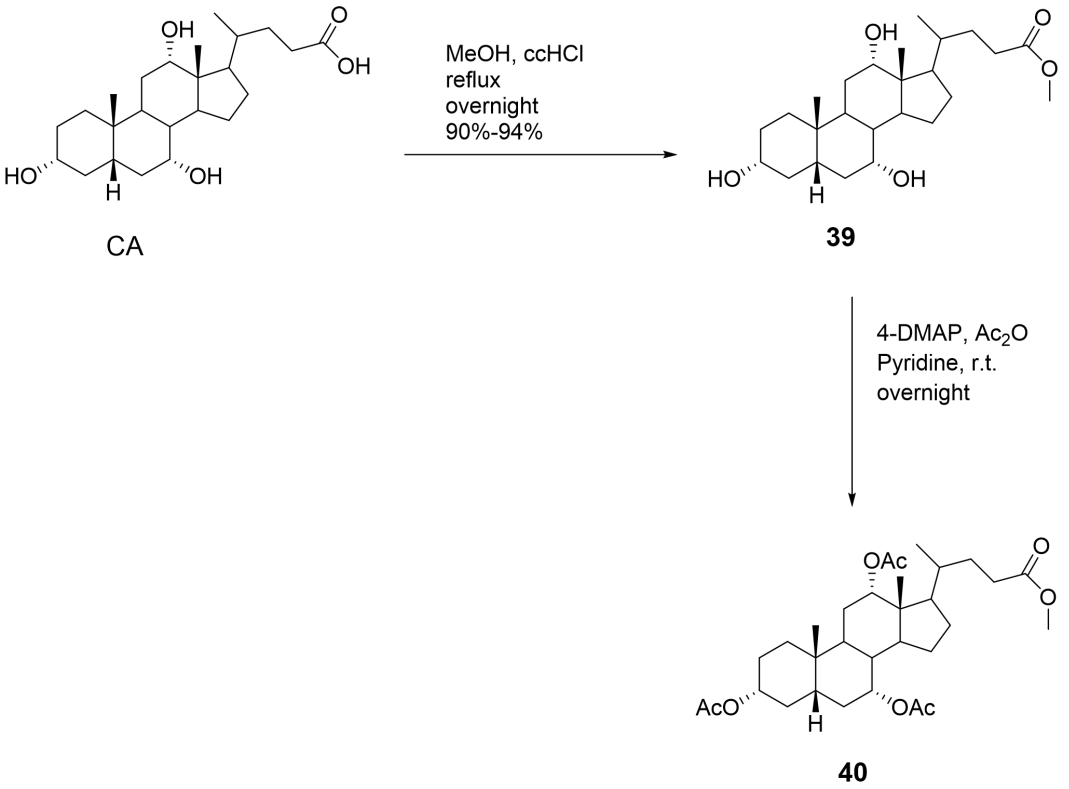

Scheme 2.2- Protection of carboxylic acid group at C-24' and hydroxyl groups at C-3', C-7' and C-12'.

The selective protection of the hydroxyl group at 7' and 12' position is not easily achieved in one step. The 3α-hydroxyl group is more reactive than 7α and 12α hydroxyl groups because 7' and 12' position are more sterically hindered and are axial in the CA case. In the present case, acetylation of all of the hydroxyl groups and then selective deacetylation at 3' position was a better synthetic strategy. The esterification of the 3, 7 and 12-hydroxyl groups was done with acetic anhydride in dry pyridine with the use of 4-DMAP as the catalyst to yield triacetate **40**. The formation of **40** was followed by TLC analysis using hexane: EtOAc=3:1 as the mobile phase. After the reaction was finished, the crude product was purified by flash chromatography to yield product **40** as white foam (88%).

2.2.3. Selective deprotection of bile acids

The selective deacetylation of compound **40** at the acetate group at C-3' position was achieved by dropwise addition of acetyl chloride (AcCl) to excess dry MeOH at cold temperature [255, 256] to produce a small amount of HCl. TLC showed the conversion of the starting material to the desired product **41** (70%) and a small amount of side product 3,7,12-trihydroxyl (**39**), 3,7-dihydroxyl-12-acetyl and 3,12-dihydroxyl-7-acetyl (30%).

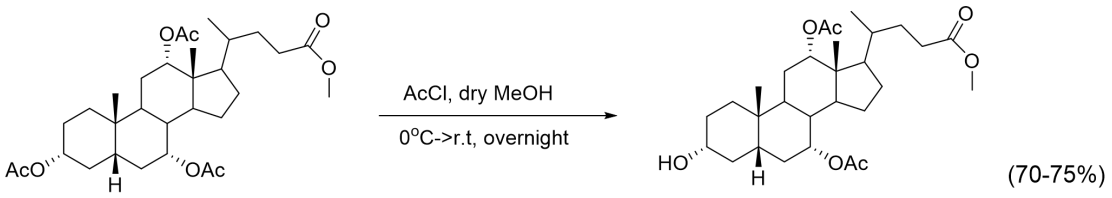

40 **41**

Scheme 2.3- Selective deacetylation of 40 with acetyl chloride in dry MeOH.

2.2.4 Oxidation of protected CA to 7-oxo derivative

Once **41** was obtained, the next stage was to convert 3α-hydroxyl group into 3β-hydroxyl group. It was decided to approach this through the 3-ketone rather than by substitution (direct inversion) since the ketone is potentially itself an interesting compound for biological evaluation. The oxidation of compound **41** with pyridinium chlorochromate (PCC) as introduced by Corey and Suggs in 1976 [257] yielded 3-oxo-7α, 12α-diacetate-5β-cholanoic acid in near 100% yield and the pure ketone could be obtained after the workup. Compound **41** was dissolved in DCM and PCC was added 3 times over an hour at RT with subsequent stirring for 4 h. The TLC showed the full conversion of compound **41**. The TLC plate was developed in hexane: EtOAc= 2:1 with vanillin solution used for detection. After the completion of the reaction, compound **42** was obtained as white solid in high yield (98%–99%).

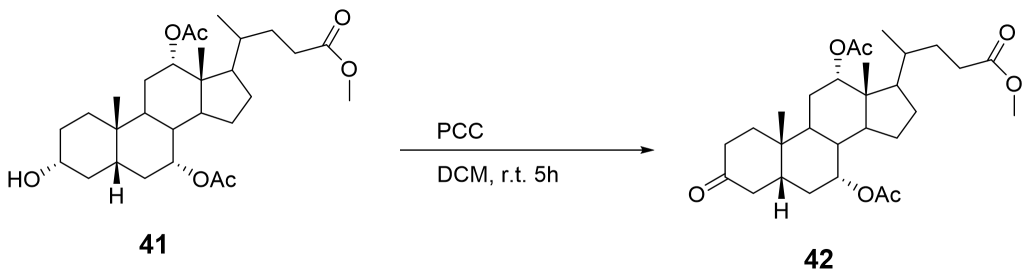

41 42

Scheme 2.4- Oxidation of compound 41 with PCC.

2.2.5 Stereoselective of hydride reduction of 3-oxo bile acids

Many different types of reducing agents have been developed for the conversion of ketones into the corresponding alcohols. Examples include sodium borohydride ($NaBH_4$), lithium aluminium hydride ($LiAlH_4$), sodium metal, catalytic hydrogenation and other more bulky reducing agent like L-selectride and LTSBH etc.

$LiAlH_4$ is an excellent reagent for the reduction of certain polar groups, for example, carboxylic acid, ester, aldehyde and acyl chloride can be reduced to corresponding alcohol. The reductions often proceed at room temperature or below and are usually very rapid and free from side reactions. However, $LiAlH_4$ was not considered in this case as it can reduce the methyl ester into undesired alcohol at C-24' position. Sodium metal reduction has a variety of uses in organic chemistry. It can easily give up a lone electron as sodium metal has a lone electron in its valence shell. It is a quite inexpensive alternative to $LiAlH_4$ reduction of esters to primary alcohol in industrial production. However, in this case, sodium can cause the same problem as $LiAlH_4$ because of its poor selectivity. Catalytic hydrogenation can be another good option for ketone reduction. By far the most common catalyst system applied tends to be palladium on activated carbon under hydrogen (Pd/C in H_2). Unfortunately, experiments showed catalytic hydrogenation was not able to reduce the 3-oxo group at ring A. $NaBH_4$ is a relatively mild and safe alternative as it is a less powerful reducing agent. Also, it is cheap and easy to handle. The use of

$NaBH_4$ as a reducing agent has been known for over 50 years. It can selectively reduce aldehydes, ketones and acid chlorides in protic solvents, but it is not able to reduce esters, carboxylic acid and nitriles. Reduction of the steroidal 3-ketone with $NaBH_4$ was quite feasible. Compound **42** was dissolved in a MeOH-THF mixture at 0^oC and then $NaBH_4$ was added with stirring for 30 min and the reaction was kept under RT overnight. TLC analysis showed the disappearance of starting material and formation of two different isomers the second day. After the work up, the crude product was purified by flash chromatography to give 3β-hydroxyl CA **43** and 3α-hydroxyl CA **41**.

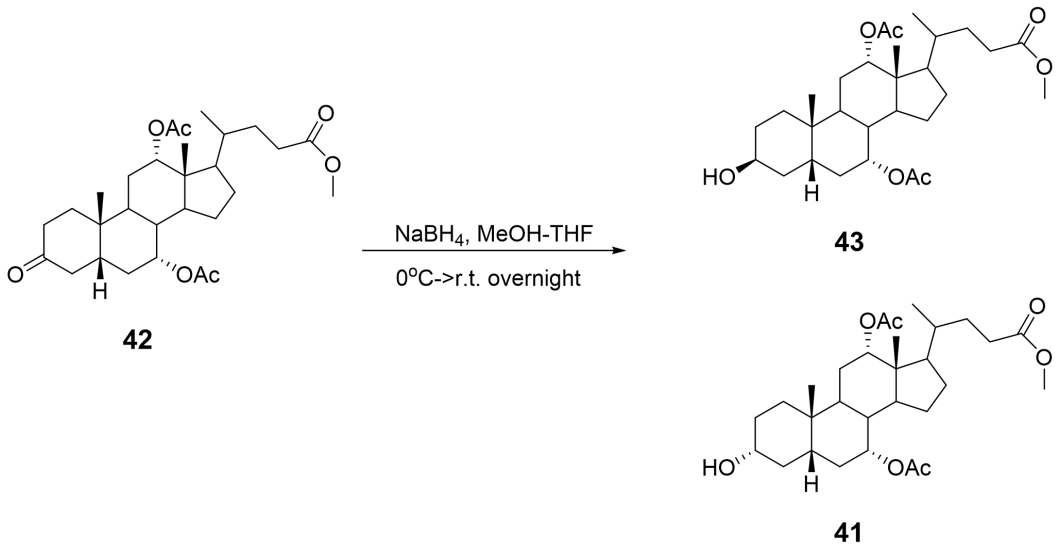

Scheme 2.5- Selective reduction of 42 with $NaBH_4$. This method yielded two different epimers, 3α-OH and 3β-OH, in different amounts.

Borane reagents are good electrophilic reducing agents and they are regarded as Lewis acid type hydrides as the boron is electron deficient. They are widely used in asymmetric reductions because of the mild reaction condition. $NaBH_4$ reacts slowly with MeOH and produces the $B(OCH_3)_4^-$ ions which changes the ratio of two different isomers.

Due to the planarity (chair conformation) of 3-ketone bile acid derivative, the borohydride ion (BH_4^-) may attack the substrate ketone from either side. This

causes both the *cis* and *trans* stereoisomer of the resulting secondary alcohol. We expect the borohydride ion (BH_4^-) approaches to the carbonyl from a less-crowded side (**b**) to yield an axial hydroxyl group which is 3β-hydroxyl group as the exo side of the molecule offers steric hindrance to attack by the BH_4^- nucleophile on the carbonyl carbon.

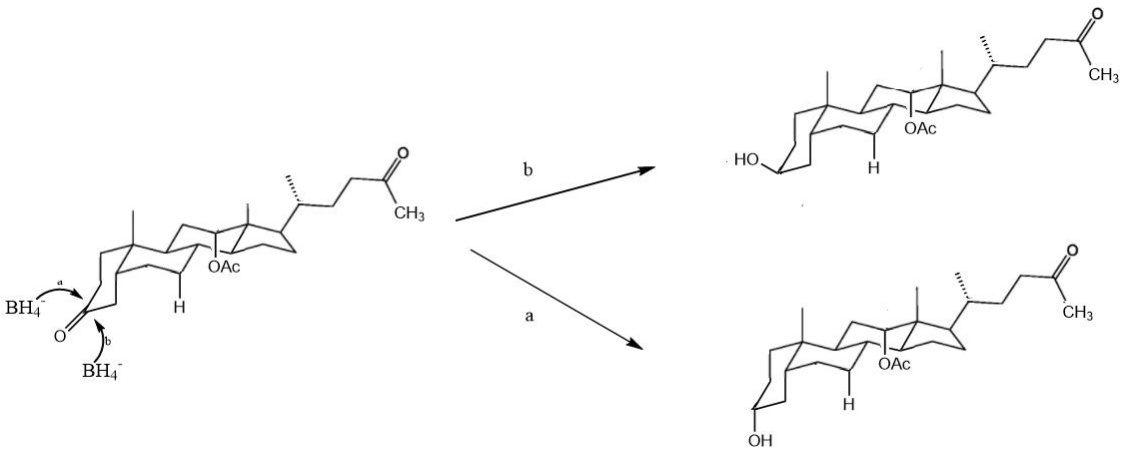

Figure 2.23- Two isomers of the desired product after the $NaBH_4$ reduction of 3-ketones. Isomer **b** is supposed to be the major product as the borohydride ion will approach the ketones from the bottom (endo attack), which is less steric-hindered side. Isomer **a** is supposed to the minor product.

After the crude product was purified by flash chromatography, two spots were separated and the NMR spectrum of each was obtained. The NMR spectra of the upper minor product (a) and the lower major one (b) are shown below in Figure 2.24.

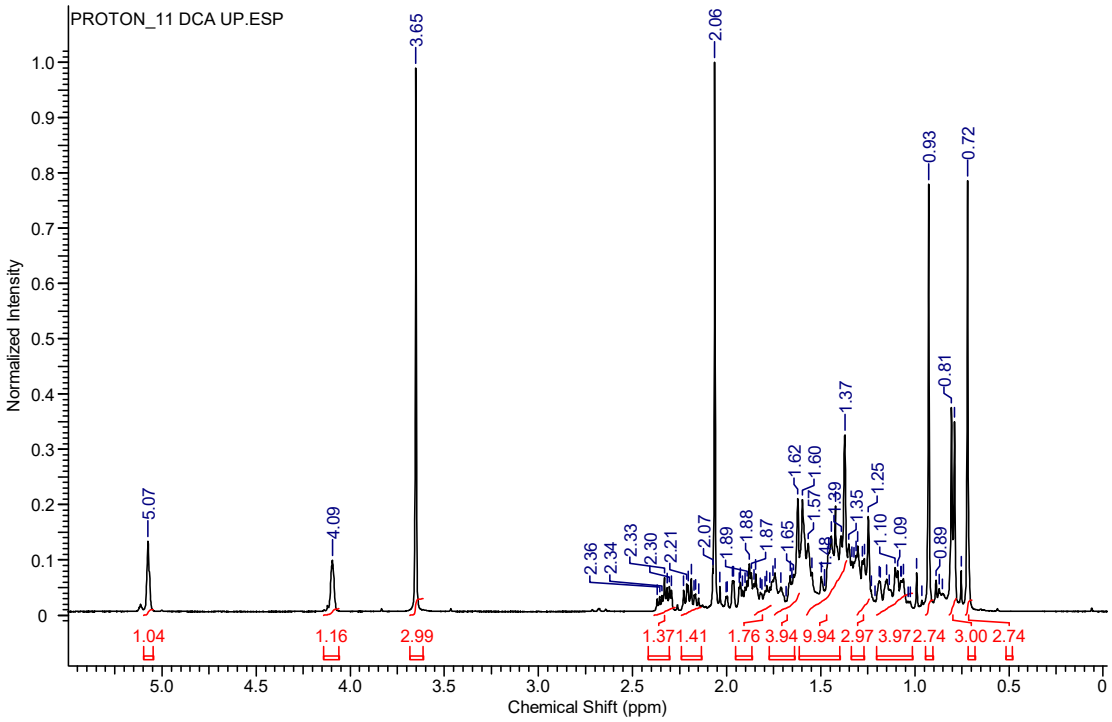

(a)

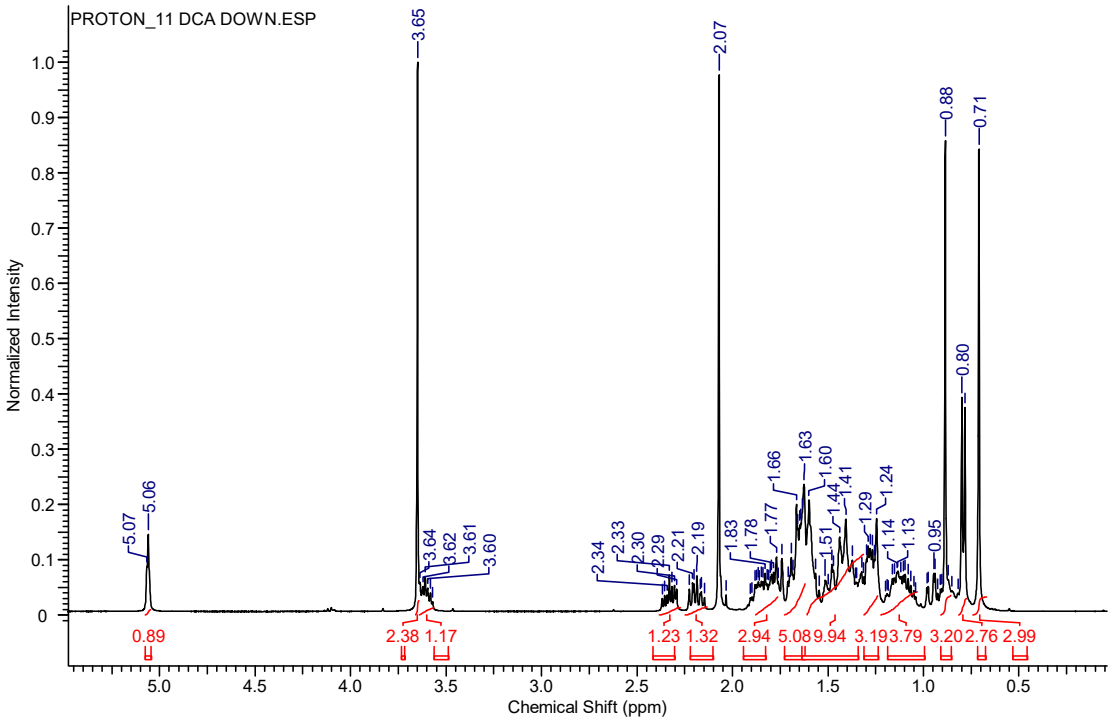

(b)

Figure 2.24- The NMR spectra of the minor spot (a) and the major spot (b) after $NaBH_4$ reduction of 3-keto-12α-acetoxy-5β-cholanoate DCA.

As can be seen from the ^{1}H-NMR spectra above, they show high similarity except there is a broad singlet peak at 4.07 ppm (in Figure 2.24 **a**) and a broad multiplet (triple-triplet) at 3.60 ppm (in Figure 2.24 **b**).

The NMR spectrum of cyclohexanol itself illustrates some common features that can be used to distinguish axial and equatorial protons. The chemical shift of the axial hydrogen is usually upfield of the equatorial hydrogen, by 0.5 ppm [258, 259]. In addition to this, the axial hydrogen shows a broad signal at higher field and equatorial hydrogen shows narrow peak at lower field [260, 261] as the axial-axial *J coupling* constant is large (~10 Hz) while the axial-equatorial and equatorial-equatorial couplings are progressively smaller [262] based on the Karplus equation.

Therefore, it is possible to reach the conclusion that **spectrum a** represents the 3α-H isomer (axial OH) and the **spectrum b** represents the 3β-H isomer (equatorial OH). **Spectrum a** is for 3β-hydroxyl-12α-acetoxy DCA **43** and the **spectrum b** corresponds to 3α-hydroxyl-12α-acetoxy DCA **41**.

In order to illustrate clearly the structural difference between 3α-OH DCA and 3β-OH DCA, the 3D models of these two compounds have been built in MOE and are shown in Figure 2.25. As expected the steroid models are similar with the main difference being the orientations of OH group at C-3'. Hydroxyl groups that are in α-orientation are located below the steroid nucleus and are equatorial to the plane of the A ring. Hydroxyl groups that are in β-orientation are located above the steroid nucleus and are axial to the plane of the steroid nucleus. For the upper diagram, the hydroxyl group at C-3' is directed downwards and the orientation is the same as the hydroxyl group at C-12'. However, for the lower diagram, the hydroxyl group at C-3' directs towards up and the orientation is against the hydroxyl group at C-12'.

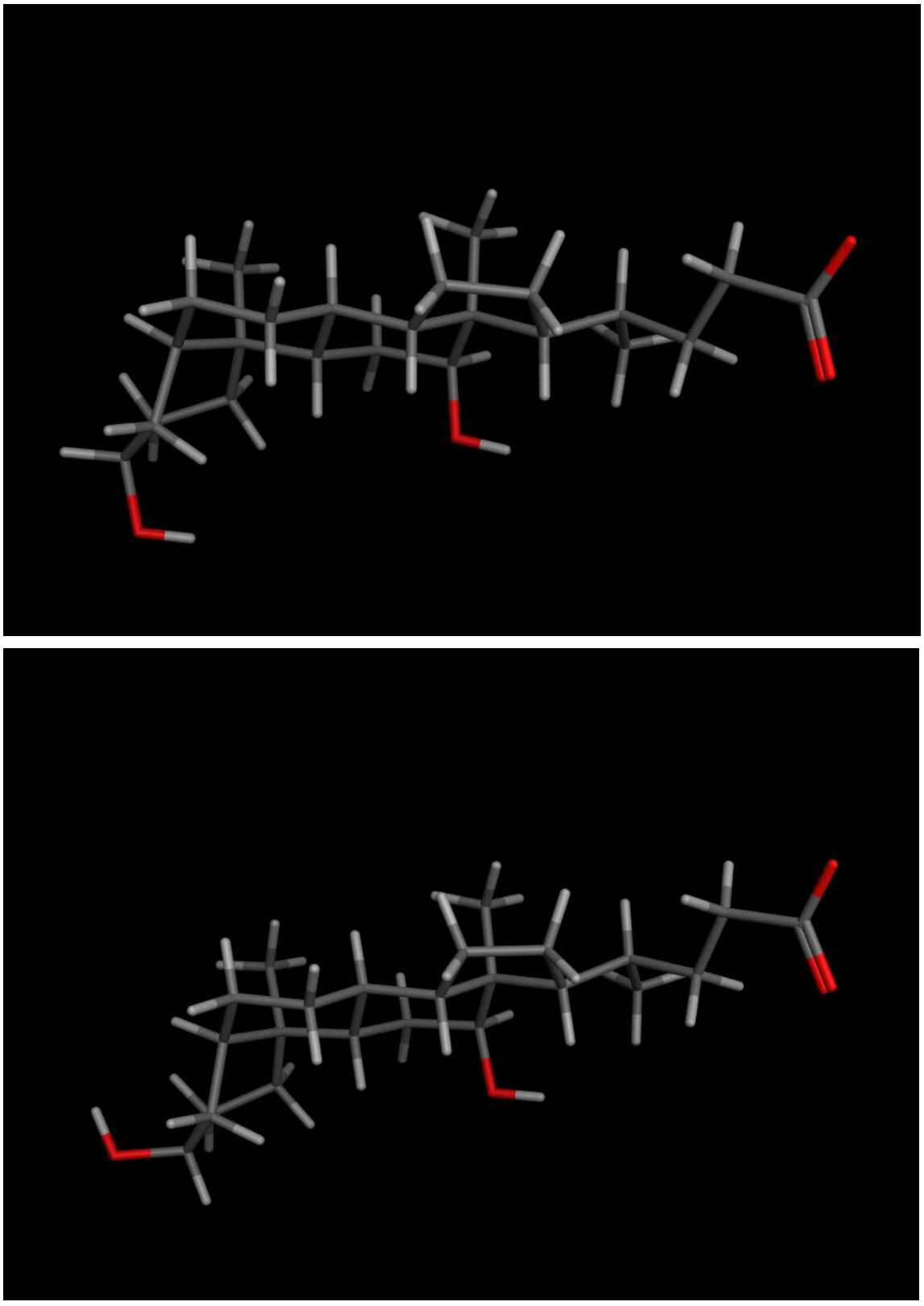

Figure 2.25- The 3D modelling of 3α-OH DCA and 3β-OH DCA. The upper diagram is for the chair conformation of 3α-OH DCA and the lower one is for 3β-OH DCA. The carbon chain is in gray, the hydrogen atoms are in white, and the oxygen atoms are in red.

After determining which peak is associated with which orientation, we can determine the ratio of 3α-H and 3β-H products based on the integration of the corresponding peaks. From the NMR of the mixture of two isomers (Figure 2.26), the integration of 3α-H is 0.49 compared with the integration of 1.47 of 3β-H. This suggests that $NaBH_4$ reduction produces more 3α-OH than 3β-OH and the ratio of 3α-OH to 3β-OH is 3.02:1.

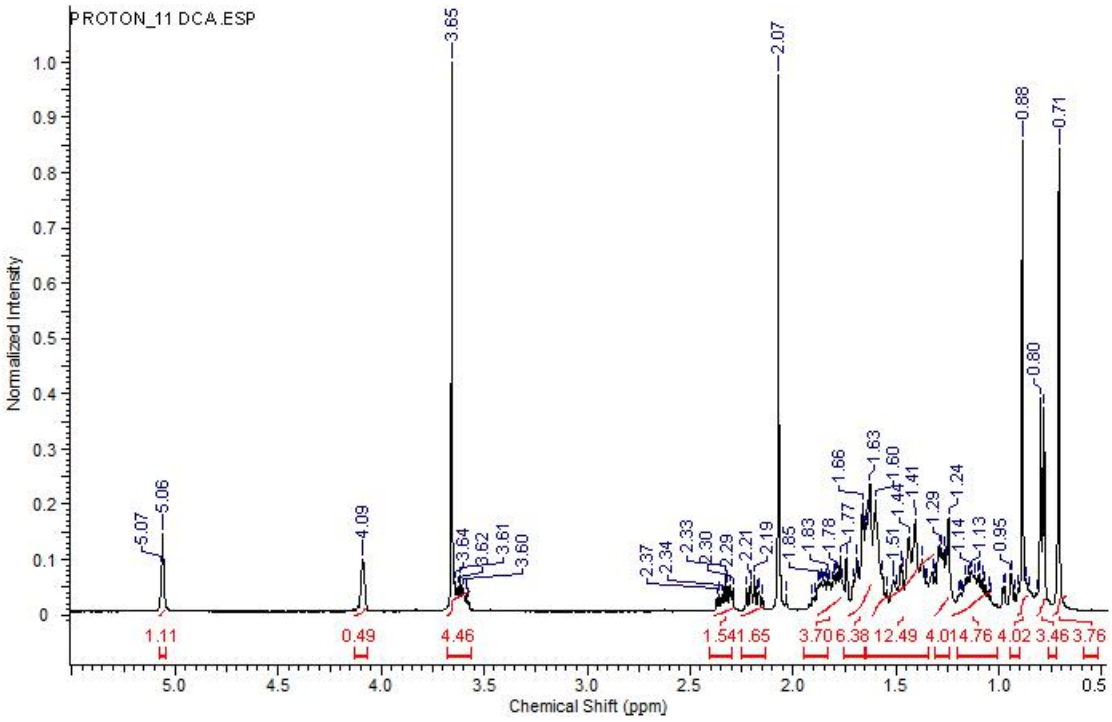

Figure 2.26- The NMR spectrum of the mixture of two different isomers after $NaBH_4$ reduction.

In general the borohydride conditions produced too little of the 3β-OH isomers for our research needs. Moreover, the purification of 3β-OH UDCA was challenging as the two isomers were close together on the TLC. Therefore, an alternative reducing agent was required that achieves greater selectivity.

From the literature, ketones are reduced by hindered boranes like selectrides with high selectivity for axial products [263]. L-selectride is a bulky reducing agent which can give predominately equatorial hydrogens (axial OH). The selective reduction is achieved as the bulkiness of the nucleophilic hydride

reagents favors addition of hydride primarily to one face of the cycloketones. The stereoselective reduction of cyclic ketones with the hindered boranes has been widely exploited in drug synthesis to produce the correct isomers of the desired intermediate [264, 265].

The commonly used reducing agents like $LiAlH_4$ and $NaBH_4$ have been reported to yield products with axial and equatorial hydrogens with the ratio of 90:10 and 85:15 respectively while the hindered borane, Li(s-Bu_3BH) and L-selectride, afford products with equatorial hydrogen as the major product.

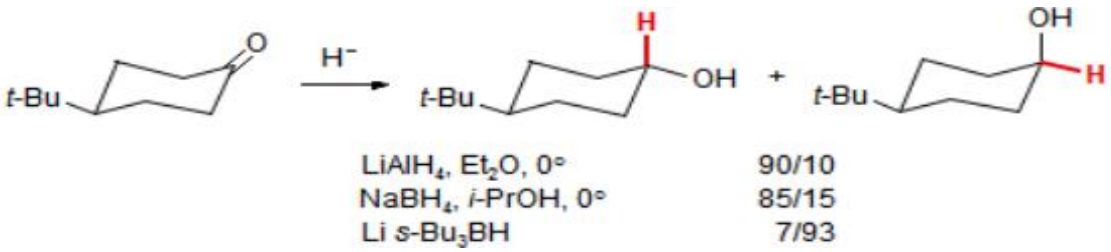

Figure 2.27- The ratio of the axial to equatorial hydrogens after using different reducing agents [265, 266].

The proportion of isomers produced also depends on the size and bulkiness of the solvent. Usually, increasing size and bulkiness results in higher amounts of the axial alcohol [268].

For the L-selectride reduction of 3-oxo bile acid, the reduction of methyl ester into alcohol occurred when the reaction was initially carried out at 0°C. Also, the starting material was not fully converted if only 1 eq. of L-selectride solution was applied. Through several attempts, optimal conditions were identified. Compound **42** was treated with four eq. of L-selectride solution in dry THF at -18°C initially and then the mixture stirred to RT. After being left overnight, TLC analysis showed the existence of both isomers, however, the axial alcohol predominated by TLC.

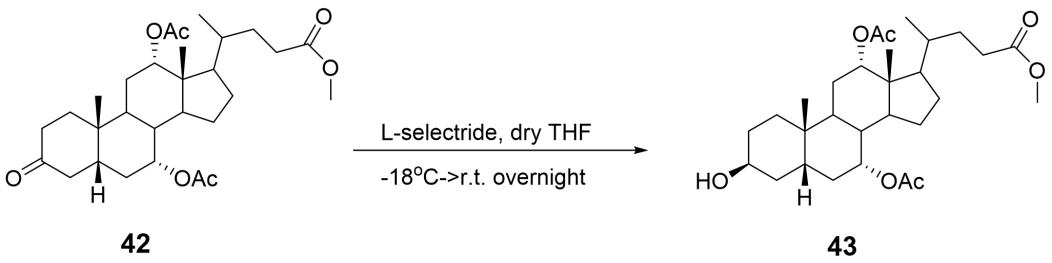

42 **43**

Scheme 2.6- Selective reduction of 42 with L-selectride solution.

As can be seen from the NMR spectrum in Figure 2.28, L-selectride reduction produces ten times more axial product (3β-OH) than equatorial product (3α-OH). This is reflected mainly in the integration for the 3α-H which is 1.03 while the integration for 3β-H is only 0.11 in this case.

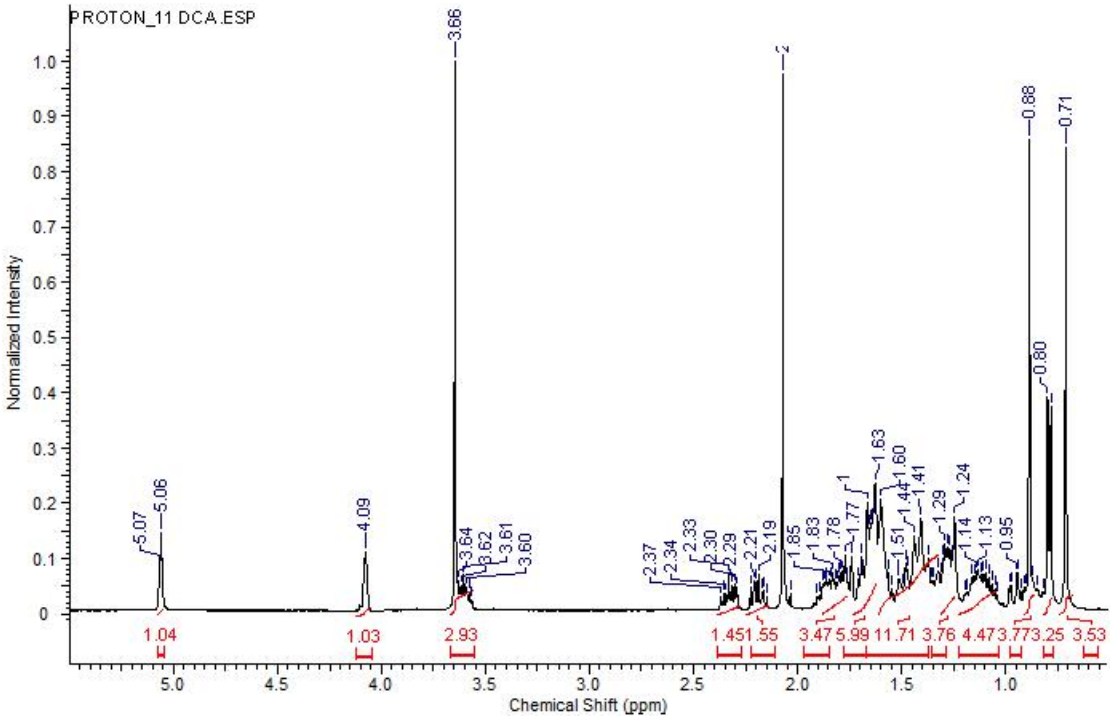

Figure 2.28- The NMR spectrum of the mixture after L-selectride reduction of 3-keto-12α-acetoxy-5β-cholanoate DCA. The ratio of 3β hydrogen to 3α is 1:9.36.

Overall, $NaBH_4$ predominately attacks from the axial side to yield equatorial alcohol products (3α-OH) while sterically bulky species such as L-selectride generate axial alcohol (3β-OH) by equatorial attack on the ketone. This was

surprising to us because the axial attack was expected to be more sterically hindered, instead, control may arise because of the bulk of the intermediate in the reduction process rather than from influences on the hydride approach.

The preferential equatorial attack by the bulky nucleophiles is due to a steric interference via axial interaction from the axial side and the axial attack by small nucleophiles is due to an electronic effect. The axial attack of the hydride on the 3-oxo contributes to the stabilization of the transition state by delocalizing the electron density from the hydride itself to the anti-bonding orbital of the anti-vicinal CH bonds.

Based on the success with the L-selectride, the same synthetic approach was carried out for reduction of other 3-oxo bile acid intermediates. Production of the relevant ketones in each case is not shown here but it followed broadly the approach already shown and it was of course simplest for LCA because this has only one secondary alcohol. The results of these experiments are summarized in Table 2.1 which shows the ratio of 3α-OH to 3β-OH after both $NaBH_4$ reduction and L-selectride reduction. The data show that across the range of bile acid ketones, $NaBH_4$ reduction produces more 3α-OH and L-selectride reduction mainly leads to the 3β-OH.

Table 2.1- The ratio of two different epimers for five different kinds of bile acids after $NaBH_4$ reduction or L-selectride reduction.

The ratio of 3α-OH:3β-OH	$NaBH_4$	L-selectride
DCA	3.02 : 1	1 : 9.36
CDCA	6.84 : 1	1 : 9.29
UDCA	5.30 : 1	1 : 11.4
LCA	3.82 : 1	1 : 8.92
CA	3.00 : 1	1 : 10.3

In conclusion, these two reducing agents have two different possible ways of delivering the hydride to the keto group. Reduction of 3-keto compounds with

$NaBH_4$ usually yields bile acids with an equatorial hydroxyl group (3α-OH) while L-selectride produces predominately bile acids with an axial hydroxyl group (3β-OH). The observed preferential addition of bulky reagents to the equatorial side is generally attributed to steric factors that the axial side is more hindered than equatorial side due to the 1, 3-diaxial interactions with the incoming nucleophile on the cyclohexane ring [269, 270].

2.2.6 Hydrolysis of 43

Compound **43** was treated with 2M aq. NaOH solution under reflux condition for 24 h. After the workup, compound **44** was obtained as a white solid in high yield (99%). A similar approach was adopted to the other epimeric bile acids that were esterified at C24.

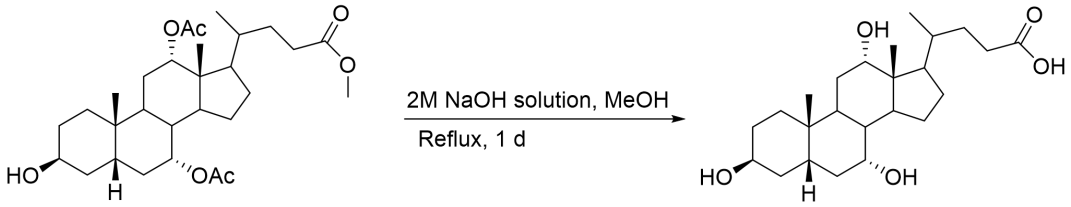

43 **44**

Scheme 2.7- Hydrolysis of 43 with NaOH/MeOH under reflux condition for 24 h.

2.3 Cytotoxicity of the isobile acids in Caco-2 cell line

In order to study the relative toxicity of the beta and alpha epimers, we used the MTT assay (3-(4, 5-dimethylthiazol-2-yl)-2, 5-diphenyltetrazolium bromide) to determine their effect on cell viability of the Caco-2 cell line which is derived from the colonic epithelium. The MTT shows the extent of mitochondrial activity in the cell population following the treatment interval and removal of detached cells. Substances that cause detachment reduce the apparent viability without causing toxicity. Meanwhile substances that are cytostatic or

able to interfere in mitochondrial activity can reduce MTT values without causing overt toxicity. The application of the MTT approach here is in the context of many studies carefully characterizing the effects of bile acids in the relevant concentration range. Bile acids induce cell death in the range 50 μM–1 mM through a combination of extrinsic and intrinsic pathways, the activation mechanism of which remains unclear. We studied cell viability effects using the Caco-2 cell line which is from the colonic epithelium because we wanted to understand the relative toxicity under (patho) physiological conditions where isobile acids are produced and occasionally reach 300 μM [79]. Stock solutions of the different bile acid epimers were prepared in dimethyl sulfoxide (DMSO) and these were diluted to 100 μM with supplement free medium. The % cell viability was measured after incubating for 24 h and it was calculated versus vehicle treated control, which was treated with same amount of DMSO (1%). Each experiment was carried out in triplicate and repeated three times to get nine data points in total for each bile acid solution. The data are presented in Figure 2.29.

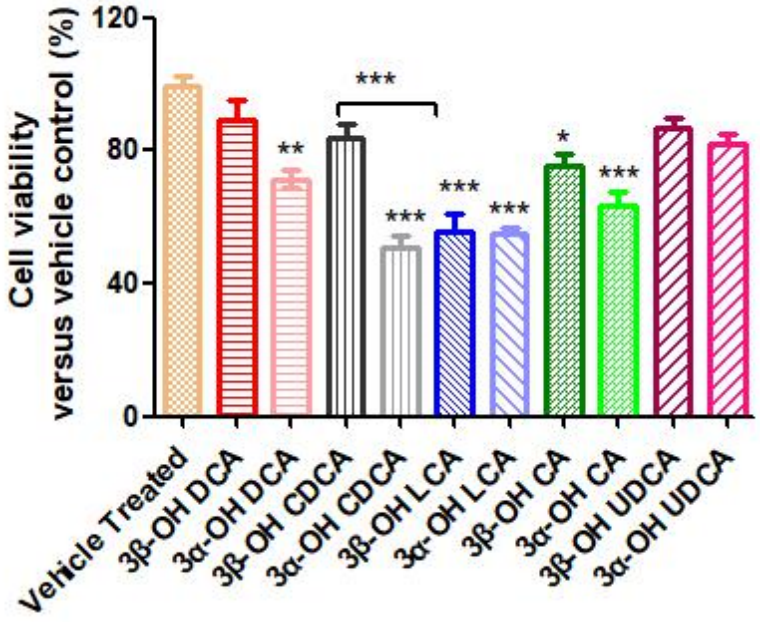

Figure 2.29- A measurement of toxicity of epimeric bile acid pairs. Caco-2 cells were seeded onto 96 well plates at a density of 1×10^5 cells/ml, and then

treated with 100 μM bile acids solution for 24 h. Cells were then treated with 10 μL of 2.5 mg/ml MTT reagent and incubated for 2 h. The assay was normalised to 1% DMSO vehicle control and absorbance of each well was read on a VERSAmax Microplate Reader (Molecular Devices, Sunnyvale, CA, USA) at a wavelength of 570 nm. Values are expressed as mean ± SEM of three triplicate experiments, * $p<0.05$, ** $p<0.01$, *** $p<0.001$ as determined by one way ANOVA with Dunnett's post-hoc correction.

Among the more commonly occurring 3α- bile acids, CDCA was found to be the most toxic, followed by LCA, CA and DCA. UDCA was least toxic and this is as expected from many studies on the relative toxicity of the bile acids. UDCA is used in medicine and is generally regarded as a non-toxic bile acid but it is toxic at higher concentration. In general, the beta compounds or isobile acids were less toxic than the alpha compounds, with greatest difference in the cases of CDCA and DCA. In the case of LCA was there no difference in the toxicity of the epimeric pairs, which indicates that conformation of the hydroxyl group in the monohydroxylated bile acid had a smaller effect. The significance of this may relate to physicochemical properties as described below. The primary bile acid CDCA (3α-OH) was highly toxic to the cells at 100 μM whereas its 3β-epimer CDCA had little effect. Overall, the data are consistent with reports that epimerization of the bile acids by the colonic microflora may reduce toxicity to the colonic epithelium [271]. This may be related to the fact that 3β-OH bile acids are more hydrophilic or have higher CMC than their 3α-counterparts.

2.4 Physicochemical characterization and relation to cellular toxicity

A relationship between lipophilicity and toxicity of bile acids has been considered to exist for quite a long time based mainly on the contrasting behaviour of LCA, DCA and CDCA and more polar di- and tri-hydroxyl bile acids such as UDCA and CA. RPTLC has been used widely for lipophilicity determination for bile acids [272, 273]. It was interesting to see if there was a

correlation between cytotoxicity of the beta compounds and their relative lipophilicity.

2.4.1 Reverse phase thin layer chromatography (RPTLC)

The hydrophobicity (or lipophilicity) is related to the tendency of non-polar molecules to form aggregates in order to reduce the surface contact with polar molecules [274]. Lipophilicity is an important characteristic for any potential drug candidate because it is essential in drug interactions with biological membranes and influences cell permeability, absorption, uptake, distribution, metabolism and in the bile acids, toxicity [275, 276]. It is also influential in pharmacodynamic and pharmacokinetic aspects of drug action. Therefore, accurate and efficient lipophilicity measurement approaches are relevant the design of drugs are selection of clinical candidates. Lipophilicity itself is typically conveyed in terms of a partition coefficient log P, the logarithmic scale of the concentration ratio of the solute at equilibrium between two immiscible solvents, one aqueous, and the other organic, typically, 1-octanol [277], a model introduced by Hansch and Leo. A negative value for log P means the compound has higher affinity for the aqueous phase and a positive value for log P indicates a higher concentration in the lipid phase.

Defining the degree of lipophilicity of bile acids is of current interest in structure-activity relationship studies since few systematic accurate data are available and are limited to only some types of bile acids. Hydrophobicity data indirectly determined chromatographically using C-18 stationary phase are often in good agreement with partition coefficients determined by static methods. The n-octanol/water system is the most widely used in the determination of log P and can offer accurate predictions of activity in complex biological system. However, it has some disadvantages including poor reproducibility, it is time consuming and requires large amount of reagents. For poorly soluble and UV transparent solutes like the bile acids, nonconventional

detection methods are required. Our lab has found RPTLC is to be a useful method for estimating relative lipophilicity of various bile acid series [278] because the bile acids can be derivatised on the plate after development overcoming the detection issue.

In the present work, the experimental retention parameter R_M values for a series of bile acids and isobile acids were calculated by RPTLC based on the R_f value at three different mobile phase compositions in methanol-water.

The correlation is defined by the following equation by Smith and Westall [279]:

$$R_M = \log\left(\frac{1}{R_f} - 1\right), \quad (1)$$

where R_f is the retardation factor.

The R_M values were determined under three different solvent systems (MeOH: water=7:3, 8:2 and 9:1) for each bile acid compound. They were linearly dependent on the concentration of organic modifier in the mobile phase, with correlation coefficient $r^2 \geq 0.99$. The R_f values were obtained in triplicate and average value is taken for determination of R_M value.

The R_{MW} value for each solute is the theoretical R_M value at 0% MeOH modifier and this value is obtained when extrapolating from the calibration curve to the zero percent of MeOH in each case (extrapolated value). This is in accordance with equation given below:

$$R_M = -S\omega + R_{MW} \quad (2)$$

where ω is the concentration of MeOH, S is the slope of the line determining how R_{MW} value be linear to the change of the concentration of MeOH [280]. The negative value of the slope in this equation suggests an increment in the migration of compounds per unit of increase in the content of the organic solvent. The highest values of the slope indicates the compounds that are

most susceptible to the change of the content of organic solvent in the mobile phase.

The log P value of test substances is determined from the calibration graph made from the log P of three reference compounds and their corresponding R_{MW} value [281].

2.4.2 Estimation of log P

As commented, log P is used to understand and predict the behavior of drug substances in the body with respect to transport and disposition. It also has influence on formulation, dosing and toxicity of drugs.

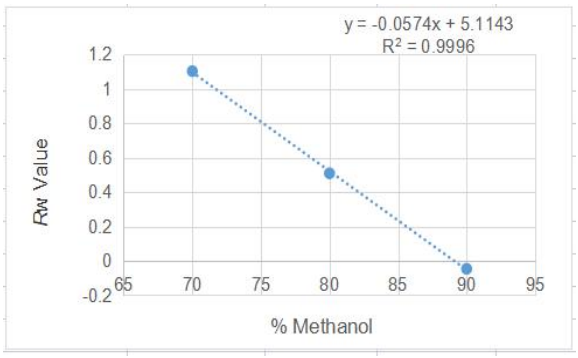

3β-OH DCA

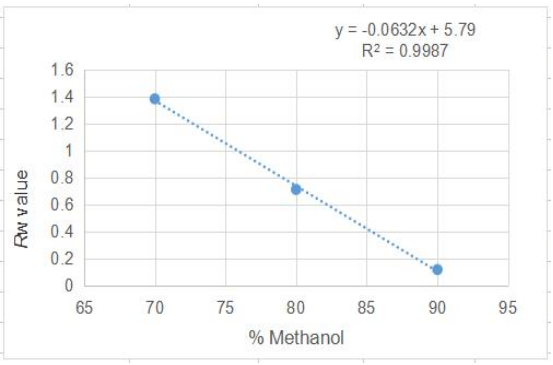

3α-OH DCA

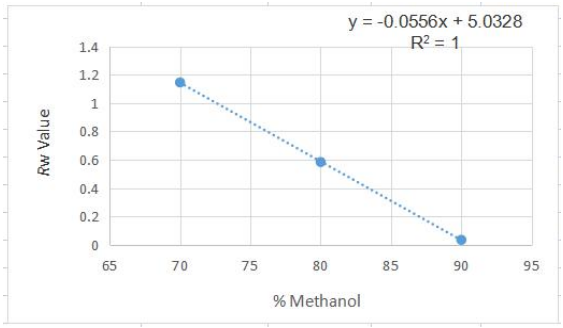

3β-OH CDCA

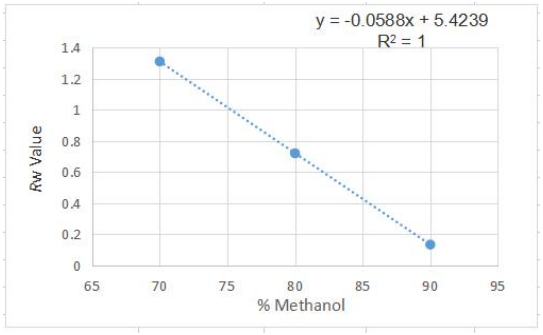

3α-OH CDCA

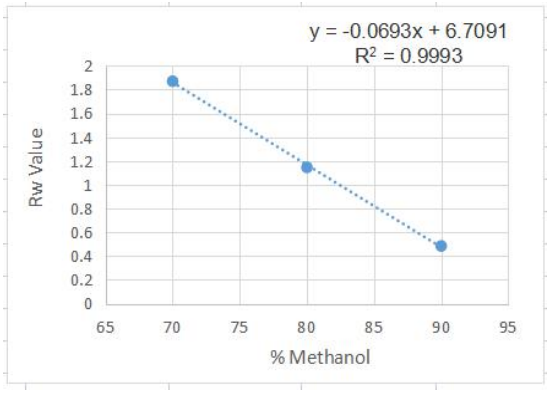

3β-OH LCA

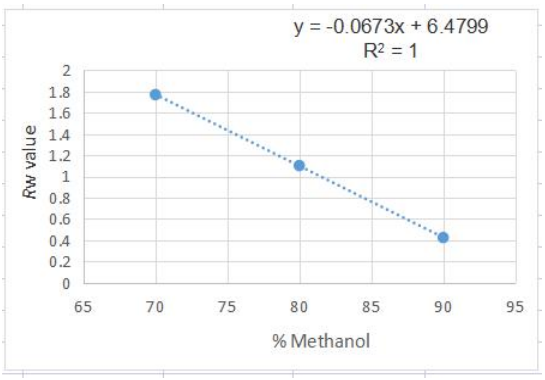

3α-OH LCA

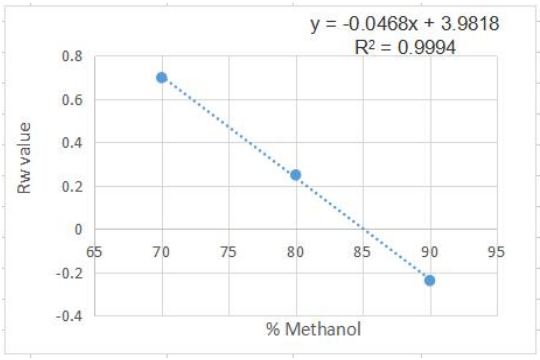

3β-OH CA

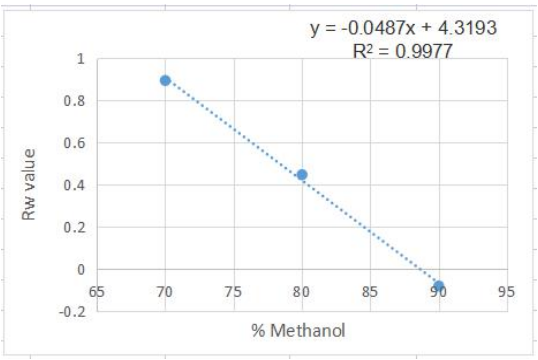

3α-OH CA

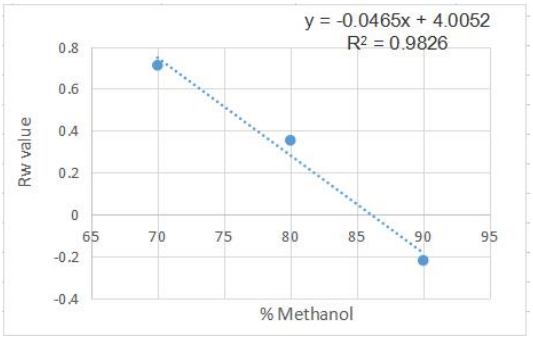

3β-OH UDCA

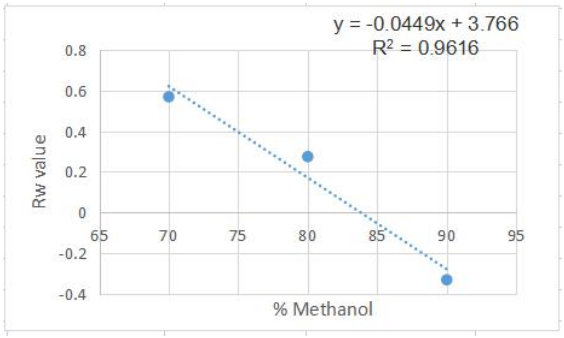

3α-OH UDCA

Figure 2.30- The linear regression curve between calculated R*m* value (Y axial) and the concentration of MeOH, 70%, 80% and 90% (X axial). The experimental R_M values for a series of (iso)bile acids were calculated based on equation (1) by knowing the R_f value for each spot on the RFTLC plate at three different mobile phase compositions. R_f of each (iso)bile acid was measured in triplicates. The R_{MW} for each (iso)bile acid is the slope of the equation (2).

The log P values of all the isobile acids were predicted based on the calibration equation of the log P value of three reference compounds and their R_{MW}. To

ensure reliable regression performance, reference compounds were selected with an optimal range of log P. Reference compounds with their corresponding log P are given below in Figure 2.31 (reference log P for DCA, CDCA and UDCA is 3.50, 3.28 and 3.00, respectively [403]).

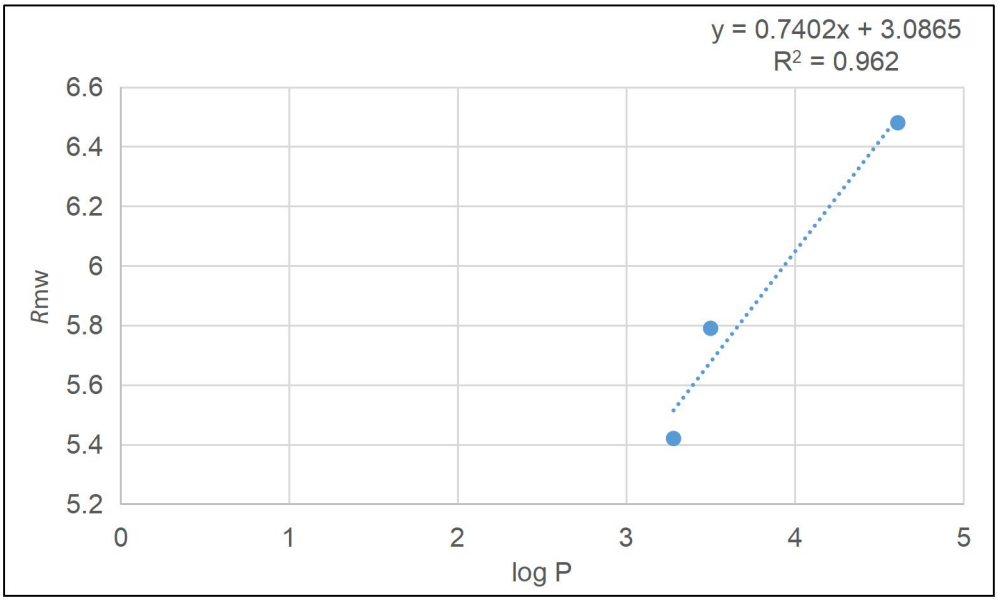

(A)

Compound	R_{MW}	log P (reference)	log P (measured)
3β-OH DCA	5.11		3.55
3α-OH DCA	5.79	3.50	4.00
3β-OH CDCA	5.03		3.50
3α-OH CDCA	5.42	3.28	3.76
3β-OH LCA	6.71		4.61
3α-OH LCA	6.48		4.46
3β-OH CA	3.98		2.80
3α-OH CA	4.32		3.02
3β-OH UDCA	4.01		2.82
3α-OH UDCA	3.77	3.00	2.66

(B)

Figure 2.31- Panel (A) is the calibration curve between log P of three reference bile acids and their corresponding calculated R_{MW}. Panel (B) is

the measured log P values of all bile acids based on the calibration equation. A standard equation for log P estimation of isobile acids was made based on published/reference log P of three bile acids (X axial) and their R_{MW} (Y axial). The log P of isobile acids was predicted by plotting their R_{MW} into the calibration equation.

The measured log P was not well correlated to the reference log P for some 3α bile acids. The distinctions may be explained by the poor retention behavior of some investigated bile acids on the RPTLC plate that their R_f was too low to be exactly determined (e.g. LCA and isoLCA) with high concentration of the organic modifier in the mobile phase.

2.4.3 Relationship between hydrophobicity and cell viability of Caco-2 cells

Many descriptors correlate with lipophilicity including hydrophobic surface area (HSA), molecular length, and solubility parameter etc [282]. Besides, the stronger intermolecular interactions (such as hydrogen bonding) between molecules and the mobile phase are, the analytes are less retained on the stationary phase and lower log P values are obtained.

Table 2.2 below summarizes the data obtained from RPTLC and the MTT assay. Combined with cell viability data, we aimed to characterise the relationship between hydrophobicity of each compound and cell viability reduction on Caco-2 cell line.

Table 2.2- Data obtained in the RPTLC and cell viability assay on Caco-2 cells. HSA was obtained from MOE software. HSA is a sum of predicted hydrophobic areas covering the surface of the molecule. Higher HSA correlates with size and hydrophilicity which correlates with increased retention in RP chromatography and higher log P. Cell viability was obtained from MTT assay on Caco-2 cells following treatment with test article at 100 μM for 24 h.

Bile acids	Hydrophobic Surface Area （HSA）	Calculated log P	R_{mw}	Cell Viability % (n=4) Mean (SD)
3β DCA	450.0706	3.55	5.11	85.4 (10.3)
3α DCA	451.0107	4.00	5.79	71.4 (4.88)
3β CDCA	454.9651	3.50	5.03	83.8 (7.13)
3α CDCA	455.5151	3.76	5.42	50.6 (6.33)
3β LCA	475.58	4.61	6.71	55.4 (9.83)
3α LCA	474.3065	4.46	6.48	55.0 (2.75)
3β CA	426.7597	2.80	3.98	75.5 (6.30)
3α CA	427.7419	3.02	4.32	63.5 (5.42)
3β UDCA	449.7198	2.82	4.01	86.9 (4.65)
3α UDCA	450.1681	2.66	3.77	82.0 (4.71)

The in silico measure of HSA of the beta isomers was in general lower than the HSA of the alpha isomers consistent with their lower R_{MW} and greater polarity.

The number, position, and orientation of hydroxyl groups in a bile acid influences the hydrophobicity [283]: The hydrophobicity of bile acids is inversely proportional to the number of hydroxyl groups on the cholane scaffold and incorporation of polar hydroxyl groups reduce hydrophobicity. Thus, the higher number of hydroxyl groups of the bile acid molecules accounts for decreasing hydrophobicity and smaller HSA. LCA is the most hydrophobic and CA is the least hydrophobic and other bile acids, DCA and CDCA, are in between. UDCA departs from this trend because of its 7β-orientated hydroxyl group.

Bile acid molecules have two different types of surfaces, the convex surface (β) and concave surface (α). The convex surface (β) is non-polar, and hydrophobic whereas the concave surface (α) tend to be hydrophilic to an extent determined by the pattern of substitution. Hence the hydrophilic groups in bile acids are arranged in the concave α-side of the steroidal rings, whereas the hydrophobic domains are aligned towards the convex β-sides [284].

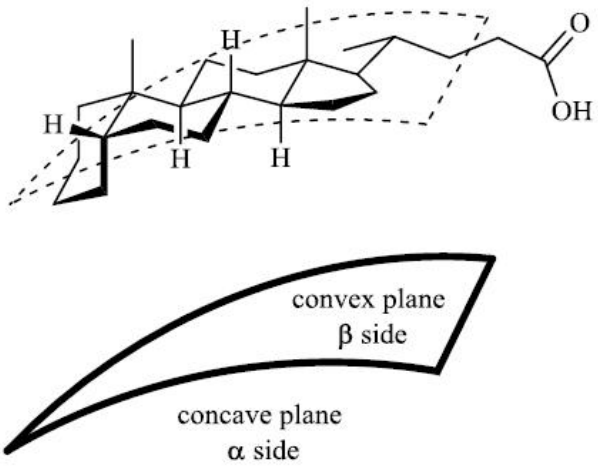

Figure 2.32- General structure of bile acids [283]. A convex plane (β side) and a concave plane (α side). The β side is more hydrophobic than α side.

CA has two α axial OH groups at C-7' and 12' and an 3α- equatorial OH group. IsoCA (3β-hydroxyl cholic acid) is less hydrophobic than CA because it has a less extended hydrophobic beta face. Dihydroxy bile acids, like isoCDCA and isoDCA, also do not have true planarity and they can be regarded as having a hydrophilic edge and their original hydrophobic face is disrupted by a β-hydroxyl group, making them more polar and less hydrophobic.

The 7β equatorial side of the bile acids is less hydrophobic compared to those with axial (α) groups. With respect to axial hydroxyl group, the water molecules from the solvation sheath can be stabilized by hydrogen bonds from the α side of the steroid. On the other hand, with the steroid having a equatorial hydroxyl group (like UDCA) the area of stabilization is completely shifted towards the β side of the molecule. This leads to increasing amount of nonstabilized water molecules (NSWM) making them less hydrophobic than other bile acids [285]. This explains why UDCA is less hydrophobic than CDCA.

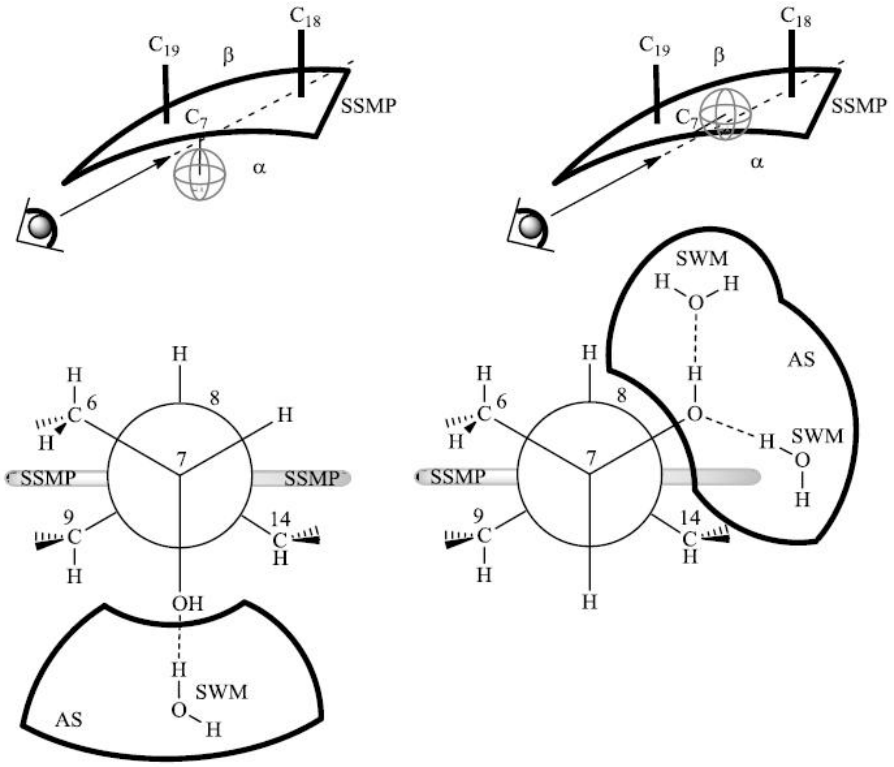

Figure 2.33- The effect of the orientation of hydroxyl group at C-7' position on the area of stabilization of water molecules [283]. 7α-OH bile acids (left) stabilize water molecule from α side while 7β-OH bile acids (right), like UDCA, stabilize water molecule from β side. (SSMP= steroid skeleton mean plane, SWM= stabilized water molecules, AS = area of stabilized water molecules)

Lastly, DCA has slightly higher hydrophobicity than CDCA because the C-12' axial hydroxyl group is hindered from solvation by the C-17' side chain.

Thus, we can conclude the order of hydrophobicity of the 3α-bile acids is: LCA>DCA>CDCA>CA>UDCA [279, 285, 286], which exactly corresponds to the order of their cytotoxicity based on the cell viability from MTT assay. At the same time, bile acids with 3β hydroxyl groups are less hydrophobic than their 3α isomer except for LCA. In the case of LCA, there are no other secondary alcohols so inversion of the 3-OH creates a uniformly hydrophobic alpha face, while causing little interruption of the beta face. In the cases of CA, CDCA and DCA, inversion of one secondary alcohol introduces hydrophilic character to the beta face while retaining hydrophilic character in the unchanged secondary alcohol on the alpha face. Interestingly, in the case of UDCA, inversion of the

3-alcohol causes a uniformly hydrophilic beta face making isoUDCA paradoxically less polar than UDCA– there is now an uninterrupted alpha face to interact with lipophilic domains, in reverse phase chromatography or indeed cell domains.

Given their relative toxicities the colonic conversion of 3α-OH bile acids to 3β-OH bile acids may be a mechanism for bile acid detoxification, particularly for unconjugated secondary dihydroxyl bile acids generated by bacterial metabolism in the gut.

Bile acid hydrophobicity (lipophilicity) is an important membrane toxicity determinant. Bile acids promotes cell membrane transport and at micellar concentration hydrophobic bile acids can disrupt the cell membrane by extraction of membrane lipids, such as phospholipids. In general, the efficiency of bile acids to solubilize phospholipids correlates with increasing hydrophobicity [287]. Hydrophobic bile acids induce mitochondrial dysfunction by causing mitochondria permeability transition (MPT) leading to easier permeability of the mitochondria membrane, which is followed by releasing of cytochrome c. The loss of cytochrome is associated with ROS generation within the mitochondria triggering apoptosis. This will be further discussed in Chapter 4.

Hydrophobicity of bile acids affects their ability to penetrate the cell membrane. In this chapter, one of interesting questions was whether it was possible to relate the cytotoxicity of 3α- bile acids and isobile acids and their hydrophobicity.

In the present set of ten compounds there was a negative correlation (R^2=0.66, n=10) between log P and cell viability (Figure 2.34). It is obvious that DCA, CDCA are out of trend being significantly more toxic than predicted based on R_{MW}. In conclusion, the lipophilicity of compounds determined in the RPTLC showed good correlation with their cytotoxicity effect.

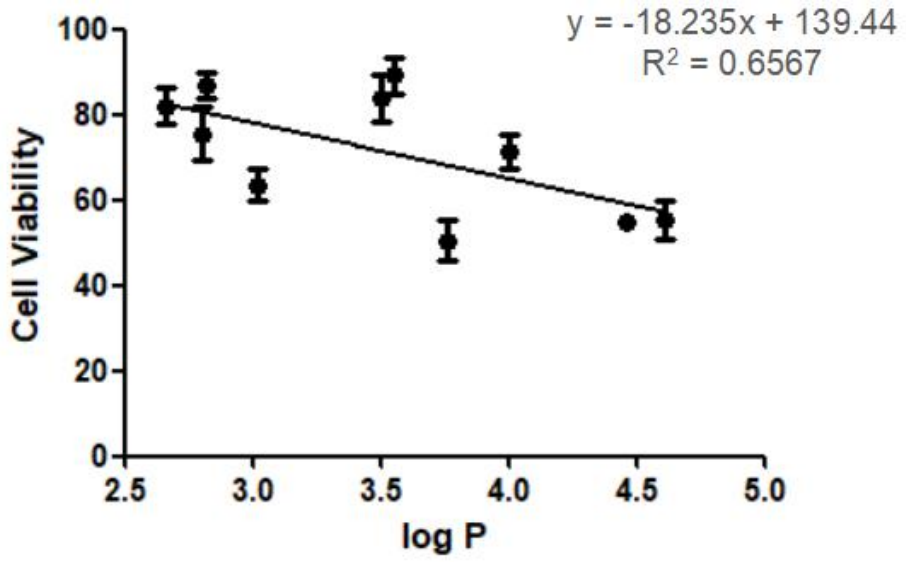

Figure 2.34- The linear correlation between the lipophilicity and cell viability of ten bile acid compounds. The coefficient of determination (R^2) is 0.66.

RPTLC retention extrapolated to zero organic modifier was predictive of bile acid toxicity in the Caco-2 cell line and it could be a useful high throughput tool for cytotoxic bile acid characterisation. There were no significant relationship between HSA and cell viability, suggesting relative bile acid hydrophobicity (lipophilicity) is a dependent property that is better predicted using chromatography. In the following sections, experimental determination of the relative effects of bile acids and their isomers on FXR is described. The results could be relevant to understanding the impact of epimerization by colonic microflora on local and liver level FXR activation. The results may also be relevant to SAR of FXR activation.

2.5 FXR FRET measurement of isobile acid interactions with FXR

Fluorescence resonance energy transfer (FRET) is a technique used to understand physical interactions between adjacent protein molecules during a bimolecular process including in living cells. The mechanism of FRET assay involves the energy transfer from a donor fluorophore in an excited state to an

adjacent acceptor fluorophore. The resonance energy transfer measurement can be used to detect the interaction.

Figure 2.35 shows the mechanism of FRET between two fluorophores attached to the same protein. The two fluorophores are close together in the distance of nanometre level. Once the protein undergoes a conformational change, the two fluorophores become much closer enabling the FRET interaction. Energy transfer measurements are applied to estimate the distance between two fluorophores. In Figure 2.37, the blue fluorophore is the donor and yellow fluorophore is the acceptor. The increasing intensity at the acceptor and decreasing in the fluorophores emission of the donor will be detected.

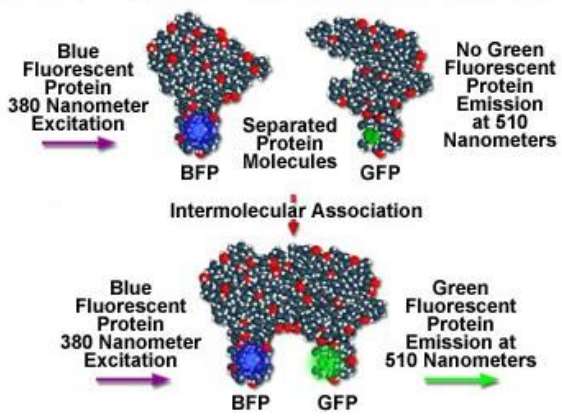

Figure 2.35- The mechanism of Fluorescence resonance energy transfer. Blue is the donor fluorophore and yellow is the acceptor fluorophore. When the molecular interaction happens, the donor-acceptor fluorophore become much closer.

Based on the mechanism of FRET, a general FXR-based bile acid sensor was reported to help understand intracellular bile acid transport dynamics on single cell level in real time and it has been used in many biomedical applications [288]. Older techniques applied to understand bile acid transport currently such have the disadvantage of damaging the samples, being not applicable for imaging in single cells and have limited time and spatial resolution. The bile acid sensor (BAS) is good alternative. It allows rapid and simple quantitation of bile acid influx and efflux of endogenous bile acids and monitoring the transport of

intracellular metabolites in single living cells. The approach as shown involves a fusion protein composed of a donor fluorophore (cerulean) and an acceptor fluorophore (citrine) that link to the FXR LBD and a co-activator peptide derived from NCoA2, containing a LXXLL motif [289]. The use of this sensor was demonstrated in cells containing NTCP and OSTα-OSTβ, functioning as an importer and exporter [290].

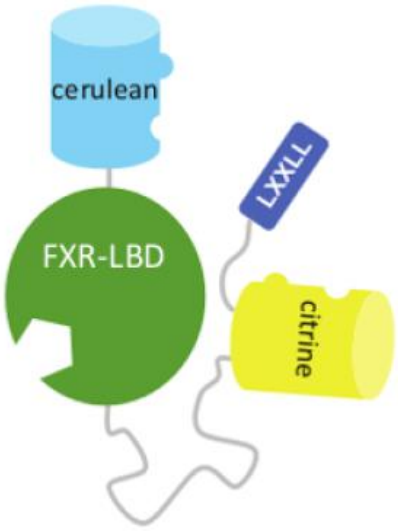

Figure 2.36- The components of the FRET bile acid sensor. It is composed of a FXR ligand binding domain, a donor fluorophore (cerulean, blue), an acceptor fluorophore (citrine, yellow) and a FXR coactivator peptide with LXXLL motif.

When bile acids and other FXR ligands bind to the LBD, FXR undergoes a conformational change and this makes the helix 12 move over and attach to FXR LBD followed by recruiting a coactivator peptide with the LXXLL motif and binding the cerulean and citrine fluorophore to close vicinity, leading to a change in FRET signal. (Figure 2.37).

FXR activation and conformational change leads to alteration in the cerulean: citrine ratio, which can be detected by average 525/450 nm emission ratio in real time. In living mammalian cells, usually an increasing average ratio is observed. This bile acid FRET sensor provides a rapid and simple method to visualize bile acid transport in living cells in real-time and it has been tested in

many cell types including U2OS, Huh-7, and HepG2 cell lines that can be transfected and have a stable phenotype. Besides, it also provides a system for direct and real-time monitoring of bile acid export in single living cells.

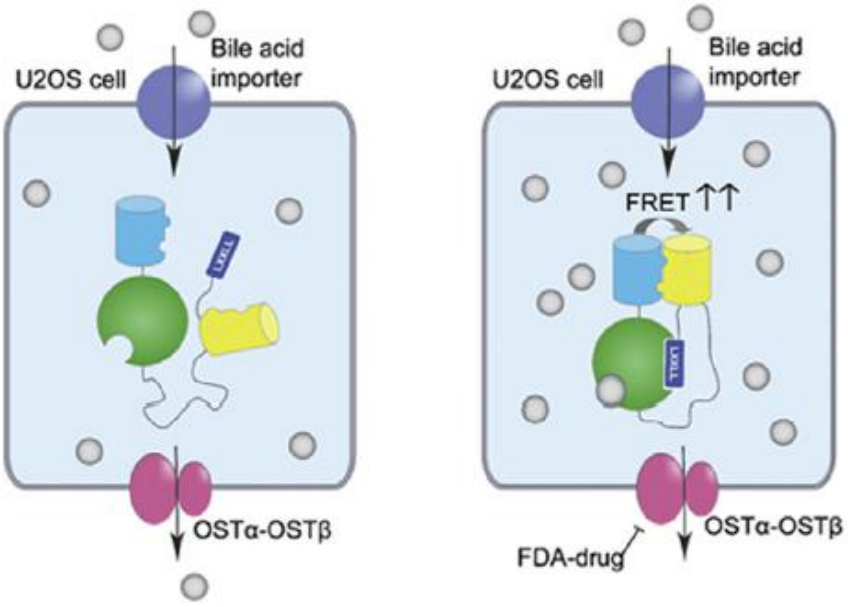

Figure 2.37- Schematic representation the mechanism of BAS upon FXR activation [290, 291]. Bile acid binding to the LBD of FXR recruits coactivator peptide (LXXLL motif) close to LBD, which causes the association between two fluorophore proteins and an increase in FRET. Also shown as 'FDA drugs' is the potential to detect drug impact on bile acid export leading to cholestasis in this context a kind of drug-induced liver injury.

In the present FXR FRET experiments, the emission ratio of cerulean fluorophore: citrine fluorophore (525/450 nm) was measured in single living cells, here transfected U2OS cells that lack expression of bile acid transporters, to quantify the FXR activation upon ligand binding. The choice of U2OS cells is because they are readily transfectable and do not endogenously express bile acid proteins. Measurements were performed by Sandra Van de Wiel in the Graaf lab in Amsterdam. Cells were grown in medium (with FBS or stripped FBS) and the confluency of cells was around 60–70% before carrying out the experiments. Bile acid was added at exactly 2 min time point (120 sec) and 5 μM GW4064 was added at 4 min time point (240 sec). GW4064 is a synthetic high efficacy agonist and it shows the maximal recruitment under the experimental conditions (a reference for max effect).

In this research, we screened whether (iso)bile acids act as FXR agonists and lead to coactivator recruitment. Experiments were firstly carried out in absence of bile acid transporter NTCP, the bile acid transport protein in the human liver that mediates uptake from the portal blood. Without NTCP, free bile acids can cross membrane by passive diffusion in a polarity dependent way (CA and to an extent UDCA are more slowly diffusing). Conjugated bile acids cannot pass through the membrane and activate FXR in the absence of a bile acid transporter. Effects therefore in cells transfected with NTCP can be attributed to the conjugated bile acids that are imported when it is active.

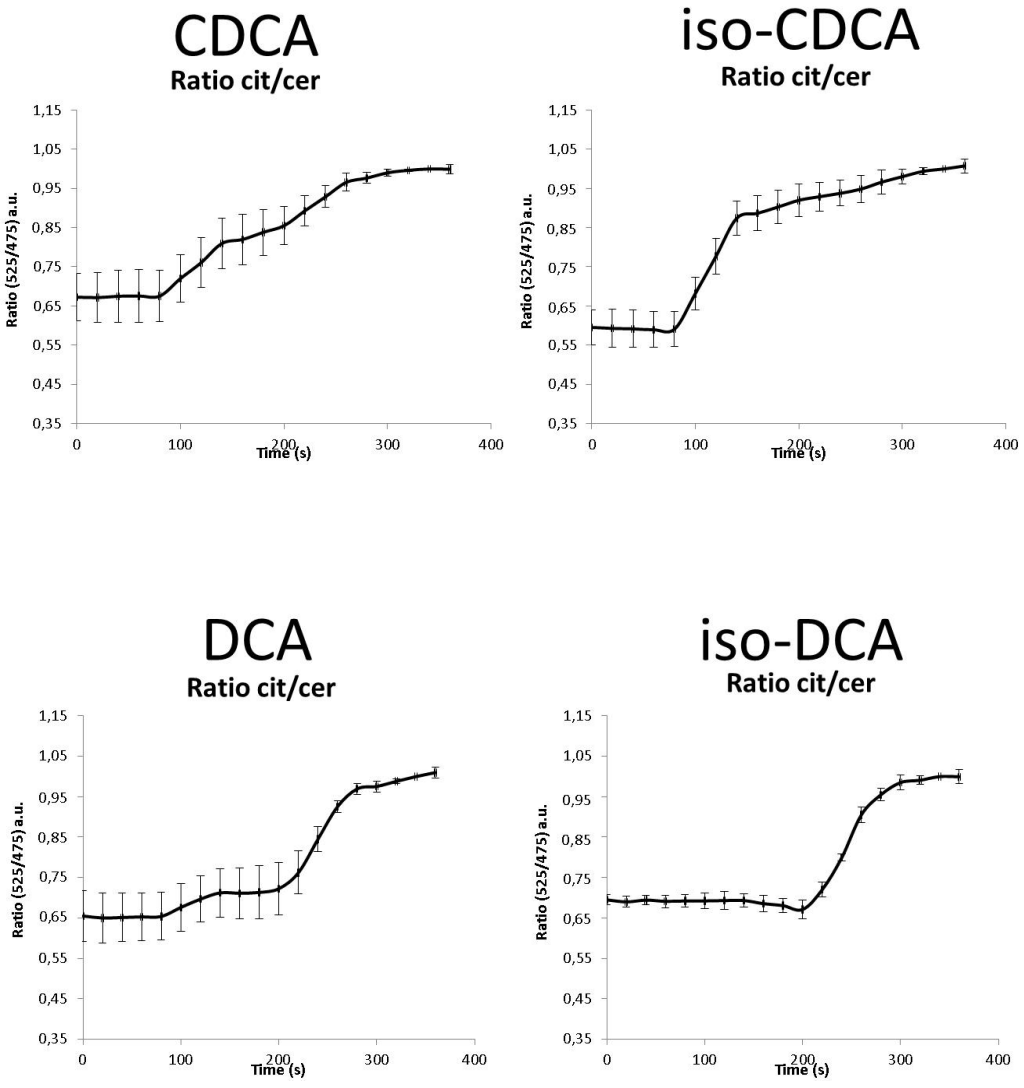

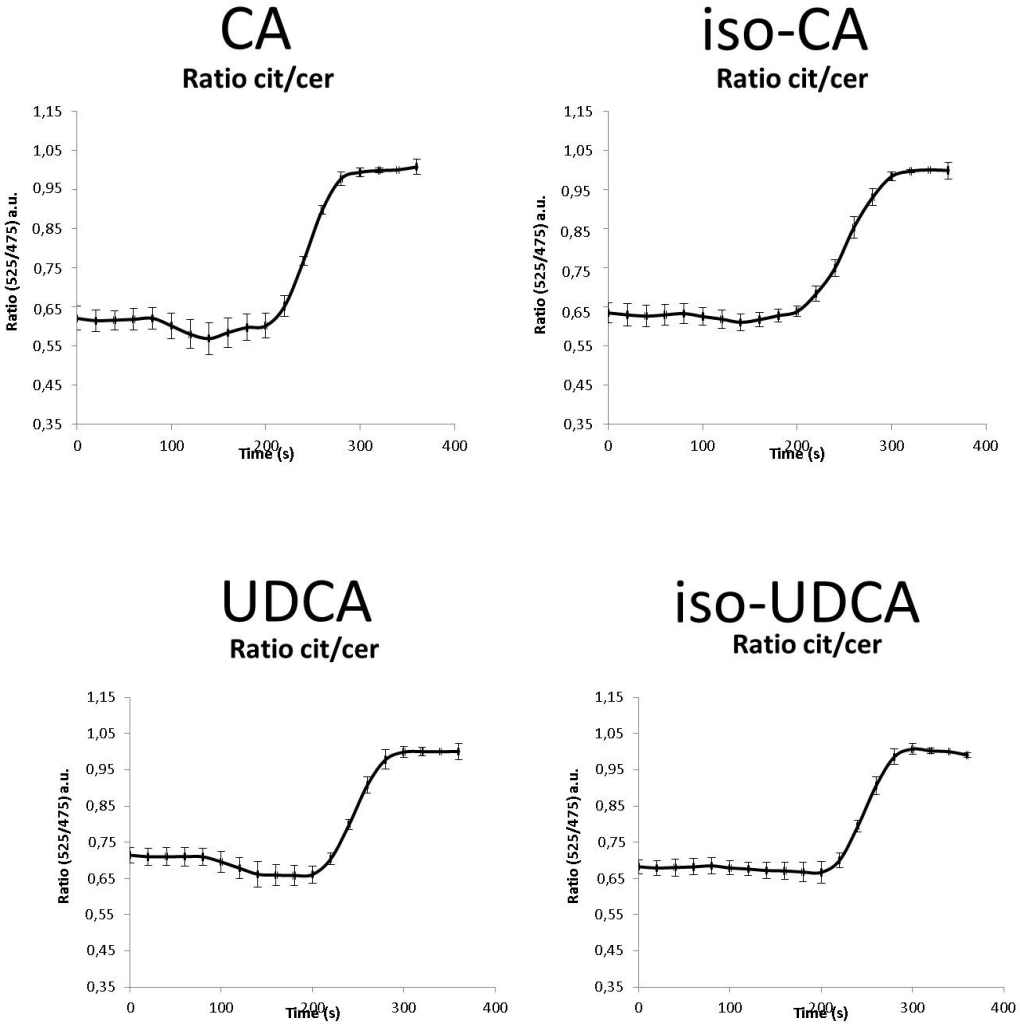

Figure 2.38- Real time monitoring of the cerulean: citrine fluorophore ratio (525/450 nm) without transfected bile acid transporter NTCP. Each bile acid compound (100 μM) was added at 2 min time point (120 sec). Data were normalized to the maximum emission ratio, which was determined by addition of concentration of FXR agonist GW4064 (5 μM) at 4 min time point (240 sec).

As can be seen from the graphs above, without the presence of NTCP, isoCDCA shows significant increase in cerulean: citrine emission ratio, even higher than CDCA indicating it is a stronger agonist [292]. Subsequent administration of the synthetic FXR agonist GW4064 could not further increase the emission ratio suggesting the maximum response was already reached by isoCDCA. In contrast, CDCA pretreated cells still showed increased FRET after addition of GW4064, indicating submaximal stimulation by CDCA alone.

DCA treatment leads to minimal increase of FRET and surprisingly addition of isoDCA even decreased the emission ratio, suggesting that binding of isoDCA to the sensor induces conformational changes opposite to alpha bile acid signaling. Other (iso)bile acids tested have no significant effect in the FRET assays. The implication of these results is that CDCA and isoCDCA are agonists in that they are able to cause conformational changes resulting in recruitment of the coactivator peptide LXXLL and positive FRET. The data suggest that isoCDCA is a more active agonist or causes a bigger effect at 100 μM than CDCA itself, the endogenous agonist of FXR. The extent of colonic isoCDCA production therefore is of interest for its effect on FXR activation.

The following set of FRET experiments involved cells transfected with NTCP. Ten different bile acids were tested in both charcoal stripped FBS and with FBS. Charcoal stripped FBS is devoid of bile acid; An estimated supernatant level of 15 μM of conjugated and free bile acids (with glycine and taurine conjugated CDCA and CA as well as unconjugated UDCA being most abundant) are present in FBS; In FBS in which the cells are grown, these bile acids cause partial saturated and constantly stimulating the FXR reporter even in the absence of additional test bile acid. This mimics aspects of an *in vivo* environment. In stripped serum, the background FRET effect is therefore lower and changes are more easily assigned to the effect of the added isobile acid or synthetic agonist GW4064.

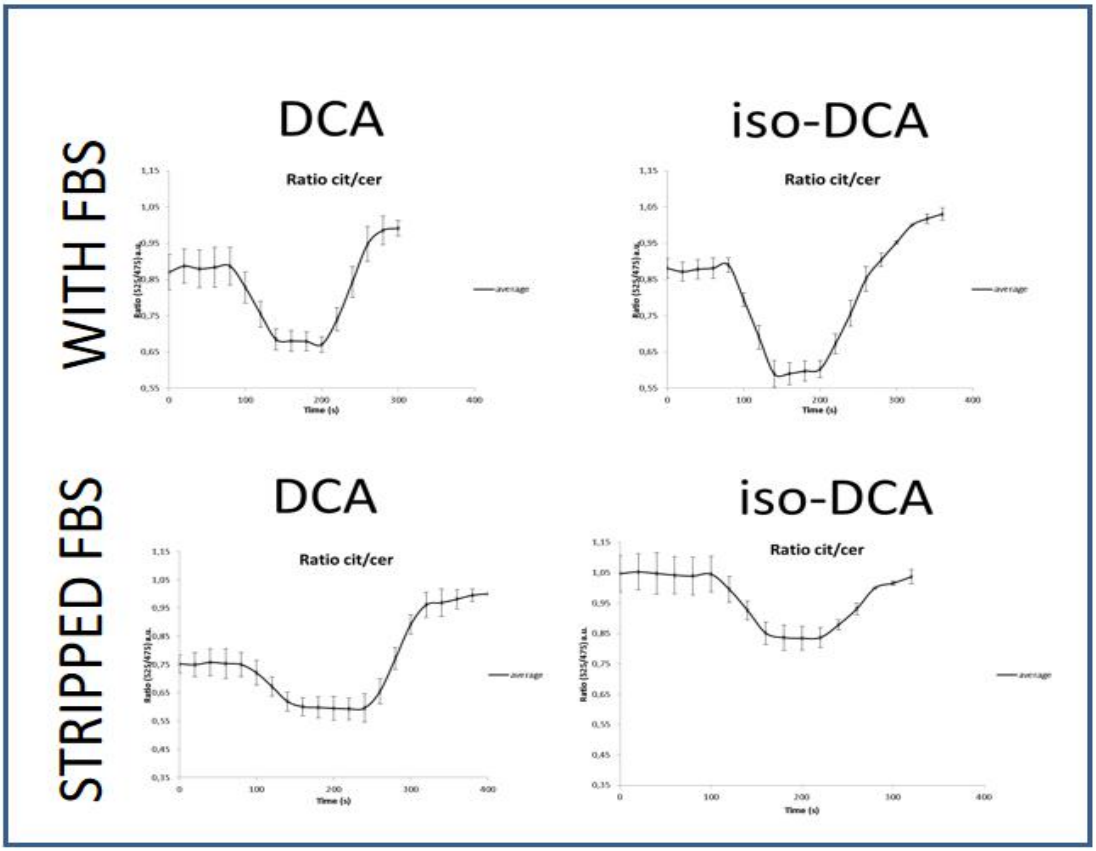
WITH FBS
DCA
iso-DCA
Ratio cit/cer
Ratio cit/cer
average
Time (s)
STRIPPED FBS
DCA
iso-DCA
Ratio cit/cer
Ratio cit/cer
average
Time (s)

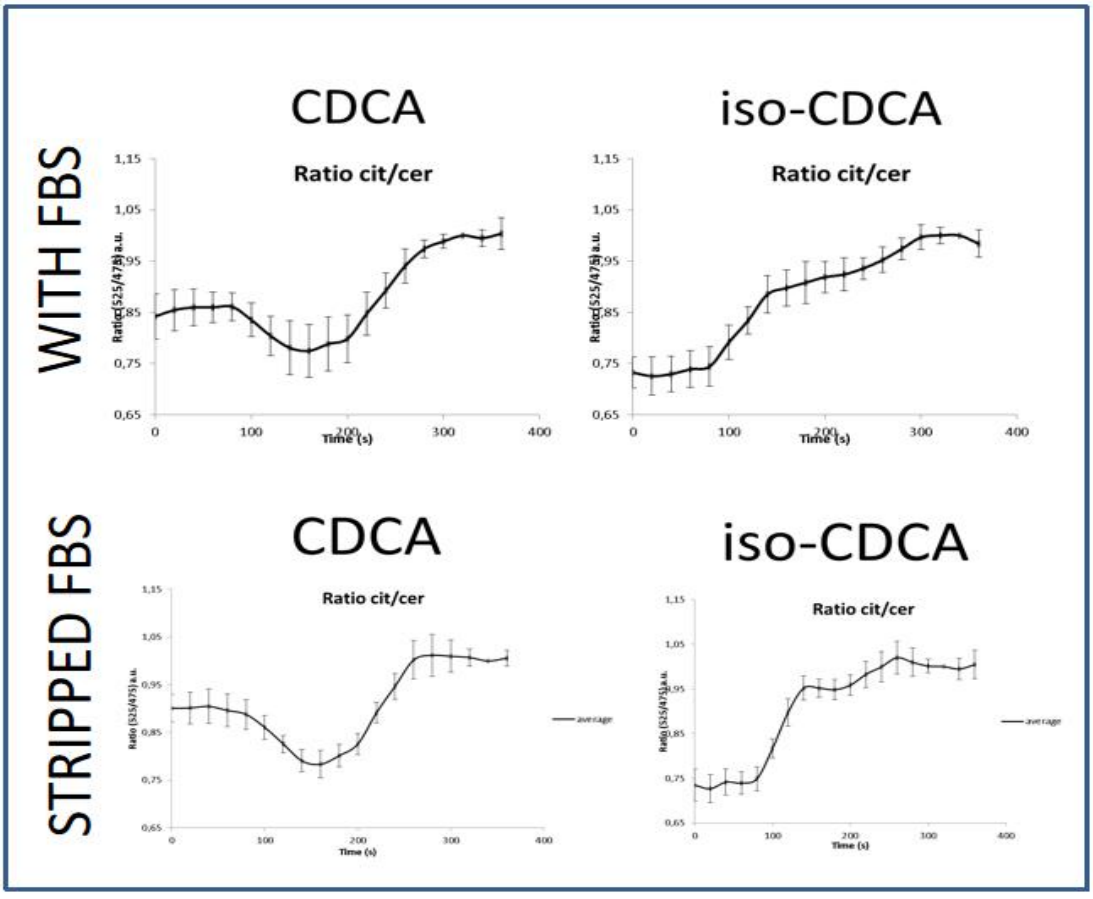
WITH FBS
CDCA
iso-CDCA
Ratio cit/cer
Ratio cit/cer
Time (s)
STRIPPED FBS
CDCA
iso-CDCA
Ratio cit/cer
Ratio cit/cer
average
Time (s)

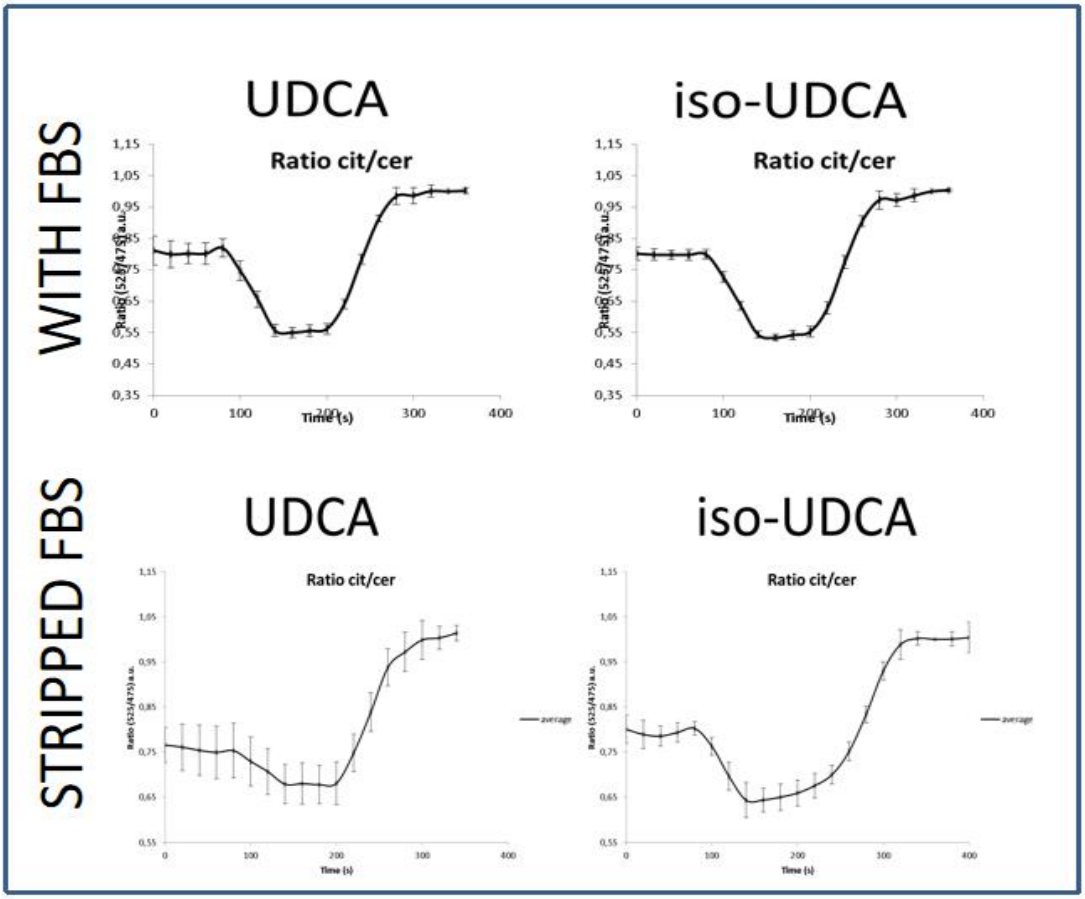
WITH FBS
UDCA
Ratio cit/cer
iso-UDCA
Ratio cit/cer
STRIPPED FBS
UDCA
Ratio cit/cer
iso-UDCA
Ratio cit/cer

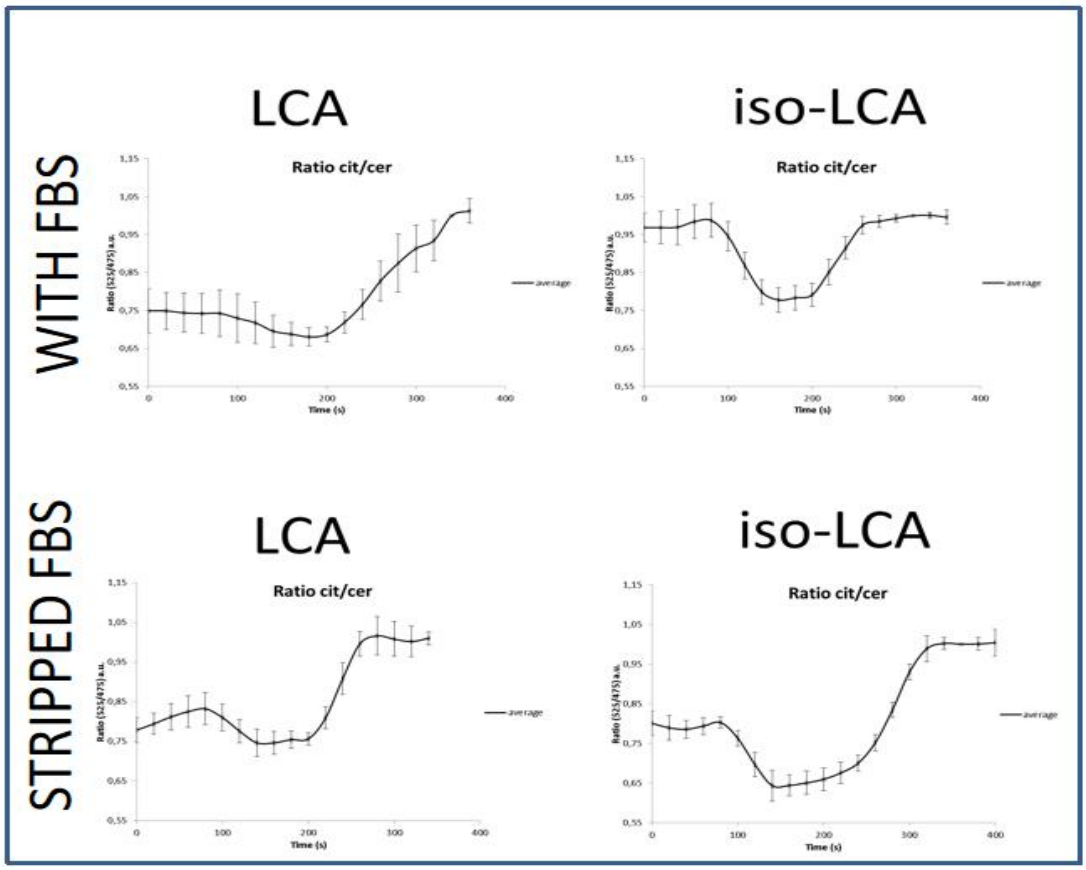
WITH FBS
LCA
Ratio cit/cer
iso-LCA
Ratio cit/cer
STRIPPED FBS
LCA
Ratio cit/cer
iso-LCA
Ratio cit/cer

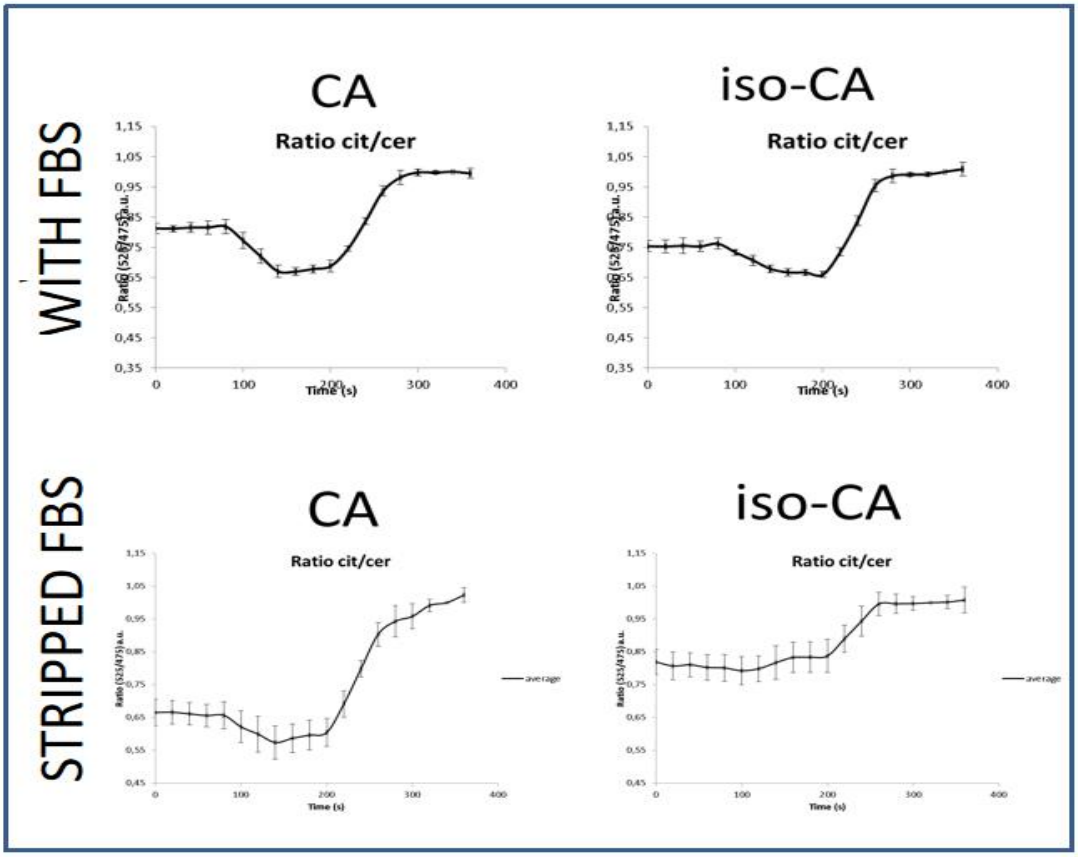

Figure 2.39- Real time monitoring of the cerulean: citrine fluorophore ratio (525/450 nm) with addition of NTCP. Ten bile acids are test in both stripped FBS and with FBS. Each bile acid compound (100 μM) was added at 2 min time point (120 sec). Data were normalized to the maximum emission ratio, which was determined by addition of concentration of FXR agonist GW4064 (5 μM) at 4 min time point (240 sec).

From the graphs above, with FBS, initial emission ratio of cerulean: citrine of the sensor at the beginning of an experiment is consistently higher than those with stripped FBS. This is because in the NTCP cells intracellular bile acids that are in FBS are enough to partially activate the sensor. In some cases above, the FRET goes down after treatment of test compounds and this is because added (iso)bile acids displace the agonists from the serum suppressing background agonist activation of FXR. They would be functionally antagonist in this context.

Of the isobile acids synthesized, only isoCDCA is a true agonist as it induces a positive FRET before treatment with GW4064 indeed only a small increase is

observed after adding GW4064. In comparison with isoCDCA, CDCA showed no significant effect in FRET which was surprising because it is generally regarded as a full agonist.

The remaining bile acids caused marked FRET decrease as they stop serum agonists from activating the sensor. The transcriptional effect of these observations was recently studied in Graz University in mice and in liver cell lines to understand if they are acting as weak agonists or as antagonists. IsoCDCA was an agonist in cells and *in vivo* in mice when administered by oral gavage. The secondary isobile acids were either weak agonists or showed some ability to antagonize the effect of synthetic agonist.

2.6 FRET-based FXR coactivator recruitment assay

Since the isobile acids had been characterized here in relation to their interaction with the FXR FRET sensor and shown to exert a range of effects on gene transcription, we were interested to assess their effect in a commonly used reporter assay for FXR.

β-Lactamase reporter system that uses the enzyme called TEM-1β-Lactamase [293]. This is a 29-KDa enzyme encoded by the ampicillin resistance gene which can be used to cleave the β-lactam ring structure molecules like penicillins and cephalosporins. The main component in this system is fluorogenic β-Lactamase substrate CCF2/4 acetoxymethylated form (CCF2/4-AM). CCF2/4-AM consists of two fluorescent dyes, 7-hydroxycoumarin-3-carboxamide and fluorescein, attached to the 7’ and 3’ positions respectively, bridged by cephalosporin.

β-Lactamase reporter assay was considered to be a robust FRET-based reporter system which can be compatible with a wide range of commonly used cell lines. Its mechanism is shown in Figure 2.40 [294, 295].

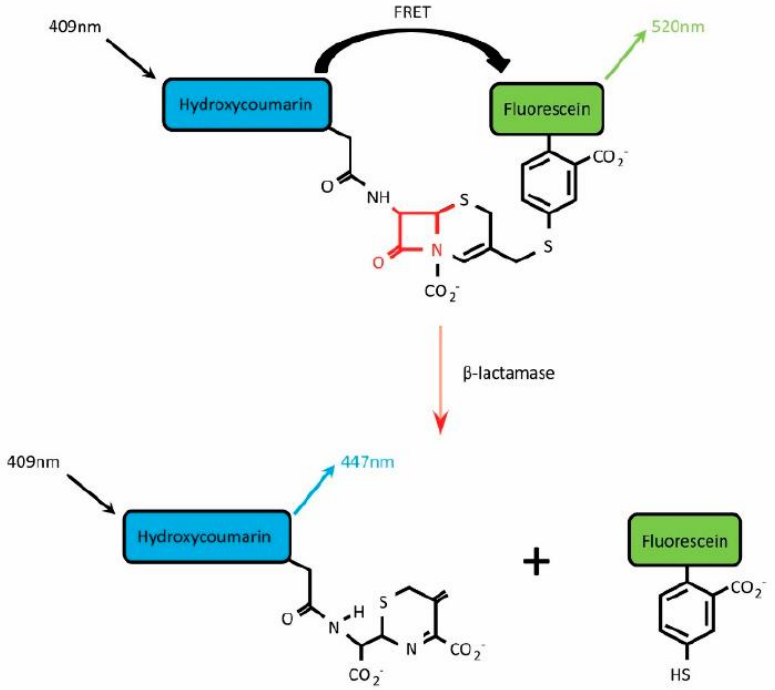

Figure 2.40- Schematic illustration of β-lactamase reporter system for quantitative measurement of membrane protein surface expression [295, 296]. When CCF2/4-AM enters the cell cytoplasm, it is cleaved by endogenous esterases into CCF2/4. Exciting of CCF2/4 at 409 nm promotes efficient FRET from the fluorescent donor and acceptor molecule, resulting in emission detectable at 520 nm. However, cleavage of β-lactam ring by β-lactamase separates the two fluorophore molecules, causes a change from green to blue fluorescence and generates a fluorescence shift from 520 nm to 447 nm.

The FXR-modulating compounds identified from this β-Lactamase FXR-bla transactivation assay are then characterized as FXR agonists or FXR antagonists based on their % FXR activity. The assay principle is shown below in Figure 2.41.

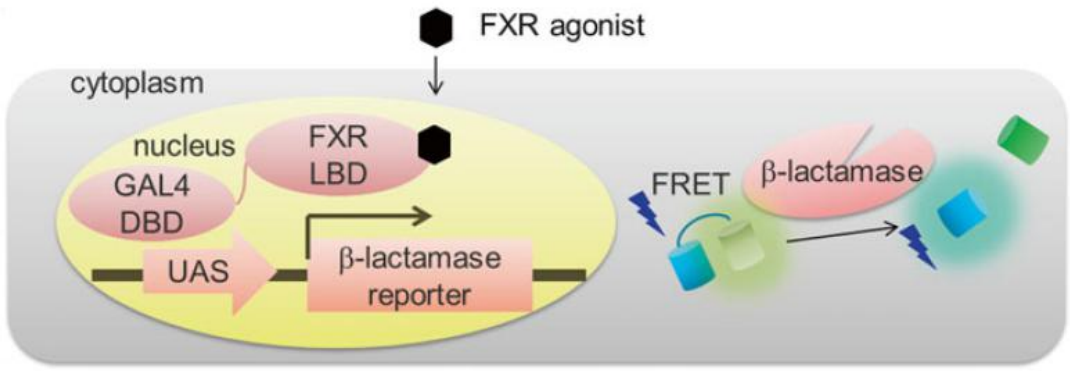

Figure 2.41- Assay principle of FXR-bla transactivation assay [297]. The activation of FXR LBD by FXR agonists leads to FRET.

To gain further insights into the regulatory functions of isobile acids with regard to FXR activity, we assessed the regulation of FXR by 3α bile acids and isobile acids using the FXR reporter assay. Non division-arrested cells called FXR-UAS-bla HEK 293T cells were grown in specific media (DMEM high glucose with GlutaMAX^{TM}). In this FXR agonist assay, cells were grown in medium (DMEM high glucose with GlutaMAX^{TM}) and the confluency of cells reaches around 60–70% before carrying out the experiments. Cells were seeded onto Greiner 384-well plate with black well, clear bottom at a density of 6×10^5 cells/ml and grew for 5–6 h in a humidified incubator set at 37^{o}C, 5% CO_2 and then a 5X stock of test compounds in assay medium was added. The agonist assay plate was then incubated for 16 h. CCF4-AM substrate mixture was loaded into each well in the absence of direct lighting for additional 2 h. The measurement was carried out at RT from the bottom of the wells, with low fluorescence background. The fluorescence plate reader was warmed up for 10–15 min before making measurements. The plate reader was set up with bottom-reader mode with optimal gain and with 5 reads. The blue channel was measured in the wavelength of 409/460 nm while green channel in 409/530 nm yielding β-lactamase activity as fluorescence emission intensity ratios [298]. The result for both blue and green channel of each well was recorded. Each experiment was carried out as quadruplicates and repeated three times to get twelve data points in total for each bile acid. The blue/green ratio was calculated for each well by dividing the background-subtracted blue emission values by the background-subtracted green values. The data was further analyzed in order to get the % agonist activity of each bile acid compound. The final data are presented in Figure 2.42.

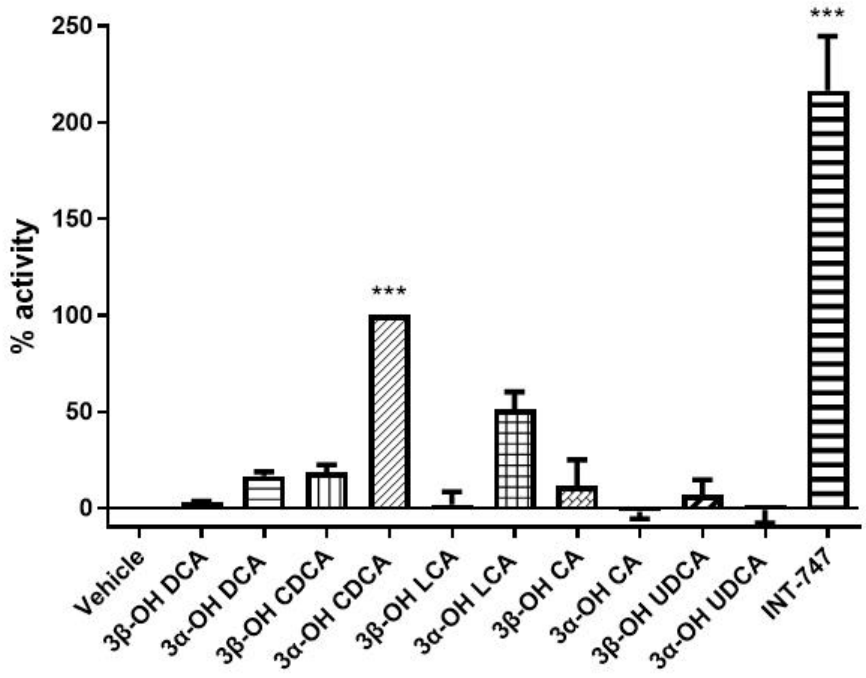

Figure 2.42- A measurement of % agonist activity of each bile acids. FXR-UAS-bla HEK 293T cells were seeded onto 396 well plates at a density of 6×10^5 cells/ml, and then treated with 100 μM bile acid solution for 16 h. Cells were then treated with CCF4-AM substrate mixture and then incubated for 2 h in the absence of direct light. The assay was normalised to 0.5 % DMSO vehicle control and absorbance of each well was read on a VERSAmax Microplate Reader (Molecular Devices, Sunnyvale, CA, USA) at a specific wavelength of excitation and emission filter for both blue and green channel. Ratios were normalized to DMSO-only wells (0.5% v/v DMSO) as 0% FXR activity. Values are expressed as mean ± SEM of three quadruplicate experiments, * p<0.05, ** p<0.01, *** p<0.001 as determined by one way ANOVA with Dunnett's post-hoc correction.

Among all bile acid compounds, INT-747 (OCA) exhibited the highest % FXR agonist activity, followed by CDCA. Both of them have been already found as good FXR agonist and this is as expected from many studies on the effect of bile acid on FXR. LCA (3α-OH), DCA (3α-OH) and isoCDCA exhibited some agonist effect on FXR but with a lower efficacy at this concentration and this corresponds to some findings on the ranking of bile acid FXR agonist potency [299–301]. 3β-epimers of DCA and LCA activated FXR, although to a much lower extent than their 3α-epimers [302, 303]. However, UDCA [304] and CA showed

negative agonist activity (not statistically significant) which was surprising. This raises the possibility that perhaps they are weak agonists [305] that act primarily as an antagonist of FXR, for example by preventing bile acids to bind and this merits further studies on their FXR antagonist effect. IsoDCA has been found to be an antagonist of FXR [306].

Isobile acids are generally weaker FXR agonists than their 3α-epimers and they may act as FXR antagonists. Another interesting finding based on the result above is that decreased FXR induction was seen for 3β-OH bile acids with a 12-hydroxy group, like isoDCA and isoCA but slightly higher FXR agonist effect occurred without this group.

Overall, the significant effect of isoCDCA on the FXR FRET assay in the previous section did not translate into an effect in the lactamase reporter assay described here that relates to functional transcriptional consequences of FXR binding. The contradiction may be explained by access or metabolism issues. Indeed in the collaborator lab in Graz in early 2019 it was discovered that isoCDCA undergoes epimerization in HepG2 cells into alphaCDCA, the primary bile acid configuration. It is also possible that isoCDCA binds the site more strongly and causes coactivator recruitment as observed in the FRET assay but has lower biochemical efficacy due to the overall shape of the assembly (antagonist). Besides, another possible explanation for the discrepancies regarding high FRET activity for isoCDCA and negligible reporter assay activity could be the difference in incubation time for these assays: for 16 h for reporter assay while only 1-2 h for FXR FRET assay.

2.7 *In vivo* mouse studies

The effects of 3α and 3β epimers of different bile acids on FXR activation were assessed *in vitro* experiments using different cell-based assays. In order to further investigate the regulatory functions of isoBAs in regard to FXR activity, our collaborators assessed FXR regulation by isobile acids comparison to their

3α epimers *in vivo* using healthy mice models.

Administration of a single dose of isoBAs alone did not lead to the expression of FXR target gene in mouse liver or intestine. Co-treatment of secondary isoBAs with endogenous FXR ligand GW4064 induced the repression of CYP7A1 and CYP8B1 mRNA expression in the mouse liver and the increase of FGF15 mRNA expression in the intestine and the effects were stronger compared to administration of already robust effect of GW4064. This indicates the robust cooperative effect of isoBAs with GW4064 in FXR activation *in vivo*.

Treatment with CA leads to increased FGF15 expression and repressed CYP7A1 levels in mice and same for UDCA and isoUDCA. The repression of CYP7A1 was even better with isoUDCA than UDCA. Although UDCA binds to FXR it shows little FXR agonistic activity based on *in vitro* reporter assay and in general is not as effective as other 3α bile aids. UDCA was unable to induce ileal FGF15 without bile acid uptake transporter proteins like ASBT and Ostα but it is associated with indirect FXR agonist activity in the presence of endogenous bile acids in liver and intestine.

2.8 Conclusion and future work

Isobile acids are of interest because of their microflora dependent production in humans and sporadic high concentration in the bowel. These secondary bile acids are less well characterized than their alpha epimers. This Chapter sought to help improve characterization through a range of approaches. We have described an efficient synthetic approach to these materials that allowed the production and physicochemical characterization of iso -CA, -DCA, -CDCA, -UDCA and -LCA. Epimerization causes these substances to become more polar, less toxic than the parent bile acids and therefore epimerisation may be a mechanism of detoxification. Considering the sinister effects of some secondary bile acids in the bowel, this could be significant in explaining causes of sporadic colorectal cancer if there are inter-individual differences in bile acid

epimerization and detoxification. In the FXR FRET in the Graaf lab, our isobile acids were shown to be largely inert or antagonist in effect by reducing signaling caused by serum bile acid. IsoCDCA was identified as a full high efficacy agonist. However in the lactamase FXR reporter assays isoCDCA and the other isoBAs were weak agonists or antagonists.

This contradiction may be partly explained by the reported rapid interconversion of alpha and beta CDCA in HepG2 cells. The impact of this on CDCA and isoCDCA effects *in vivo* is subject of ongoing study and referred to in the appended paper.

Bile acids and bile acid receptors are therapeutic targets for development of drugs for treating cholestatic liver diseases, fatty liver diseases, diabetes and obesity. The ongoing development of natural, semi-synthetic and synthetic compounds that regulate the activity of these bile acid receptors, and of some other drugs that alter bile acid pool by modulating in the species of gut microbiota, will exploit this potential. Synthetic approaches to isoBAs and their physicochemical characterization here will hopefully contribute to this and explain the effects of theses interesting endogenous products of microflora metabolism.

Chapter 3. Synthesis of muribile acids and biological evaluation of their effect on cytoprotection

Muricholic acids (MCA) are a group of bile acid compounds that are found in mice and at a very low concentration in human urine. MCAs are more polar and hydrophilic than bile acids found in humans as they contain an additional hydroxyl group at C-6'. Interestingly muribile acids are found in high concentration in human newborns. This leads some researchers to believe that MCAs may have a role in human development, and may offer some potential in the treatment of degenerative disorders later in life. They disappear from the human circulation in the first months of life. Muribile acids are challenging to synthesize and not readily available commercially. The work described in this chapter involves the synthesis of the MCAs and investigation of their protective effects in liver stem cells. The research work was also concerned with provision of sufficient quantities of MCAs to research collaborators in Lund (Sweden) and Graz (Austria). The coordinated aim of our research is to help to expand our understanding of MCA biochemistry and therapeutic potential in humans. A brief overview of work to date is provided here.

3.1 Brief introduction to muribile acids

The discovery of the muribile acid family can be traced back to the 1950s. Edward Doisy at St. Louis University won the Nobel Prize for his work on the identification of the 3, 6, 7-trihydroxy bile acids in rats and discovered the αMCA, βMCA and ωMCA [307]. His student, William Elliott, synthesized these bile acids and described their chemical properties [308].

In terms of the chemical structure, CDCA (3α, 7β) is the primary mammalian bile acid from which many of the C_{24} bile acids are considered to be derived. The most common modification of CDCA is the additional hydroxylation of the steroid nucleus. Trihydroxyl- bile acids with hydroxyl groups at C-3', C-7', and one additional site are generated. In mammals, the most common 'third site' hydroxylation positions are C-6 (α or β) or C-12 (α). The trihydroxyl bile acid

with one additional hydroxyl group at C-12 is known as CA; additional hydroxyl analogues at C-6 are so called muricholic acids (MCA). This hydroxylation greatly changes the physicochemical properties of bile acids, resulting in a bile acid pool that is more hydrophilic and less cytotoxic.

Human and mice have remarkably different bile acid pool compositions, with mice possessing a more hydrophilic bile acid profile [309]. Mice synthesize three bile acids not found in adult humans. Two of these compounds are synthesized directly by the mouse, αMCA and βMCA. The third, ωMCA is produced by oxidation of 6β-hydroxyl of βMCA followed by reduction to 6α-hydroxyl group by mouse colonic microbiota [310, 311]. Current knowledge about bile acid metabolism is highly influenced by studies in mice. This is largely due to the development of mouse models in research due to their advantages of small size, short gestation period and life span [312]. But there are several major differences between mice and human bile acid metabolism including as mentioned hydroxylation at the C-6' position. CDCA is not metabolized at C-12' in the rat, instead it is hydroxylated at C-6' to form α-MCA. A number of other bile acids are metabolized similarly in the rat, contributing not to 12α-hydroxyl derivatives, but to the 6-hydroxylated muribile acids via mouse 6β-hydroxylase. The presence of the 6-OH group protects MCAs from 7-dehydroxylation via bacterial enzymes in the intestine [313]. Muribile acids have a variety of interesting potentially therapeutic effects, for example, they have the potential to reduce infections caused by *Clostridium difficile* germination [314], which is considered a leading cause of a debilitating antibiotic-associated colitis.

Based on the findings from the previous chapters, it is interesting that the therapeutic bile acid, UDCA, which has a hydroxyl group on the β side of the steroid nucleus, shows less cytotoxicity than most of the naturally occurring bile acids and reduces tumorigenesis in humans [315]. In humans, UDCA is generated mainly from CDCA by the gut microbiota via a 2-step process [316]. UDCA is a primary bile acid synthesized in the absence of the gut microbiota

constituting around 3% of the total bile acid pool in humans [317]. Besides, it should be emphasized that while the bile acid pool in humans consists mostly of hydrophobic bile acids, the bile acid pool in mice is predominantly composed of a large proportion of hydrophilic 6-hydroxylated bile acids, including all the MCAs (constituting half or more of the bile acid pool [318]). The presence of these MCAs may help explain why the incidence of colon cancer is low in mice.

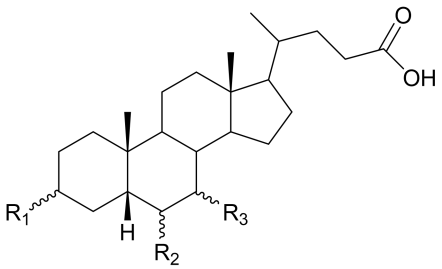

BAs	R_1	R_2	R_3
α-MCA	α-OH	β-OH	α-OH
β-MCA	α-OH	β-OH	β-OH
ω-MCA	α-OH	α-OH	β-OH
γ-MCA	α-OH	α-OH	α-OH

Figure 3.1- The structures of four common muribile acids. Muribile acids are derivatives within a steroid skeleton of 5β-cholanic acid with a C3 α-OH group and OH groups on C6 and C7 carbons with different orientations.

MCAs are prenol lipids structurally characterized by a bile acid alcohol which bears three hydroxyl groups (Figure 3.1). αMCA (3α, 6β, 7α) and βMCA (3α, 6β, 7β) being the primary bile acids in mice are well described in the literature. In mouse liver, most CDCA can be converted to αMCA and βMCA [319]. βMCA is a principal bile acid biosynthesized by rat and mouse liver. This is usually

5-fold more abundant than αMCA, mainly due to epimerization of αMCA into βMCA mediated by intestinal microbiota [320]. βMCA is a natural primary bile acid in rat and mouse but does not occur in significant amounts in humans. βMCA is more hydrophilic acid than UDCA because of the presence of a hydroxyl group in the 6β position of the steroid ring. It has been found that βMCA is more effective than UDCA in preventing and dissolving cholesterol gallstones in mice [321]. αMCA is a hydroxylated bile acid found in normal human urine and in free glycine and taurine conjugated forms detected in human feces. Natural αMCA and βMCA are powerful inhibitors of cholesterol absorption in mice [322].

ωMCA (3α, 6α, 7β) is among the most abundant bile acids in the gut content and feces of male rat [323] but little is known about its role or effects. It is a secondary bile acid in the rat and mouse, constituting around 20% of total fecal bile acids of the conventional rat. Anaerobic bacteria in mice and rats can convert primary bile acid β-MCA into ω-MCA by three strains in a cooperative way. The conversion of β-MCA into ω-MCA proceeds in two steps: *E. lentum* oxidizes the 6β-OH group into 6-oxo group, followed by reduction into 6α-OH group [310]. Besides, HDCA (3α, 6α), itself can be absorbed from the gut and converted to ωMCA by the rat liver. The formation of ωMCA play a critical role in the increase of total bile acid fecal excretion [324]. ωMCA has an interesting series of effects on host health. It shows promise for treatment of obesity and hypercholesterolemia in relevant mouse models of disease [325]. The synthesis and biochemical properties of ωMCA will be discussed in detail in this chapter. The research described relates to investigations into approaches to its synthesis for biochemical investigations in this and other labs. In the Gilmer group there is additional interest in its cytoprotective properties, and some preliminary studies are described.

3.2 Biosynthesis of muribile acids

The biosynthesis of human primary bile acids and secondary bile acids has been explained in detail in Chapter 2. Current knowledge on bile acid metabolism is largely based on animal studies where the mouse becomes the preferred model for study [326, 327]. In humans, around 7 mg per day per kg body weight of cholesterol is converted to bile acids while in mice this figure increases to 50 mg per day per kg body weight [328, 329]. However, in both species, cholesterol catabolism to bile acids accounts for a similar overall fraction of daily cholesterol elimination (approximately 45%). Even so, there are many differences between mice and humans with respect to bile acid metabolism. Different types of primary bile acids are synthesized by various hydroxylases and epimerases, depending on species [330]. The human primary bile acid pool is composed of about 40% CDCA, 40% CA and 20% DCA [85], whereas CA (60%) and more hydrophilic MCAs (40%) are the predominant bile acids in mice [331]. Although primary bile acid synthesis is notably similar between human and mouse, bile acid composition and pool size in the mouse liver is strikingly different from humans [332], with LCA as a typical example. However, LCA is produced from CDCA in both human and mouse large intestine. LCA is present at only trace levels in mouse liver, perhaps due to the low concentration of CDCA. LCA is known as a toxic bile acid, however, LCA is efficiently conjugated in mice, contributing to decreased hepatotoxicity. Besides, the alternative pathway accounts for very little in terms of overall bile acid composition in humans, whereas it contributes as much as 50% of bile acid composition in rodents.

The differences in bile acid and cholesterol metabolism between mice and human are strongly dependent on the production of MCAs. In mice, several other bile acids are produced that are not seen in humans. 6β-Hydroxylation and 7α-epimerization on CDCA lead to the synthesis of αMCA (3α, 6β, 7α) and UDCA, respectively. As mentioned, UDCA (3α, 7β) is considered as a primary

bile acid in mice whereas it is a secondary bile acid in humans. At the same time, βMCA (3α, 6β, 7β) is formed by epimerization at 7α-hydroxyl group of αMCA. It has been reported recently that the mouse enzyme sterol-6β-hydroxylase (*CYP2C70*) is key for the synthesis of MCAs in the alternative pathway as confirmed by siRNA inhibition studies in primary mouse hepatocytes bearing recombinant *CYP2C70* gene [333]. This gene encoded the principal enzyme is responsible for the differences in bile acid metabolite profile between humans and mice [334]. The *CYP2C70* gene is necessary for the formation of αMCA from CDCA as well as βMCA from UDCA in mice [335]. These bile acids are not formed at significant levels in human liver, reflecting again the remarkable differences between various species in MCA synthesis.

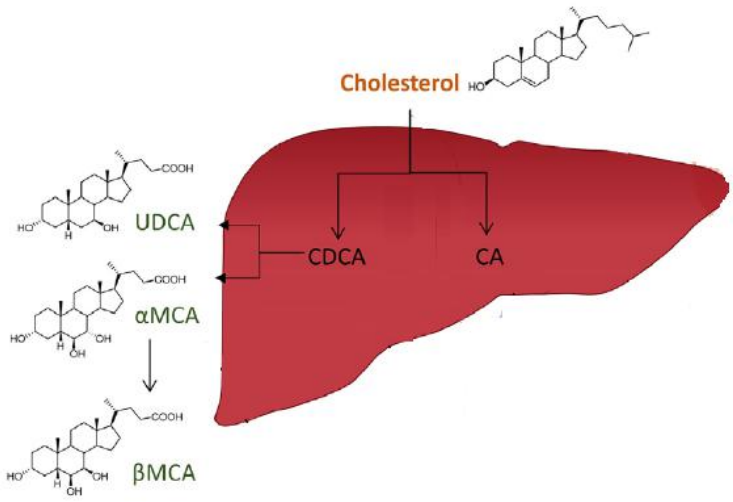

Figure 3.2- The biosynthesis of primary bile acids from cholesterol in the mouse liver [323]. The classic pathway in mice favors the synthesis of CA and the alternative pathway is quantitatively significant and favors the production of MCAs.

CA, αMCA and βMCA are most abundant in mouse liver. More than 95% of mouse bile acids are taurine conjugated for secretion into bile. The selection of taurine or glycine for bile acid conjugation is regulated by the BAAT enzyme [336, 337] and the availability of the taurine precursor [338]. The BAAT enzyme is particularly inefficient at using glycine for conjugating bile acids in mice. The taurine conjugates of bile acids have been demonstrated to be less cytotoxic

than glycine conjugated or unconjugated forms. Most of the conjugated bile acids that pass into the small intestine are reabsorbed. For the fraction entering the colon, the glycine or taurine moiety is removed by BSH and then deconjugated bile acids in mice undergoes additional microbial-mediated reactions, bacterial 7α or 7β-dehydroxylation. The secondary bile acids found in the mouse intestinal lumen includes DCA, HCA (3α, 6α, 7α) and ωMCA, which are converted from CA, αMCA and βMCA, respectively. Among these, the formation of αMCA and βMCA is of only minor quantitative importance as compared to the 7α-dehydroxylation of CA [339]. The formation of HCA and ωMCA (3α, 6α, 7β) is via epimerization of the 6β-OH group. HDCA is produced also through the C-7 dehydroxylation of ωMCA. LCA and ωMCA are secreted into faeces while other bile acids are reabsorbed and circulated back to mouse liver [340].

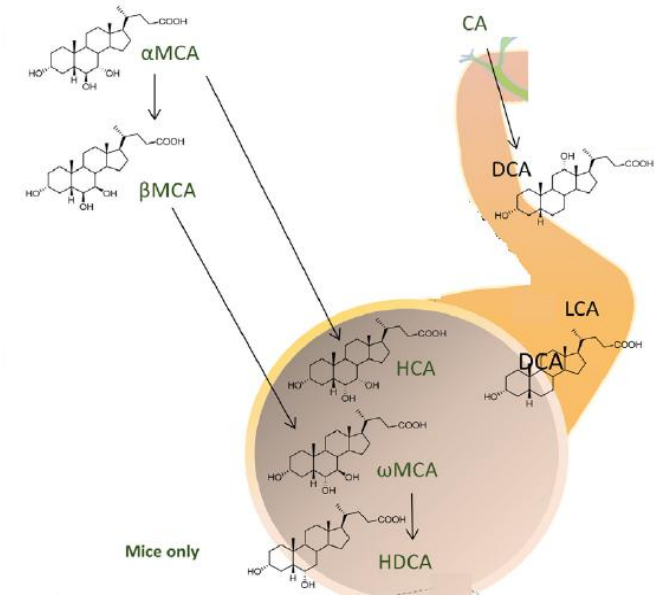

Figure 3.3- The biosynthesis of secondary bile acids from primary bile acids in the mouse intestine [323]**.** The secondary bile acids produced in the mouse are DCA, HCA, ωMCA and HDCA.

To sum up, in mice, the two pathways (classic and alternative pathway) contribute equally to form a highly hydrophilic bile acid pool containing approximately 50% of CA and 50% of MCAs, with very little DCA and CDCA

(see Figure 3.4).

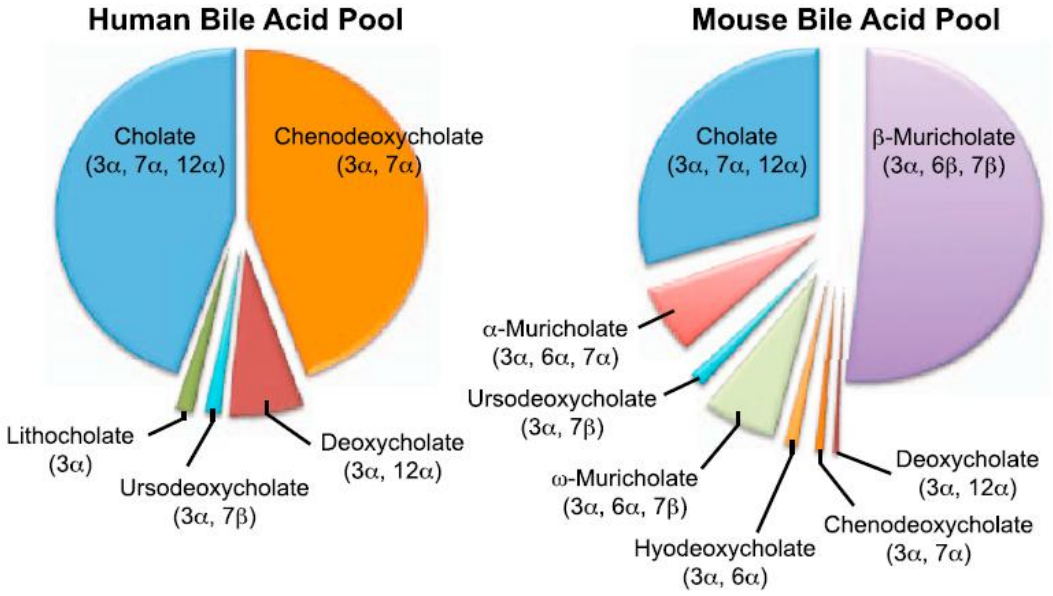

Figure 3.4- Bile acid composition in the human and mouse bile acid pool [3][341]. Humans and mice have remarkably different bile acid pool compositions. As the major primary bile acid, human mainly synthesize CA and CDCA, whereas mice have major CA and 6-hydroxylated MCAs made from CDCA.

MCAs are regulators of bile acid biosynthesis via a positive feedback mechanism in mice, which is quite different from the negative feedback mechanism that influences the biosynthetic process in humans [342]. Induction of CDCA synthesis in mouse liver results in the production of MCAs and UDCA [343]. With increasing amount of MCAs entering the small intestine, their intestinal absorption also increases, presumably via both ASBT and ASBT-independent mechanisms. In the enterocyte, MCAs exert FXR antagonistic effects, strongly reducing ileal FGF15 expression [342]. This depresses ASBT expression, which increases bile acid absorption enlarging the bile acid pool [344]; this pool will be further enriched with different MCAs by the hepatic conversion of CDCA. At the same time, in the hepatocyte, MCAs reduce CYP7A1 expression due to its local FXR antagonistic action and thereby increases hepatic bile acid synthesis. In parallel, reducing FGF15 expression from the gut to the liver may lead to suppression of hepatic CYP7A1 expression.

Muribile acids only exist in infant humans and then disappear from the circulation in the early stages of life because of colonization of the bowel by bacteria. Bacterial colonization starts in intrauterine life and increases during birth and the first days of life [345, 346].

The biosynthesis of muribile acids in human neonates may have a role in protecting the fetal liver against bile acid toxicity by reducing overall hydrophobicity while other detoxification pathways are under-developed [347]. In early neonatal development, an alternative (acidic) synthesis pathway is the major route for bile acid synthesis due to lack of CYP7A1 enzyme [348–350]. This enzyme is negatively correlated with MCA levels in human neonates [351, 352]. In this stage of human development, the presence of the *CYP2C70* gene makes it possible for synthesis of MCAs to occur in humans [353] because the *CYP2C70* gene leads to the formation of muribile acids from (conjugated) CDCA.

MCAs may offer therapeutic potential in some health conditions. For example, they are reported to reduce the absorption of cholesterol. Production of significant amounts of MCAs by human intestine and liver would contribute to beneficial metabolic effects such as reduced body weight, reduced liver lipids and improved insulin sensitivity. It has recently been found that increased conversion from conjugated CDCA to MCAs may be beneficial in the development and treatment of cholestasis and NASH [354]. βMCA is possibly available for NAFLD treatment by influencing bile acid and lipid homeostasis [355].

3.3 Chemistry of ωMCA

ωMCA (3α, 6α, 7β) is most abundant in the feces of male rats, and it is transformed from β-MCA by 6α-epimerization. While ωMCA is of considerable interest in this field of research, it is in short supply. The most complete set of synthetic procedures for production of ωMCA were early devised by the Toshio

group (Japan) in 1989 [356, 357].

ωMCA with an axial-equatorial cis glycol structure can be synthesized from naturally occurring bile acids. CDCA (3α, 7α) is an excellent starting material as its structure resembles the final product distinguished only by the C-6 hydroxyl group and CDCA is in abundant supply. Furthermore, it has previously been demonstrated that the administration of CDCA to mice promotes the formation of MCAs and CDCA should be at least one substrate for the formation of MCAs [320]. However, in the synthesis of muribile acids, problems arise around the introduction of the α-hydroxyl group at C-6' and how to convert 7α-OH into its 7β epimer.

The earliest synthesis of muribile acids was achieved by enzymes, in work reported by an Italian group [358]. In their work, selective oxidation and reduction of 7-hydroxyl bile acids was catalyzed by specific HSDHs in biphasic media. They found the regioselective oxidation of 7α-OH and following stereoselective reduction of the 7-keto group can afford muribile acids in high yields (Scheme 3.1).

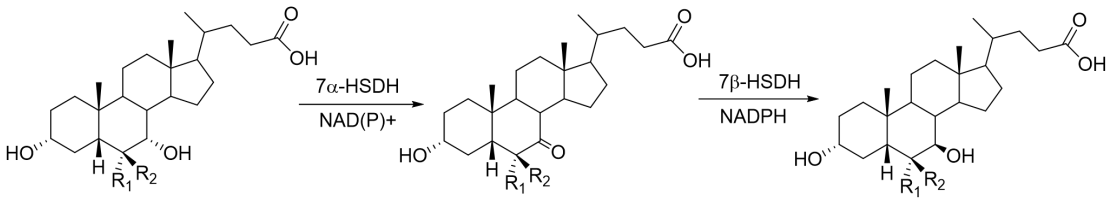

Scheme 3.1- The earliest published synthetic mechanism for producing muribile acids through enzyme catalysts [358]. The oxidation of 7-hydroxyl bile acids was catalyzed by the 7α-HSDHs, while the reduction was catalyzed by the NADP-dependent 7β-HSDHs (cofactor regenerated by the glucose-glucose dehydrogenase system). Here R_1 and R_2 represent H or OH, depending on bile acid species)

Afterwards, based on the idea of oxidation and subsequent reduction at C-7' position, Toshio's group started their ongoing program that leads to the synthesis of a complete set of all muribile acids [359]. ωMCA was prepared from

the CDCA through a series of steps to give 3α, 6α-dihydroxyl-7-oxo ester as the intermediate (shown in Scheme 3.2). It is the monohydroxylated form of CDCA. This intermediate compound was synthesized from CDCA via potassium chromate oxidation and subsequent bromination. Then the intermediate was further disilylated at C-3' and C-6' with the use of tert-butyl-dimethylsilyl chloride and the resulting ester was readily hydrolyzed. Finally, the hydrolyzed carboxylic acid was reduced by metal potassium in tert-amyl alcohol to afford the desired product after cleavage of the t-butyldimethylsilyl ether linkage.

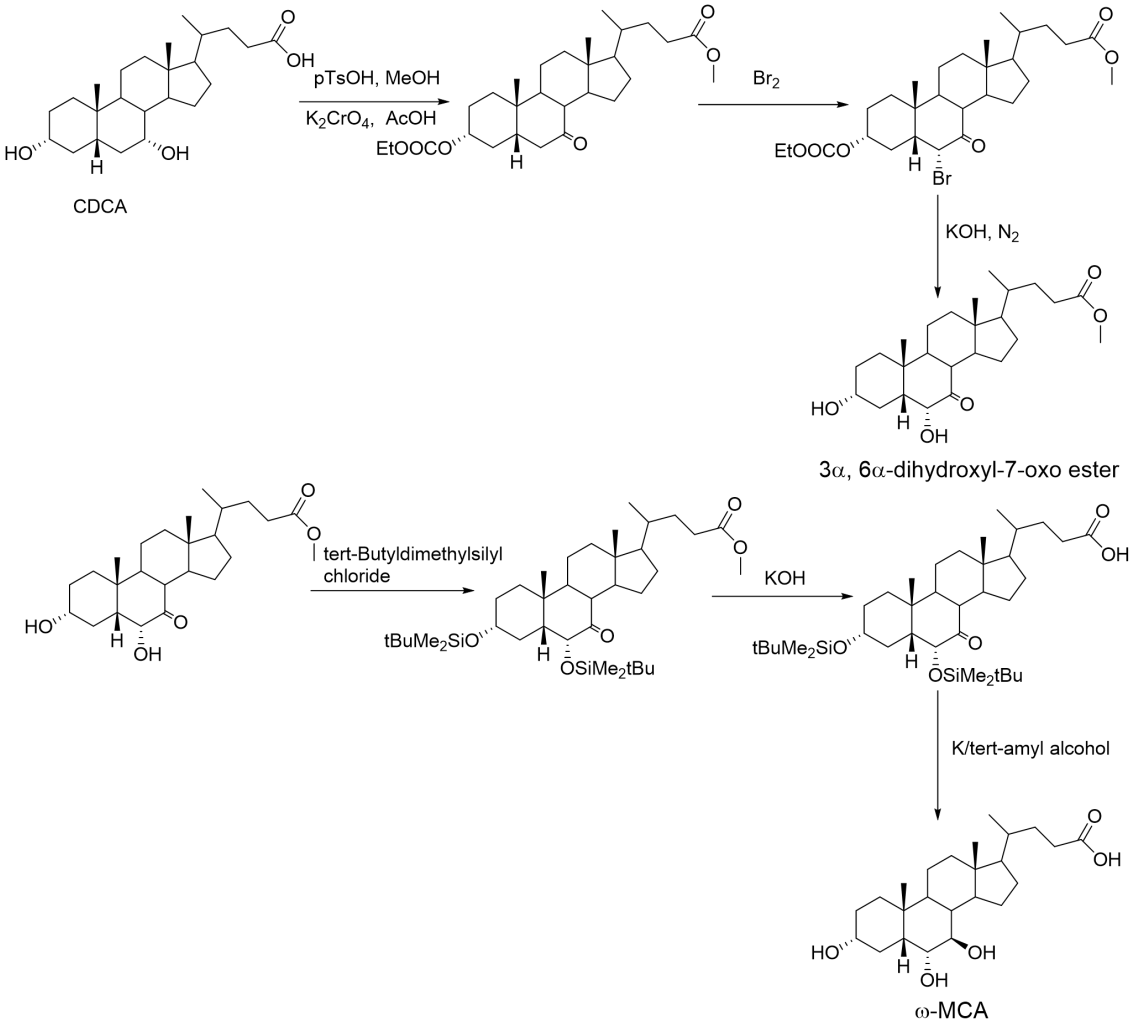

Scheme 3.2- The synthetic route for the synthesis of ω-MCA from CDCA by Toshio's group [357].

The synthetic approach seems inefficient because of the number of steps involved and the low overall reported yield (only 37% from the intermediate 3α, 6α-dihydroxyl-7-oxo ester). In 2013, a Korean research group reported the synthesis of αMCA, involving a nine step synthetic route from CDCA with an overall yield of 26%. They provided a viable synthetic route to produce high levels of high quality MCAs that afford these materials (shown in Scheme 3.3) [360]. In their study, the C-3' hydroxyl group was protected by an acetylation protecting group resulting in a significant improvement in yield.

The starting material CDCA underwent esterification at C-24', selective oxidation using NBS in aqueous sodium bicarbonate and subsequent bromination at C-6' to generate 3α-acetoxy, 6α-bromo-7-oxo-5β-cholanoate. This was subjected to conditions that caused elimination with treatment of zinc powder in acetic acid to provide 3α-acetoxy-5β-chol-6-enoate, which was then treated with 3-chloroperbenzoic acid in 1, 2-dichloroethane to afford 3α-acetoxy-6α, 7α-epoxide. The αMCA could be synthesized in a reasonable yield through reacting 6α, 7α-epoxide with boron trifluoride methyl etherate in DMF to give 3α-acetoxy-6β, 7α-dihydroxy-5-cholanoate which was finally hydrolyzed with 10% methanolic potassium hydroxide.

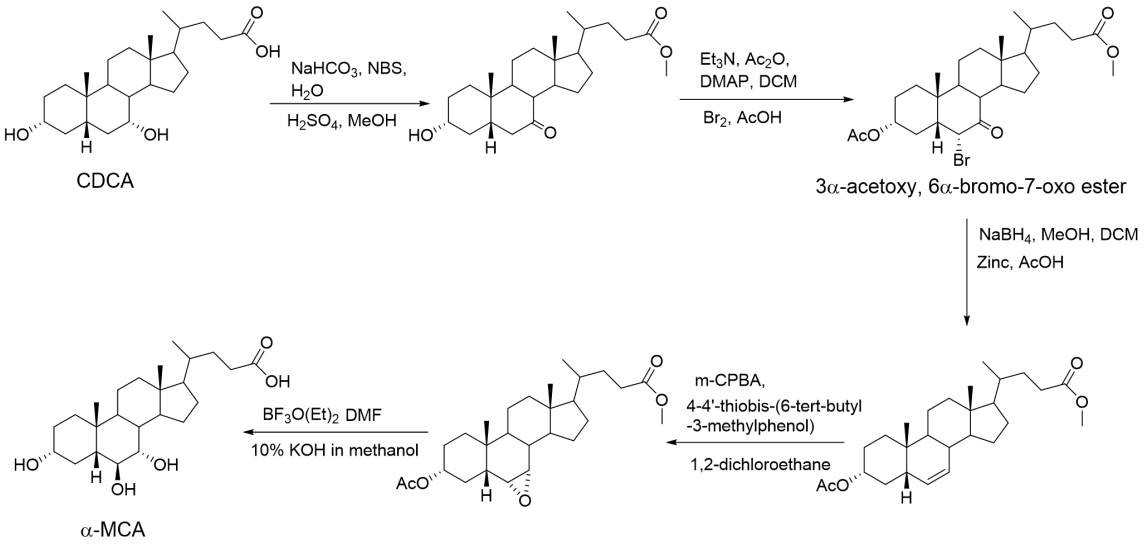

Scheme 3.3- The synthetic route for the synthesis of α-MCA from CDCA by Korean group [360].

Based on the synthetic strategies from previous work, we focused on designing a simpler and higher-yield synthetic approach for making ω-MCA in order to support further research on synthetic routes and support our collaborating research groups in the area of bile acid biology.

Scheme 3.4 below shows our synthetic strategy to produce ω-MCA and γMCA in the current work. These routes involved the selective introduction of the acetate protecting group at position C-3', PCC oxidation of the hydroxyl group to keto at C-7', bromination at C-6' making 6α-bromo derivatives followed by substitution to yield 6α-OH and the final selective reduction of 7-keto with $NaBH_4$.

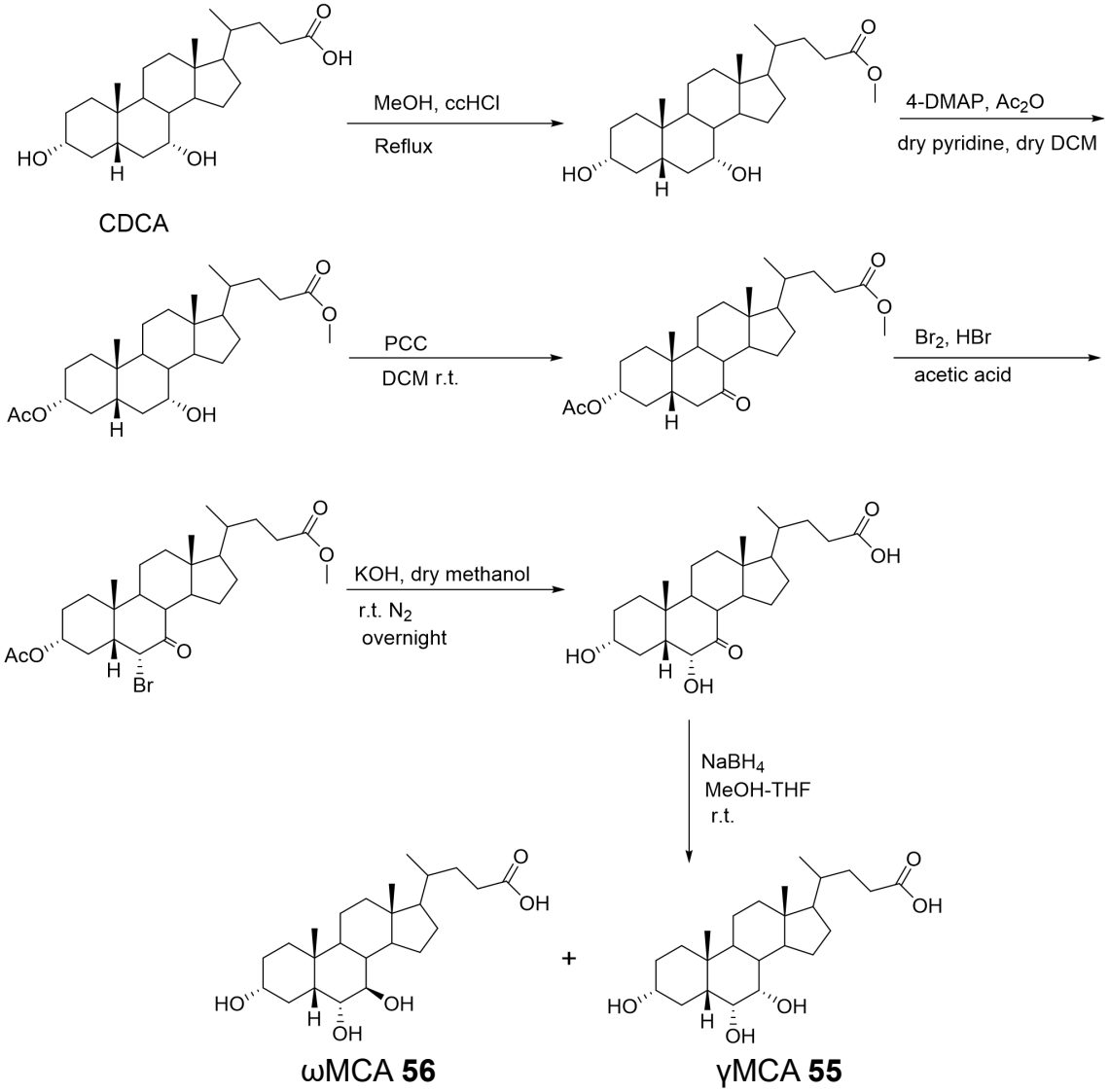

Scheme 3.4- The synthetic route for the synthesis of ωMCA 56 and γMCA 55 from CDCA. ωMCA was prepared in a sequence of six reaction steps from CDCA and in comparable yields (32%) compared with previous reports. This represents an improvement over previous published synthesis routes. The final yield could be improved by stereoselective reduction.

3.3.1 Selective protection of CDCA

This synthetic route begins with the protection of the carboxylic acid at C-24' and hydroxyl group at C-3'. The most efficient way to protect carboxylic acid is to form the ester linkage. The formation of methyl ester was carried out in MeOH by adding half eqv. of 37% HCl at reflux. After overnight reaction TLC showed the full conversion to methyl ester. The product **50** appeared with a higher R_f value on TLC plate (hexane: EtOAc=1:2). After workup, the CDCA methyl ester **50** was obtained as a white powder in high yield (97%).

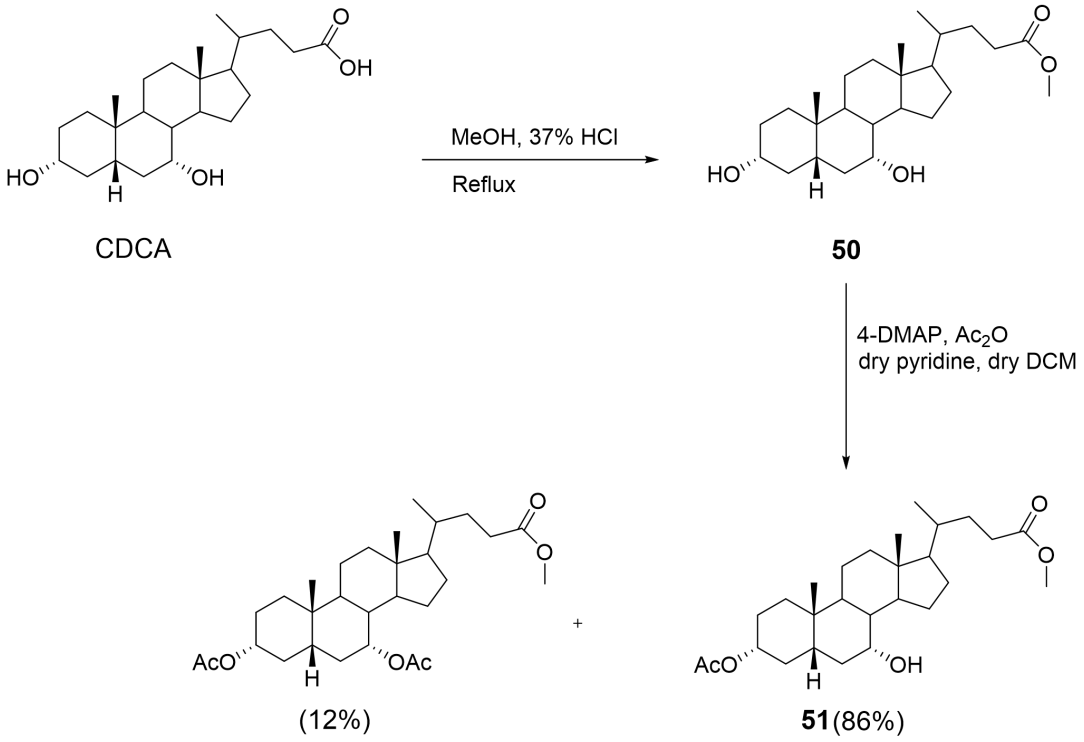

CDCA **50**

(12%) **51** (86%)

Scheme 3.5- Selective protection of CDCA at C-3' and C-24' position.

The selective protection of the 3α-OH required appropriate experimental condition in order to achieve regioselectivity. Selective protection of 3α-position was achieved by using Ac_2O in dry pyridine. The reaction was stopped by adding 1 ml MeOH after 16 h to prevent further acetylation at C-7' position. The formation of **51** was followed by TLC analysis using hexane: EtOAc=3:1 as the mobile phase. When the reaction finished, the crude product containing monoacetate and trace diacetate was purified by flash column chromatography to yield product **51** as a white foam (86%).

3.3.2 PCC oxidation of the CDCA 7-OH

After successful protection of CDCA at position C-3', an oxidation reaction was conducted to convert 7α-OH into 7-oxo with PCC. Compound **51** was dissolved in dry DCM and PCC was added 3 times over one hour at r.t. with subsequent stirring for 4 h. TLC showed the full conversion of compound **51**. The TLC plate was developed in hexane: EtOAc= 3:1 with vanillin solution used for detection. After workup, compound **52** was recovered as a white foam with 98%-99% yield.

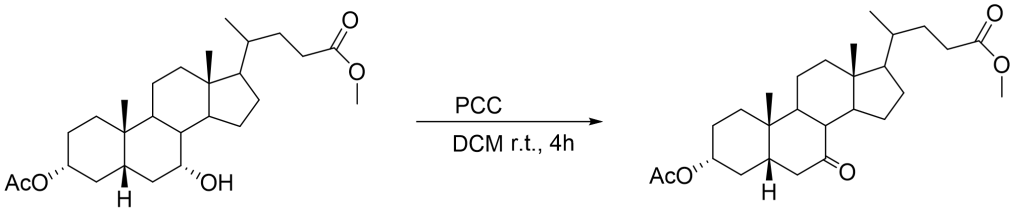

51 **52**

Scheme 3.6- Oxidation of 51 with PCC.

3.3.3 Bromination at C-6' position

The most critical stage in this synthetic route was the introduction of a 6α-OH to the steroid ring. In the bromination of 7-keto-steroids, it has been known that the bromine atom entered the position of C_6 [361]. The bromination of compound **52** in acetic acid containing 48% hydrobromic acid was attempted at RT by

dropwise addition of bromine. The reaction proceeded for overnight. A mixture of two isomers of 6-bromo-7-oxo could be detected on TLC (hexane: EtOAc= 4:1 with vanillin solution). The 6-bromo-7-keto is a secondary alkyl bromide which should follow SN1 mechanism on substitution, which means it would give two isomers (the ratio of two isomers is quantified by the integration of the signals on NMR) [362]. Column chromatography was not necessary in this step as the next step will produce two isomers as well.

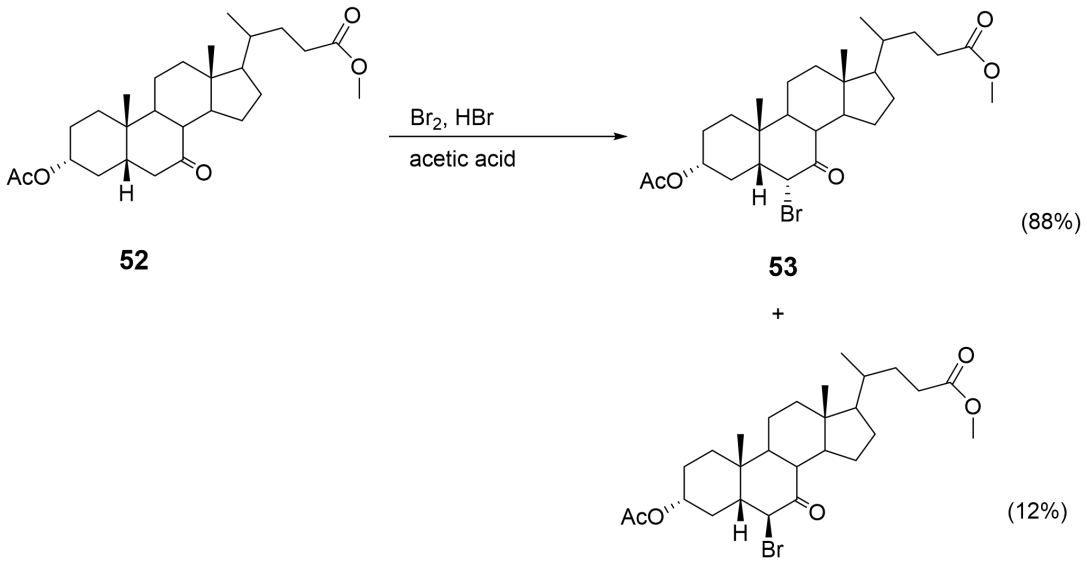

Scheme 3.7- Bromination of 52.

3.3.4 Alkaline hydrolysis to obtain 3α, 6α-dihydroxyl-7-ketoetiocholanate 54.

KOH pellets were ground into powder and added to a stirred suspension of two 6-bromo-7-keto isomers in dry methanol. The mixture was stirred at RT overnight under N_2. The mixture turned brown after adding KOH. A mixture of what transpired to be desired product **54** and trace side product 3α, 6β-dihydroxyl-7-ketoetiocholanate could be detected on TLC plate. After workup and column chromatography (hexane: EtOAc= 1:3), **54** was recovered with 91% yield. The NMR of the major spot on TLC is shown in Figure 3.5 below.

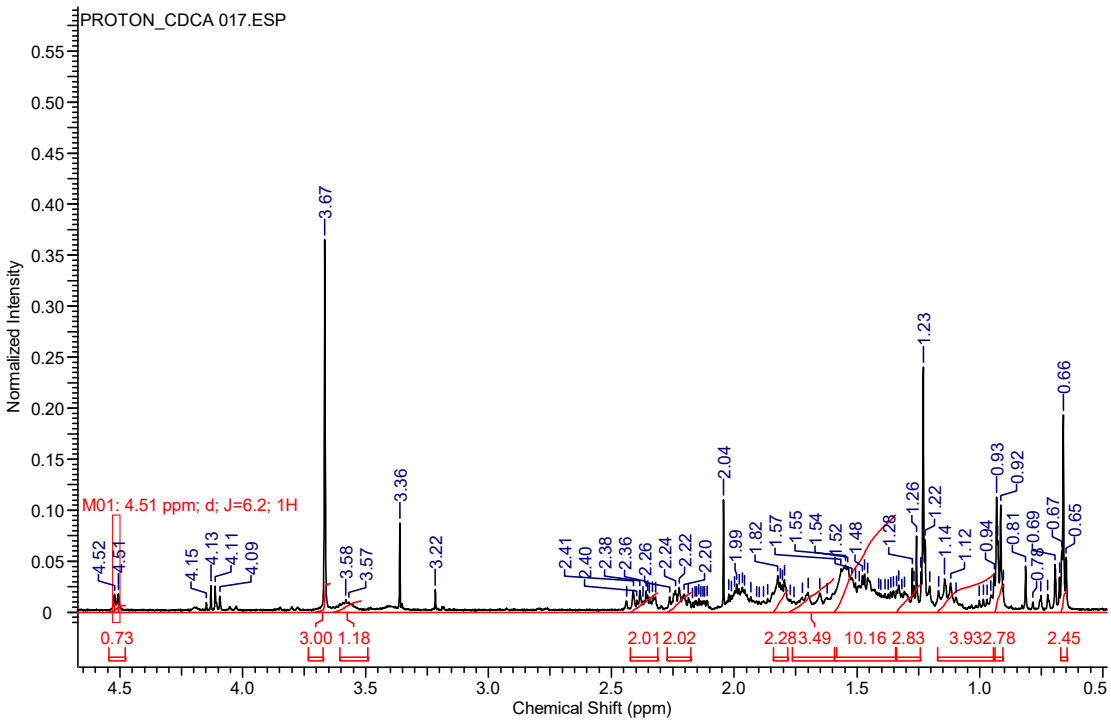

Figure 3.5- The NMR of 3α, 6α-dihydroxyl-7-ketoetiocholanate 54.

Next it was necessary to distinguish between the 6α-OH isomer from NMR. The CH of the 6α-OH isomer is equatorial, and its dihedral angle to the 5β-H is large (over 90°), whereas the CH of the 6β-OH isomer is axial and it is near to being co-planar with 5β-H with the dihedral angel around 0°. Based on the Karplus equation/Karplus graph, J value= 6.2 Hz in the NMR looks consistent with a large angle of perhaps 130° in the 3D modelling of the alpha compound, whereas a very small angle would have J value around 10 Hz. Therefore, the major product obtained was assigned as 3α, 6α-dihydroxyl-7-ketoetiocholanate **54**.

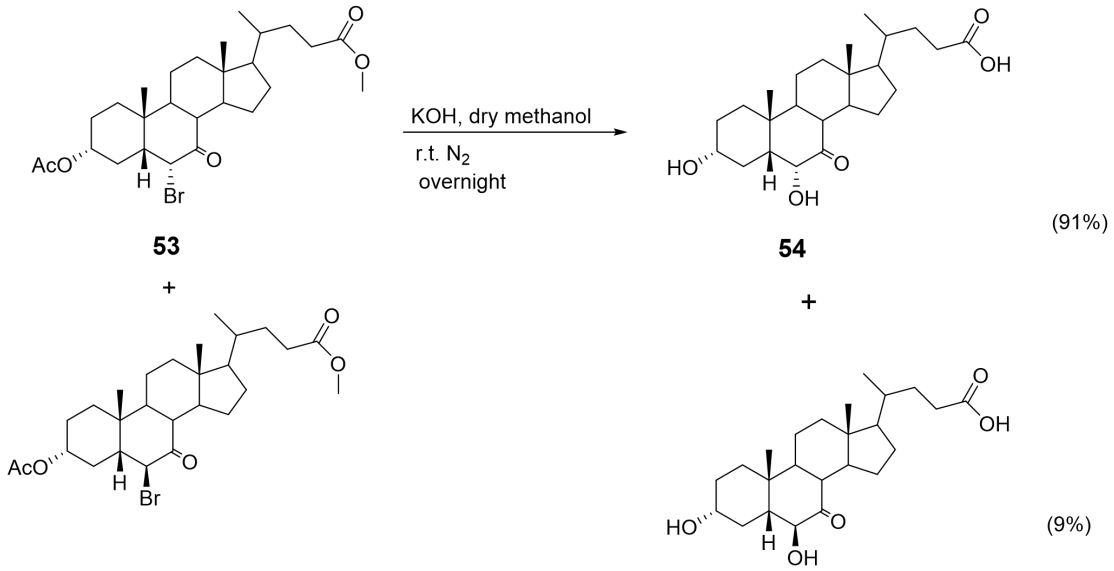

Scheme 3.8- Alkaline hydrolysis of 53 with KOH/MeOH in inert condition. This method yields two different isomers, with compound **54** the main product.

3.3.5 Reduction of compound 54 with $NaBH_4$

As discussed in Chapter 2, there are many reducing agents described in the literature that can achieve reduction of steroidal 7-ketones. $NaBH_4$ is the cheapest and most useful in this case. Reduction of the 7-oxo with $NaBH_4$ was quite feasible. Compound **54** was dissolved in a MeOH-THF mixture at 0°C and then $NaBH_4$ was added with stirring for 30 min and the reaction was kept under RT overnight. TLC analysis showed the disappearance of starting material and formation of two different isomers after 24 h. After the work up, the crude product was purified by flash chromatography to give 3α,6α,7β-trihydroxy acid (ω-MCA, 32%) and 3α,6α,7α-trihydroxy acid (γ-MCA, 45%). Some of the final product got lost in the aqueous phase during the aqueous workup due to high product polarity.

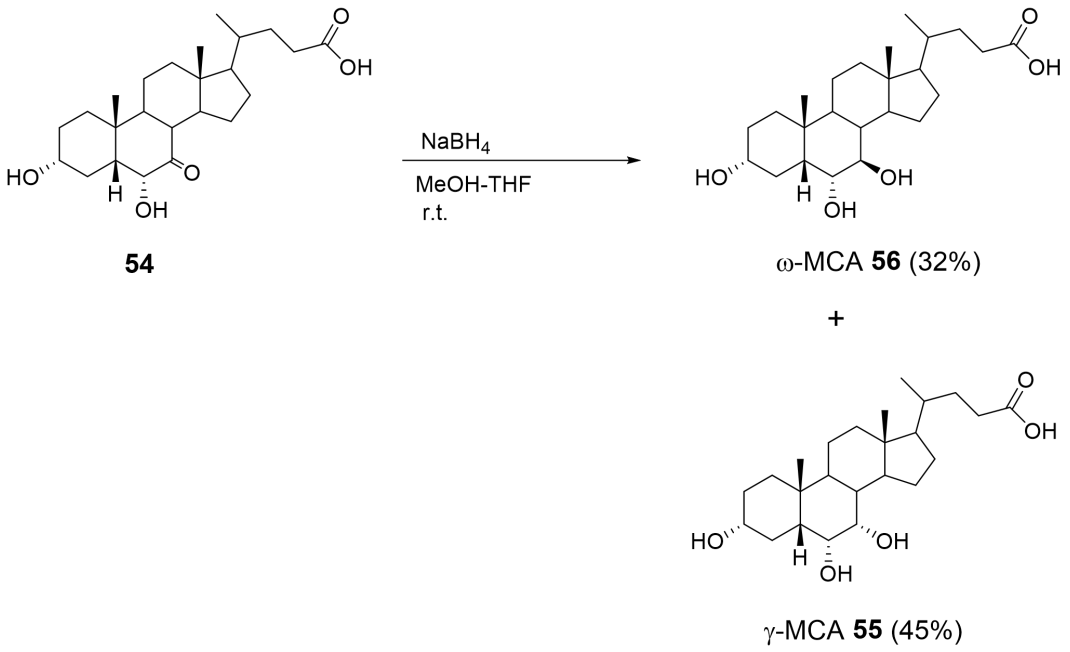

Scheme 3.9- $NaBH_4$ reduction to yield two final muricholic acids, ω-MCA and γ-MCA.

Both ω-MCA and γ-MCA are produced after nonselective $NaBH_4$ reduction and they were characterized with NMR. As can be seen from two NMR spectra below, the isomers show high similarity. A double-doublet at 5.10 ppm for both arises from the 6α-OH. A multiplet at 4.58 ppm is due to the 3α-OH. The main difference between them is that there is a singlet peak at 3.90 ppm (Panel A) and a triplet peak at 5.21 ppm (Panel B). The spectra have been assigned based on the chemical shifts of the alpha and beta protons at C-7' in γMCA and ωMCA respectively.

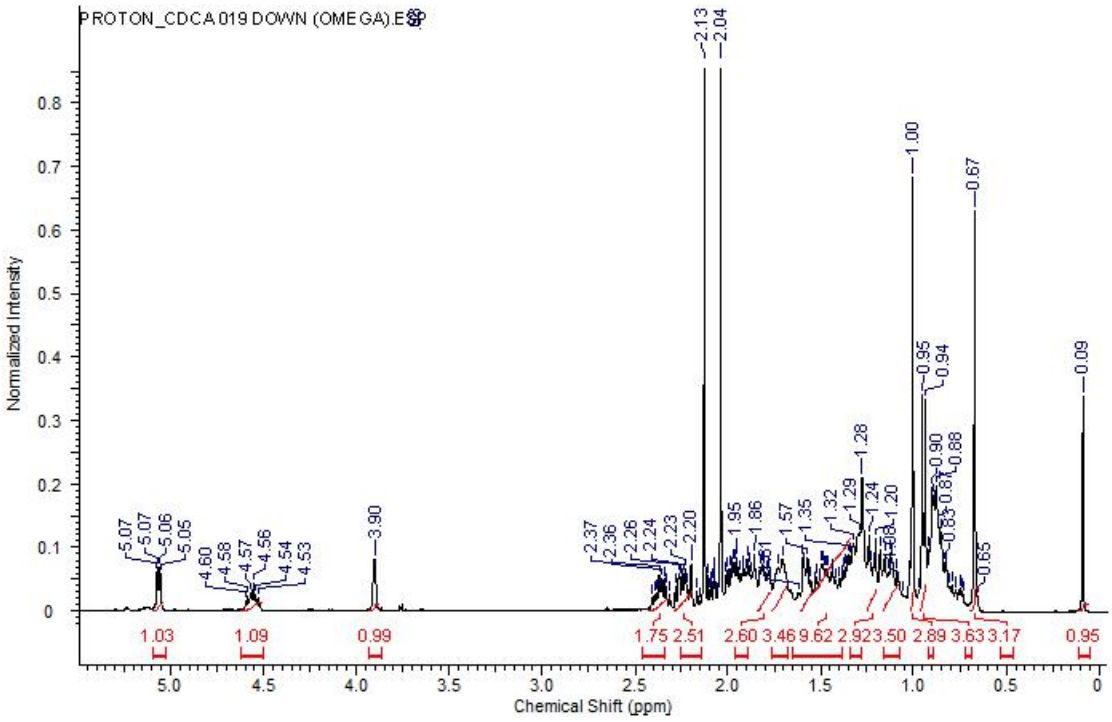
PROTON_CDCA 019 DOWN (OMEGA).ESP
Normalized Intensity
Chemical Shift (ppm)

(A)

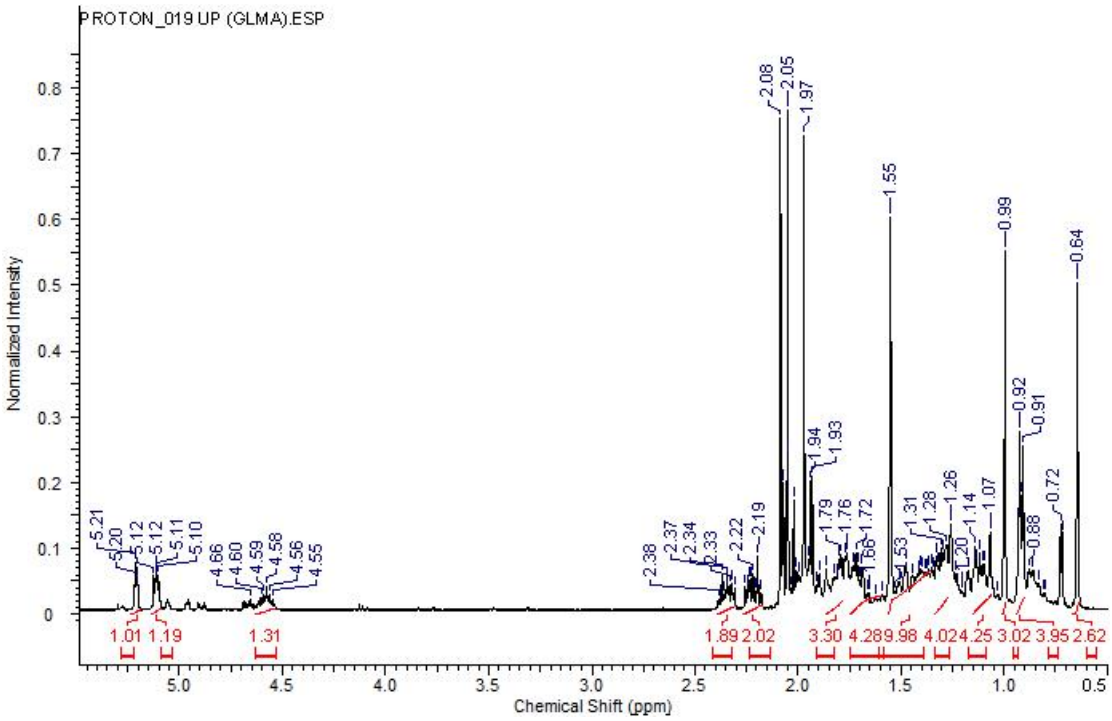
PROTON_019 UP (GLMA).ESP
Normalized Intensity
Chemical Shift (ppm)

(B)

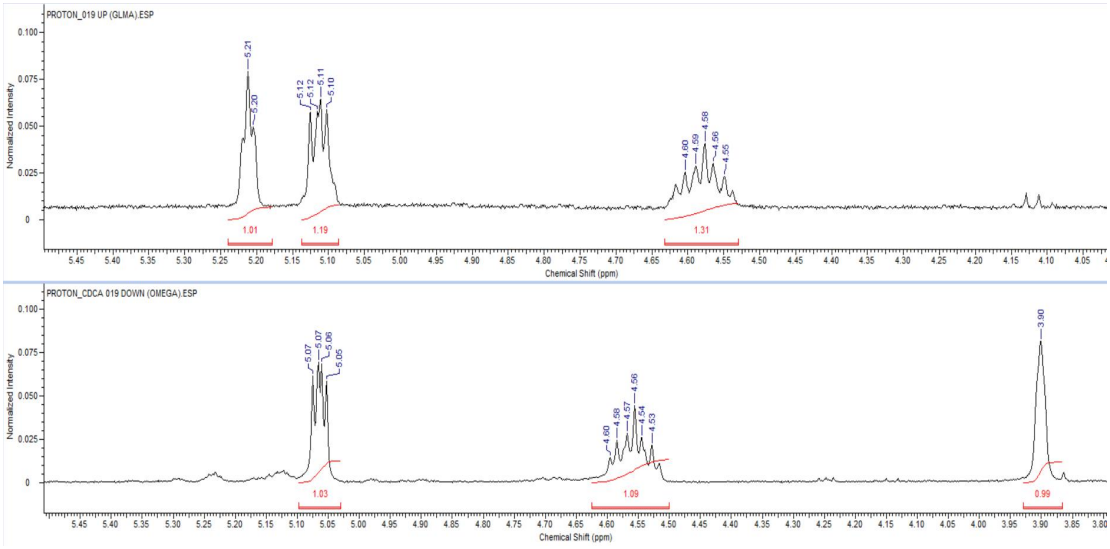

(C)

Figure 3.6- Panel A represents the NMR of ω-MCA (3α, 6α, 7β) and panel B is assigned to γ-MCA (3α, 6α, 7α). Panel C is the inset of 3.5-5.5 ppm of two spectrum.

The final yield for both MCAs was higher than that reported by the Toshie group. The yield of ω-MCA could in principle be further improved by applying L-selectride reduction in the final step to achieve better stereoselectivity. Based on the conclusion from Chapter 2, L-selectride reduction produces predominately bile acids with an axial hydroxyl group, ω-MCA in this case. Future work could focus on further chemical optimization of the synthetic process to improve yields in the final step and overall yield and provide optimal quantities of this valuable material for further biological studies.

3.4 Cytoprotective effect of muribile acids

Bile acids with hydrophobic properties are known to cause cytotoxicity due in part to their amphilicity and related membrane activity and detergent effects [363]. On the other hand, hydrophilic bile acids such as UDCA have been found to exert therapeutic effects partly attributable to a blockade of cytotoxic hydrophobic bile acids [364, 365]. It is well known that cytoprotective and cytotoxic properties of bile acids correlate well with hydrophilicity and hydrophobicity,

respectively. CA, hyocholic acid and even the hydrophobic CDCA exhibit cytoprotection against DCA induced cytotoxicity [366]. It is likely that the cytotoxicity of the hydrophobic bile acids is reduced by a lower concentration of more hydrophilic bile acids under certain circumstances, but the precise mechanism of this cytoprotection needs to be further investigated.

Submillimolar concentrations of cytotoxic bile acids (such as DCA) may induce cell death via apoptosis as they disrupt the ordering of the membrane [367]. DCA is known to cause DNA fragmentation, oxidative stress, Golgi fragmentation and apoptosis [368] and pretreatment with UDCA and TUDCA inhibits DCA induced apoptosis and Golgi fragmentation in colon cancer cells [369]. UDCA and its taurine conjugate TUDCA have been found to diminish the overall toxicity in biological and animal studies and they exhibit choleretic and cytoprotective properties *in vivo* and *in vitro*. Although the exact mechanism of cytoprotection is not entirely clear (see below), their effect seems to be achieved by blocking the interaction of Bcl-2-associated X protein, Bax, which plays a key role in apoptosis (detail will be discussed in Chapter 4) [370].

Besides, DCA increases the overall hydrophobicity of the bile acid pool, decreases hepatic insulin signaling and increases ER stress signaling. It has been found that cholestasis promotes ER stress in the liver. The ER is an important intracellular site for the synthesis of secretory and membrane proteins, modulating their folding, transport and degradation, while ER stress is associated with the improper protein folding and the accumulation of misfolded proteins. The accumulation of these proteins is harmful to cells. Bile acids can modulate ER stress and in turn induction of ER stress suppresses bile acid synthesis and ER stress is an important factor in the development of obesity-related inflammation, insulin sensitivity and type 2 diabetes and involved in a wide range of hepatic diseases including cholestatic liver diseases. Hydrophilic bile acid subtypes, such as TUDCA, have been shown to improve insulin sensitivity by decreasing ER stress [371]. UDCA alleviates ER

stress by improving intracellular osmotic balance and glucose homeostasis [372]. These observations suggest that bile acid hydrophobicity influences ER homeostasis regulation. Recent studies found that TαMCA, a rodent specific bile acid, has a potential to lower ER stress level, similar to TUDCA [373]. These observations aroused our interest in further investigation on the cytoprotection effect of muribile acids and their therapeutic use.

It has been found that TUDCA and TβMCA exert cytoprotective effects against DCA or CDCA induced toxicity because of their optimal hydrophilicity [374] and these cytoprotective bile acids have no harmful effect towards membrane properties [375]. In addition, βMCA and its conjugates can prevent liver damage, cholestasis caused by cytotoxic bile acids [376, 377]. Muribile acids are found to be even more hydrophilic than UDCA and TUDCA the question arises; will these more hydrophilic muribile acids reduce ER stress and exhibit possible cytoprotective effects.

The objective of this work was to determine the cytoprotective effect of synthesized muribile acids, at physiologically relevant concentrations. Briefly, liver cells of human origin were pretreated with the muribile acids before addition of cytotoxic bile acids.

In order to study the cytoprotective property of the muribile acids, the Alamar Blue assay method was used to determine the % cell viability here. The Alamar Blue assay is a fluorometric method for detection of mitochondrial activities of cells ranging from bacteria to mammalian cells and it is a simple, reliable, stable and nontoxic method working on both attached and suspended cells [378]. Moreover, cells are not destroyed during the test procedure. Mainly for these reasons, the Alamar Blue assay is considered superior to many classic tests for determining % cell viability such as the MTT test [379].

The interpretation of results requires some care and insight into their biochemical meaning. The application of the Alamar Blue assay approach here

is in the context of many studies carefully characterize the effects of bile acids in the biologically relevant concentrations. Cells were harvested in log phase of growth and cell counting was done to optimize the cell density into 1×10^4 cells/ml. Cells were then pretreated with 200 μM muribile acids for 24 h before adding cytotoxic bile acid, DCA, in this case in order to compare the difference with treating only with muribile acids or DCA over the same period. Stock solutions of the different bile acid compounds were prepared in DMSO and these were diluted to 200 μM with supplement free medium. The % cell viability was measured after incubating for 48 h and it was calculated versus vehicle treated control, which was treated with same amount of DMSO (1%). Each experiment was carried out in triplicate and repeated three times to get nine data points in total for each test solution. The data are presented in Figure 3.7.

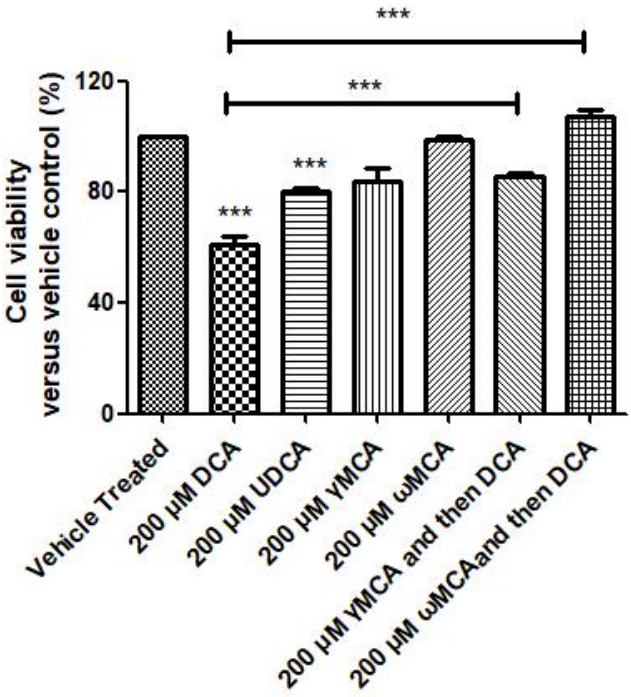

Figure 3.7- A measurement of toxicity of different bile acids with Alamar Blue assay method. Huh-7 cells were seeded onto 96 well plate at a density of 1×10^5 cells/ml, and then treated with muribile acids at 200 μM for 48 h. Cells were then treated with 10 μl Alamar Blue reagent in an amount equal to 10% of the volume in the well and incubated for 2 h in the dark. The assay was normalised to 1% DMSO vehicle control and absorbance of each well was read on a VERSAmax Microplate Reader (Molecular Devices, Sunnyvale, CA, USA) with excitation wavelength at 530–560 nm and emission wavelength at

590 nm. Values are expressed as mean ± SEM of three triplicate experiments, * $p<0.05$, ** $p<0.01$, *** $p<0.001$ as determined by one way ANOVA with Tucky's post test.

Results of this assay were consistent with our previous experience with DCA. Treatment at 200 μM resulted in around 40% cell death in Huh-7 cell cultures. Muribile acids themselves do not exhibit significant toxicity towards Huh-7 cells after incubating for 48 h consistent with their hydrophilicity. Indeed their toxicity is even lower than hydrophilic UDCA, which is established as a cytoprotective agent. Pretreatment with muribile acids (200 μM) for 24 h significantly reduced cell death caused by DCA. At 200 μM ωMCA completely protected cells from loss of viability in response to 24 h DCA 200 μM treatment and γMCA had some effect in cell protection towards Huh-7 cells. The data indicate that pretreatment of cells with muribile acids particularly ωMCA is cytoprotective against cytotoxic bile acid insult.

These results indicate that ωMCA has efficient cytoprotective effects against DCA-induced cell death. Its superiority of the beta isomer is consistent with the observations of UDCA and TUDCA that have been examined by Gilmer's group. Both UDCA and TUDCA contain a 7β-hydroxyl group suggesting that this is important for cytoprotection. Although the cytoprotective properties of muribile acids have been found against DCA insult, the nature of their protective effect is still unclear. Further work carried out to explore the mechanistic basis for the cytoprotection by ωMCA is described below.

3.5 Mechanism of cytoprotective effect of ωMCA

The cytoprotective effect of UDCA and TUDCA has been recognised for many years and continues to be extensively investigated. One of the preferred explanations is that they counteract ER stress. As described earlier, this is a form of cellular stress associated with the overwhelming of protein folding machinery. It can be simulated *in vitro* by treating cells with DCA or with

tunicamycin (TM). As seen already DCA can induce cell death and this is partly due to prolonged ER stress. TM also induces cell death through ER stress.

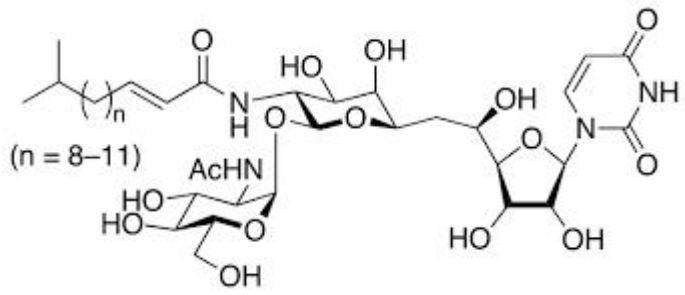

Figure 3.8- Chemical structure of TM [380]. TM is a nucleoside antibiotic complex isolated from *Streptomyces lysosuperificus.* Its activity is attributed to a mixture of compounds, each of which contains one mole of fatty acid with various carbon chain lengths. TM blocks the N-linked glycosylation of proteins and DNA synthesis, commonly used in inducing the unfolded protein response (UPR) [381, 382], a group of signal transduction pathways responding to ER stress.

TM, a naturally occurring antibiotic, interferes with protein N-linked glycosylation causing proteins to be incorrectly folded in eukaryotic cells and directly leading to ER stress, a key disease driver [383]. ER is the site of protein synthesis and folding found in all eukaryotes. ER stress is caused by an imbalance between the demand for protein folding and the capacity of the ER for protein folding. In persistent ER stress, cells undergo apoptosis. As an inducer of ER stress, TM causes apoptosis in liver cells [384] (Figure 3.9).

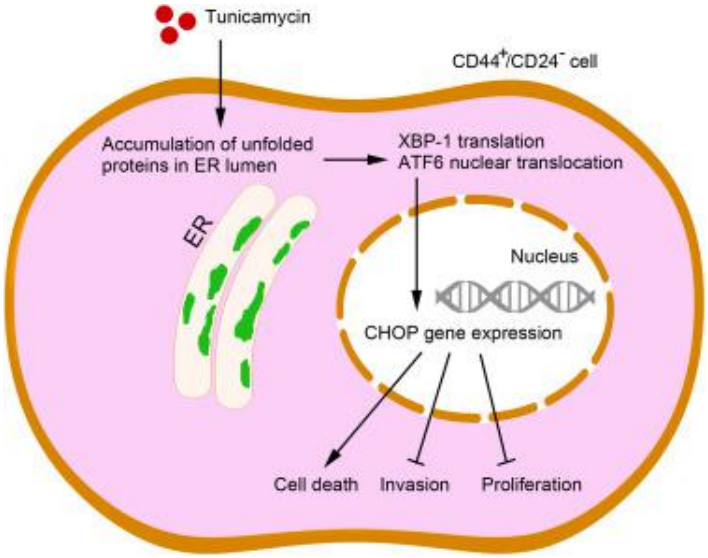

Figure 3.9- Model of TM-induced ER stress [385]. TM causes accumulation of unfolded proteins in the ER inducing UPR in the cell. This is followed by the induction of CHOP protein, which provokes cell death via different pathways. CHOP is a proapoptotic factor that provokes programmed cell death via apoptosis.

Since ωMCA reduces the extent of apoptosis induced by DCA we tested its ability to protect Huh-7 cells from apoptosis caused by TM. As shown in Figure 3.10, TM induced around 60% cell death in Huh-7 cells when they were exposed to it at 5 μM. When the cells were co-incubated with ωMCA, substantial cytoprotection was observed and cell viability was restored.

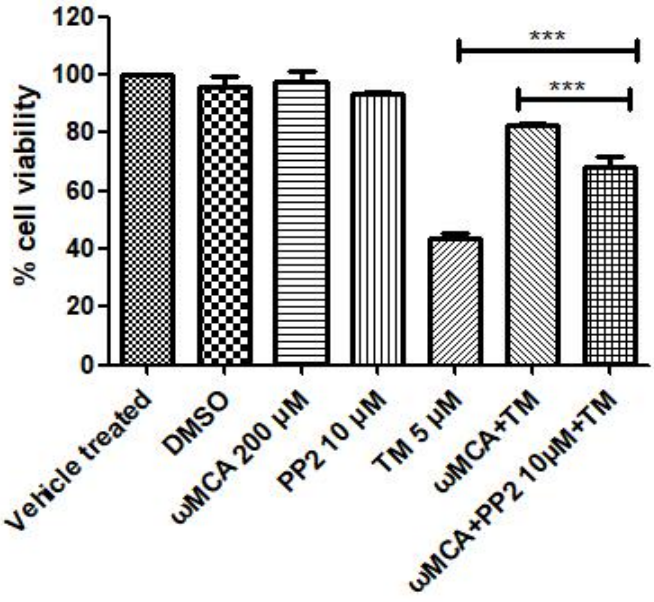

Figure 3.10- Measurement of cytoprotective effect caused by ωMCA and SRC inhibitor PP2. Huh-7 cells were seeded onto 96 well plates at a density of 1×10^4 cells/ml, and then treated with PP2 at 10 μM for 3 h before co-incubation with ωMCA at 200 μM and TM at 5 μM for 8 h. Cells were then treated with 10 μl Alamar Blue reagent in an amount equal to 10% of the volume in the well and incubated for 2 h in the dark. The assay was normalised to 1% DMSO vehicle control and absorbance of each well was read on a VERSAmax Microplate Reader (Molecular Devices, Sunnyvale, CA, USA) with excitation wavelength at 530–560 nm and emission wavelength at 590 nm. Values are expressed as mean ± SEM of three triplicate experiments, * $p<0.05$, ** $p<0.01$, *** $p<0.001$ as determined by one way ANOVA with Tucky's post test.

Further mechanistic studies were performed by Dr Nadhim Hante in the Gilmer lab. Cytoprotection by UDCA and TUDCA is speculated to be due to activation of cell surface integrin receptors that trigger activation of FAK and SRC proteins. SRC, a non-receptor protein tyrosine kinase, localizes to cellular membranes, in particular the plasma membrane (Figure 3.11). It plays an important role in regulating signal transduction by cell surface receptors and is involved in numerous essential functions to maintain cellular homeostasis such as regulation of cellular migration, proliferation, adhesion and survival, and other fundamental cellular processes. Nadhim had shown that TUDCA is unable to express its cytoprotective effect against TM when the members of the network of proteins related to integrin αVβ1 are inhibited. This includes SRC proteins that are directly downstream of the integrins. Inhibition of SRC proteins by PP2 diminishes TUDCA protective effects against apoptotic insult by TM.

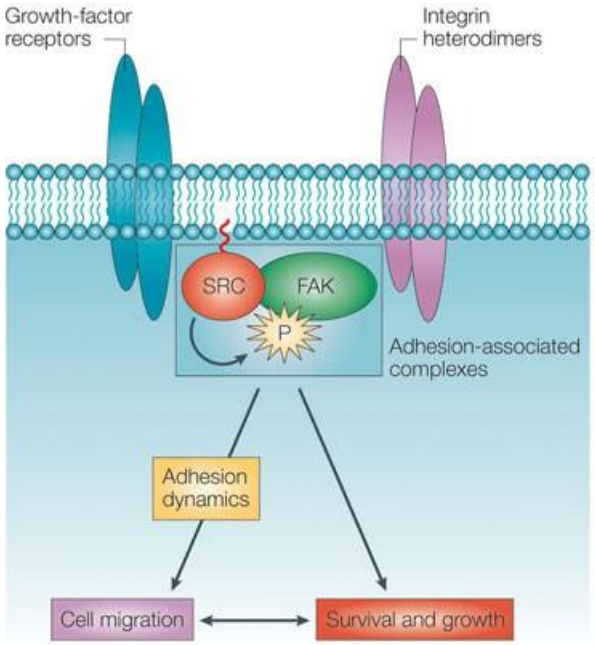

Figure 3.11- SRC as a cell surface signal integrator in cell survival and growth [386]. SRC binds to growth factor receptors on the cell membrane and focal-adhesion kinase (FAK) to integrins and they bind to each other. SRC binding to growth factor receptors is generally considered to be important and it involves in adhesion regulation, as well as in growth and survival signaling.

We speculate, that like TUDCA, the polar muribile acid stimulate the cell surface integrin or other growth factor receptors. This leads to increased cell survival signaling that is able to overcome the apoptotic effect of TM. When the SRC inhibitor PP2 is present, ωMCA is not as protective. This is consistent with ωMCA stimulating SRC directly or more likely, indirectly, through integrins or growth factor receptors.

3.6 Conclusion and future work

Hydroxylation at the C-6 position of the bile acid changes the polarity of bile acids, making compounds more hydrophilic and water soluble. This decreases their cytotoxicity, a feature that is consistent with their presence in human neonates where liver detoxification processes are underdeveloped and prone to significant ER stress. Murible acids are interesting substances but are inaccessible and expensive.

This work has provided some improvements to the synthesis of key muribile acids and valuable observations in relation to their *in vitro* cytoprotective potential. With assistance from the Gilmer group, it was also shown that protection by muribile acids involves SRC protein and in this respect, their protective mechanisms may be some commonality with UDCA/TUDCA. For future work, the biochemical properties of the compounds in the series will be further characterised and the cytoprotective effects further investigated. The new synthetic approaches exemplified in this work will improve accessibility and availability of the compounds, potentially supporting their therapeutic developments in indications such as NASH and other liver diseases where ER stress and/or cell death plays a significant role.

Chapter 4. Toxic bile acid analogues related to UDCA

Studies over the past two decades have provided a better understanding of the mechanisms underlying the cytotoxic and the beneficial effects of bile acids. Exposure to bile acids at high concentrations primarily causes cell death. Bile acids are generally toxic to cells though cytotoxicity is influenced by bile acid structure and their degree of hydroxylation and conjugation. This chapter focuses on the amplification of bile acid toxicity through a series of synthetic and biomedical studies involving structurally modified bile acids.

The mechanism of bile acid-induced cell death is incompletely understood. It appears to relate to the generation of ROS within cells. Bile acids are amphipathic compounds sometimes described as facially amphipathic as they have both hydrophilic and hydrophobic faces. The facial amphilicity of bile acids enable them to promote detachment of the phospholipids and proteins within biological membranes in the concentration 1–10 mM. This leads to the disruption of cell membrane. The permeability of the cell membrane increases greatly and this causes cell death. Lower concentrations of bile acids promote cell death through apoptotic pathways while high concentration of bile acids induce cellular necrosis. Again there is a strong structural dependence with hydrophilic bile acids such as CA and UDCA being least cytotoxic, though even these so-called non-toxic bile acids are still capable of inducing apoptosis and necrosis. It is important to improve our understanding of bile acid toxicity because of its contribution to disease– intestinal carcinogenicity and hepatoxicity in cholestasis in particular.

4.1 Introduction

4.1.1 ROS

ROS, defined as oxygen-containing reactive chemical species, is a byproduct of aerobic metabolism. The main members of ROS family include non-radical ROS like H_2O_2 and free radical ROS like $O^{\cdot -}_2$, $OH^{\cdot}$. Free radical ROS is highly active because of the unpaired free radicals [387]. ROS has long been

associated with the cancer treatment as high intracellular concentrations of ROS cause cancer cell apoptosis [532]. Generating ROS provides a mechanistic basis that is common in non-surgical therapeutic interventions in many cancer treatments.

ROS may arise from exogenous sources or within cells. The majority of ROS species are generated inside the mitochondria. ROS is converted from superoxide ($O_2^{\bullet-}$), which results from the reactions between electrons leaking from the mitochondrial respiratory chain and oxygen. ROS has various biological functions including modulating cell proliferation, differentiation, survival and death [388]. It controls many signal transduction pathways by modifying the protein structures and is involved in signaling cell growth. ROS species also regulate enzyme activity and change the functions of many biological molecules by causing oxidative modifications. Short term responses to ROS protect cells by adjusting gene expression to prevent harmful effects and even inhibits apoptosis via activating NF-κB signaling. However, long-term exposure to elevated levels of intracellular ROS has detrimental effects. While a slight increase of the ROS level only causes short-period cellular alteration while a significant increase of ROS results in oxidative DNA damage including mismatch DNA repair within the p53 gene for example. Such oxidative DNA damage may result in cell death via the induction of apoptosis or necrosis. The accumulation of DNA mutations associated with protracted exposure to ROS and increases the risk of progression to cancer. ROS generation is a common feature associated with all phases of carcinogenesis including initiation, promotion, and progression. In the meantime, ROS damages various cellular biological macromolecules such as lipids, cellular proteins and DNA [389], if they accumulate to threshold concentrations. The diversity of molecular damage to key cellular components may lead to cell cycle arrest, replication error and genetic instabilities, all of which are associated with the development of cancer.

Excessive intracellular ROS levels are toxic to cancer cells. Elevated intracellular oxidative stress leading to a lethal accumulation of ROS induced DNA and other molecular damage can arise via exogenous agents such as ionizing radiation. This is the principle underpinning the targeted delivery of radiological cancer therapies. The selective induction of lethal levels of intracellular ROS species via directed ionizing radiation therapy can kill cancer cells while, reducing damage to adjacent normal cells [390].

Oxidative stress is an important trigger of cell death and has been associated with the development of cholestatic liver injury. Bile acids have been proved to promote the generation of ROS in different cell lines. Retention of hydrophobic bile acids inside hepatocytes disrupts cell membrane through their detergent properties and helps the generation of ROS in hepatic mitochondria. This is considered a major cause of liver disease [391] and cancer development. Bile acids induced apoptosis results from the oxidative stress with increasing ROS level. Bile acids are likely to generate ROS from multiple sources. Another source of ROS production is bile acid induced damage to mitochondria which causes the electron transport chain to withdraw one electron from O_2 to form superoxide. This is typically involves activating plasma membrane enzyme, such as NADPH oxidases.

Synthesizing bile acid compounds which can generate ROS and increase ROS levels in cancer cells directly or indirectly via ROS mediated cytotoxic molecules, is an important focus of this chapter. One mechanism involves the reaction of ROS with the free radical nitric oxide to produce peroxynitrite ($ONOO^-$). Peroxynitrite is very toxic and oxidizes a wide variety of cellular macromolecules, including DNA and proteins (Figure 4.1) [392]. This is an oxidizing and nitrating molecule that has been associated with cancer and other acute diseases.

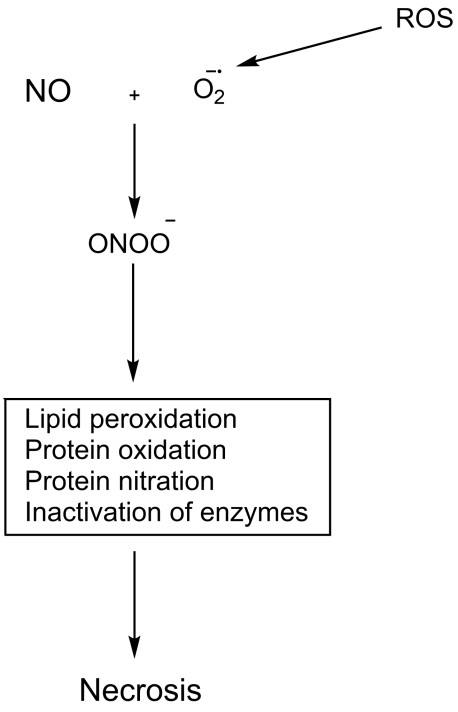

Figure 4.1- The mechanism of generating peroxynitrite inside cells. It is generated by the interaction between nitric oxide ($NO^{\cdot}$) and superoxide ($O_2^{\cdot-}$) [393].

Mitochondria are the major site of ROS production in mammalian cells. A significant quantity of mitochondrial ROS generation takes place at the electron transport chain (ETC) [394]. Mutations in mitochondrial genes encoding components of the electron transport chain can result in increasing ROS levels. Accumulation of ROS in the mitochondria, whether from mutations or the influence of bile acids, promotes the opening of the mitochondrial permeability transition pore (MPTP) in the inner mitochondrial membrane and subsequent matrix swelling and outer membrane fracture. This is followed by the release of the apoptotic signaling molecule cytochrome c (a terminal oxidase component of the ETC) [395, 396]. The mechanism is shown in Figure 4.2.

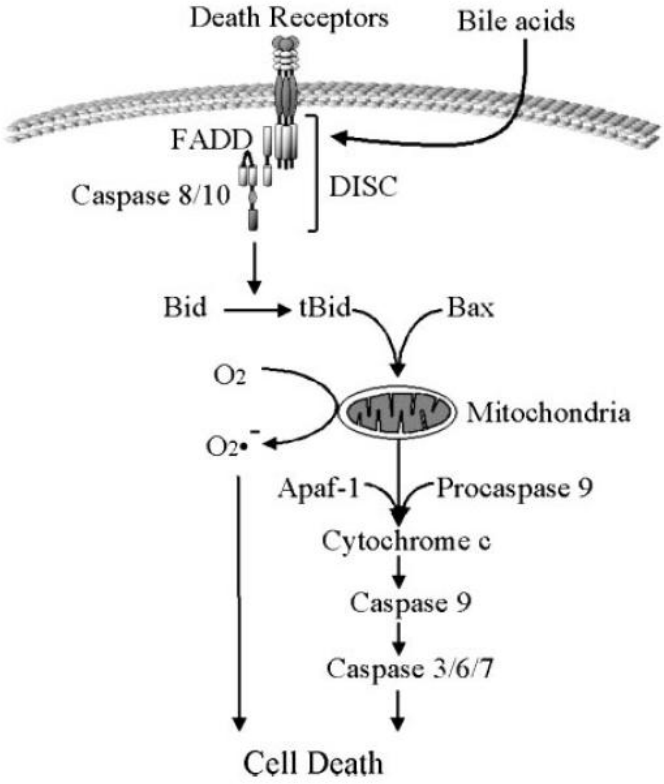

Figure 4.2- The mechanism of hydrophobic bile acids in generating ROS and causing cell apoptosis [397].

Hydrophobic bile acids contribute to the activation of caspase-8 and Bid (a pro-apoptotic protein in the Bcl-2 family essential for death receptor-mediated apoptosis) dissolution. Bid permeates the mitochondria and opens MPTP resulting in the release of factors such as the apoptosis-initiating factor and cytochrome c [398]. MPTP is a non-specific channel formed by proteins inside or outside mitochondrial membranes. Hydrophobic bile acids stimulate Bax, a death-promoting and pro-apoptotic protein in the Bcl-2 family. Bax also exerts an enhanced permeability or a perforation effect, within the outer membrane of the mitochondria. When Bax enters the mitochondria, it triggers the release of proapoptotic factor cytochrome c into the cytosol [399–401]. Cytochrome c interrupts the normal electron current produced by electronic transport respiratory complexes I and III, which contributes to electron leak. These electrons bind directly to oxygen atoms and increase the generation of superoxide. Activation of MPTP leads to the increased level of ROS and

accumulation of ROS subsequently promotes the MPTP, amplifying the levels of ROS within the mitochondria, leading to mitochondrial fragmentation. Thus, bile acid cytotoxicity is associated with the generation of ROS [402] and inhibition of MPTP prevents bile acid-induced hepatocyte cytotoxicity. A feedback loop forms as shown in Figure 4.3.

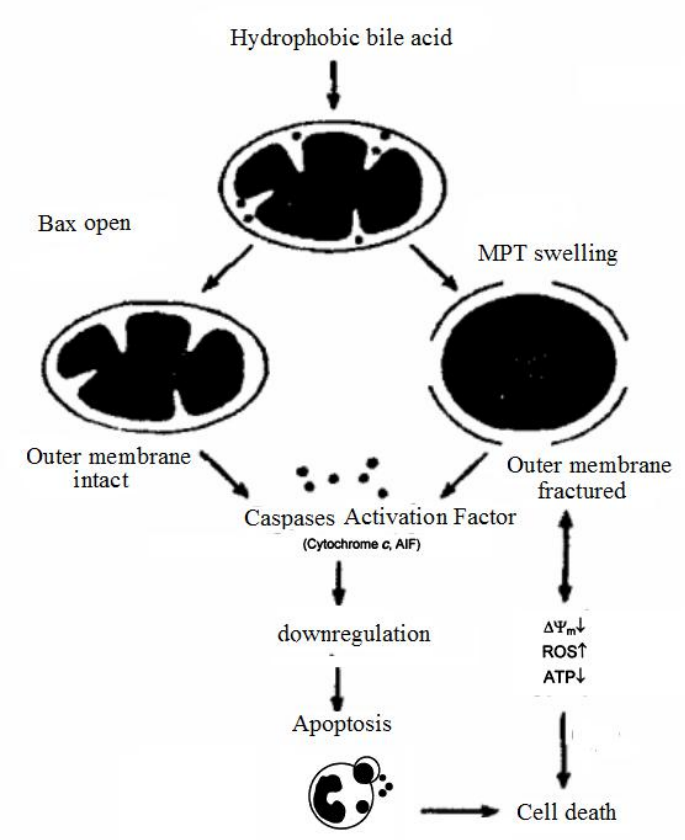

Figure 4.3- The feedback loop of hydrophobic bile acids in opening MPTP and increasing ROS [33].

4.1.2 Toxic bile acid apoptosis pathways

Apoptosis is highly regulated mechanism of controlling cell death which is considered a program of cell suicide. Apoptosis is an indispensable part of embryonic development. The ‘sculpture’ of fingers and toes in a developing human embryo is a typical example of the value of apoptosis. Studies on apoptosis greatly increased from the early 1990s. Apoptosis is the key process for the elimination of damaged cells and maintenance of the homeostatic control of cell number [404, 405]. It plays a vital role in immune regulation and

tissue homeostasis. Importantly, apoptosis is involved in many pathological conditions, influencing a large variety of tissues including heart, liver, kidney, and the central nervous system. Activation of apoptosis in tumor cells leads to the elimination of cancer cells. However, apoptotic cells undergo a wide variety of biochemical events, including the loss of mitochondrial membrane potential, protein cleavage and DNA fragmentation [406]. Excessive apoptosis, that may be triggered by free radical insult can lead to uncontrolled cellular responses, including a variety of metabolic syndrome [464] including obesity and neurodegenerative diseases (Alzheimer's disease).

Exposure to high physiological levels of bile acids induces apoptosis. The *intrinsic toxicity* is linked to the hydrophobicity of bile acids. Hydrophobic bile acids solubilize lipids on the cell membrane causing cell membrane damage. Bile acids exert great toxicity when their intracellular or extracellular concentration reaches an elevated threshold level. However, bile acids are toxic even at lower concentrations. Toxicity is mediated by increasing the levels of the superoxides within affected cells by molecules such as malondialdehyde, a byproduct in cells. At lower concentrations, hydrophobic bile acids induce mitochondrial dysfunction by increasing the permeability of the mitochondrial membrane.

The induction of apoptosis by toxic bile acids is mainly related to two fundamental molecular pathways (see Figure 4.4): 1) the death receptor-mediated pathway (extrinsic pathway), and 2) the mitochondrial pathway (intrinsic pathway) [407]. Both pathways involve the activation of caspases, a family of cysteine proteases that cleave on the carboxyl side of aspartic acid. The intrinsic pathway includes the direct effect on mitochondria and following release of pro-apoptotic factors. The extrinsic pathway (Fas pathway) involves binding to death receptors by death receptor ligands, followed by the activation of initiator caspases and effector caspases. Toxic bile acids at concentrations below 100 μM, mainly initiate the death

receptor-mediated pathway. This involves the promotion of ligand-independent Fas aggregation. When bile acid concentrations exceed 150 μM this can lead to mitochondrial dysfunction mediated by increasing ROS levels [408].

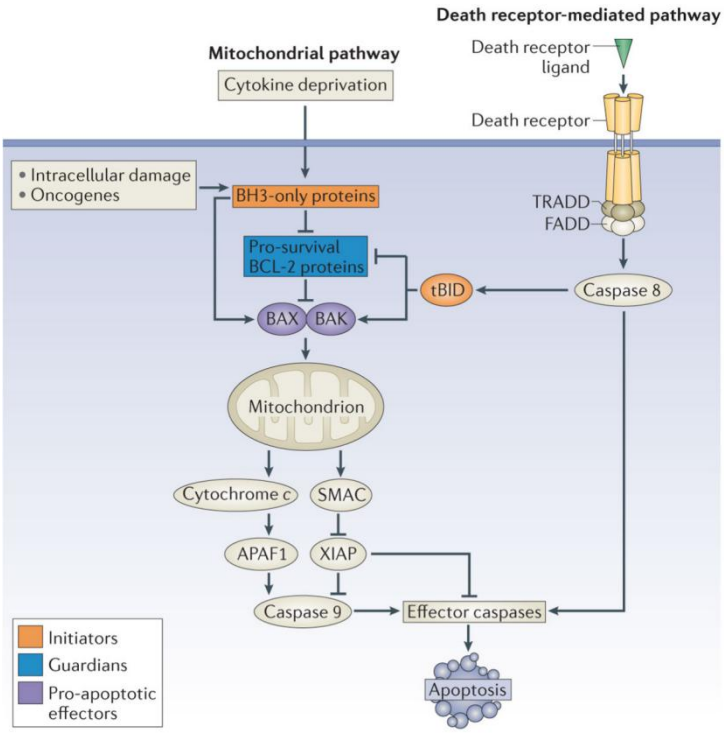

Figure 4.4- Hydrophobic bile acids cause cell apoptosis through two pathways: the death receptor-mediated pathway and the mitochondrial pathway [409, 410]. Both two cell apoptosis pathways converge at activation of the effector caspases (such as caspase-3, caspase-7 and caspase-6).

The mitochondrial pathway (intrinsic pathway)

Mitochondria are organelles bounded by a membrane bilayer, present in cytosol and are critical to the maintenance of homeostasis within cells. The destruction of mitochondria is an important feature of apoptosis. The mitochondrial pathway of apoptosis is induced by intracellular stresses that converge on mitochondria, leading to the generation of ROS, followed by mitochondrial depolarization, membrane permeabilization and disruption of the mitochondrial membrane potential. The mitochondrial pathway is initiated with the activation of membrane-associated enzymes (mainly NAD(P)H oxidases)

by toxic bile acids, which promotes MPT (Mitochondrial Permeability Transition). The promotion of MPT induces perturbations in the mitochondria and allows the release of pro-apoptotic factors such as cytochrome c [411–414]. The loss of the electron carrier, cytochrome c from the respiratory chain, results in the impairment of the electron transport chain and generation of ROS. The release of the pro-apoptotic factors can activate the initiator caspase-9. At the same time, caspase-9 is processed to the mature enzyme. This in turn activates downstream effector caspases such as caspase-3, caspase-6 and caspase-7 via a caspase cascade, promoting the cleavage of Bcl-2 located in the mitochondrial outer membrane. The Bcl-2 family is responsible for regulation of the release of pro-apoptotic factors and regulates the mitochondrial pathway both positively and negatively [415], and contributed to induced mitochondrial dysfunction. Reducing levels of Bcl-2 trigger the activation and oligomerization of Bax, a cytosolic mediator of bile acid-induced mitochondrial cytochrome c release [416]. Initial cytochrome c release induces Bax translocation to the mitochondria and leads to further cytochrome c release [417]. This establishes a feedback loop that amplifies apoptosis. Excessive cytochrome c release leads to the development of new pores within the mitochondrial membrane, and also leads to the cellular membrane integrity disruption and subsequent cell lysis [418].

The death receptor-mediated pathway (extrinsic pathway)

Death receptors are type 1 transmembrane proteins, that may activate apoptosis via the interaction of the receptor with specific cognate ligands. These receptors belong to the TNF receptor superfamily. Among the most widely studied death receptors are Fas and TRAIL membrane proteins. Fas is associated both with cell proliferation in human fibroblasts for example and with the induction of apoptosis. Death receptor-mediated pathways also include Fas-independent apoptosis [419]. Typical death receptor pathways are

triggered by ligand-induced activation of death receptors at the cellular membrane [420], which is followed by recruitment and oligomerization of intracellular adaptor molecules [421]. High concentrations of toxic bile acids result in cell death by activating this death receptor localized at the plasma membrane from the Golgi apparatus. This pathway is activated when certain death receptor ligands engage their cognate death ligands such as FADD (Fas-associated protein with death domain) and its caspase-8. FADD contains a death effector domain that initiates apoptosis by directly activating initiator caspase-8. This is distinct from mitochondrial pathways that result in the activation of caspase-9 [408], followed by the initiation of effector caspase. LCA induced apoptosis in colon cancer cell lines is mediated through this pathway initiated by caspase-8 [422]. Protease caspase-8 has been found to be a signaling caspase involved in the initiation of apoptosis caused by the Fas [423]. Transcription factor p53 is implicated in bile acid induced apoptosis [424] and has been shown to transiently increase Fas expression at the cellular surface to stimulate Fas-FADD binding [425].

Activation of death receptors by bile acids always signals the mitochondria pathway of apoptosis in type II cells, such as hepatocytes. In hepatocytes, activated caspase-8 (dominant death receptor-activated initiator caspase) cleaves the cytosolic pro-apoptotic protein, Bid, a member in proapoptotic Bcl-2 family. The truncated form of BID (tBID) activated by caspase-8 engages in the mitochondrial pathway to amplify the apoptotic response [409] and trigger pore formation, which finally leads to mitochondrial dysfunction and irreversible hepatocyte death. Thus, this Fas death receptor activation appears to be a critical pathway for bile acid related hepatocyte apoptosis.

Genetic removal of Fas only reduces hepatocyte apoptosis by 50% [426]. In the absence of Fas, enhanced expression and oligomerization of TRAIL receptor, synthesized in Kupffer cells [427], can cause cholestatic liver injury. Inhibition of this death receptor-mediated signaling would be essential for the treatment of

cholestatic liver diseases. Compounds capable of causing cell death specifically through the extrinsic pathway are promising candidates for the future drug discovery and development because cancer cells often remain sensitized to death receptor signals [428].

Activation of death receptors invariably signals the mitochondrial pathway of apoptosis in hepatocytes. Both the direct mitochondrial and caspase 3 mediated pathways cooperate in causing apoptosis and their coordination underscores the vital role of mitochondria in programmed cell death.

The ER stress pathway

Some studies challenge the central role of mitochondria in causing apoptosis and suggest that some apoptotic signals can directly activate caspase without involvement of mitochondria [429]. Bile acids with similar concentrations to those found in cholestatic liver diseases, can induce apoptosis via the intrinsic pathway even when the death receptor activation is repressed [430]. Inhibition of death receptor signaling solely is not sufficient to repress hepatocyte apoptosis and subsequent bile acid induced liver damage in cholestatic diseases.

More recently, it has been found that hydrophobic bile acids induce apoptosis in hepatocytes through another intracellular pathway of hepatocyte cell death by causing endoplasmic reticulum (ER) stress. This involves bile acid mediated Ca^{2+} release localized at the ER membrane and subsequent activation of caspase-12, triggering apoptosis. This has been verified in the liver-derived cell line Huh-7. A variety of agents, including inhibitors of glycosylation, toxins and oxidative stress can induce ER stress and contribute to cell death. Recent researches suggested that ER stress might be associated with hepatocyte cell death caused by cholestasis or bile acids [431].

TUDCA, the taurine conjugation of UDCA, has been demonstrated to regulate this ER mediated pathway by reducing Ca^{2+} efflux and subsequent activating

of caspase-12. TUDCA is used in the treatment of many diseases like type 2 diabetes and the metabolic syndrome.

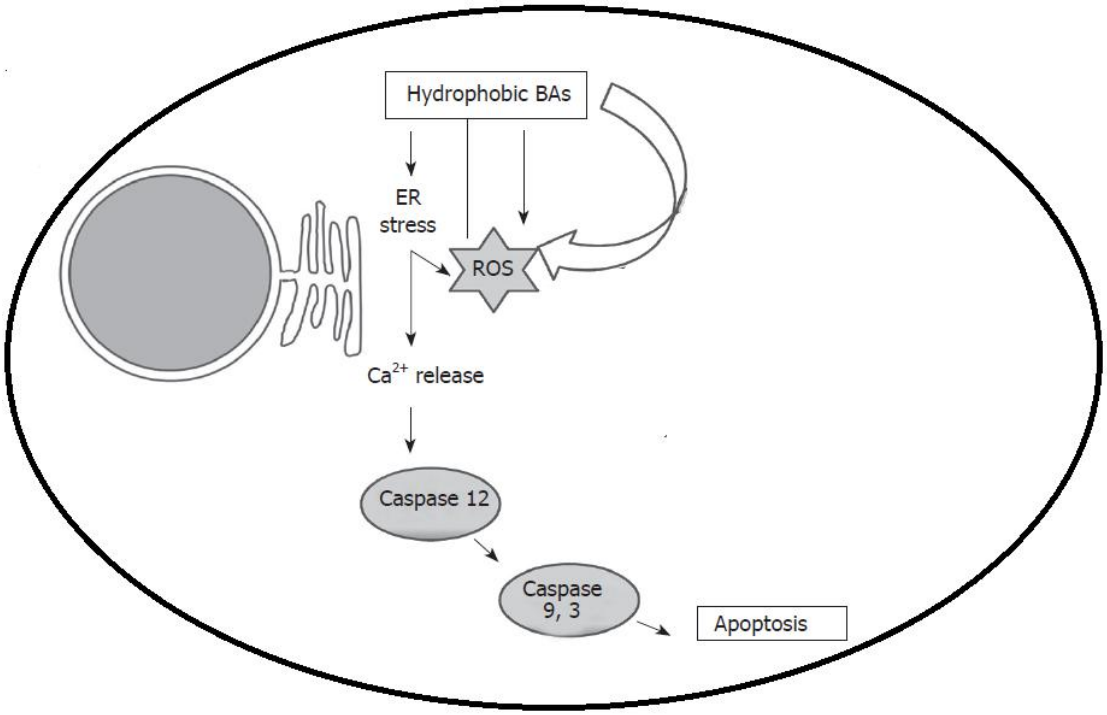

Figure 4.5- Intracellular mechanisms of bile acid-induced hepatocyte apoptosis by ER stress [391].

Bile acids affect intracellular signaling and gene expression, which contributes to alterations in cell growth and even tumorigenesis [432]. Many hydrophobic bile acids cause cellular apoptosis via the mechanisms shown above that pathophysiological concentration of those bile acids activate death receptors [59] and induce oxidative damage and mitochondrial dysfunction [434, 435]. These hydrophobic bile acids have the potential to induce apoptosis through both detergent effects and receptor-mediated interactions. However, UDCA, a chemoprevention agent, can inhibit cell proliferation without inducing apoptosis and this inhibition causes cells to arrest in the G1 phase of the cell cycle [436]. Moreover, UDCA inhibition of apoptosis involves modulation of p53-mediated cell death involving reducing p53 transcription and DNA binding activities. UDCA is also anti-apoptotic [437, 438] and also indirectly blocks apoptosis of

damaged cells by activating several survival signaling pathways, like MAPK and NF-κB. UDCA and its taurine and glycine conjugates protect cells against apoptosis induced by hydrophobic bile acids like DCA. DCA has been found to activate epidermal growth factor receptor (EGFR) in many metabolic disorders and UDCA inhibits this. Besides this, the protective mechanism of UDCA against toxic bile acids involves the direct prevention of mitochondrial membrane perturbation [439] by reducing the pro-apoptotic protein Bax in mitochondria, repressing the generation of ROS [413] and inhibiting cytochrome c release. UDCA plays an important role in modulating the classic mitochondrial pathway of apoptosis in different cell types [440], therefore designing molecular targets mediating UDCA signaling to the mitochondria arouses many interests on the cytoprotection effect of UDCA. UDCA also interferes with the death receptor pathway, blocking caspase-3 activation.

Apoptosis became a topic of intensive research to identify molecular targets and bile acids, especially UDCA, propose effective therapies in the treatment of a wide variety of apoptosis-related diseases. It interferes with cellular apoptosis both at mitochondrial and transcriptional level. UDCA has been the first-line treatment of certain liver diseases for quite a long time. Besides, UDCA has the ability to treat neurological disorders associated with increased level of apoptosis in pre-clinical neurodegenerative models because administration of UDCA in high doses can be delivered to brain [441].

4.1.3 Bile acid toxicity and protection

Different bile acids produce a diversity of cellular effects, some of which may cause harm while others may be cytoprotective. Bile acids have various functions in mammals, including the stimulation of bile formation and cytoprotective effects that enhance the survival of cells. However, the juxtaposition of the cytoprotective effect of bile acids and their capacity to induce apoptosis is dependent on the concentration of bile acids. They are

highly cytotoxic and induce cell death when present in abnormally high concentrations. Cytotoxicity is associated with the capacity of those bile acids that exhibit greater hydrophobicity such as CA and its conjugates, to disrupt the cell membrane and membrane bound organelles.

The retention of hydrophobic bile acids, CDCA and DCA, both disrupts cell membranes through their effect on lipid components and facilitates the generation of ROS through the intrinsic and extrinsic pathways of apoptosis. ROS is generated by activation of Kupffer cells which further contributes to hepatocyte injury. The accumulation of hydrophobic bile acids has historically been long considered a major cause of liver damage as it may lead to the deterioration of existing bile duct, endothelial injury in the lungs and kidney and also have toxic effects on other cells and tissues.

Gut bacteria produce the bile acid LCA from the dehydroxylation of CDCA. It was shown that LCA induces cirrhosis and its taurine conjugate causes cholestasis based on animal experiments. These toxic bile acids correlate to some extent with human liver diseases. However, other bile acids, especially hydrophilic UDCA, were shown to inhibit apoptosis in the same concentration range. UDCA represses apoptosis induced by toxic bile acids and ethanol by decreasing mitochondrial depolarization and repressing translocation of Bax to the mitochondrial membrane with subsequent inhibition of cytochrome c release and caspase activation and formation of ROS [414, 442]. It has been found to modulate bile acid injury in hepatocytes and is currently used to in the treatment of cholestatic liver diseases like PBC and PSC [443, 444].

Because of the potential therapeutic value, UDCA and its derivatives have become the subject of considerable research focus. Many human clinical trials demonstrate that UDCA is effective in CRC prevention and treatment. UDCA is found to inhibit bile acid synthesis in the liver, alter the composition of colonic bile acid, and reduce overall cytotoxicity of the circulating bile acid pool. It is evident that UDCA can prevent the activation of all apoptosis pathways

although its underlying molecular protective mechanisms remain to be established with certainty. In cholestatic liver disease, uptake of UDCA decreases hepatocyte injury and slows disease progression. A variety of studies have shown the potential use of bile acids for the treatment of paediatric cholestatic disorders, including drug induced liver injury. Because of these, UDCA and its derivatives arouse interest based on their protective properties. On the other hand, UDCA is found to suppress the toxicity of lipophilic bile acids at the level of mitochondrial electron chain, up to a concentration of 100 μM. However, at higher concentrations, UDCA can increase bile acid-induced toxicity.

Emerging evidence suggests that the accumulation of cellular mutations, DNA damage and the emergency of cancer are associated with the development of apoptosis resistant cells. This is may also arise as a consequence of repeatedly exposure to high concentrations of hydrophobic bile acids, like DCA. Therapeutic approaches in such instances, include targeting of the apoptosis resistant pathway, to restore apoptosis competence, which results in more effective killing of tumor cells.

UDCA has been found to induce apoptosis via extrinsic pathway as well as intrinsic pathway in human cancer cell lines [445]. It could induce apoptosis in liver cancer, gastric cancer and colon cancer cell lines [446–448]. It is effective in reducing ROS production in tumor cells by inhibiting the MPT formation and preventing the release of cytochrome c from mitochondria. In light of these studies and the minimal side effects associated with the clinical administration of UDCA, our research targeted the development of a novel class of UDCA derivatives which can induce apoptosis in specific tumor cells and provoke cell death. Two UDCA derivatives, HS-1030 (conjugate form of UDCA with N-[(3α,5β,7β)-3,7-dihydroxy-24-oxocholan-24-yl] glycine methyl ester of UDCA) [449] and HS-1183 (conjugate form of UDCA with *N*-[(3α,5β,7β)-3,7-dihydroxy-24-oxocholan-24-yl] L-phenyl alanine benzyl ester)

have already been synthesized to reinforce the UDCA effect in apoptosis initiation [450] and have been demonstrated to be effective in induce apoptosis in CRC cells.

4.2 Design and synthesis of 3α-UDCA derivatives

By understanding how bile acids cause cancer cell damage, we may be able to design agents that can mitigate the damage. On the other hand, in the medical management of cancer the therapeutic objective is to kill tumor cells and agents that are able to kill tumor cells are continually being sought. It is beneficial to use bile acids because of their intrinsic toxicity can be useful leads in the identification of new cytotoxic agents. The synthetic and biochemical studies in this aspect of my work are motivated by this idea.

A panel of 3-azido-24-amides derived from CDCA are capable of reducing cell viability and inducing apoptosis in cancer cells with low micromolar IC_{50} [292]. Dr. Jason Galvin who was awarded a PhD degree from research work carried out in our lab, discovered during the course of his work that a 3-ethanesulfonylamide analogue of UDCA **29** can induce apoptosis in liver (Huh-7) and intestine (Caco-2) cell lines at relatively low concentration and surprisingly cause entire cell death. The objective of this work was to further explore new bile acid analogues related to 3α substituted UDCA in search of greater potency and selectivity and to understand the structural requirements imparting high toxicity. UDCA analogues were made through synthetic manipulation of the functional groups in C-3' (by incorporating sulfonamides or trifluoromethyl) and C-24' position (see Table 4.2). In this work, we began with the synthesis of a library of 3α derivatives of UDCA in an effort to investigate the SAR around the steroid nucleus regarding cytotoxicity (Figure 4.6).

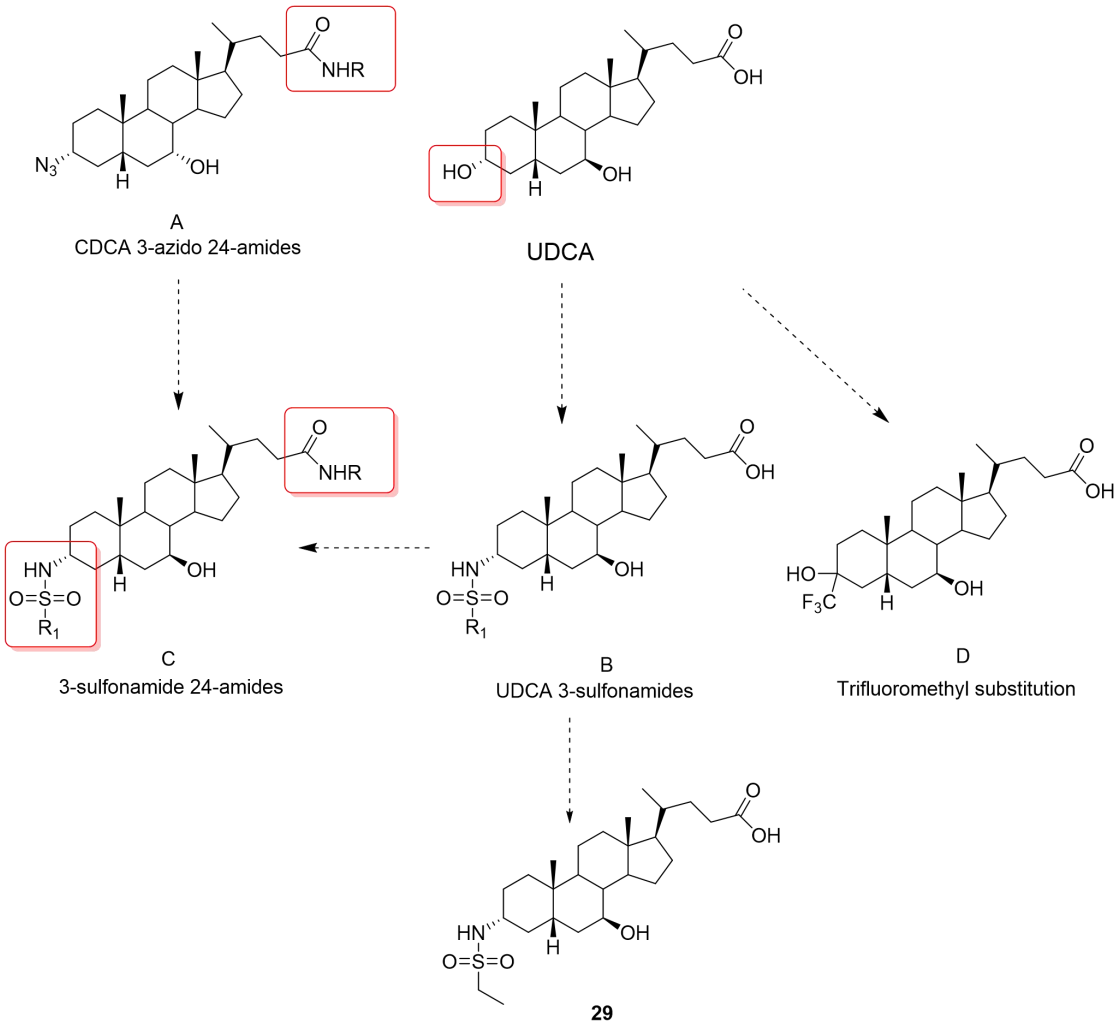

Figure 4.6- Chemistry strategies in improving cytotoxicity based on the SAR around the structure of UDCA and CDCA 3-azido-24-amides. A) CDCA 3-azido-24-amides were identified with low IC_{50} for reducing cell viability in the Caco-2 and HT-1082 cell lines [292]. B) UDCA 3α-sulfonamides were found to be toxic, among which 3α-ethanesulfonamide UDCA **29** displayed unexpectedly high cytotoxic activity. C) A series of 3-sulfonamides 24-amides were designed based on the SAR around UDCA in increasing toxicity. D) Trifluoromethyl substitution at C-3 of UDCA is another strategy to enhance potency towards reduction of cell viability.

4.2.1 Synthesis of 3α-Boc protected UDCA

This section relates to the synthesis of 3α-Boc-protected amine groups, which is an important intermediate to produce corresponding UDCA sulfonamides. The synthetic route to different 3α-amide derivatives of UDCA was quite complicated. Firstly, in order to obtain stereospecific synthesis of 3α-Boc

derivatives of UDCA, we anticipated an inversion of configuration during the formation of the azide group at 3α position. Conversion of the 3α-OH to an appropriate leaving group then allows azide displacement and obtains 3α-Boc compound. Scheme 4.1 shows the synthetic route of 3α-Boc protected UDCA.

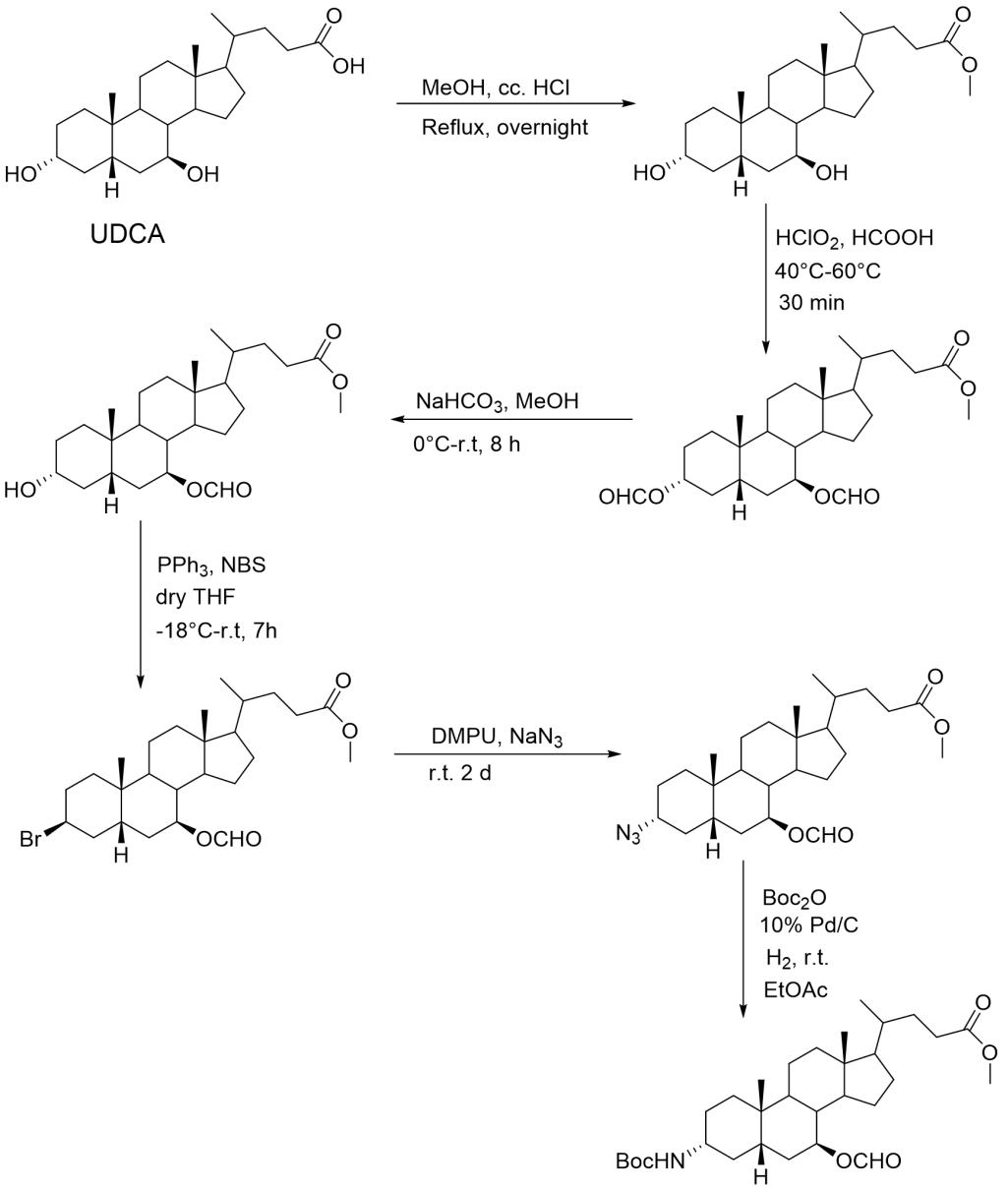

Scheme 4.1- Synthesis of 3α-Boc protected UDCA. (here F=formic protecting group for secondary alcohol)

4.2.1.1 Protection of UDCA

The first step in this synthetic route was the selective protection of C-24'

carboxylic acid and the 7β-hydroxyl group. The protection of C-24' carboxylic acid was done in first. The most widely used method in carboxylic acid protection is esterification. In many cases, bile acid methyl esters can be obtained in a high yield in an acid catalyzed reaction [451]. The formation of methyl ester **1** was carried out in MeOH by adding half eqv. of acid catalyst at reflux. After overnight, TLC showed 100% conversion of the starting material. The TLC plate was developed in hexane: EtOAc=1:2 with vanillin solution used for detection. After workup, the methyl ester was obtained as white solid in high yield (96%). (Scheme 4.2)

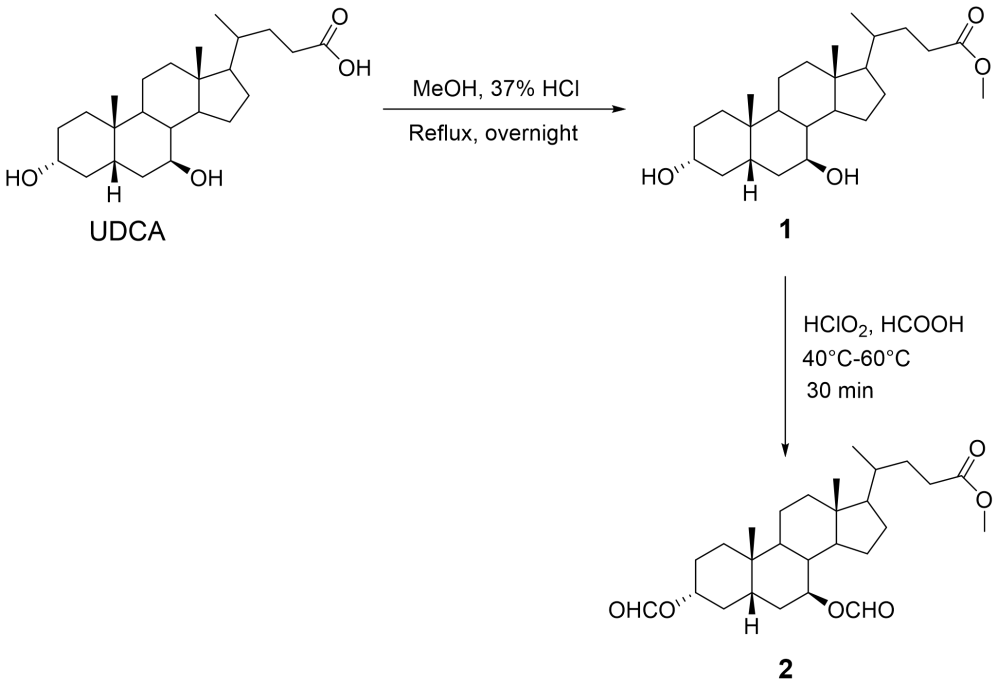

Scheme 4.2- Esterification of C-24' carboxylic acid and protection of hydroxyl groups at C-3' and C-7'

The selective protection of the hydroxyl group at C-3' and 7' position is not easily achieved in one step. The 3α-hydroxyl group is more reactive than 7β-hydroxyl groups because C-7' position are more sterically hindered and are equatorial in the UDCA case. Our approach was to protect both C-3' and C-7' hydroxyl group with formic acid and then selective cleavage of the formic protecting group on the less hindered A-ring. The protection of the 3 and

7-hydroxyl groups was done with concentrated perchloric acid in formic acid under 60°C to yield di-formate **2**. The formation of **2** was followed by TLC analysis using hexane: EtOAc=3:1 as the mobile phase. After the reaction was finished, the crude product was purified by flash chromatography to yield product **2** as white foam (90%).

4.2.1.2 Selective deprotection of 3, 7-diformate UDCA 2

The most generally used method to achieve cleavage of the formate group is hydrolysis in the presence of weak base condition. Concentrated KOH or NaOH solution deprotect both hydroxyl groups in a short time. $NaHCO_3$ is a commonly used reagent to selectively hydrolyse formate group without converting methyl esters to carboxylic acid. The selectivity over the methyl ester is that formate group are more susceptible to hydrolysis and they hydrolysed first. The hydrolysis was carried out in anhydrous MeOH at pH~10 at RT. After 8 h, The TLC showed the conversion of the starting material to the desired product **3** (75%) and a certain amount of side product (15%). The reaction time needed to precisely control and 8 h was found to be the best reaction time to achieve mono-acetate product. Overlong reaction time led to the synthesis of more side product.

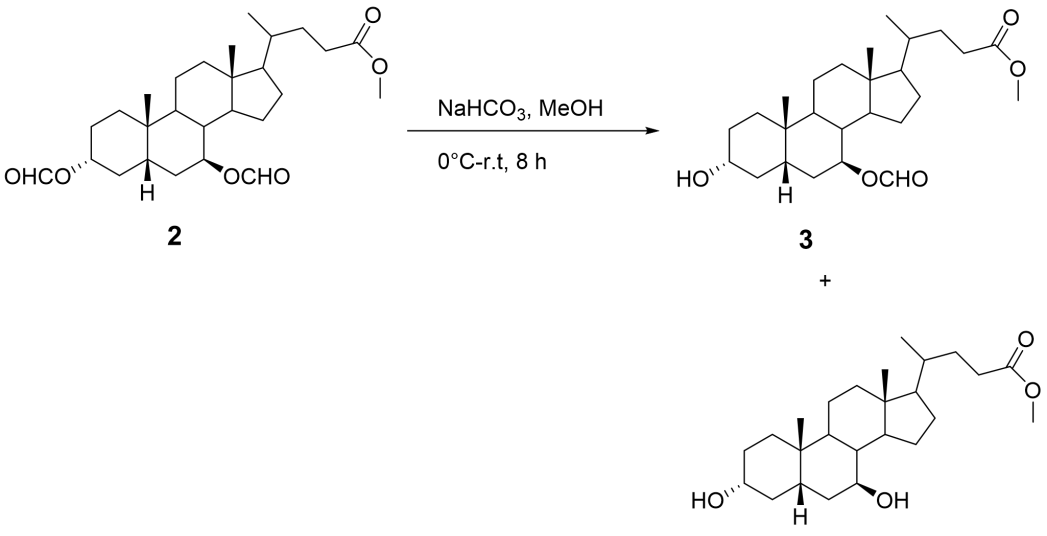

2 **3** +

Scheme 4.3- Selective deprotection of 2 with $NaHCO_3$ in inert MeOH.

4.2.1.3 Synthesis of 3α-bromo UDCA

The direct synthesis of azide from the corresponding alcohol is only limited to tertiary alcohol [452]. A reported synthetic route involves general reaction steps via a bromo intermediate [453]. To obtain the final 3α-azide compound, the 3α-alcohol should undergo a nucleophilic substitution into 3β-bromo intermediate, which is subsequently converted into 3α-azide.

A novel reaction system for transformation of hydroxyl groups into bromodeoxy group consists of PPh_3 together with halogen source in dry THF at RT [454]. Here, NBS is used as the halogen source as bromine is much easier to be displaced. 3α-Hydroxyl group is replaced by bromine via oxyphosphonium intermediate with inversion of configuration. Compound **3** was treated with 2 eqv. of PPh_3 and NBS in dry THF at -18^{o}C and the reaction proceeded at RT for around 7 h. After TLC (hexane: EtOAc= 5:1) shows the full conversion of starting material, the crude product was workup and purified by flash column chromatography to obtain 3β-bromo, 7α-acetyloxy-5β-cholanoate **4** as colourless oil in 87% yield. The initial reaction temperature was set to quite low in order to reduce potential side reactions.

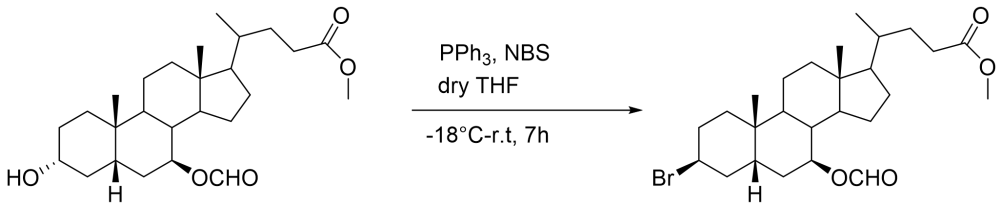

3 **4**

Scheme 4.4- Synthesis of 3β-bromo UDCA via Mitsunobu displacement.

4.2.1.4 Synthesis of 3α-azide UDCA

Compound **4** was then transformed to the corresponding 3α-azide **5** in a nucleophilic SN2 substitution reaction. Sodium azide is a good source in preparing azide compound as the pseudohalogen azide anion can displace the bromo group to produce the azide compound. Compound **4** was treated with

10 eqv. of NaN_3 in DMPU at RT and stirred for 2 d. During the process, the flask needed to be covered by tin foil to reduce the degradation of NaN_3. The formation of the 3α-azide was followed by TLC analysis using hexane: EtOAc=5:1 as mobile phase. The R_f difference of the starting material and final product was quite small so that it is hard to follow the changes only based on the R_f value of the spots. But the colour of two spots was quite different after development with vanillin solution that product spot showed white compared to dark purple for the starting material. After 2 d, the crude product was worked up and cleaned by column chromatography to obtain compound **5** as light-yellow oil in 85% yield.

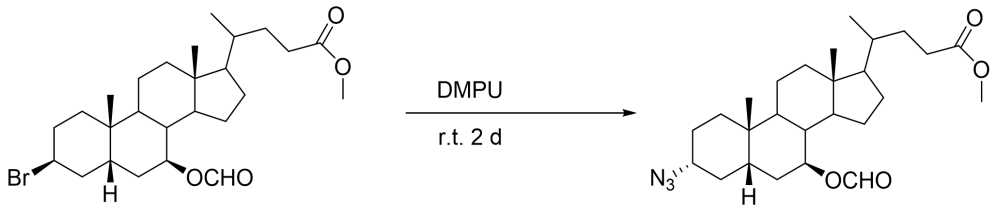

4 **5**

Scheme 4.5- Synthesis of 3α-azide UDCA 5.

4.2.1.5 Reduction of 3α-azide UDCA and subsequent Boc protection

The next step involves the reduction of 3α-azide UDCA **5** and immediate Boc protection on produced amine. Boc-protection of amines produced is widely needed because of amine's instability. In this case, the UDCA azide **5** was carbamoylated in situ with Pd/C under H_2 atmosphere in the presence of Boc_2O to give Boc-protected amino compound **6**. 1.2 eqv. of Boc_2O was added to a mixture of Pd/C and compound **5** in EtOAc and the reaction was stirred overnight under H_2. The formation of **6** was followed by TLC analysis using hexane: EtOAc=4:1 as the mobile phase. After the reaction was finished the second morning, the crude product was purified by flash chromatography to yield product **6** as white foam (90%) and also a small percentage of 3-keto product.

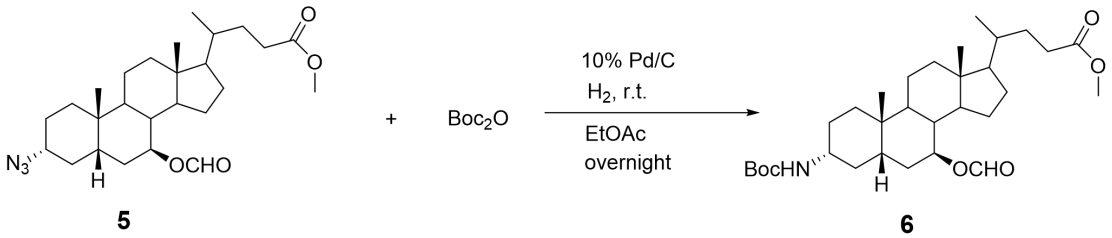

5 6

Scheme 4.6- Synthesis of 3α-Boc protected UDCA 6.

4.2.2 Alkaline hydrolysis and further amidation on C-24'

In order to synthesize different kinds of amides on C-24', the next step would be the hydrolysis of 3α-Boc protected UDCA. The hydrolysis of the protecting groups usually takes place under strong alkaline condition (pH=14). Compound **6** was treated with 2M aq. NaOH solution in MeOH under reflux condition for 4-6 h. After the workup, compound **7** was obtained as a white solid in high yield (99%).

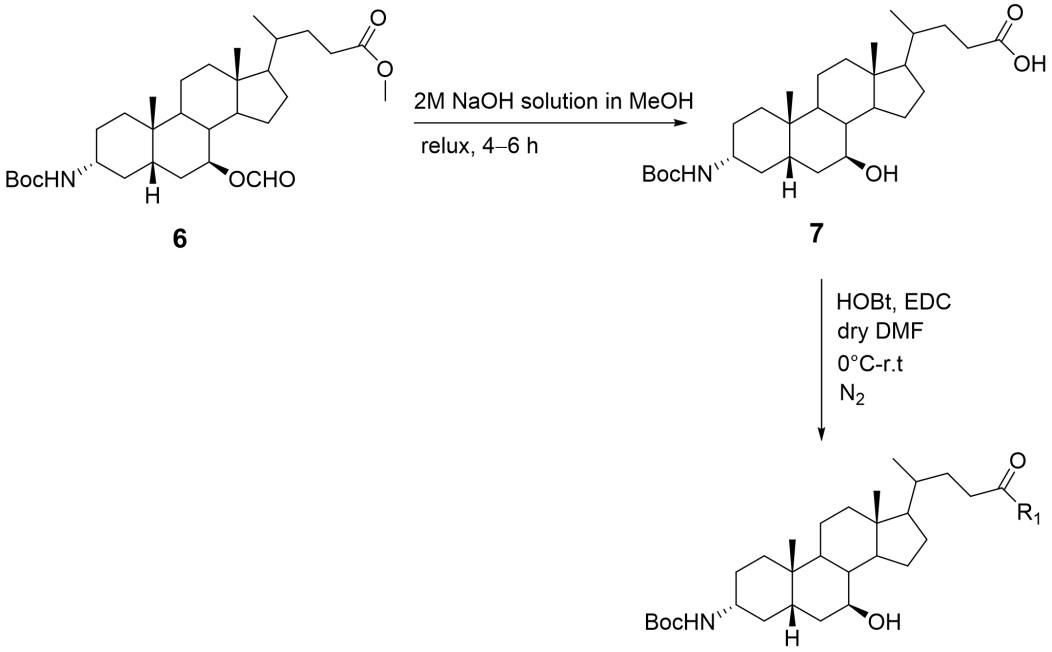

6 7

Scheme 4.7- Alkaline hydrolysis of 3α-Boc protected UDCA and subsequent amide coupling into different C-24' amides. Here R_1 represents different amines.

A relative low cost and easy method for transformation to desired amides from carboxylic acid at C-24' was to employ the well characterised coupling of

carboxylic acid and amine or anhydrides with HOBt and EDC. Using this method, we were able to avoid the isolation of the active ester. This reaction was carried out in dry DMF at 0°C. The formation of intermediate was monitored by TLC analysis (hexane: EtOAc=1:1). When the intermediate formed, amine was added dropwise into the mixture and was stirred to RT for overnight. The formation of intermediate was usually very fast at 0°C, usually 30 min. After workup and subsequent column chromatography, the C-24' amides were afforded in the yield of between 55%–70%, depending on the type of amine applied. The amine reactants and amide products are listed in Table 4.1 below.

Table 4.1- A list of C-24' amides with Boc protection on C-3'.

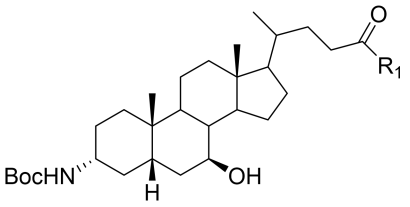

Amine used	R_1	Product
butan-1-amine	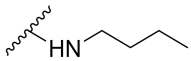	**8**
pyrrolidine	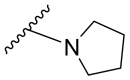	**9**
cyclopentanamine	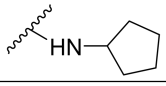	**10**
ethylamine	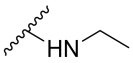	**11**
ammonia		**12**
cyclopropylamine	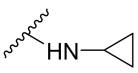	**13**

^{1}H-NMR characterization of C-24' amide with 3α-Boc protected

As can be seen from the ^{1}H-NMR spectrum below, two doublet peaks observed at δ 5.48 and δ 4.42 represent the NH proton on cyclopentamine and on Boc protecting group respectively. Compared with the ^{1}H-NMR spectrum of compound **6**, the chemical shift of 9 protons of tert-butyloxycarbonyl protecting group ($3\times CH_3$) does not change at all. A multiplet between δ 3.48 and δ 3.52 indicates the presence of 7α-H. Another multiplet localized between δ 3.35 and δ 3.37 represents the 3β-H. Overall this ^{1}H-NMR spectrum corresponds to the structure of compound **10**.

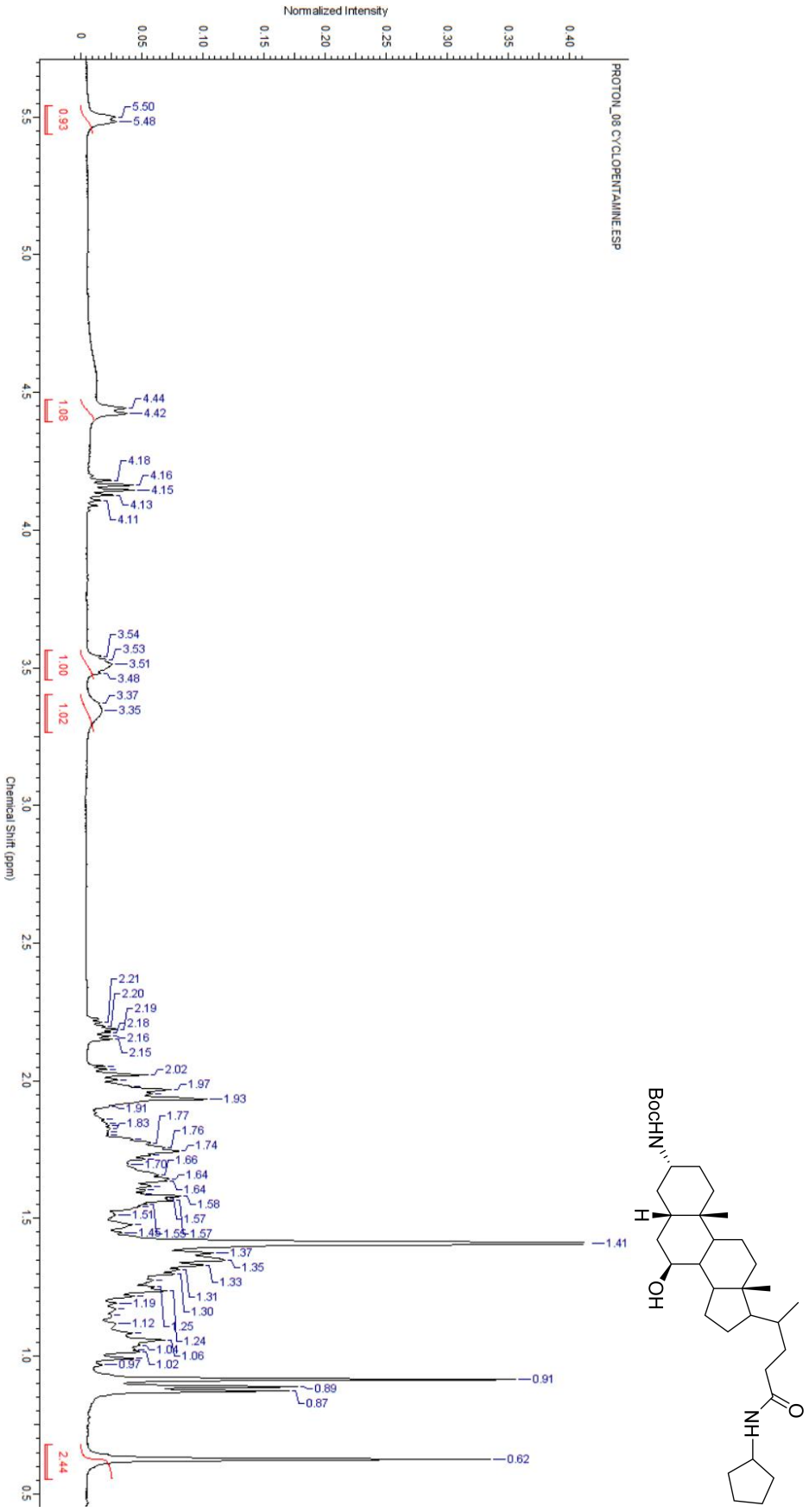

Figure 4.7- ^{1}H-NMR spectrum of compound 10.

4.2.3 Deprotection and final coupling with sulfonyl chlorides

Different sulfonyl chlorides were attached to the deprotected amine to afford 3α-sulfonamide UDCA derivatives. The removal of the Boc-protecting group of the C-24' amides was done by employing a 33% solution of TFA in dry DCM at RT. After full disappearance of the starting material (approximately 25–30 min), the mixture was neutralized first and the volatiles were removed and the secondary amine was dried under high vacuum. The trifluoroacetate salt was used immediately without any further purification and coupled with the sulfonyl chlorides in anhydrous DMF at 0ºC and then turned to RT for overnight.

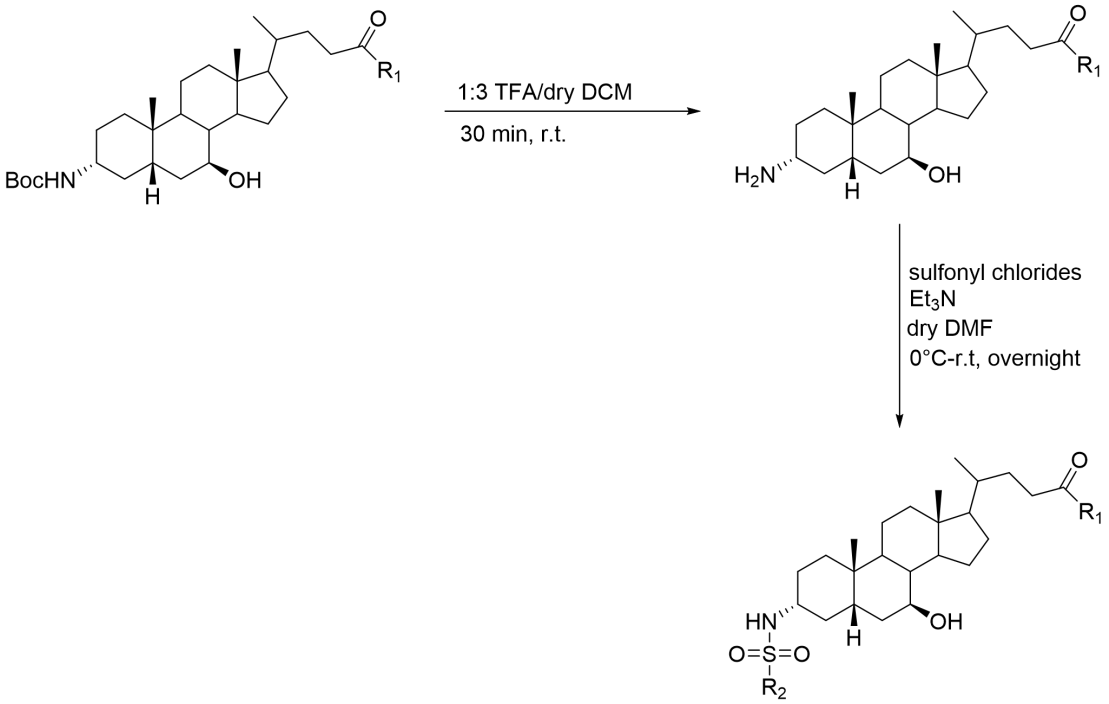

Scheme 4.8- Deprotection and coupling with sulfonyl chlorides to afford final 3α-sulfonyl, 24-amido UDCA derivatives. R_1 here represents different amines used and R_2 alkyl groups of different sulfonamides. (A list of R_1 and R_2 can be found in Table 4.2)

Table 4.2- A list of 3α-sulfonyl, 24-amido UDCA compounds. C-3' position is attached by four different types of acid chlorides while C-24' side chain is modified into different amides.

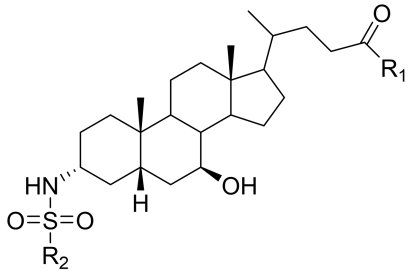

R_1= 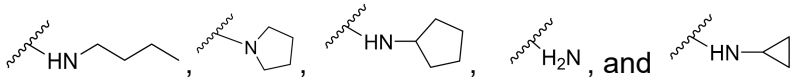 and

R_2= -CH_3 (methyl), -CH_2CH_3 (ethyl), -$CH_2CH_2CH_3$ (propyl), and -Ph (benzyl)

Butan-1-amine series 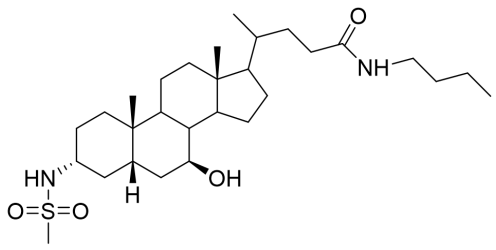 **14** 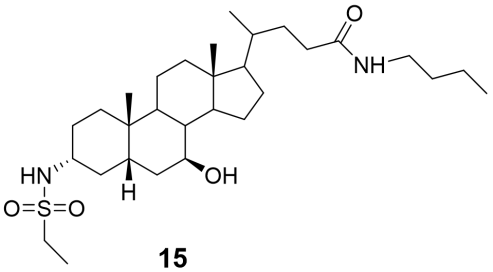 **15** 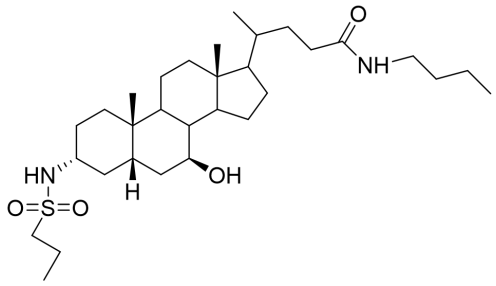 **16** 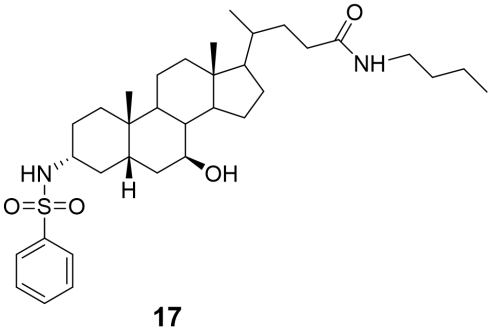 **17**
Pyrrolidine series

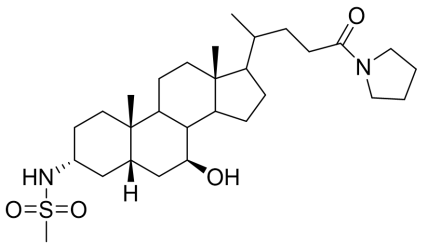

18

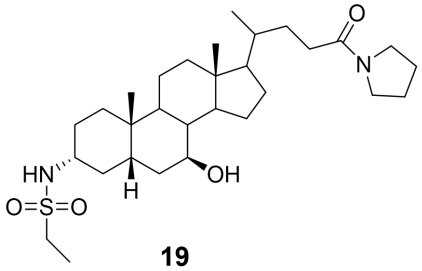

19

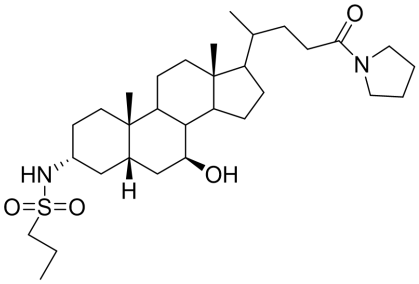

20

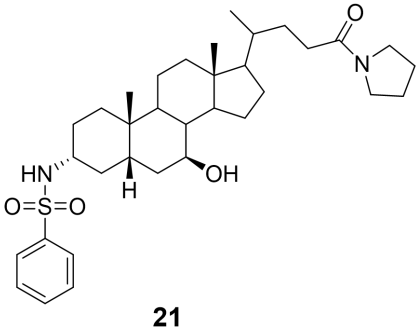

21

Cyclopentanamine series

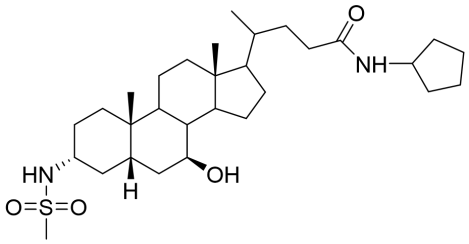

22

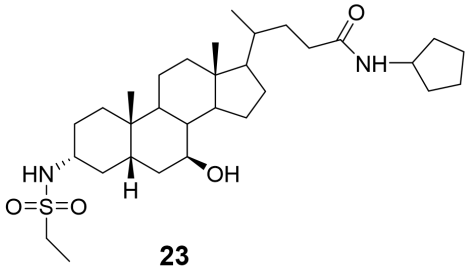

23

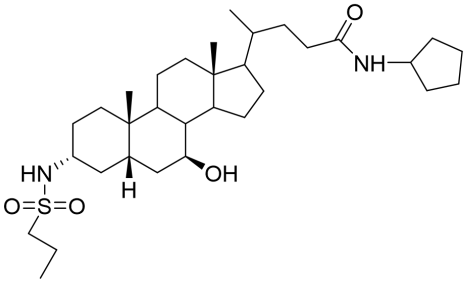

24

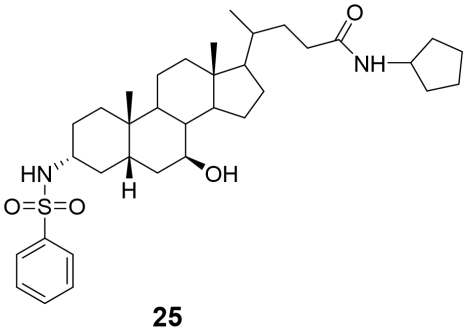

25

Ammonia

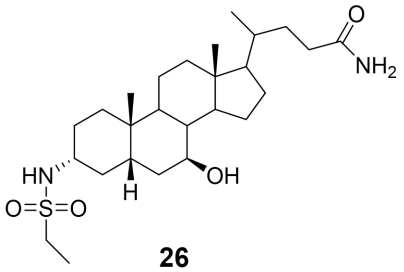

26

Cyclopropylamine

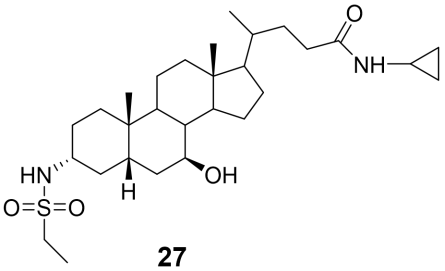

27

The % yield of desired 3α-sulfonyl, 24-amido UDCA was low mainly because of complex reaction scheme and their physicochemical property. They are very polar and therefore large quantities of compound were lost to the aqueous layer in the workup step. More work needs to be done to improve the % yield.

^{1}H-NMR characterization of 3α-sulfonyl, 24-amido UDCA derivatives

The disappearance of the Boc protecting group can be clearly observed. Compared to the ^{1}H-NMR spectrum (Figure 4.7) of **10**, the chemical shift of 7α-H does not change at all. A quartet peak found at δ 3.02, integrated to 2 protons, represents the CH_2 of ethanesulfonyl group and this is an important signal for compound **15**. Besides this, a doublet between δ 3.96 and δ 3.98 is assigned to the NH of ethanesulfonyl group. A multiplet localized between δ 3.21 and δ 3.26, with the integration of 3H, indicates the signal for N-CH_2 and 7α-H. Overall this ^{1}H-NMR spectrum corresponds to the structure of compound **15**.

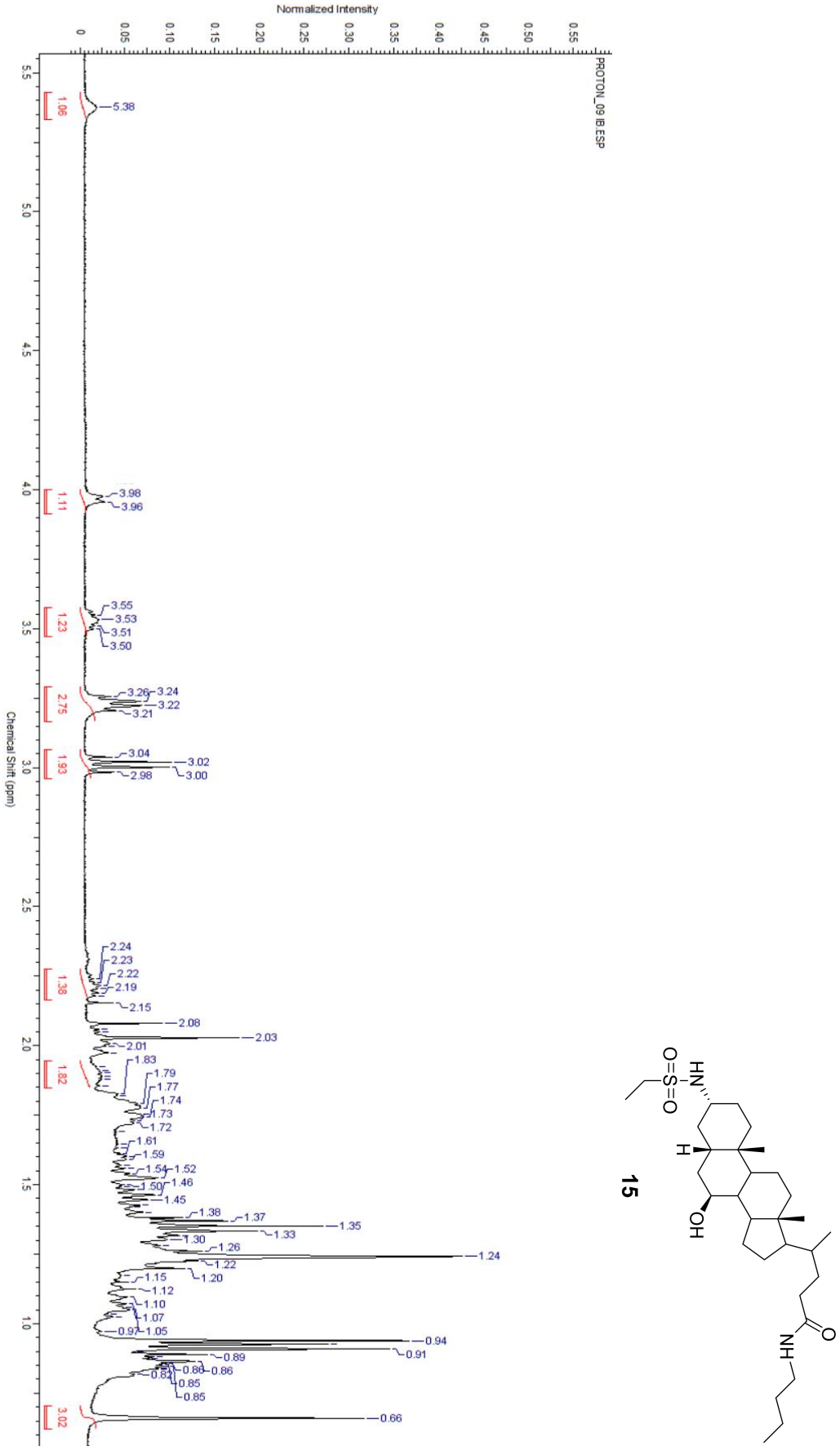

Figure 4.8- ^{1}H-NMR spectrum of compound 15.

4.3 Cytotoxicity of the 3α-UDCA sulfonamides in Huh-7 cell line

In order to study the potential toxicity or relative toxicity of 3α-UDCA sulfonamide compounds, we used the MTT assay method to determine the % cell viability. The application of the MTT approach here is in the context of many studies carefully characterizing the effects of bile acids in the relevant concentration range, which has been used as an important research tool in the second chapter of this thesis. We studied cell viability effects using the Huh-7 cell line which is a type of hepatocellular carcinoma (HCC) cell line because we wanted to understand the relative toxicity of these 3α-UDCA sulfonamides **29** at the concentration of 50 μM. Stock solutions of the different 3α-UDCA sulfonamides were prepared in DMSO and these were diluted to 50 μM with supplement free medium. The % cell viability was measured after incubating for 24 h and it was calculated versus vehicle treated control, which was treated with same amount of DMSO (1%). Each experiment was carried out in triplicate and repeated three times to get nine data points in total for each bile acid drug solution. The data are presented in Figure 4.9.

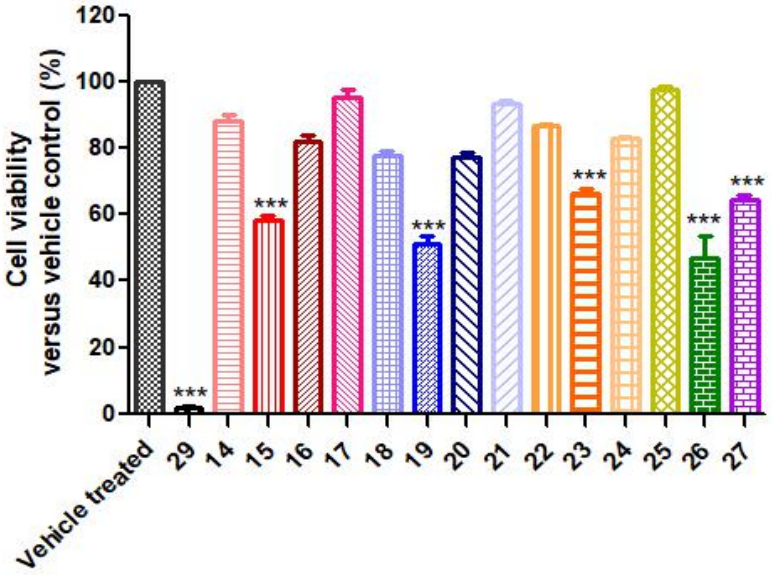

Figure 4.9- A measurement of toxicity of a panel of 3α-sulfonamide UDCA compounds. Huh-7 cells were seeded onto 96 well plate at a density of 1×10^5 cells/ml, and then treated with 50 μM bile acid solution for 24 h. Cells were then treated with 10 μl of 2.5 mg/ml MTT reagent and incubated for 2 h. The

assay was normalised to 1% DMSO vehicle control and absorbance of each well was read on a VERSAmax Microplate Reader (Molecular Devices, Sunnyvale, CA, USA) at a wavelength of 570 nm. Values are expressed as mean ± SEM of three triplicate experiments, * $p<0.05$, ** $p<0.01$, *** $p<0.001$ as determined by one way ANOVA with Dunnett's post-hoc correction.

It is manifest from the Figure 4.9 above, among this panel of 3α-UDCA sulfonamides, 3α-ethanesulfonamide UDCA **29** without any conjugation was found to be the most toxic, which corresponds to Jason Gavin's findings in his thesis that this compound exhibited unexpectedly high cytotoxic activity. Conjugation to other amines at C-24' will obviously decrease their relative toxicity compared to **29**. At the same time, coupling with ethanesulfonamides shows the highest toxicity compared with other sulfonamides, followed by propanesulfonamides and methanesulfonamides. Conjugation to benzenethanesulfonyl chlorides caused the lowest toxicity.

Most of the UDCA sulfonamides did not exhibit any cytotoxicity effect but some of them seem to protect cells from death (for example **17**, **25**). It will be interesting to further explore the SAR of the UDCA sulfonamides on the cytoprotection effect.

4.4 Further toxicity screen of 3α-ethanesulfonamides

The data, which were collected for a panel of the new 3α-amides, indicated that the cell viability reductions observed with the MTT assay were due to the structure differences in general. An understanding of the structural basis for the cytotoxicity effects of bile acids is important to ongoing efforts to the design of selective cytocidal agents [455–458]. Based on initial toxicity screen in Huh-7 cells, the 3α-amides causing a significant drop in count at 50 μM were compound **26** and **29** shows some effect. Many studies indicate the incorporation of alcohol on the C-24 position increase the overall toxicity and we supposed that addition of an alcohol group can even boost the cytotoxicity

of 3α-ethansulfonamide UDCA. The objective was to extend the structure activity relationships already established to include derivatives at the C-24 position and explore whether the alcohol derivative of 3α-ethansulfonamide UDCA **28** exhibits significant cytotoxicity effect on Huh-7 cells.

Our initial synthetic strategy revolved around producing the desired compound based on direct $LiAlH_4$ reduction. $LiAlH_4$ is a good reducing agent producing hydroxyl derivatives from methyl ester directly. A simple two-step synthesis using compound **5** as the starting material was designed (Scheme 4.9).

The first step was to reduce the methyl ester into the hydroxyl group while reducing the azide group into amine simultaneously. The second step was the attachment of the ethanesulfonyl group. However, this synthesis did not work as expected because an unknown impurity was produced in the meantime and it cannot be purified. The impurity proved hard to remove by column chromatography.

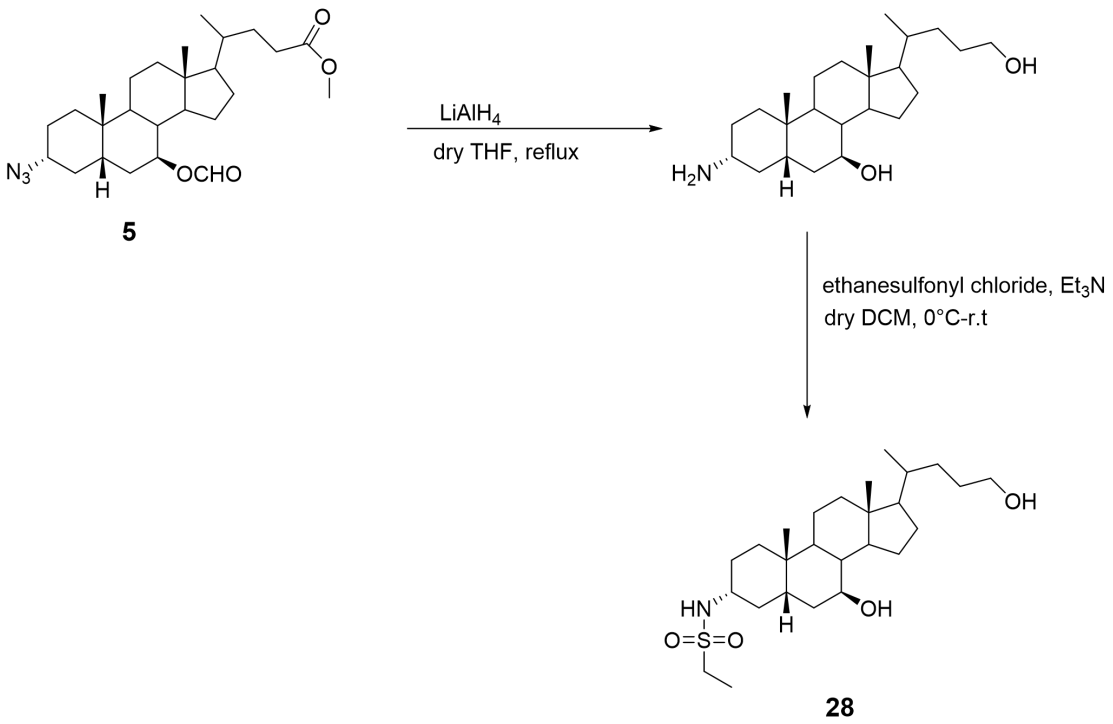

Scheme 4.9- Initial designed synthesis of the alcohol derivative of 3α-ethansulfonamide UDCA 28 based on $LiAlH_4$ reduction.

The problem with the synthesis of **28** forced us to shelve this synthetic procedure. A more complex synthetic route was redesigned in Scheme 4.10. This followed the classic sodium reduction (Bouveault-Blanc reduction discovered in 1903) in the last step that an excess of Na was added to a solution of the carboxylic acid in increments to the alcohol, which functions both as solvent and as reducing alcohol. In this synthetic route, Na/EtOH was applied to efficiently reduce the carboxylic acid into the primary alcohol while it has no effect on the 3α-ethanesulfonyl group compared with $LiAlH_4$ reduction. What is worth mentioning is that Na is a strong reducing agent and the use of Na in this reaction needs to done very carefully as it is very active and exposure of Na in air may cause explosion. Besides, large amount of Na and ethanol tended to increase hazards and made the handling of the reaction products difficult. The first step of this approach involved the direct reduction of 3α-azide UDCA into the primary amine and then subsequent incorporation of the 3α-ethanesulfonyl group in the presence of Et_3N. After purification, the intermediate was hydrolysed by refluxing in MeOH/NaOH at pH 14 to afford the product 3α-ethanesulfonyl UDCA. The final compound **28** was obtained by subsequent reduction with sodium metal in EtOH (the synthesis pathway is shown in Scheme 4.10). The reaction was quite successful and roughly 60% of final yield was obtained from the starting material 3α-azide UDCA.

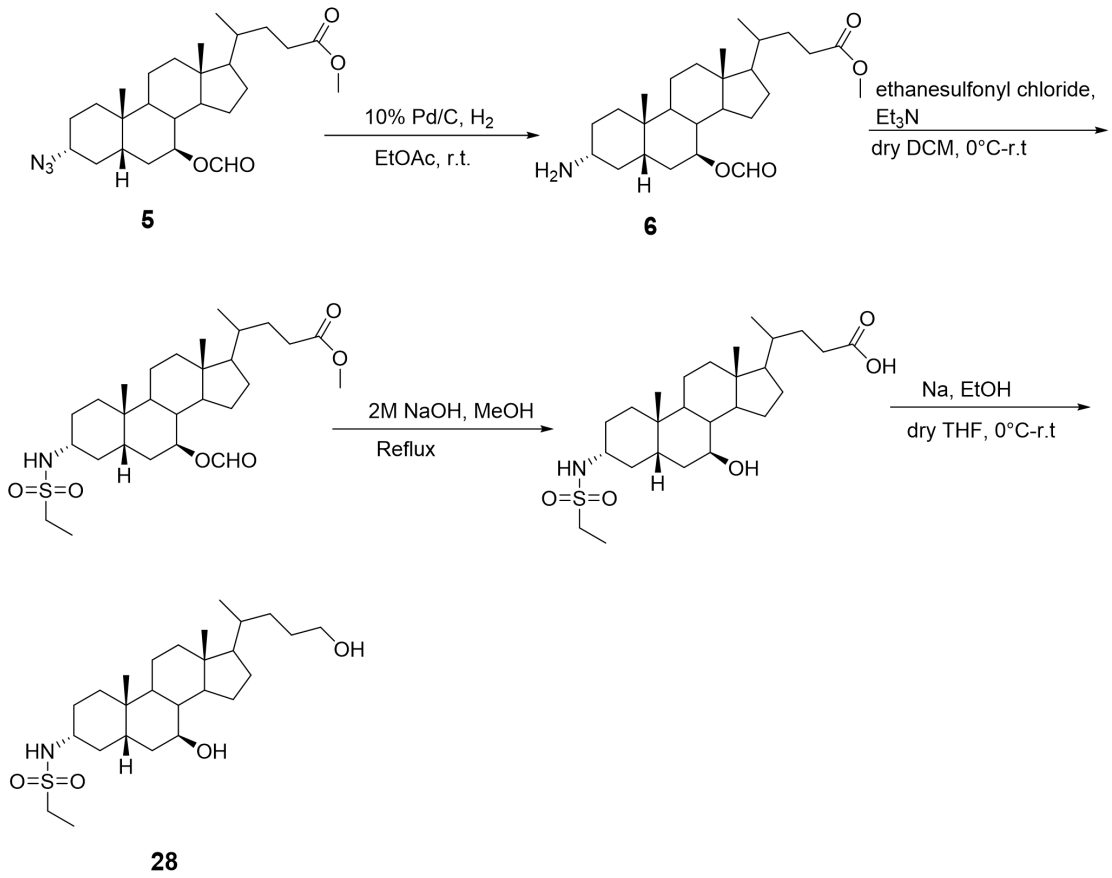

Scheme 4.10- Synthetic route of the alcohol derivative of 3α-ethansulfonamide UDCA 28 based on Na/EtOH reduction.

Once this panel of 3α-ethansulfonamide UDCA analogues was synthesized, next stage of work was to characterize their toxicity pattern on specific cell line, here Huh-7 cells and Caco-2 cells and study their agonist effect on FXR via the β-lactamase reporter assay.

4.5 Cytotoxicity of the 3-ethanesulfonyl UDCA analogues in Huh-7 and Caco-2 cell line

The MTT assay was applied to assess the % cell viability after treating of the specific cell line with this panel of 3-ethanesulfonyl UDCA amides. The main purpose was to evaluate how UDCA amides affect Huh-7 cells, the hepatocyte-derived cancer cell line. At the same time, we also examined the cytotoxic effect of the UDCA amides on Caco-2 cell line, human epithelial

colorectal cancer cell line in order to compare. Caco-2 cell line exhibits the feature of the normal intestinal epithelium, including expression of various important bile acid transporter proteins, like sodium-dependent bile acid transport (ASBT) and efflux proteins. It serves a model for a variety of transcellular pathways and is routinely used on the research into bile acid uptake and transport [459]. All stock solutions of the UDCA amides were prepared in DMSO which were diluted to the required concentration with serum free medium. Four concentrations (100 μM, 50 μM, 25 μM and 10 μM) of the stock solution were tested and % cell viability was measured after incubating for 24 h. The % cell viability was calculated versus vehicle treated control, which was treated with same amount of DMSO (1%). Each experiment was carried out in triplicate and repeated three times to get nine data points in total for each bile acid drug solution.

It has been found previously in the group that 3-ethanesulfonyl UDCA compound **29** cause significant apoptosis. In this project, we wanted to explore the cytotoxicity of other 3-ethanesulfonyl UDCA derivatives using two different cell lines (Huh-7 and Caco-2 cell line). The % viability results are presented in the figures shown below. (Figure 4.9 and Figure 4.10)

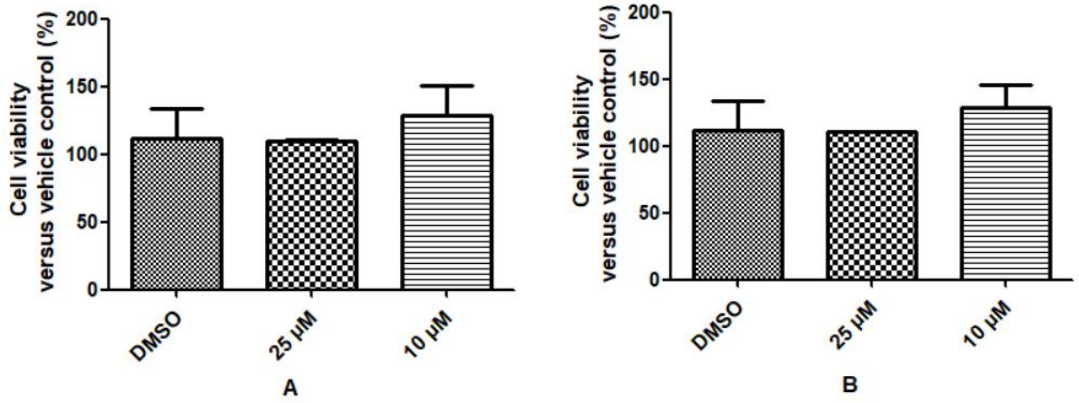

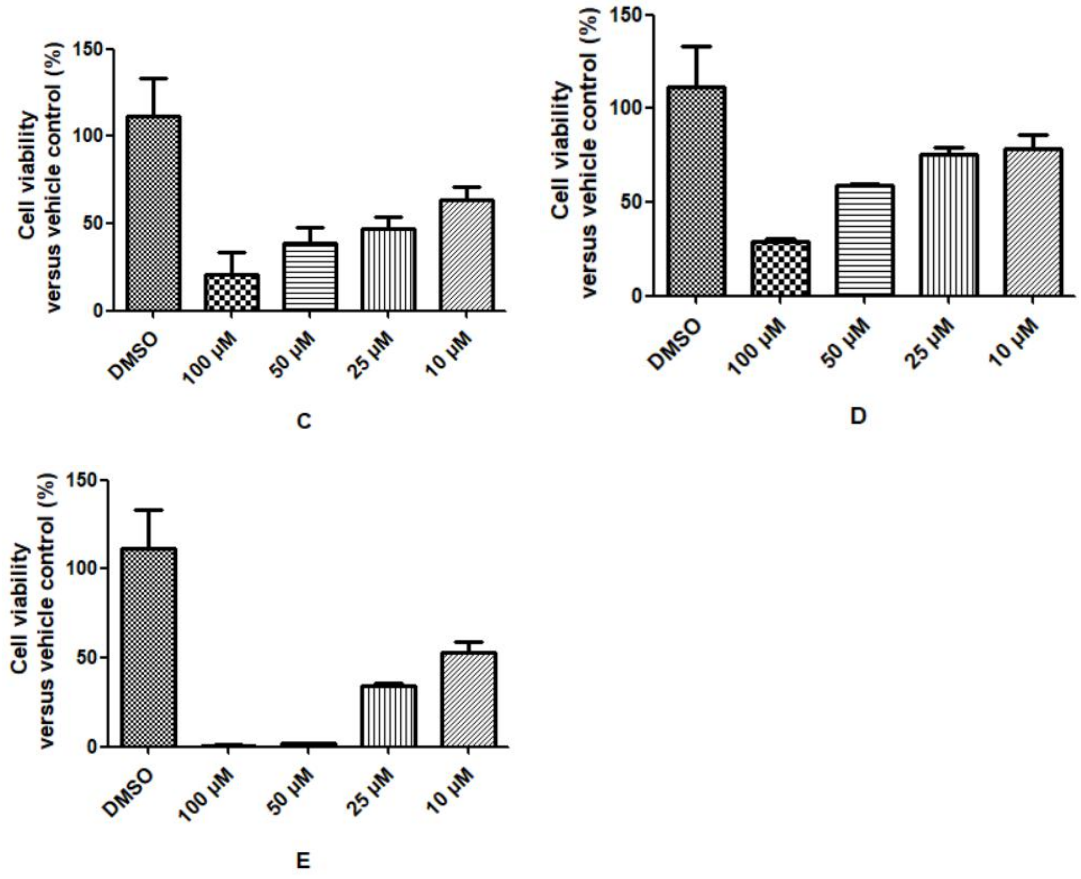

Figure 4.9- The effect of 3-ethanesulfonyl UDCA analogues on Huh-7 cell viability at 24 h. Figure A-E represent data for 15, 19, 26, 28 and 29, respectively. Huh-7 cells were seeded onto 96 well plates at a density of 1×10^5 cells/ml, and then treated with different concentrations of 3α-ethanesulfonyl analogues for 24 h. Two hours before the end of treatment, 10 µl of 2.5 mg/mL MTT was added. At 24 h the medium was gently aspirated and crystals dissolved in DMSO. Absorbance at 570 nm was normalised to 1% DMSO vehicle control. Values expressed as mean ± SEM of three triplicate experiments.

From Figure 4.9 above, compound **15** and **19** were evaluated at the two lower concentrations and they did not show cytotoxicity on the Huh-7 cell line after 24 h. Compound **29** showed most cytotoxic effects at 100 µM and 50 µM compared with other compounds, causing less than 10% survival, and higher than compound **26**. Compound **28** treatment led to cytotoxic effect on Huh-7 cells at higher concentration.

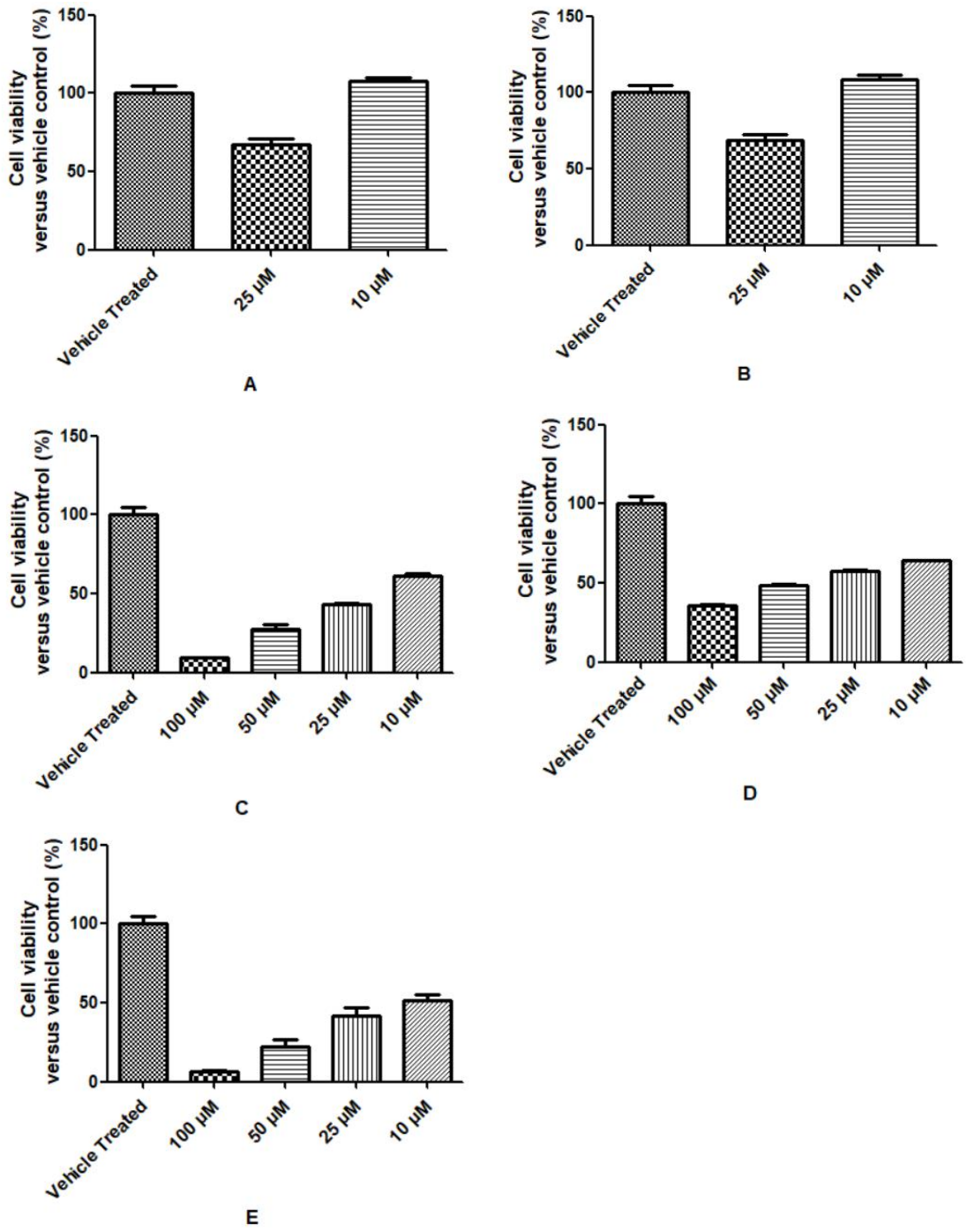

Figure 4.10- The effect of 3α-ethanesulfonyl UDCA analogues on Caco-2 cell viability at 24 h. Figure A-E represent data for 15, 19, 26, 28 and 29, respectively. Caco-2 cells were seeded onto 96 well plates at a density of 1×10^5 cells/ml, and then treated with different concentrations of 3α-ethanesulfonyl analogues for 24 h. Two hours before the end of treatment, 10 µl of 2.5 mg/ml MTT was added. At 24 h the medium was gently aspirated and crystals dissolved in DMSO. Absorbance at 570 nm was normalised to 1% DMSO vehicle control. Values expressed as mean ± SEM of three triplicate experiments.

From Figure 4.10 above, both compound **15** and **19** were evaluated at the two lower concentrations and they did not show cytotoxicity effect towards Caco-2 cell line after 24 h. Compound **26** and **29** showed similar effect and they both caused high cytotoxicity under 100 μM and 50 μM, but up to 10 μM both compounds lead to more than 50% survival. The cytotoxic effect of compound **28** on Caco-2 cells is not as significant in higher concentrations comparing with **29**, suggesting structural modification from carboxylic acid to an alcohol at C-24' reduces overall compound cytotoxicity.

Further research was carried out to investigate the % cell viability difference between two different cell lines with same bile acid solution. As can be seen from Figure 4.11 below, nearly all the 3-ethanesulfonyl UDCA amides exhibited more cytotoxicity towards Caco-2 cells than Huh-7 cells at similar concentrations.

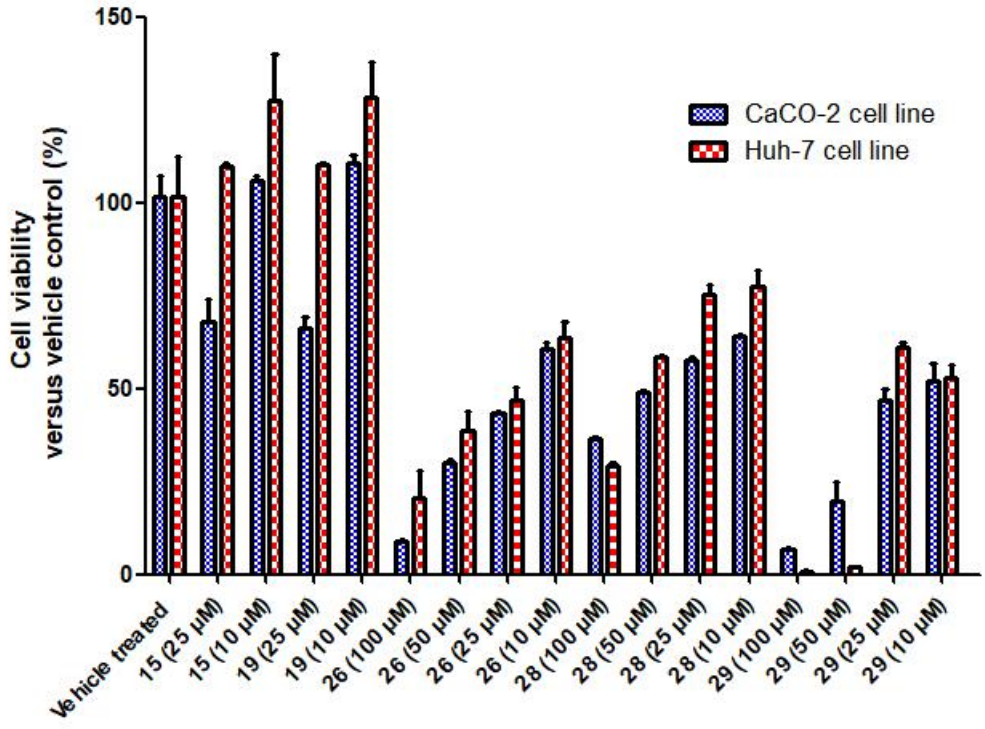

Figure 4.11- The effect of 3α-ethanesulfonyl UDCA analogues on both Huh-7 and Caco-2 cell viability after incubating for 24 h.

Compound **26**, **28** and **29** resulted in a cell viability of below 50% even at low concentration of 50 μM. Approximate IC_{50} values were subsequently roughly estimated over 24 h at four concentration levels. The results estimated using Graphpad Prism are presented below in Figure 4.12 and 4.13.

Compound	**Huh-7 MTT**	**Caco-2 MTT**
	IC_{50} (μM) (95% CI)	**IC_{50} (μM) (95% CI)**
28	21.68 (13.52–34.78)	10.36 (7.909–13.58)
26	10.66 (6.258–18.17)	14.40 (12.12–17.11)
29	10.30 (5.690–18.66)	11.89 (8.937–15.82)

Figure 4.12- IC_{50} values calculated for Huh-7 and Caco-2 cells after treatment with 3α-ethanesulfonyl UDCA compounds for 24 h.

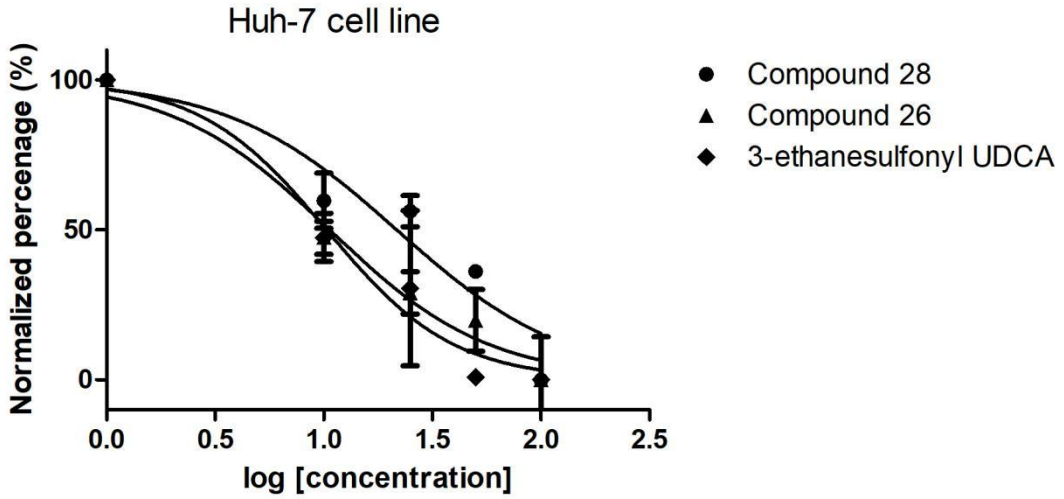

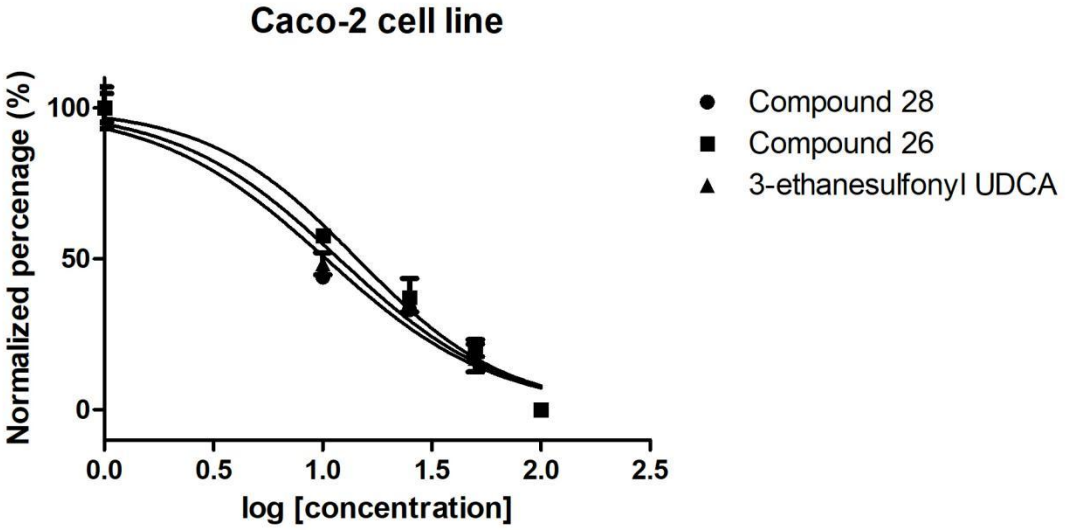

Figure 4.13- Representative IC_{50} curves generated using MTT assay in Huh-7 and Caco-2 cells. Huh-7 and Caco-2 cells were treated with varying concentrations (10–100 μM) of different 3α-ethanesulfonyl UDCA for 24 h. Cell viability was assessed using MTT assay and curve fitted using non-linear regression to calculate IC_{50} values. Values represent mean ± SEM of three experiments performed in triplicate.

Compounds **26**, **28** and **29** were identified with low micromolar IC_{50} values for reducing cell viability in the Caco-2 and Huh-7 cell line, making them among the potent bile acid agents. They were in general more active against Caco-2 cells than Huh-7 cells. Caco-2 cells were especially more susceptible to cytotoxicity from compound **29** than Huh-7 cells.

UDCA can induce apoptosis via both the extrinsic pathway and intrinsic pathway [460]. Huh-7 cell line is Fas negative, known to be Fas deficient, and has minimal Fas expression [461]. Apoptosis and mitochondrial cytochrome c release were inhibited by transfection with dominant negative FADD. Therefore, the apoptosis observed in the Huh-7 cell line may be death receptor mediated (the extrinsic pathway).

These compounds may act through the intrinsic pathway, which in many cases is faster and more potent/efficacious. This may explain why the Caco-2 cells were more sensitive in general than the Huh-7 cells.

At the same time, Caco-2 cells express various BA transporter proteins such as ASBT and OATP [462, 463] that are not highly expressed in Huh-7 cells therefore Caco-2 cells may take up bile acids much easier.

4.6 Analogues of UDCA sulfonamides developed for action on FXR

The approval of drug OCA opened a new area of bile acid therapy and many pharmaceutical companies put much effort on the identification, optimization, and final development of steroid FXR agonists all the way from initial discovery of lead compound to last-stage clinical trials. New bile acid analogues are very likely to lead to the activation of multiple nuclear receptors including FXR and TGR5.

The aim of this section was to explore the effect of various UDCA sulfonamides on their FXR agonist activity since the appropriate assay was operational to address research questions raised in other chapters in this thesis. The same procedures as the β-Lactamase FXR reporter assay introduced in the second chapter were followed. CDCA and OCA, generally known good FXR agonists, were used as the reference in this case. Some of compounds made previously in this lab by Jason Galvin were also tested in this time and all the UDCA sulfonamides.

Each experiment was carried out in quadruplicate and repeated three times to get twelve data points in total for each UDCA sulfonamide analogue. The blue/green ratio was calculated for each well by dividing the background-subtracted blue emission values by the background-subtracted green values. The data was further analyzed in order to get the % agonist activity of each UDCA sulfonamide. The final result is presented in Figure 4.14.

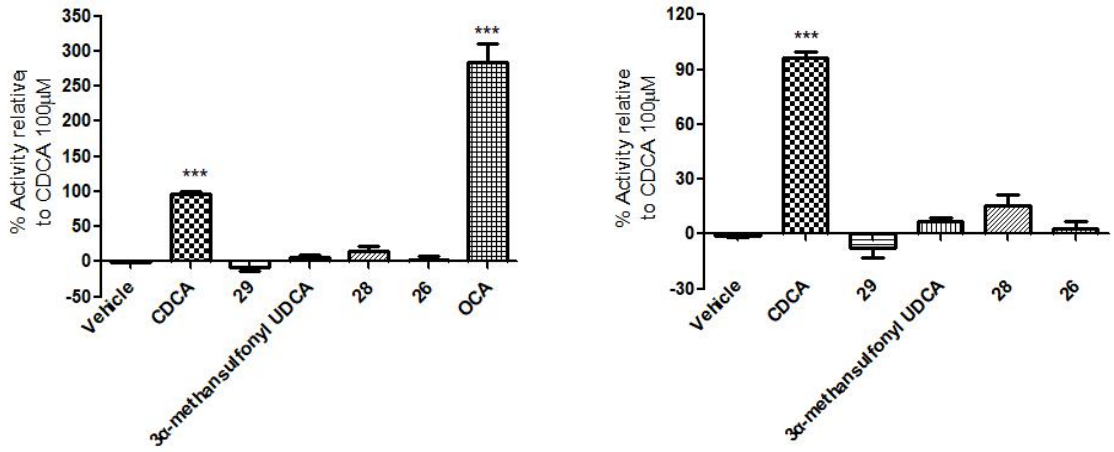

(A)

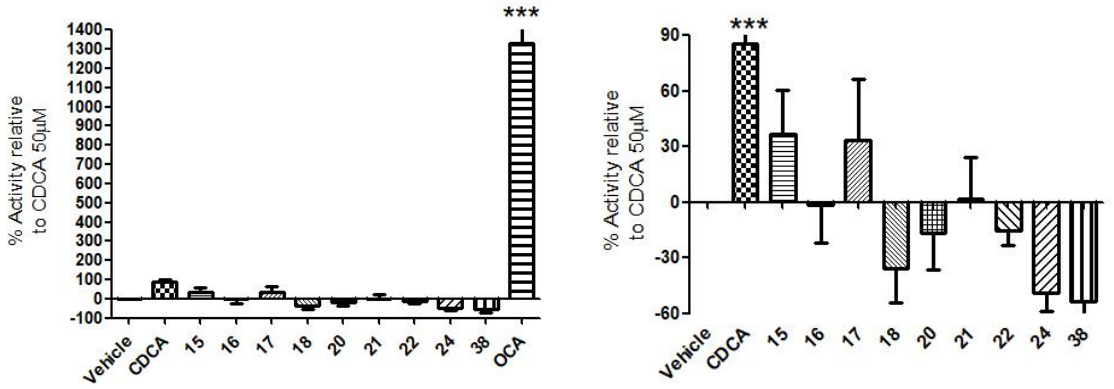

(B)

Figure 4.14- A measurement of % agonist activity of each UDCA sulfonamide. (A) under 100 μM; (B) under 50 μM. Left are with OCA, and right are without OCA. FXR-UAS-bla HEK 293T cells were treated with specific concentration of bile acids solution for 16 h. Cells were then treated with CCF4-AM substrate mixture and then incubated for 2 h in the absence of direct light. The assay was normalised to 0.5 % DMSO vehicle control and absorbance of each well was read on a VERSAmax Microplate Reader (Molecular Devices, Sunnyvale, CA, USA) at a specific wavelength of excitation and emission filter for both blue and green channel. Values are expressed as mean ± SEM of three quadruplicate experiments, * $p<0.05$, ** $p<0.01$, *** $p<0.001$ as determined by one way ANOVA with Dunnett's post-hoc correction.

As shown in Figure 4.14 above, none of the compounds appears to have significant FXR agonist activity apart from CDCA and OCA, known potent FXR agonist. In the 100 μM group, compound **28** exhibited the strongest agonist

effect, followed by 3α-methanesulfonyl UDCA and **26**. To our surprise, 3α-ethanesulfonyl UDCA **29** showed a negative result relative to vehicle control. This may have been due to its cytotoxicity which had been observed towards Huh-7 and Caco-2 cells. In the 50 μM test group, **15** and **17** had a minor agonist effect and the remaining compounds produced negative results compared with vehicle control. The possibility they are FXR antagonists and merits further study.

As described in the introduction, the purpose of this chapter was to describe efforts made to design a bile acid analogue with high toxicity towards mammalian cell lines by taking account of observations in various previous studies in the Gilmer lab. Having explored the amidation of 3-sulfonamido analogues of UDCA, on the basis that amidation in previous 3-azido series had produced highly toxic analogues we next turned our attention to 3-trifluoromethylation in bile acid analogues. The novel compounds were designed to achieve enhanced hydrophobicity, a chemical characteristics long associated with toxicity in the bile acids.

4.7 Synthesis of 3-trifluoromethyl bile acids

4.7.1 Introduction to fluorine chemistry and trifluoromethyl compounds

Fluorine is considered as the next most interesting atom for incorporation into small molecules after nitrogen in the life sciences field. Fluorine as a substituent in active ingredients is important in drug discovery. Usage of fluorinated compounds in medicine can be traced back to the 1940s. Advances in modern chemistry have enhanced understanding of the importance of fluorine in the periodic table and its impact on the structure, reactivity and functions of fluorine-containing molecules. Consequently, lots of materials, ligands, catalysts, polymers and pharmaceutical drugs contain fluorine substitutes. The fluorine atom has a strong electronegativity (4.0), a low polarizability and a small atomic radius. In terms of chemistry, The F-C bond is

very stable and has an effective Van der Waals radius (1.47 Å) similar to C-H bond. The F-C bond is the strongest carbon-atom single bond, which is reflected in the applications of organofluorine compounds. Fluorine has been widely applied to modulate the biological properties of drug molecules such as pK_a value of nearby functional groups, hydrophilic-hydrophobic balance, permeability, metabolic stability, protein binding affinity and lipophilicity because of its large electron-withdrawing inductive effect and its steric resemblance to hydrogen [465]. Moreover, the introduction of ^{19}F nuclear magnetic resonance imaging has become the most promising method in biological studies.

X	H	F	O	Cl	N	CF_3	CH_3
Electronegativity (Pauling Scale)	2.1	4.0	3.5	3.2	3.0	3.5	2.3
van der Waals radius (Å)	1.20	1.47	1.52	1.75	1.55	2.74	2.23
C-X bond distance (Å)	1.09	1.40	1.43	1.77	1.47	1.49	1.51
CH_3-X bond dissociation energy (kcal/mol)	105	110	92	85	85	103	90

Figure 4.15- Chemistry properties involving fluorine, and trifluoromethyl groups [465].

It is well known that introducing fluorine atoms and/or fluorine-containing groups into bioactive molecules can have lots of positive effects, such as allowing them to be more selective, potent, increasing efficacy, and making them easier to administer [466]. Fluorine substitution also leads to substantial conformational changes, therefore changing the bioactivity of organic compounds. Because of these, introduction of fluorine atom to the ring system of bile acid compounds is of great interest to investigate their roles in a variety of metabolic disorders. Fluorination of biologically active molecules promotes the development of contemporary pharmaceutical industry and the advantages of incorporating fluorine into pharmaceuticals has been generally recognized.

To date, 20% of prescribed pharmaceuticals and 30% of the leading blockbuster drugs are estimated to contain a C-F bond. More fluorinated drugs are predicted to be discovered in the near future as fluorine-containing compounds continue to draw attention in the field of chemistry [467]. Many anticancer, and anti-inflammatory drugs have all been successfully modified by fluorine substitution to produce more active compounds.

The development of fluorinated pharmaceuticals is well related to the advances in synthetic organofluorine chemistry. In principle, fluorine-containing organic compounds can be synthesized via both fluorination and fluoroalkylations. However, fluoroalkylation is superior in terms of efficacy and compatibility under many conditions, particularly when fluoroalkyl groups consists of multiple fluorine atoms. Among various fluoroalkylations, trifluoromethylation arouses much interest in medicinal chemistry. Trifluoromethyl groups can be introduced to dramatically change physicochemical properties and related biological activities and to increase binding affinity of drug molecules. Actually, many new drugs approved by FDA contain a trifluoromethyl group, for example efavirenz, sitagliptin, mefloquine and fluoxetine. Their structure indicates that setting up the aromatic/heteroaromatic CF_3 group being the most advanced. The addition of fluorine atoms will enhance its lipophilicity and membrane permeability, thus leading to increased stability and bioavailability [468].

The main purpose of the work in this chapter was to explore synthetic approaches for producing different 3-trifluoromethyl bile acids to help in the characterization of their effect on cellular toxicity, hydrophobicity and FXR activation.

4.7.2 Synthesis discussion of 3-trifluoromethyl bile acids

Nucleophilic trifluoromethylation of carbonyl compounds fundamentally relies on the utilization of trifluoromethyltrimethylsilane, $TMSCF_3$. The synthesis of

3-trifluoromethyl bile acid has been previously investigated in our group by Florian Gegenfurtner.

The aim of this section was to synthesize and characterize a small set of trifluoromethyl CDCA, DCA and UDCA derivatives. The synthesis pathway is shown below in Scheme 4.11. One of the objectives of this work was to characterise the stereochemistry of the trifluoromethyl addition and in relation to their cytotoxicity.

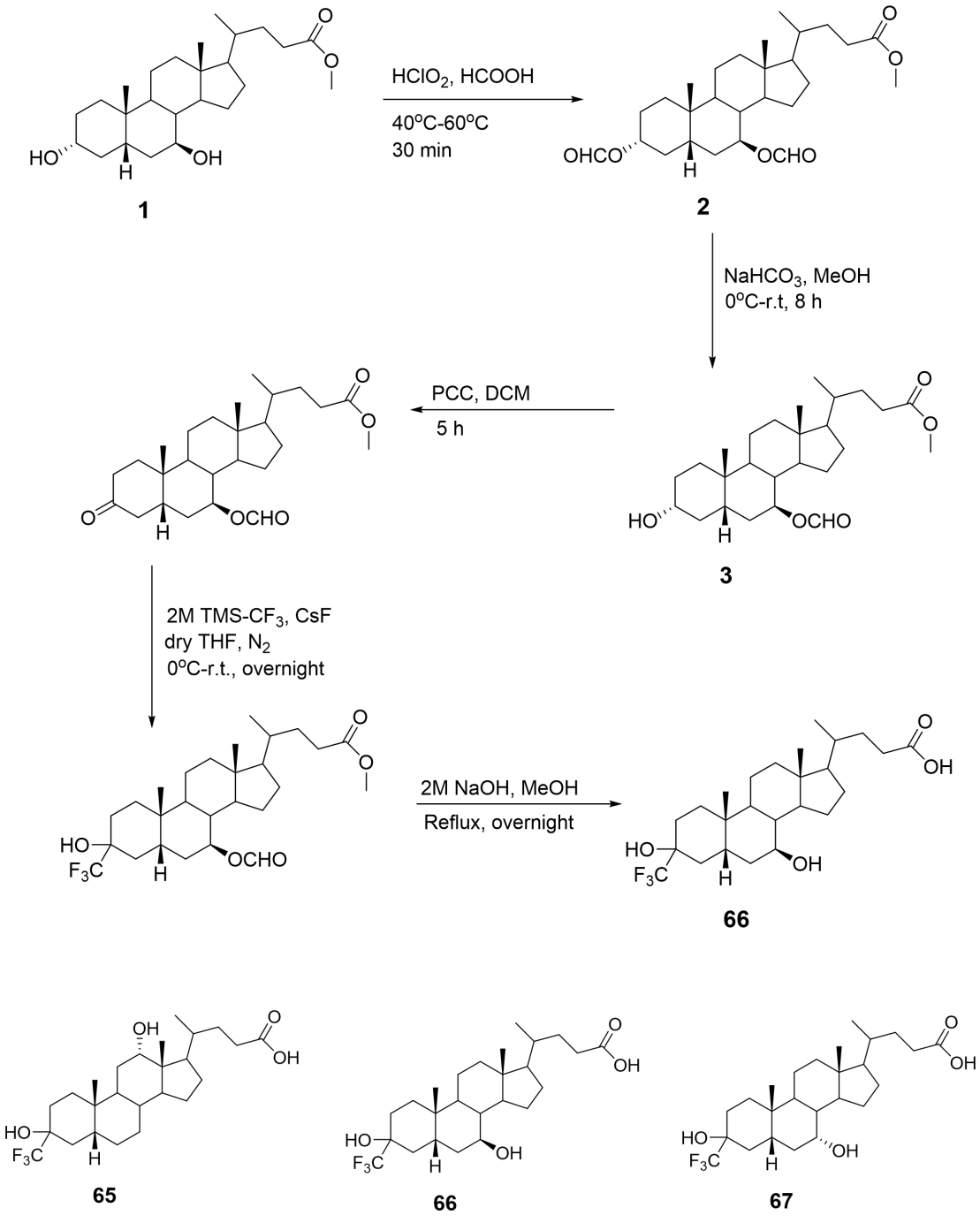

Scheme 4.11- The synthetic pathway for the synthesis of prevalent isomer of 3-trifluoromethyl UDCA 66 and the chemical structure of 3-trifluoromethyl bile acids 65, 66 and 67.

Trifluoromethylation is most commonly achieved via activation of the Ruppert-Prakash reagent, Me_3SiCF_3 which was firstly used for carbonyl compounds in 1989. This is usually achieved in the presence of suitable initiator TBAF or CsF to release the final product. Fluoride activation converts commercial Me_3SiCF_3 into a $^-CF_3$ equivalent, even at low temperature [469]. However, the installation of a 3-trifluoromethyl moiety is challenging mainly because the intermediates formed during the trifluoromethylation reactions are unstable under the conditions necessary for the reaction to proceed [470]. Initially the Ruppert-Prakash trifluoromethylation was performed in the presence of catalytic amount of TBAF [471], however, the reaction did not work as the starting material 3-oxo did not react under these experimental conditions. Afterwards lots of attempts were made to solve the problem, like optimizing the ratio of Me_3SiCF_3, the solvent volume and the initiator category. The choice of fluoride anion activator is very important in this case and the best experimental condition for the synthesis of trifluoromethyl bile acid was finally identified. This involved the employing of a slight excess of Me_3SiCF_3 (1.1 eqv), and a catalytic amount of CsF (0.2 eqv.) and a minimal amount of dry THF under N_2 atmosphere [472] followed by acidic workup affords the trifluoromethylated alcohols in quite good yield (72%).

4.7.3 Characterization of 3-trifluoromethyl bile acids

The configuration of the trifluoromethyl substituent was challenging to determine. 1D ^{19}F NMR showed the presence of a single peak at -79.10 ppm, indicating the existence of only one isomer (Figure 4.16 b). Besides, a signal in 2D HMBC had a J value of 285 Hz indicates the $^{19}F^{13}C$ coupling (typical 1JCF~272 Hz). Heteronuclear 2D NOE experiments were applied to study the

dipolar interactions between heteronuclei and nearby protons to help identify the orientation. The heteronuclear 2-D NOE experiments have proven to be useful for structural elucidation and conformational analysis in ^{13}C and ^{19}F NMR spectroscopy [473]. The characterization of the final product further benefited from DQF-Phase-Sensitive CoSy. This helps suppress the CoSy diagonal, meaning that it is easier to identify cross-peaks near the diagonal. The chemical shift of 3α-H and 3β-H is close on the diagonal and their off-diagonal cross-peaks will be close to the diagonal and thus hard to see on a standard CoSy. Besides, it distinguishes whether J value is positive or negative by using different colors (black for positive and red for negative). It is beneficial for the determination of two pairs of multiplets with similar chemical shifts obscuring each other. The black peak (positive J value) in my case indicated the existence of 3α-CF_3 bile acids. The trifluoromethylation in other words produces the alpha or equatorial isomer.

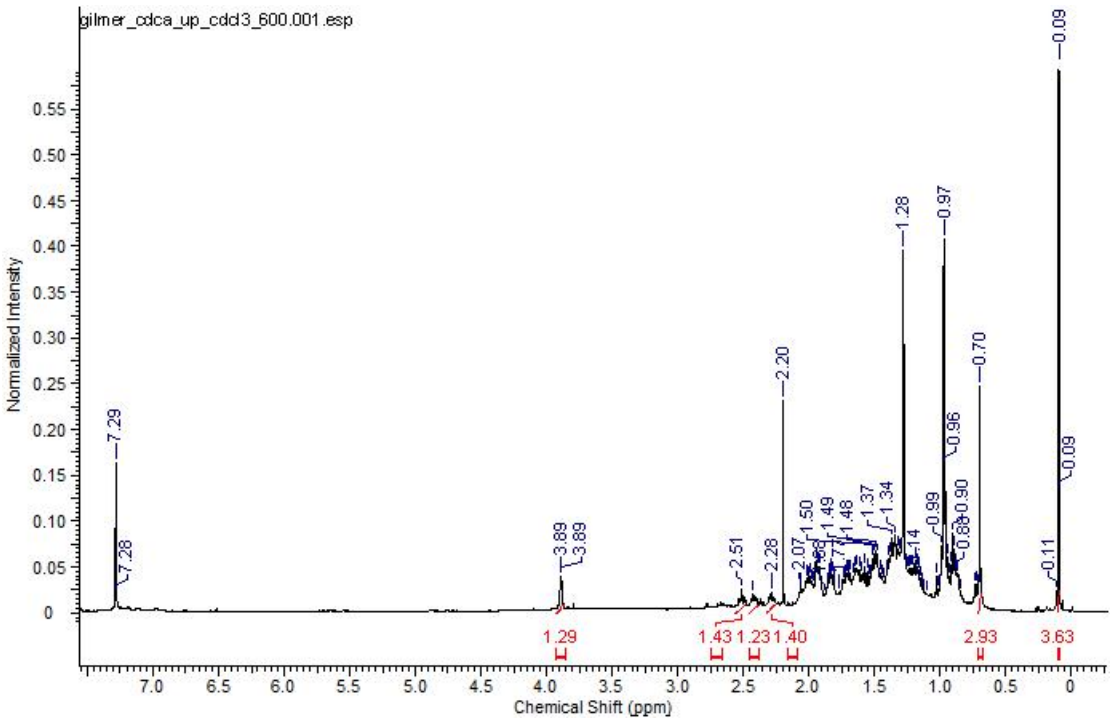

(a)

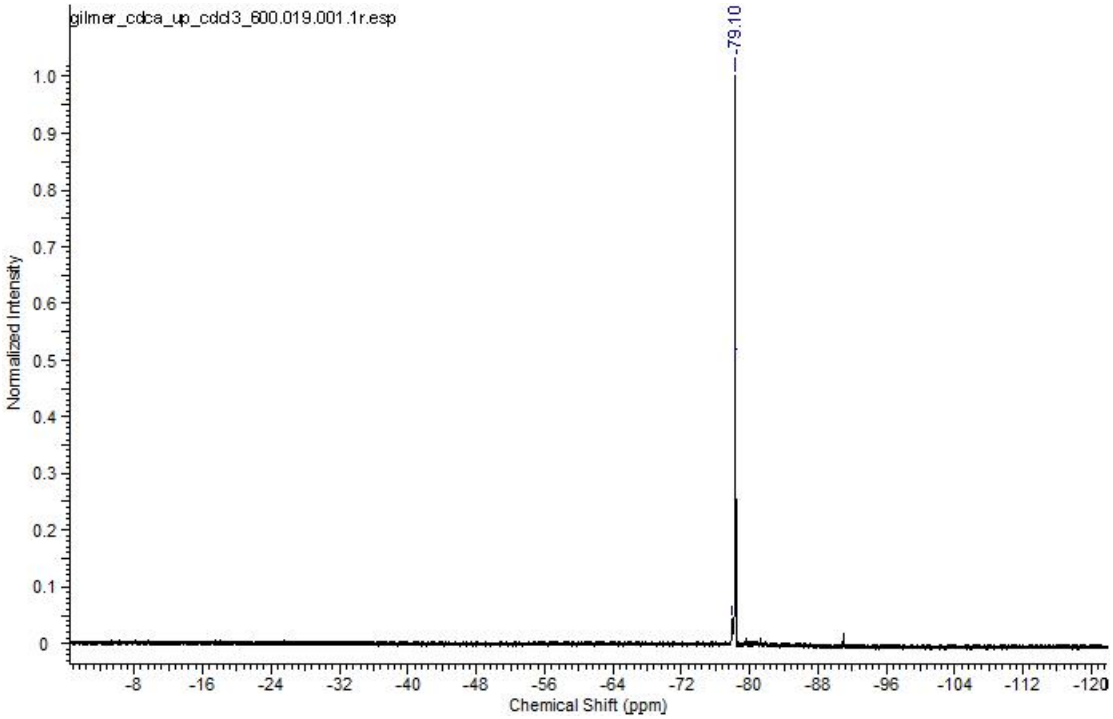

(b)

Figure 4.16- (a) the ^{1}H NMR of 3-trifluoromethyl CDCA 67; (b) the ^{19}F NMR of 67.

4.7.4 Determination of lipophilicity of 3-trifluoromethyl bile acids

The lipophilicity of the 3-trifluoromethyl bile acids was investigated by RPTLC using methanol-water in different compositions. The estimation of log P is based on R_f value of each compound on the RPTLC plate. Although the R_f value is not directly correlated to the lipophilicity of the compounds, a significant relationship was found between the lipophilic parameter R_{MW} value and known log P values of reference compounds, which has been described in Chapter 2.

The purpose of this section was to compare the lipophilicity of these 3-trifluoromethyl bile acids determined by RPTLC using three different mobile phase systems with lipophilicity values estimated by statistical methods.

Estimation of log P

The log P values of the three 3-trifluoromethyl bile acids were estimated using a calibration equation of the log P value of three reference compounds (DCA, CDCA and UDCA) and their measured R_{MW}. The result is shown below in Figure 4.17.

Compound	R_{MW}	log P (reference)	log P (measured)
DCA	5.26	3.50	
CDCA	5.56	3.28	
UDCA	4.31	3.00	
3-trifluoromethyl DCA **65**	6.72		4.09
3-trifluoromethyl CDCA **67**	6.27		3.87
3-trifluoromethyl UDCA **66**	6.16		3.59

Figure 4.17- The the measured log P values of all 3-trifluoromethyl bile acids based on the calibration equation. The reference log P for DCA, CDCA and UDCA is 3.50, 3.28 and 3.00, respectively [533].

The order of measured hydrophobicity of the 3-trifluoromethyl bile acids is: 3-trifluoromethyl DCA **65**>3-trifluoromethyl CDCA **67**>3-trifluoromethyl UDCA **66**, which exactly corresponds to the order of the parent bile acids. The presence of a 3-trifluoromethyl group significantly increases their hydrophobicity/lipophilicity by approximately 0.6 log P units [474–476]. The impact of this on their cytotoxicity is addressed in the following section.

4.7.5 Toxicity characterization of trifluoromethyl compounds in Huh-7 cells

We studied % cell viability effects using the Huh-7 cell line and the Alamar Blue assay. Stock solutions of these bile acid compounds were prepared in DMSO

and they were diluted to 100 μM with supplement free medium (with 1% DMSO). The % cell viability was measured after incubating for 24 h and it was calculated versus vehicle treated control, which was treated with same amount of DMSO (1% in assay medium). Each experiment was carried out in quadruplicate and repeated three times to get twelve data points in total for each drug solution. The data are presented in Figure 4.18 below.

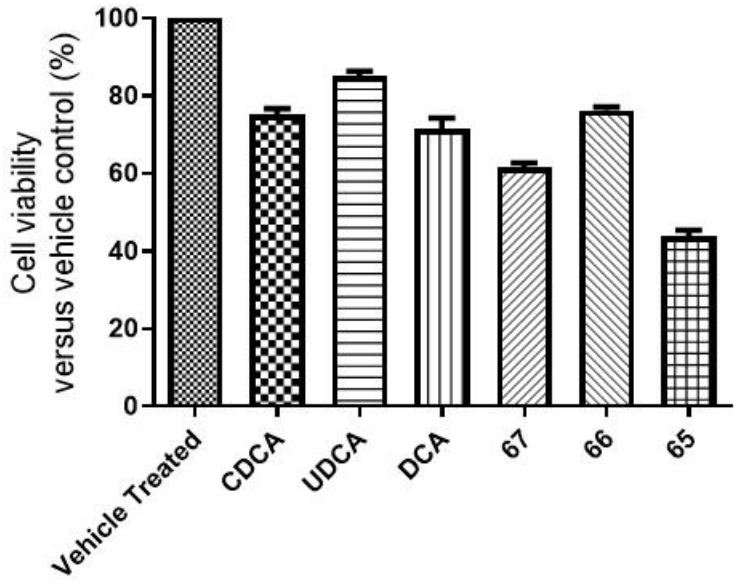

Figure 4.18- A measurement of toxicity of trifluoromethyl bile acids. Huh-7 cells were seeded into 96 well plates at a density of 1×10^5 cells/ml, and then treated with 100 μM bile acids solution for 24 h. Cells were then treated with 10 μl Alamar Blue reagent in an amount equal to 10% of the volume in the well and incubated for 2 h in the dark. The assay was normalised to 1% DMSO vehicle control and absorbance of each well was read on a VERSAmax Microplate Reader (Molecular Devices, Sunnyvale, CA, USA) at a wavelength of 570 nm. Values are expressed as mean ± SEM of three quadruplicate experiments, * $p<0.05$, ** $p<0.01$, *** $p<0.001$ as determined by one way ANOVA with Dunnett's post-hoc correction.

Compared with the toxicity pattern for normal bile acids, addition of 3-trifluoromethyl group increases their cytotoxicity in a manner that corresponds precisely to the order of their calculated hydrophobicity from RPTLC.

4.8 Conclusions

Bile acids are known to induce cell death through a variety of pathways that are related to their detergency and non-specific cell surface effects. However apoptosis in response to bile acids occurs at lower concentration than the CMC at which detergency effects are expected. The Gilmer group have studied a range of bile acid derivatives to detect their potential to interact with specific protein mediators in propagating a cell death signal (as opposed to non-specific detergency effects). One of the better examples of this is the 3α ethyl sulfonamide analogue of UDCA **29** which is potently cytotoxic across multiple cell lines, whereas its methyl and propyl analogues are not. Indeed the UDCA analogue was more toxic than its DCA sulfonamide isomer and is perhaps the most potently cytotoxic bile acid or bile acid analogue discovered. The present study extents the SAR knowledge of this class showing that substitution on the 24-carboxylic acid with amide does not enhance activity (as it had in the 3α- and 3β- azido steroids already published). However the work showed that the carboxylic acid is not essential since it could be reduced to alcohol without compromising activity. This may be useful for the design of cytotoxic bile acid analogues for potential use in cancer treatment or indeed for investigating the mechanism of bile acid – induced cell death which remains obscure. For the application of compounds in this context their effect on FXR as principal bile acid receptor was considered interesting. The compounds were shown not to activate FXR although several may have antagonist effects that could be further investigated. In a final attempt to generate compounds with sub-micromolar toxicity, the sulfonamide design explored in the earlier part of the chapter was replaced with trifluoromethyl. This had the expected effect of increasing hydrophobicity across the panel of UDCA, CDCA and DCA, and increasing toxicity but these analogues were still less toxic than the sulfonamide compounds that were characterized earlier. The 3α orientation of the trifluoromethyl installation was determined by a variety of NMR methods.

Chapter 5. Towards targeted bile acid conjugates

5.1 Studies on dansyl and dansyl taurine compounds

5.1.1 Introduction

The dansyl group has been widely used as a fluorescent reporter in diverse applications. The dansyl group, in which dimethylamino moiety functions as a donor part and naphthalene sulfonyl as an acceptor part, exhibits intense absorption bands in the near UV and a strong fluorescence in the visible region [477]. Dansyl chloride (5-dimethylamino-1-naphthalenesulfonyl chloride) itself is a fluorescence dye for fluorescence labeling of albumin and primary and secondary amines [478] and reaction of dansyl chloride with both aliphatic and aromatic amines produces blue- or blue-green fluorescent sulfonamide adducts [479]. This dye exhibits the advantage of not overlapping with commonly used fluorophores for labeled targets. It was then routinely applied in protein analysis for determining terminal amino acids. Thus, the binding of the dansyl group to an amino acid offers many advantages, for example, the conjugates have strong fluorescence, relatively long emission wavelength and good solvatochromism [480]. These small fluorescent molecules display convenient photophysical properties for monitoring different physiological functions. Besides, it has been demonstrated that derivatization can make slight changes to the parent compounds which do not affect significantly their physiological behavior [481]. Fluorescent bile acid derivatives have been applied to monitor several functional aspects of steroids, transport properties [482], for example, dansyl derivatives of DCA have been found to monitor the kinetics of bile acid transport [483] and bile acid-HSA interaction, an important parameter for liver function test [484].

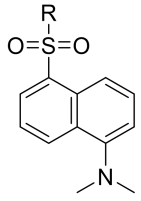

Figure 5.1- Molecular structure of dansyl fluorophore [477]. The dimethylamino moiety acts as an electron donor whereas the naphthalene

sulfonyl group functions as an acceptor. Here, R = Cl (dansyl chloride) or R = $NHCH_2COOH$ (dansyl glycine).

Dr. Ferenc Majer and Dr. Jason Galvin in the Gilmer group previously carried out work on C3-dansyl compounds such as those shown below in Figure 5.2. One of the findings was that these compounds undergo extensive rapid cellular uptake that is apparently active (temperature dependent) but not through a transporter protein. Surprisingly, in further studies, it was found that the uptake rate and extent of the dansyl compounds was far greater than the natural bile acids from which they are derived. In responding to the observations made in Chapter 4, and apparent ceiling on non-specific bile acid toxicity, the purpose of present study was to investigate the possibility for using dansyl bile acid uptake properties to design compounds that can specifically target tumor cells with a toxic payload. First compounds **57** and **59** and taurine conjugated derivatives **58** and **60** were prepared and evaluated for their intrinsic toxicity.

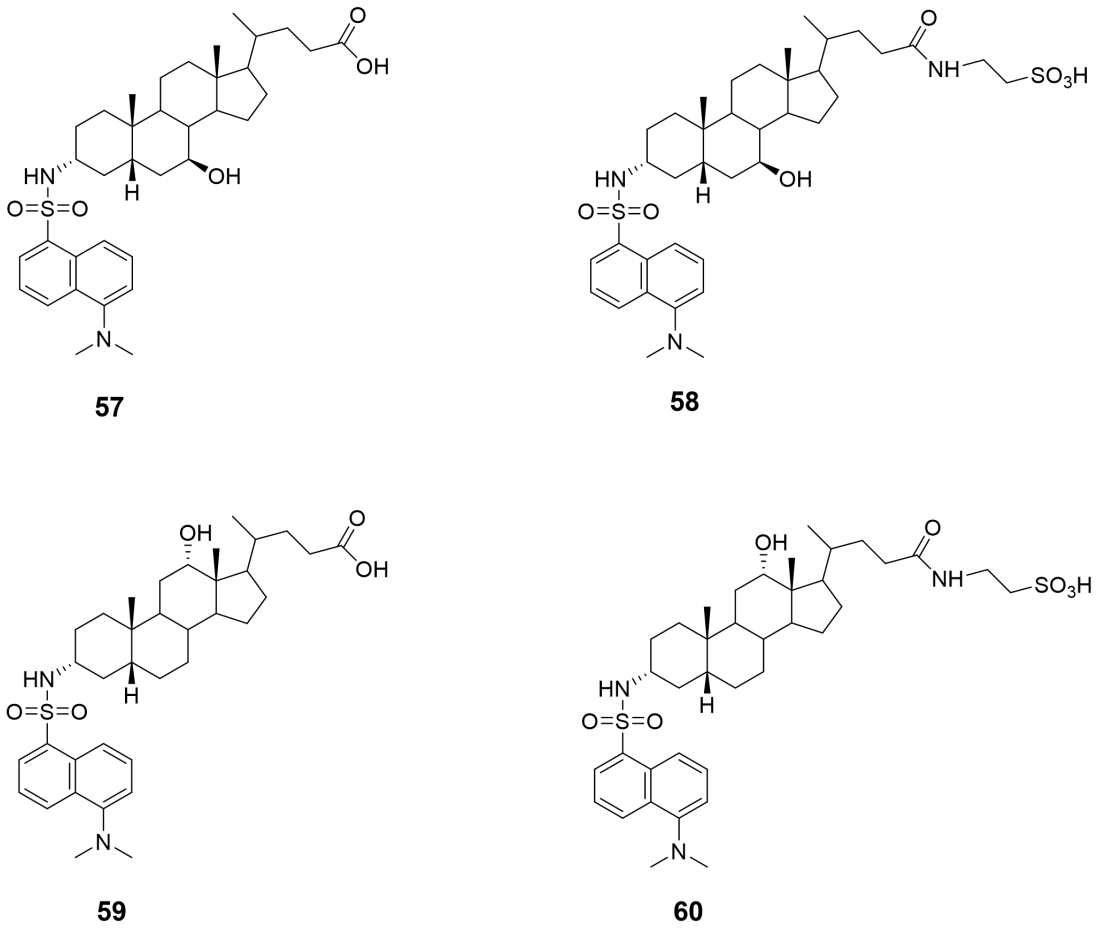

Figure 5.2- The chemical structure of 3α-Dansyl UDCA 57 and 3α-Dansyl DCA 59 and their corresponding taurine conjugated derivatives 50 and 60.

The synthetic approach adopted to these compounds was similar to that has been reported in our previous work on 3α-dansyl moiety of UDCA and DCA [485].

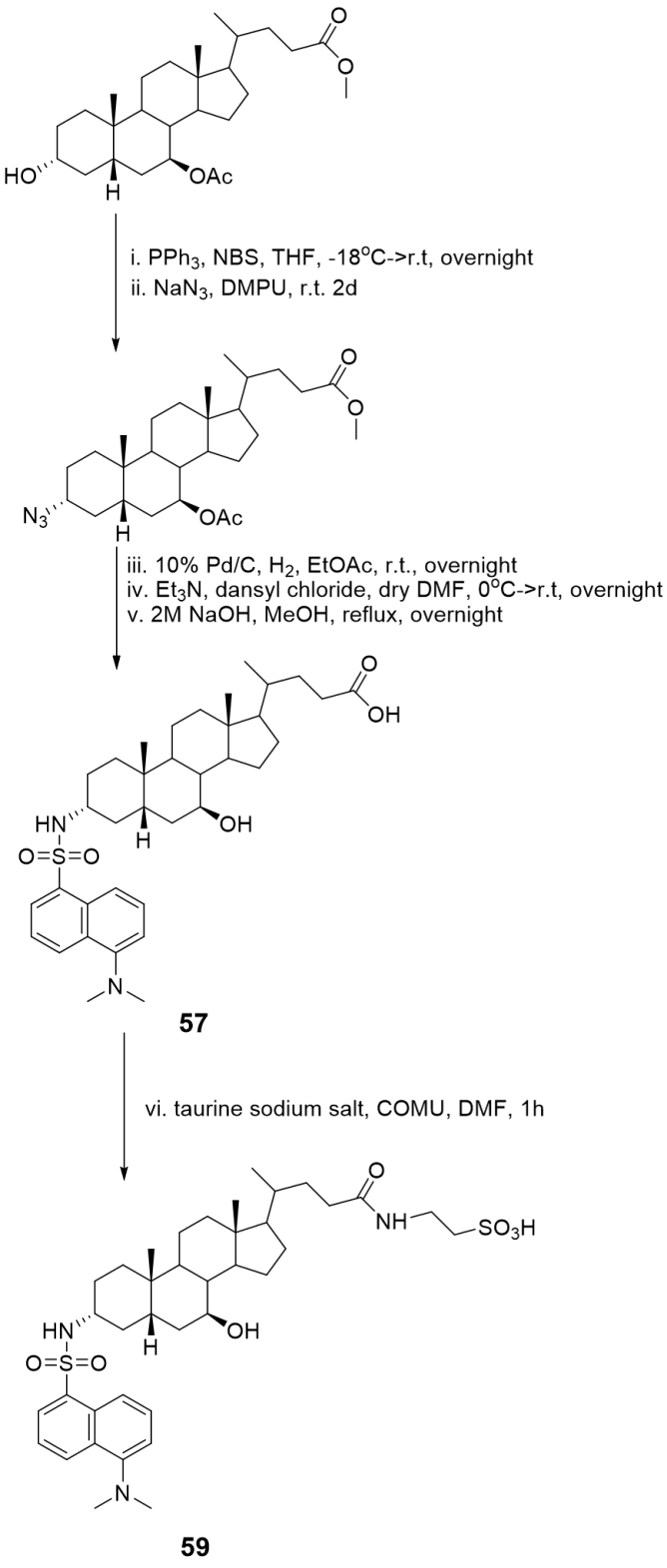

Scheme 5.1- The synthetic route for 3α-dansyl UDCA 57 and its taurine conjugated form 59.

This synthetic route mainly involves the replacement of 3-OH with nitrogen containing group but with retention of configuration. Treatment of the starting

material with NBS in the presence of triphenylphosphine afforded the corresponding 3β-Br, which could be converted to 3α-azide via SN2 substitution. Pd/C reduction with hydrogen gas gave primary amine and amidation with dansyl chloride was performed in sequence to avoid the unstable primary amine degradation. This was followed by ester hydrolysis with sodium hydroxide solution. Synthesis of bile acid taurine conjugates with standard amide coupling technology can be challenging. The final yields are usually poor because of either low conversion or complicated purification due to the high polarity of the ionised sulfonic acid. A recently developing coupling reagent called COMU [486], a safe and effective peptide coupling agent, was found to enable simple conversion to final compounds **58** and **60** and give taurine conjugates in excellent yield (80–85%) as the water soluble byproducts could be washed away in the workup.

5.1.2 Toxicity characterisation of dansyl compounds in Huh-7 cells

In order to characterize the relative toxicity of the dansyl and dansyl taurine compounds, the Alamar Blue assay was used to determine the % cell viability, following treatment of the Huh-7 cell line. Stock solutions of the bile acid compounds were prepared in DMSO and they were diluted to 100 μM with supplement free medium (with 1% DMSO). The % cell viability was measured after incubating for 24 h and was calculated versus vehicle treated control, which was treated with same amount of DMSO (1% in assay medium). Here UDCA was used as reference. Each experiment was carried out in quadruplicate and repeated three times to get twelve data points in total for each drug solution. The data are presented in Figure 5.3 below.

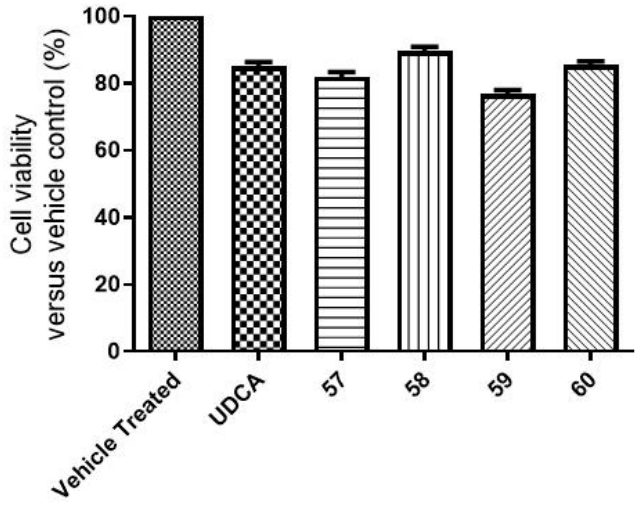

Figure 5.3- A measurement of intrinsic toxicity of dansyl and dansyl taurine bile acids in Huh-7 cells. Huh-7 cells were seeded into 96 well plates at a density of 1×10^5 cells/ml, and then treated with 100 μM bile acids solution for 24 h. Cells were then treated with 10 μl Alamar Blue reagent in an amount equal to 10% of the volume in the well and incubated for 2 h in the dark. The assay was normalised to 1% DMSO vehicle control and absorbance of each well was read on a VERSAmax Microplate Reader (Molecular Devices, Sunnyvale, CA, USA) at a wavelength of 570 nm. Values are expressed as mean ± SEM of three quadruplicate experiments, * $p<0.05$, ** $p<0.01$, *** $p<0.001$ as determined by one way ANOVA with Dunnett's post-hoc correction.

From Figure 5.3, it is clear that incorporation of dansyl moiety slightly reduces the % cell viability after 24 h compared with natural bile acids. Conjugation with taurine, however, reduces the overall toxicity of dansyl compounds, which means taurine-conjugated bile acids were less toxic than their unconjugated counterparts [487]. The result are promising for the application of the compounds as fluorescence reports, however the dansyl group imparts insufficient cellular toxicity compared with the ethyl sulfonamide studied in the previous chapter. Considering that the dansyl reporter group in this series was however known to impart active transport and uptake, we decided to investigate the replacement of the dansyl group with a toxic warhead that has similar overall shape characteristics for active uptake. Chlorambucil, an aromatic mustard will be investigated in the following content.

5.2 Design and development of cell-targeted cytotoxics

5.2.1 Cytotoxic-bound steroid conjugates

Chemotherapy has been the main method for treatment of cancer patients since the middle of the 20th century. The long-standing limitation to most cancer-chemotherapeutic agents is that they are not selective in their action against cancer cells and they often lead to side effects in therapeutic dose caused by the acute toxicity of the agents towards normal cells and tissues. Insufficient accumulation of drugs within the tumor cells is also a big issue. Besides, they are also restricted by multi-drug resistance of tumor cells and a large dose of drug can be required to achieve adequate local concentration. However, with the advent of monoclonal antibodies, which recognize antigens related to many types of human cancers, over the past 15 years, cancer treatment has shifted from conventional chemotherapy towards receptor-target chemotherapy (selective chemotherapy) considering the non-specific toxicity of most chemotherapeutic agents against normal cells. The conjugation of an anticancer molecule with a steroid towards its cognate receptor can be more selective and less toxic than the non-target approach [488–490]. An important approach to enhance the profile of an anticancer drug is to conjugate selected chemotherapeutic agents (warhead) to various carriers/targeting motif, including estrogen, peptide and steroid hormones via the enzyme-labile bond or spacer molecules, which can preferentially recognize tumor cells [491–493]. The advantage of this design is that cytotoxic agents can be specifically targeted to receptors and thus selectively delivered to the nucleus of the cancerous cells where they exert their cytotoxic effect [494–496] because these conjugates recognize the intrinsic morphological and physiological differences between cancerous and normal cells. This has the potential to increase or prolong therapeutic concentrations in the target cancerous area, compared to the normal tissues or cells, and peripheral toxicity would be significantly reduced. Targeted chemotherapy also provides possibility for overcoming

intrinsic resistance of some tumors to traditional chemotherapeutic agents [497].

The coupling of cytotoxic agents to steroidal skeletons has been studied since the late 1960s. The first hormone targeting chemotherapeutic agents developed for the treatment of cancer used estrogens as carriers for various alkylating agents. Nitrogen mustard compounds were chemically bound to carrier estrogens for improving cytotoxicity and selectivity on estrogen-positive cells. The clinical application of estramustine (Emcyt®, synthesized in the 1960s), is an early example of hormonally targeted chemotherapeutic drug effective against breast cancer and advanced prostate cancer [498]. It is a conjugated derivative of a potent estrogen named estradiol and a nitrogen mustine moiety called chlormethine. The design of these cytotoxic estrogen derivatives was based on the mechanism that linking 17β-estradiol with the alkylating agent would promote the transport of the cytotoxic agent directly to the nucleus of tumor cells by targeting active estrogenic hormone receptors with high affinity [499]. This would result in improved specificity and efficacy for the target cells, and at the same time, reducing overall toxicity [500]. In general, targeting hormone dependent tumors through the estrogen receptor is an effective strategy in the development of more potent cancer chemotherapy agents [501].

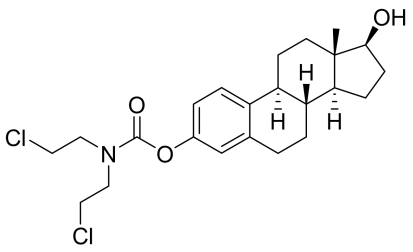

Figure 5.4- The chemical structure of Estramustine. It is a synthetic compound linking the 3-hydroxyl group of 17β-estradiol with the carboxyl group of bis (2-chloroethyl)carbamic acid through a carbamate link.

Drug-bile acid conjugates have been synthesized based on this idea at first proposed in 1982. Pioneering work in developing bile acid-derived prodrugs

origins from the research team of Kramer, who studied bile acid drug conjugates [7][525]. Bile acid-based drug conjugates are discussed as delivery systems for anticancer drugs and therapeutic peptides [502]. Bile acids are selected as effective carrier and absorption enhancer because of their biological compatibility and favorable toxicity profiles [503]. Bile acids are selectively taken up into the liver by the specific transporters in the hepatocyte plasma membrane and specific interaction with hepatic and ileal bile acid transporters could in principle be achieved for drug-bile acid conjugates. In drug-bile acid conjugates the bile acid moiety increases affinity of the conjugates to bile acid transporters.

5.2.2 Nitrogen mustards and chlorambucil

The most suitable target for receptor-based cytotoxic agents used for chemotherapy against cancer is DNA. Many effective drugs used for the treatment of cancer have a common feature of alkylating DNA [504]. Alkylation of DNA occurs through three different mechanisms: 1) attaching alkyl groups to DNA bases, leading to the repression of DNA synthesis and RNA transcription due to the altered DNA, 2) DNA damage via the formation of cross-links, and 3) the mispairing of nucleotides.

Nitrogen mustards were among the first chemotherapeutic drugs for cancer treatment. They are types of drugs showing very potent antineoplastic effects and highly effective in the treatment of Hodgkin disease, lung, ovarian and breast cancers as well as several lymphomas [505]. Nitrogen mustards present a major class of alkylating agents derived from mustard gas, which are commonly used in the treatment of cancer since the discovery of their anticancer effect in 1942, however their poor selectivity to cancer cells, high toxicity, and limited therapeutic activity restricts their further clinical application. Nitrogen mustards are a kind of bio-alkylating agent which can form electron deficient intermediates with active electrophilic groups. They finally lead to

blockade of cell division by reacting with DNA, cross linking two DNA strands and preventing DNA duplication. The mechanism of action arises from the presence of an N, N-bis (2-chloroethyl)-amine group. They show the highest toxicity by binding to N-7 on the DNA base guanine, the preferred site of initial attack [506–509]. The formed cross-linking is irreversible and leads to cellular apoptosis.

Nitrogen mustards alkylate DNA in two steps [510]. Firstly, they undergo a first order SN2 intramolecular cyclization at neutral or alkaline condition by single step and an unstable aziridinium cation is formed. The aziridinium ion is highly reactive towards the DNA of cancer cells as well as normal cells. In the second step, a monoalkylation adduct is produced from the strained aziridinium cation through SN2 mechanism. The mechanism repeats again on the other side to resulting in cross linking between two DNA strands.

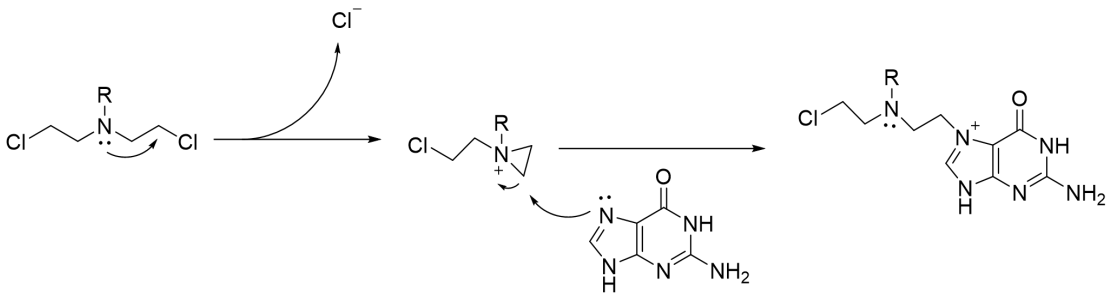

Figure 5.5- The mechanism of Guanine Alkylation by Nitrogen Mustards [511]. Nitrogen mustard alkylating agents react with DNA in a sequence selective manner.

Due to its high reactivity and cytotoxicity, numerous modifications have been made to improve its efficacy and selectivity. Combination of nitrogen mustards with a steroidal hormone with affinity for its receptor leads to the improvement in activity, safety, pharmacokinetics and pharmacodynamics of the leading compounds [512, 513]. Among all the conjugated molecules, steroid hormone-nitrogen mustard combination has been found to be the most successful *in vivo* [514]. It can be imagined that a lipophilic steroid carrier molecule would aid transport of the nitrogen mustards more effectively to

specific target.

The first reported nitrogen mustard compound was bis (2-chloroethyl) sulfide (known as mustard gas), used as poison gas in the Second World War. Mechlorethamine was the first nitrogen mustard introduced in clinical practice and the first cytotoxic agent to show antineoplastic activity. However, it is cytotoxic and induces several severe side effects, for example, severe injuries to the eyes, respiratory tract and skin [515] and severe gastrointestinal and bone marrow depression.

Chlorambucil was among the first drugs in the treatment of cancer and it is first line anti-cancer agent in the management of various types of tumors. Chlorambucil (N, N-bis(2-chloroethyl)-p-aminophenylbutyric acid, see Figure 5.6) is an acidic aromatic derivative of nitrogen mustard synthesized by Everett et al. in 1953. It is also known as the drug Leukeran®. It is clinically used in the treatment of Hodgkin's disease, chronic lymphocytic leukaemia (CLL) and PBC as well as some types of lymphoma. Its clinical use is limited as it causes toxic side effects, for example, bone marrow suppression, immune system injure, vomiting, nausea and increased risk of infection [516]. It is available in tablets of 2 mg. The daily dose ranges from 2 to 10 mg, and often given long term.

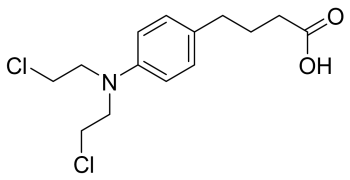

Figure 5.6- The chemical structure of chlorambucil. It is a monocarboxylic acid that is butanoic acid substituted at position 4 by a 4-[bis(2-chloroethyl)amino]phenyl group.

The mechanism of anti-tumor effect of chlorambucil relates to its ability to alkylate DNA by cross-linking guanine bases in DNA double helix strands [517] (the primary mechanism involves the formation of N7G:N7G crosslinks),

making the strands unable to uncoil and separate. As this is important in DNA replication during all phases of cell cycle, cells can no longer divide. Although it is classified as a cytostatic drug (stops cell division) the DNA damage via the formation of cross-links may induce apoptosis. Cellular apoptosis is associated with activation of an apoptosis promoter Bcl-2 protein and activation of p-53 protein (see Figure 5.7).

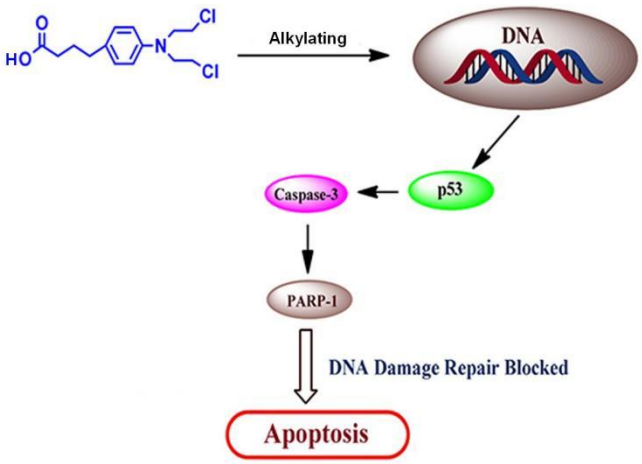

Figure 5.7- The mode of mechanism of the anti-tumor effect of chlorambucil [518].

Although it is much less toxic than most other nitrogen mustards, there is sufficient evidence for the carcinogenicity of chlorambucil and it remains listed as a known carcinogen. Besides, dose and duration of treatment were considered to be two important determinants of chlorambucil from several clinical trials [519]. The problem of drug resistance is a key challenge restricting the application of chlorambucil [520].

Improving the therapeutic properties of chlorambucil by exploring tumor specific targeting of drug delivery became a hot topic in recent years. Bile acid chlorambucil conjugates have been investigated to address the problems of poor drug delivery and drug resistance. This belongs to a broader field of harnessing the well characterized selective uptake of bile acids to target cells. From early 1990s, much efforts were focused on using the C-3 position on the

steroid nucleus based on the analysis of the SAR for the relevant transporters [521]. Indeed Kramer et al. employed taurocholic acid as a carrier in an attempt to deliver chlorambucil to hepatocytes [522]. Chlorambucil can be conjugated to bile acids via either an ester or peptide bond in a way that conserves the negatively charged side chain of natural bile acid that is critical for active uptake [523]. The covalent coupling of chlorambucil to bile acids has potential to improve intracellular accumulation of this cytostatic drug [524, 525] as the conjugates can be taken up into the liver by transporter proteins on the hepatocyte membrane. Such approaches would in principle also retain to an extent chlorambucil in the liver system avoiding kidney partitioning and elimination. Transport of bile acid chlorambucil-taurocholate conjugate by NTCP and OATP present in human liver cancer cells (HCC) [526] demonstrated in principle that cytostatic agents coupled to bile acids could be a chemotherapeutic approach to treat HCC in humans. However a serious challenge to selectivity in this approach is the reduced expression of NTCP and OATP on liver cancer cells compared with normal liver cells, with potential for effects opposite to what is intended [527].

In this study, we focused on the synthesis of bile acid chlorambucil conjugates shown in Figure 5.8 based on the rapid and extensive uptake of the dansyl compounds described earlier in the chapter, which had little toxicity. Following initial synthetic studies preliminary, biological evaluations of their effect on cell viability were carried out to determine if the bile acid modified the profile of the payload drug. The partitioning of these substances into liver cells was studied using HPLC.

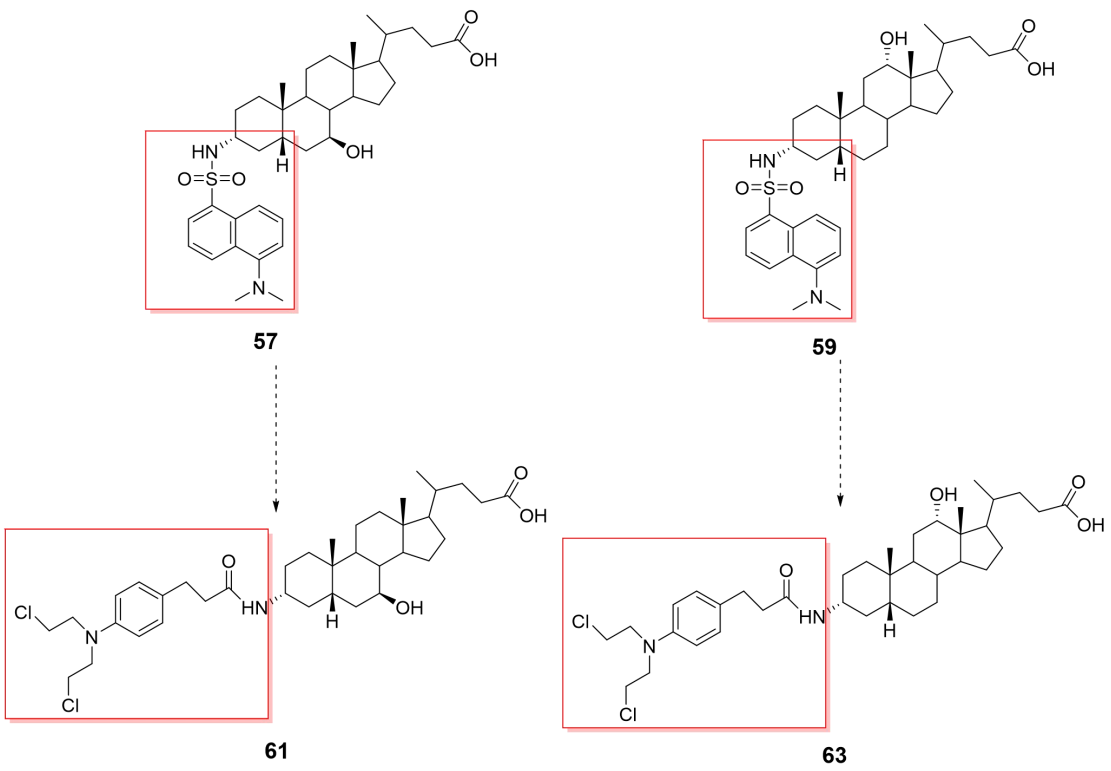

Figure 5.8- Chemistry strategy in replacement of the dansyl group with a toxic payload, chlorambucil. UDCA chlorambucil conjugate **61** and DCA chlorambucil conjugate **63** have potential as chemotherapeutics in hepatocellular carcinoma.

5.2.3 Design and synthesis of bile acid chlorambucil conjugates

The synthesis of these chlorambucil bound bile acid was based on the amide bond formation (-NHCO-) between chlorambucil and a linker-modified CDCA/DCA ester to mimic the amide bond in the dansyl compounds. Thus, chlorambucil conjugated UDCA **61** was synthesized from UDCA azide **5** through Pd/C reduction, HOBt·DCC coupling and final deprotection step (Scheme 1). A similar synthetic approach was adopted to the chlorambucil conjugated DCA **63**.

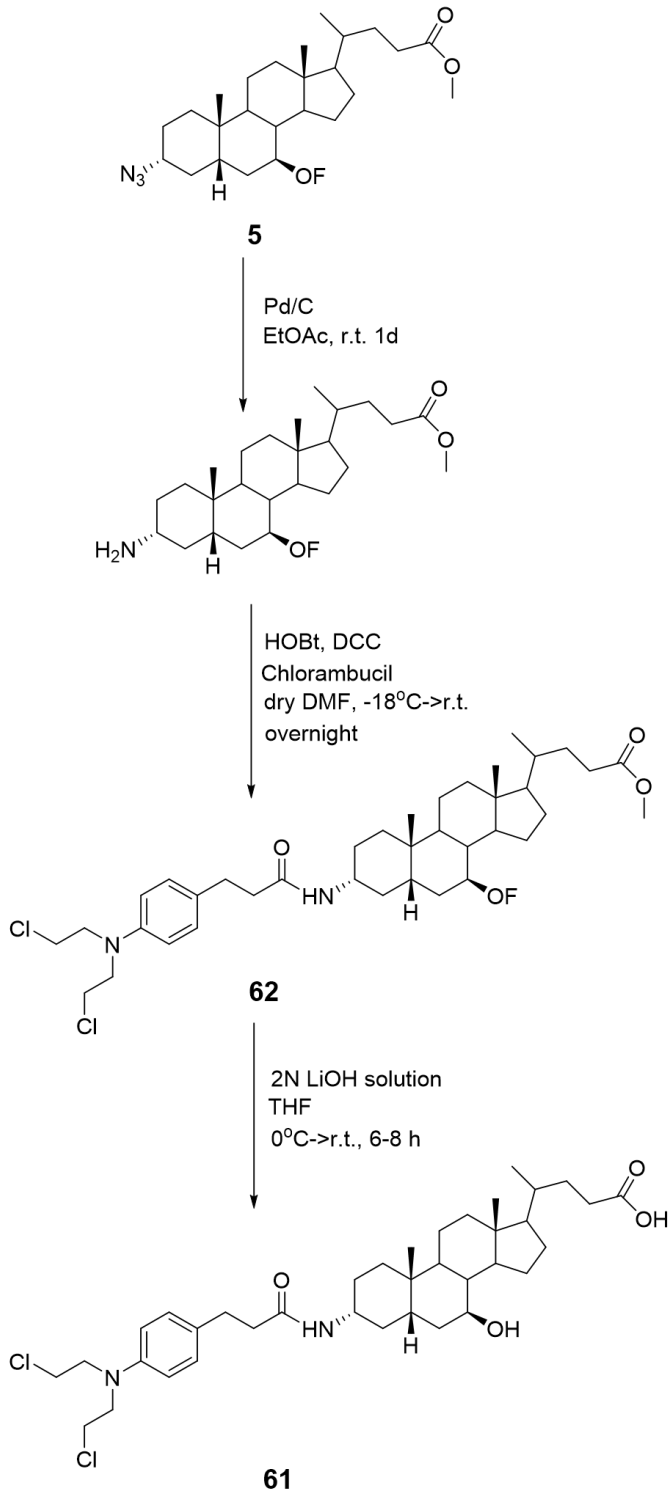

Scheme 5.2- The synthetic route for the synthesis of UDCA chlorambucil conjugate 61.

The first step in the synthetic approach was the Pd/C reduction into amine over H_2. After 24 h, TLC showed 100% conversion of the starting material. The TLC plate was developed in hexane: EtOAc= 5:1 with vanillin solution used for

detection and a big spot was found on the baseline, consistent with formation of the amine intermediate.

Reaction of chlorambucil with the amino bile acid derivative methyl ester, using conventional HOBt and DCC as condensing agents (Steglich esterification), gave the product in good yield [528]. The formation of chlorambucil amide was followed by TLC using hexane: EtOAc=2:1 as the mobile phase. The crude product was purified by flash chromatography to yield UDCA chlorambucil amide **62** as brown foam (63%).

UDCA-chlorambucil amide was treated with 2M aq. NaOH solution in methanol (pH=14) under reflux condition for overnight with no success probably because of hydrolysis of the amide linkage [529]. The protected UDCA chlorambucil adduct in THF was treated with a 2 N aq. solution of LiOH in MeOH/H_2O to pH~10 and stirred for 6-8 h until TLC analysis showed the hydrolysis was complete. The crude product was then purified by flash chromatography (hexane: EtOAc=1:2) to afford final UDCA chlorambucil conjugate **61** as a white solid (50%). Two newly synthesized bile acid conjugates as well as the parent drug chlorambucil were screened for cytotoxicity test in the Huh-7 cell line using the colorimetric MTT assay. The purpose of this study was to investigate putative mechanisms of action of chemotherapy with chlorambucil and bile acid chlorambucil conjugates against cancer cell line, here Huh-7 cell line.

5.2.4 Toxicity characterisation of chlorambucil bound bile acids in Huh-7 cells

The effect of drug chlorambucil and adducts **61** and **63** on cell viability was determined in the relevant cell lines using the Alamar Blue assay. We studied % cell viability effects on the Huh-7 cell line. Stock solutions of the test compounds were prepared in DMSO and these were diluted to 100 μM with supplement free medium (with 1% DMSO). The % cell viability was measured

after incubating for 24 h and it was calculated versus vehicle treated control, which was treated with same amount of DMSO (1% in assay medium). Here UDCA is used as the reference in this experiment. Each experiment was carried out in quadruplicate and repeated three times to get twelve data points in total for each drug solution. The data are presented in Figure 5.9 below.

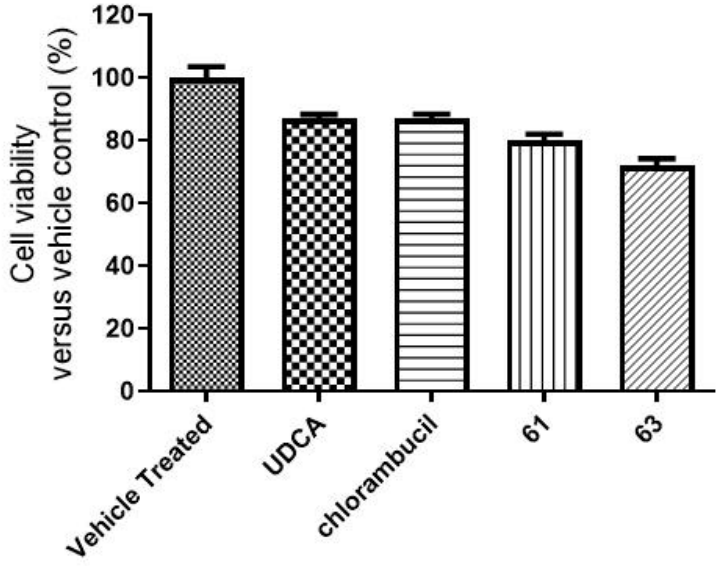

Figure 5.9- A measurement of toxicity of chlorambucil bound bile acids. Huh-7 cells were seeded into 96 well plates at a density of 1×10^5 cells/ml, and then treated with 100 μM bile acids solution for 24 h. Cells were then treated with 10 μl Alamar Blue reagent in an amount equal to 10% of the volume in the well and incubated for 2 h in the dark. The assay was normalised to 1% DMSO vehicle control and absorbance of each well was read on a VERSAmax Microplate Reader (Molecular Devices, Sunnyvale, CA, USA) at a wavelength of 570 nm. Values are expressed as mean ± SEM of three quadruplicate experiments, * $p<0.05$, ** $p<0.01$, *** $p<0.001$ as determined by one way ANOVA with Dunnett's post-hoc correction.

From Figure 5.9 above, the bile acid chlorambucil conjugates show increased overall effect on cell viability compared to chlorambucil. The parent drug had weak activity in the Huh-7 cell line resulted in 14.1 % ± 1.499% of cell viability reduction compared with vehicle treated. UDCA and DCA chlorambucil conjugates show some cytotoxicity effect on Huh-7 cells after incubating for 24 h, causing 19.83% and 27.93% cell reduction respectively. Chlorambucil is frequently classified as a cytostatic rather cytotoxic drug and therefore its

effect in a cell viability assay depends on the extent of cell division or doubling time of the cell line.

Therefore Huh-7 cells were treated again, this time for 48 h with the same test articles and otherwise similar conditions to assess the effect over further proliferation time.

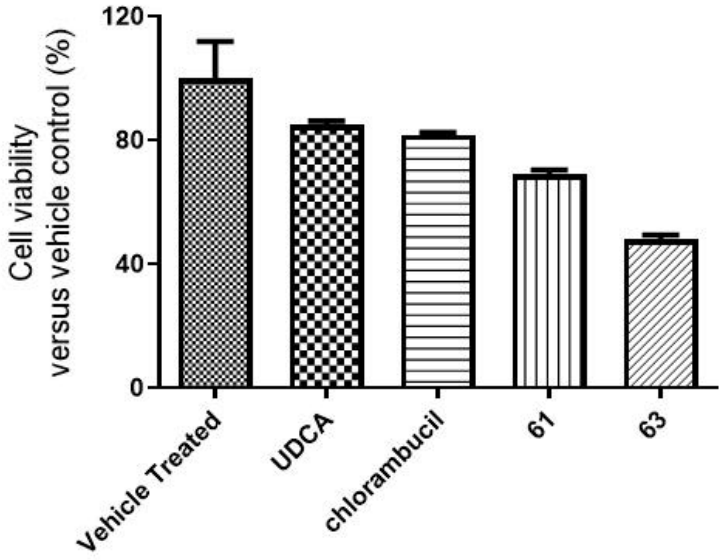

Figure 5.10- Further results of toxicity screen of chlorambucil and chlorambucil bound bile acids in huh-7 cells. Huh-7 cells were seeded into 96 well plates at a density of 1×10^5 cells/ml, and then treated with 100 μM bile acids solution for 48 h in this case. Cells were then treated with 10 μl Alamar Blue reagent in an amount equal to 10% of the volume in the well and incubated for 2 h in the dark. The assay was normalised to 1% DMSO vehicle control and absorbance of each well was read on a VERSAmax Microplate Reader (Molecular Devices, Sunnyvale, CA, USA) at a wavelength of 570 nm. Values are expressed as mean ± SEM of three quadruplicate experiments, * $p<0.05$, ** $p<0.01$, *** $p<0.001$ as determined by one way ANOVA with Dunnett's post-hoc correction.

There was no significant reduction in Huh-7 signal after treatment with chlorambucil for 48 h compared with 24 h. In contrast, the bile acid conjugates showed greater activity over the longer incubation time. UDCA chlorambucil by around 30% (69.2% ± 1.235 % cell survival), The DCA chlorambucil conjugate, caused cell viability loss of 72.1 % compared to 47.9 % at 24 h. Although a

small study, the bile acid conjugates with chlorambucil appear to be worth further investigation in that they have enhanced effect on cell viability compared with the bile acids themselves and the parent nitrogen mustard.

Further studies could look at the concentration dependence of the effect and at the mechanism and involvement of cell death in the effect.

5.2.5 Cellular uptake of the chlorambucil and bile acid chlorambucil conjugates in Huh-7 cell line by HPLC

It was of interest to understand if the conjugation to the bile acids improved the cell viability reducing effects of chlorambucil through increasing cellular uptake or through some other effect for example by changing protein binding to a modulator of cell survival/apoptosis.

There are three main ways that molecules move across a membrane and these include passive diffusion (simplest mechanism), active transport (ATP driven and require the aid of transporter) and endocytosis. UDCA and DCA are in their free form generally taken up through so-called passive diffusion.

Although chlorambucil has been in medical use for many years, the mechanism of its transport and cellular uptake remains incompletely understood. Cellular uptake of chlorambucil does not proceed against a concentration gradient [530]. The pK_a value of chlorambucil is 5.8, causing the drug to exist largely in the unionised form at upper intestinal pH. Cell culture models, here tumorigenic Huh-7 cells, offer the possibility of using pharmacological methods to gain more precise information on the mechanisms of cellular uptake. The extent of cellular uptake of chlorambucil the related bile acid conjugates into Huh-7 cells in this context was quantified by a HPLC method with UV detection.

The uptake was studied by incubating solutions of the test articles, removing the supernatant, washing and lysing the cells and analyzing both supernatant

and cell lysate portion using HPLC. Huh-7 cells were seeded into 24 well plates at the cell density of 80,000 cells per well in a volume of 250 µl and incubated for 48 h. The supernatant was removed and 250 µl of chlorambucil or analogue compound (at 100 µM) in serum free medium was added to each well and incubated for 30 min. The supernatant was then fully removed again and added to Eppendorf tube A. The cells remaining in the wells were washed with cold PBS twice to reduce non-specific binding effects (outside cells and plastic). The washings were also analysed by HPLC to eliminate non-specific binding contribution to the effects observed. RIPA lysis buffer (250 µl) was then added to each well for 30 min. After 30 min, the mixture was removed and collected into another Eppendorf tube B. These Eppendorf tubes collected were stored at 4^{o}C for further analysis. Supernatant and cell lysate concentrations were determined by HPLC. They were diluted 1 in 1 with mobile phase and the samples were centrifuged at 10,000 rpm for 10 min at 4^{o}C to remove cell residues and to precipitate the cellular debris and membrane proteins. The prepared samples were then measured based on the developed HPLC method and the results were calculated in the estimation of expected concentrations versus the external reference standard controls, 100 µM chlorambucil, UDCA chlorambucil conjugate or DCA chlorambucil conjugate. All of the experiments were performed in triplicate and carried out at 37^{o}C. It was found that the water/ACN (50:50) mixture ratio with 0.1% formic acid was the optimal mobile phase and the flow rate was set at 1.5 ml/min. The detection wavelength was 254 nm and the retention times of drug chlorambucil, UDCA chlorambucil conjugate and DCA chlorambucil conjugate were 5.4 min, 13.3 min and 24.8 min, respectively (see Figure 5.11).

SAMPLE INFORMATION

Sample Name:	CLB	Acquired By:	System
Sample Type:	Unknown	Sample Set Name	Jerry 14092020
Vial:	2	Acq. Method Set:	Jerry method
Injection #:	1	Processing Method	Jerry
Injection Volume:	20.00 ul	Channel Name:	2487Channel 2
Run Time:	20.0 Minutes	Proc. Chnl. Descr.:	2487Channel 2
Date Acquired:	9/14/2020 9:34:02 PM IST		
Date Processed:	9/15/2020 5:07:21 PM IST		

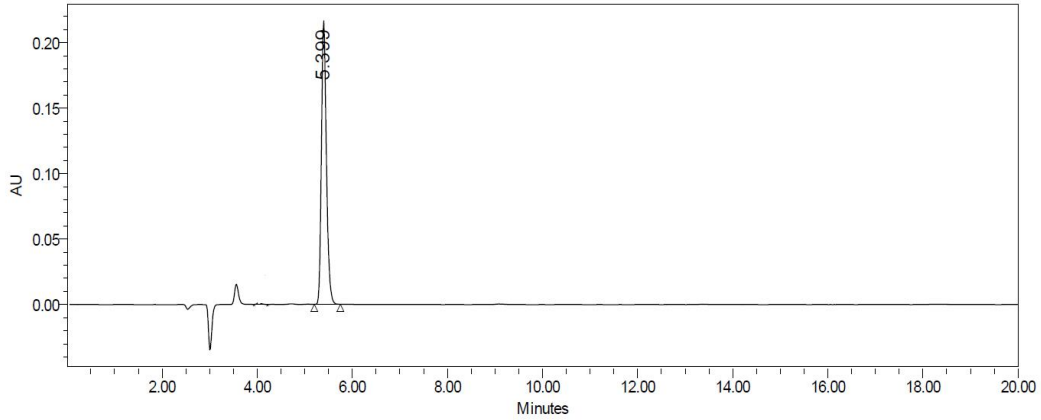

	RT	Area	% Area	Height
1	5.399	1582152	100.00	215692

(a)

SAMPLE INFORMATION

Sample Name:	DCA CLB	Acquired By:	System
Sample Type:	Unknown	Sample Set Name	Jerry 14092020
Vial:	4	Acq. Method Set:	Jerry method
Injection #:	1	Processing Method	Jerry
Injection Volume:	20.00 ul	Channel Name:	2487Channel 2
Run Time:	30.0 Minutes	Proc. Chnl. Descr.:	2487Channel 2
Date Acquired:	9/14/2020 10:15:52 PM IST		
Date Processed:	9/15/2020 5:07:23 PM IST		

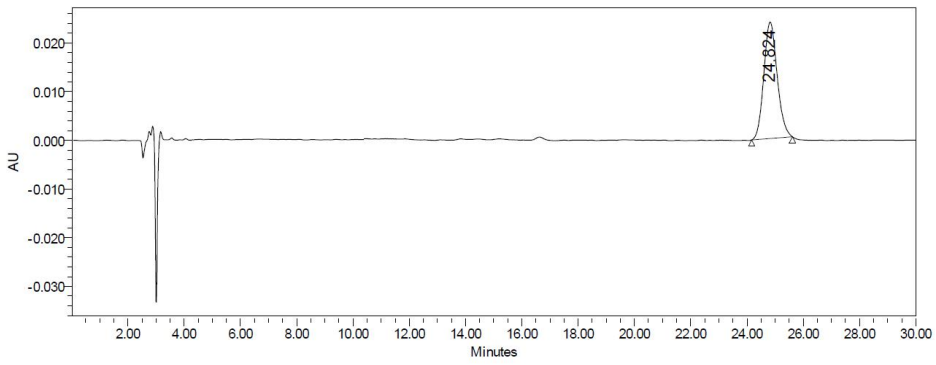

	RT	Area	% Area	Height
1	24.824	788593	100.00	23934

(b)

Figure 5.11- Chromatogram of chlorambucil (a) and DCA chlorambucil

conjugate (b) (100 μM) dissolved in mobile phase (water: ACN=1:1) without any cell. The chromatograms show only single peak and no other major peaks for any other metabolites.

The peak area found in the HPLC chromatograms can be quantitated into the concentration of test articles compared with the standard injection concentration (100 μM), therefore cellular uptake could be quantitatively determined based on the variation of the peak area in the HPLC chromatogram of supernatant versus the standard. Low levels of test articles were found in the supernatant (Figure 5.12). The samples taken into PBS to indicate non-specific binding were analysed by HPLC and in a similar manner to the lysate and supernatant samples. The HPLC analysis indicated that a small amount of the analytes remained on the bottom or inner wall of the 24 well plate after the supernatant was taken. However, washing the cells with PBS after removal of supernatant made no difference to the following analysis of cellular concentration after cell lysis, indicating negligible binding to the plate.

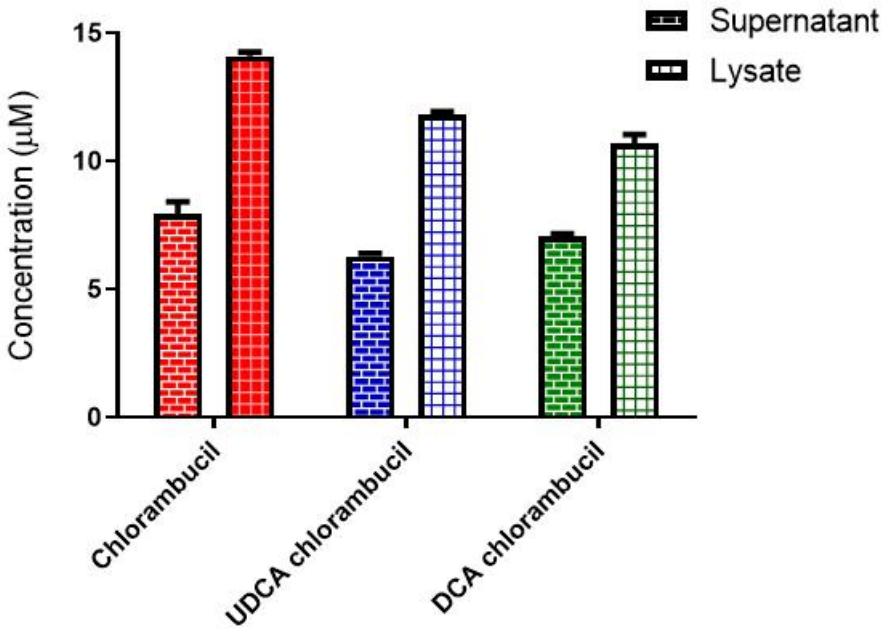

Figure 5.12- Supernatant and lysate concentration of chlorambucil and two bile acid chlorambucil conjugates after treating for 30 min.

Work for the next stage was to compare the differences of supernatant and cell lysate portion after treatment with chlorambucil, UDCA chlorambucil and DCA chlorambucil for longer time, 6 h, 24 h and 48 h in order to explore the difference. HPLC followed the same procedures as work that had been done previously.

Decreasing concentrations of test articles in the supernatant over time indicates more compounds were uptaken by Huh-7 cells with the prolonging of incubation time (Figure 5.13a). Bile acid chlorambucil conjugates more rapidly accumulated in cells and this probably relates to their physicochemical property that they are hydrophobic and more readily to permeate through the cell membrane.

UDCA and DCA chlorambucil concentrations in cell lysate reduce with the increment of treatment time whereas concentration of chlorambucil increases (Figure 5.13b). Besides, concentration of UDCA and DCA chlorambucil was lower in cell lysate at 48 h compared to 24 h.

(a)

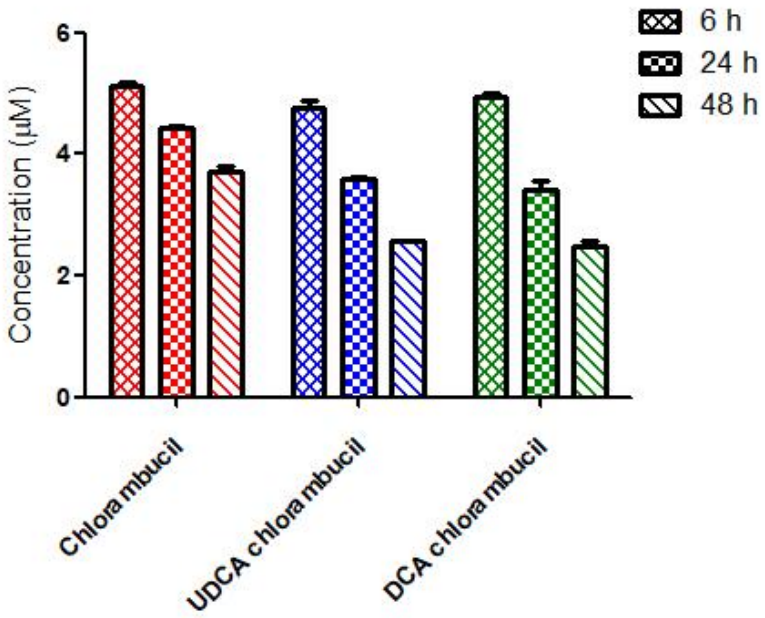

(b)

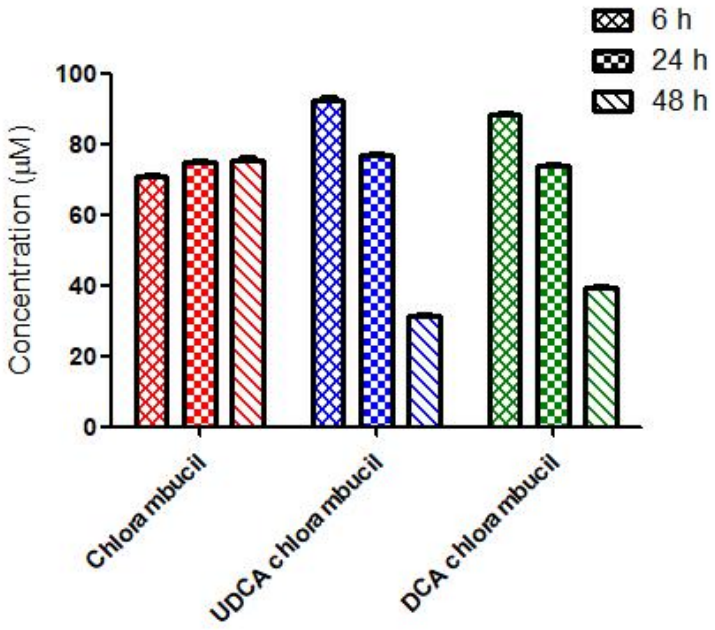

Figure 5.13- Plots showing supernatant (a) and lysate concentration (b) (Y axis) of chlorambucil and two bile acid chlorambucil adducts (X axis) after treating for 6 h, 24 h and 48 h. They show the variations in concentration of chlorambucil, UDCA chlorambucil and DCA chlorambucil inside the supernatant and lysate portion, respectively, at each time.

A peak for chlorambucil was found on the HPLC chromtagram of bile acid chlorambucil conjugate at 24 h and 48 h. This was not evident at 6 h indicating that it results from cellular processing of the bile acid conjugates that is time dependent. The graph plotted below (Figure 5.14) shows the decrease of bile acid conjugates level and production of chlorambucil inside the cell lysate. This suggests that that bile acid chlorambucil conjugates can be broken down by Huh-7 cells into parent chlorambucil.

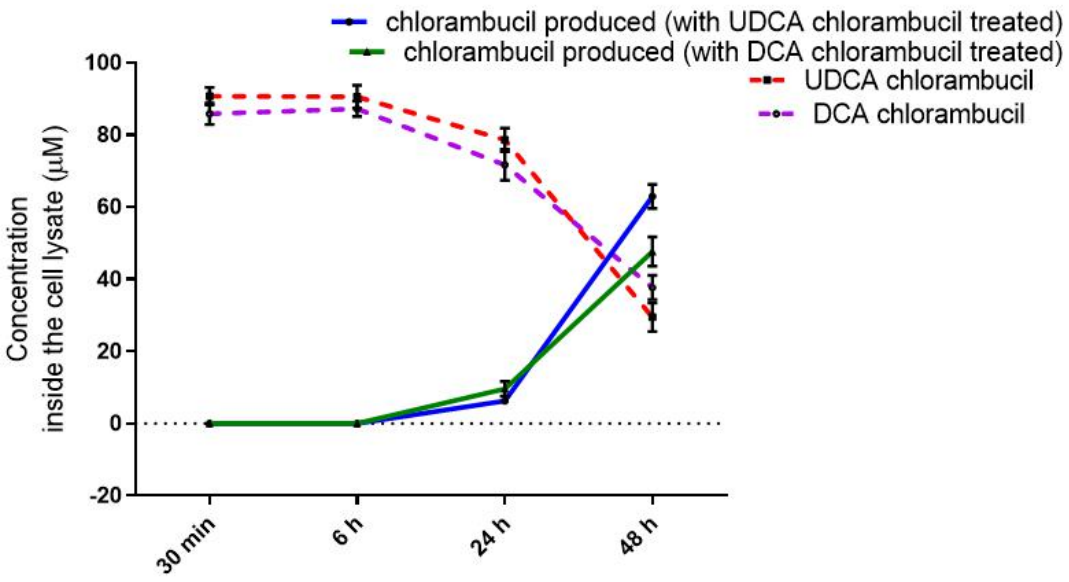

Figure 5.14- Graph shows the variation of the levels of chlorambucil produced and bile acid conjugates concentration inside cell lysate versus the increment of treatment time.

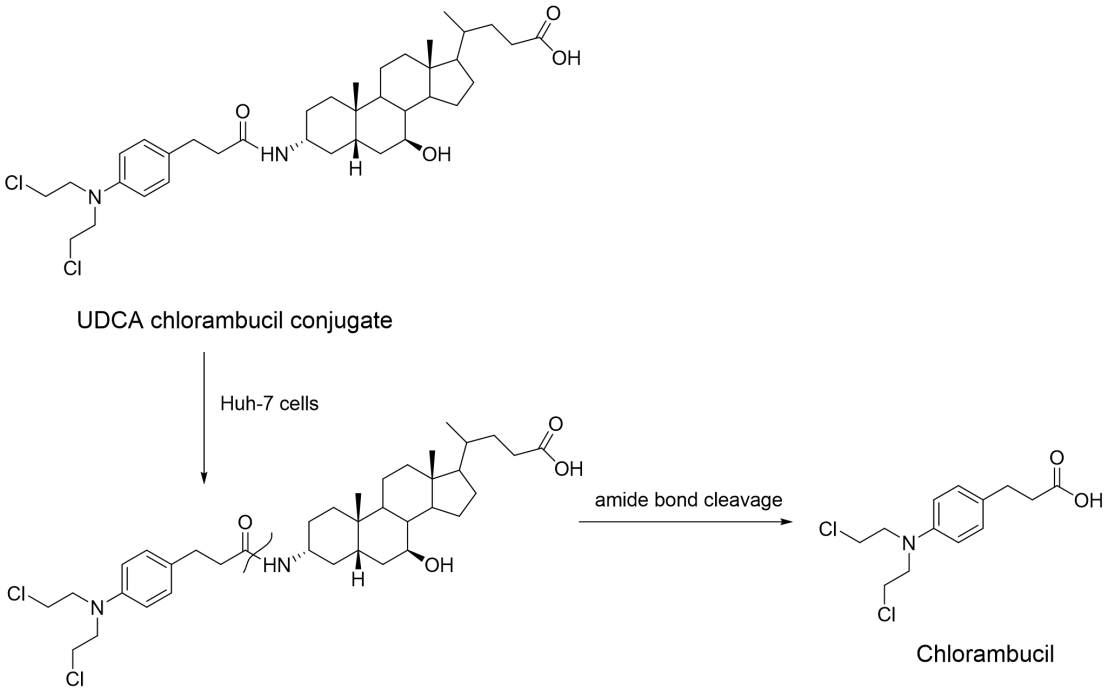

Scheme 5.3- The production of chlorambucil in the conjugate treated cells. It shows the reversal of the formation in chemistry by cleavaging the amide bond to the reformation of parent chlorambucil.

There is only a small increase in uptake of bile acid chlorambucil conjugate relative to chloramucil and in any case the conjugates do not produce more chlorambucil than the drug itself, therefore intracellular uptake attributed to transport of chlorambucil bound bile acid or cellular availability of the parent does not explain their higher antiproliferative activity. The reason for increased cytoxicity of bile acid chlorambucil is not clear but likelihood of intrinsic toxicity from the known structures of bile acid conjugates, which might relate to their differences in physical properties such as solubility and permeability or biochemical properties such as enzyme inhibition.

To sum up, human hepatocellular carcinomas cells as represented by Huh-7 are capable of mediating the uptake of chlorambucil conjugated bile acids, proving the feasibility of bile acid drug conjugates in liver-specific drug targeting [531]. Our study demonstrated a drug design approach to improve the drug absorption and enhance the efficiency of native chlorambucil, as its bile acid derivatives displayed higher intracellular accumulation and cytotoxicity against liver cancer cell line. Tumor targeting with hormone peptides, estrogen, androgen and bile acids provides a basis for the development of more effective diagnostic and therapeutic approaches for cancer.

Chapter 6. Experimental

6.1 Chemistry

6.1.1 General synthetic methods

All chemicals used in this project were purchased from Sigma-Aldrich (Dublin, Ireland), excepted where stated. All chemical reactions were monitored by TLC. Uncorrected melting points were measured using a Stuart SMP11 melting point apparatus and were uncorrected. IR spectra were acquired on an Elmer 205 FT infrared Paragon 1000 spectrometer, with wavenumber given in unit cm^{-1}. ^{1}H and ^{13}C nuclear magnetic resonance (NMR) spectra were measured at the temperature of 27^{o}C on a Bruker DPX 400 and an Agilent 40MR DD2 spectrometer (400.13MHz, ^{1}H; 100.61MHz, ^{13}C) using tetramethylsilane (TMS) as internal standard, in $CDCl_3$. Coupling constants were measured in Hz. For ^{1}H-NMR, chemical shifts were reported: shift value (number of protons, multiplicity of the peak, coupling constants where applicable). Electrospray ionization mass spectrometry (ESI-MS) was performed in the positive ion mode on a liquid chromatography time-of-flight mass spectrometer (Micromass LCT, Waters Ltd., Manchester, UK). Compound purity/accuracy was confirmed using a combination of ^{1}H-NMR, ^{13}C-NMR, IR, melting point and HR-MS. (Compound **1-13** are the important intermediate compounds but not final products)

General procedure for the formation of 24-carboxylic acid-3α-Boc-7β-hydroxyl-5β-cholanoate (3α-Boc UDCA 7):

24-methyl ester-3α, 7β-dihydroxy-5β-cholanoate (1)

To a solution of UDCA (5 g, 12.74 mmol) dissolved in MeOH (100 ml), concentrated HCl (37%, 6.37 mmol, 0.2 ml) was added drop-wise. The mixture was stirred at reflux (86^{o}C) and allowed to react for overnight. The formation of the UDCA methyl ester was followed using TLC analysis (Hexane: EtOAc=1:3). When the reaction finished, the solvent was removed under reduced pressure and then extracted with EtOAc (3×75 ml) and followed by washing with water (2×100 ml) and brine (1×100 ml). The organic phase was dried over $MgSO_4$,

filtered and the solvent was removed under reduced pressure to yield a white, odourless solid (4.90g, 12.05 mmol, 94.62%).

24-methyl ester-3α, 7β-diformyloxy-5β-cholanoate (2)

To a solution of **(1)** (4 g, 9.84 mmol) in formic acid (30 ml) was added several drops of concentrated perchloric acid at 40^{o}C. The mixture was allowed to heat to 60^{o}C with stirring for 30 min. When all the starting material was reacted, the reaction mixture was poured into water and then extracted with EtOAc (3×75 ml) and washed with water (2×100 ml) and brine (1×100 ml), dried over $MgSO_4$, filtered and the solvent was removed under reduced pressure. The crude product was purified by flash chromatography using Hexane: EtOAc=3:1 as the mobile phase to yield a white foam (3.2 g, 6.92 mmol, 70.3%).

24-methyl ester-3α-hydroxyl, 7β-formyloxy-5β-cholanoate (3)

To a solution of **(2)** (3.2 g, 6.92 mmol) in MeOH (100 ml) was added sodium bicarbonate (1.24 g, 14.72 mmol) in 3 times at 0^{o}C within one hour and stirred to RT for 7 h. When the starting material was reacted, the solvent was removed under reduced pressure. The reaction mixture was then poured into 150 ml water and extracted with EtOAc (3×100 ml). The organic phase was washed with water (2×100 ml) and brine (1×100 ml), dried over $MgSO_4$, filtered and the solvent was removed under reduced pressure. The crude product was purified by flash chromatography using hexane: EtOAc=2:1 as the mobile phase to yield a white solid (2.5 g, 5.72 mmol, 83.2%).

24-methyl ester-3α-bromo, 7β-formyloxy-5β-cholanoate (4)

PPh_3 (2.55 g, 9.71 mmol) was added to a stirred solution of **(3)** (2.11 g, 4.856 mmol) in anhydrous THF (80 ml) and the mixture cooled to -18^{o}C. NBS (1.73 g, 9.71 mmol) was added drop-wise to the reaction mixture and then allowed it stir to RT for 6 h. When TLC showed no more starting material present, THF was removed by rotary evaporator. The reaction mixture was poured into water

(100 ml) and extracted with EtOAc (3×75 ml). The organic phase was washed with brine (2×100 ml), dried over $MgSO_4$, filtered and the solvent was removed under reduced pressure. The product was purified with flash column chromatography using hexane: EtOAc=7:1 as the mobile phase to yield colourless oil (2.08 g, 4.18 mmol, 86.6%).

24-methyl ester-3α-azide, 7β-formyloxy-5β-cholanoate (5)

To a solution of **(4)** (2.00g, 4.02 mmol) in DMPU (50 ml), was added sodium azide (2.61 g, 40.2 mmol) at RT. The reaction mixture was left stirring for 2 d and then poured into water (100 ml) and extracted with EtOAc (3×75 ml). The organic phase was washed with water (3×100 ml) and brine (1×100 ml) to fully remove DMPU, dried over $MgSO_4$, filtered and the solvent was removed under reduced pressure. The residue was purified by flash column chromatography, using 20% EtOAc in hexane as mobile phase. The yield product was white foam (1.80 g, 3.92 mmol, 97.4%).

24-methyl ester-3α-tert-butyloxycarbonyl-7β-formyloxy-5β-cholanoate (6)

To a pre-reduced 10% Pd/C (0.1 g) in EtOAc (40 ml) was added a solution of **(5)** (1.80 g, 3.92 mmol) and di-tert-dicarbonate (1.03 g, 4.7 mmol) in EtOAc (20 ml) and stirred under H_2 at RT for 1 d. When all the starting material was reacted, the reaction mixture was filtered through a celite pad and washed with EtOAc. The solvent was removed under reduced pressure. The residue was purified by flash column chromatography, using 20% EtOAc in hexane as mobile phase. The yield product was white foam (1.45g, 2.72 mmol, 69.4%).

3α-tert-butyloxycarbonyl-7β-hydroxyl-5β-cholanoate (7)

To a solution of **(6)** (400 mg, 0.75 mmol) in MeOH (32 ml) was added 2M NaOH solution (10 ml) at reflux and stirring for 4 h. When the reaction finished, the solvent was removed under reduced pressure. The mixture was poured into 1 M HCl (50 ml) and extracted with EtOAc (3×50 ml). The organic phase

was washed with water (2×100 ml) and brine (1×100 ml), dried over $MgSO_4$, filtered and the solvent was removed under reduced pressure to yield white foam (360 mg, 0.732 mmol, 97.6%).

24-butylamino-3α-tert-butyloxycarbonyl-7β-hydroxyl-5β-cholanoate (8)

To a solution of **(7)** (100 mg, 0.203 mmol) in dry DMF (10 ml) were added EDC (180 µl, 1.017 mmol) and HOBt·H_2O (0.138g, 1.017 mmol) at 0°C under N_2 atmosphere for 3 h. When intermediate formed, butan-1-amine (30 µl, 0.305 mmol) was added drop-wise at 0°C and then stirred to RT for overnight. Reaction completion was monitored by TLC using hexane:EtOAc=1:1 as the mobile phase, then the mixture was poured into 1 M HCl solution (50 ml) and extracted with EtOAc (3×50 ml). The organic phase was washed with water (2×50 ml) and brine (1×50 ml), dried over $MgSO_4$, filtered and the solvent was removed under reduced pressure. The crude product was purified by column chromatography using hexane: EtOAc=1:1 as the mobile phase to yield the product as white foam (96 mg, 0.18 mmol, 86.3%).

^{1}H-NMR δ ($CDCl_3$): 0.63 (3H, s, 18-CH_3), 0.88 (3H, s, 19-CH_3), 0.91 (3H, d, J = 6.2 Hz, 21-CH_3), 1.00-1.21 (4H, m, 8-CH, 9-CH, 14-CH, 17-CH), 1.24-1.31 (3H, m, 1-CH_2, 20-CH), 1.32-1.39 (10H, m, 2-CH_2, 4-CH_2, 6-CH_2, 7-CH_2, 11-CH_2), 1.40 (9H, s, COOC($C\underline{H}_3$)$_3$), 1.66-1.77 (4H, m, 15-CH_2, 16-CH_2), 1.78-1.86 (2H, m, 22-CH_2), 1.94-2.02 (2H, m, 22-CH_2), 2.19-2.25 (2H, m, 23-CH_2), 3.21 (2H, q, NH-$C\underline{H}_2$), 3.34 (1H, m, 3β-H), 3.51 (1H, m, 7α-H), 4.42 (1H, d, $N\underline{H}$-COOC(CH_3)$_3$), 5.60 (1H, d, $N\underline{H}$-CH_2).

24-pyrrolidin-3α-tert-butyloxycarbonyl-7β-hydroxyl-5β-cholanoate (9)

To a solution of **(7)** (100 mg, 0.203 mmol) in dry DMF (10 ml) were added EDC (180 µl, 1.017 mmol) and HOBt·H_2O (0.138g, 1.017 mmol) at 0°C under N_2 atmosphere for 3 h. When intermediate formed, pyrrolidine (25 µl, 0.305 mmol) was added drop-wise at 0°C and then stirred to RT for overnight. Reaction

completion was monitored by TLC using hexane:EtOAc=1:2 as the mobile phase, then the mixture was poured into 1 M HCl solution (50 ml) and extracted with EtOAc (3×50 ml). The organic phase was washed with water (2×50 ml) and brine (1×50 ml), dried over $MgSO_4$, filtered and the solvent was removed under reduced pressure. The crude product was purified by column chromatography using hexane: EtOAc=1:2 as the mobile phase to yield the product as white foam (88 mg, 0.162 mmol, 79.4%).

^{1}H-NMR δ ($CDCl_3$): 0.64 (3H, s, 18-CH_3), 0.90 (3H, s, 19-CH_3), 0.92 (3H, d, J = 6.2 Hz, 21-CH_3), 1.00-1.22 (4H, m, 8-CH, 9-CH, 14-CH, 17-CH), 1.25-1.31 (3H, m, 1-CH_2, 20-CH), 1.32-1.40 (10H, m, 2-CH_2, 4-CH_2, 6-CH_2, 7-CH_2, 11-CH_2), 1.41 (9H, s, COOC($C\underline{H}_3$)$_3$), 1.67-1.77 (4H, m, 15-CH_2, 16-CH_2), 1.78-1.85 (2H, m, 22-CH_2), 2.13-2.18 (2H, m, 22-CH_2), 2.28-2.33 (2H, m, 23-CH_2), 3.41 (4H, m, N-$C\underline{H}_2$), 3.45 (1H, m, 3β-H), 3.53 (1H, m, 7α-H), 4.38 (1H, d, $N\underline{H}$-COOC(CH_3)$_3$).

24-cyclopentylamino-3α-tert-butyloxycarbonyl-7β-hydroxyl-5β-cholanoate (10)

To a solution of **(7)** (100 mg, 0.203 mmol) in dry DMF (10 ml) were added EDC (180 µl, 1.017 mmol) and HOBt·H_2O (0.138g, 1.017 mmol) at 0^{o}C under N_2 atmosphere for 3 h. When intermediate formed, cyclopentamine (30 µl, 0.305 mmol) was added drop-wise at 0^{o}C and then stirred to RT for overnight. Reaction completion was monitored by TLC using hexane: EtOAc=1:1 as the mobile phase, then the mixture was poured into 1 M HCl solution (50 ml) and extracted with EtOAc (3×50 ml). The organic phase was washed with water (2×50 ml) and brine (1×50 ml), dried over $MgSO_4$, filtered and the solvent was removed under reduced pressure. The crude product was purified by column chromatography using hexane: EtOAc=1:1 as the mobile phase to yield the product as white foam (95 mg, 0.17 mmol, 83.6%).

^{1}H-NMR δ ($CDCl_3$): 0.62 (3H, s, 18-CH_3), 0.89 (3H, s, 19-CH_3), 0.91 (3H, d, J = 6.2 Hz, 21-CH_3), 1.01-1.23 (4H, m, 8-CH, 9-CH, 14-CH, 17-CH), 1.24-1.31 (3H,

m, 1-CH_2, 20-CH), 1.32-1.40 (10H, m, 2-CH_2, 4-CH_2, 6-CH_2, 7-CH_2, 11-CH_2), 1.41 (9H, s, COOC($C\underline{H}_3$)$_3$), 1.64-1.76 (4H, m, 15-CH_2, 16-CH_2), 1.77-1.83 (2H, m, 22-CH_2), 1.97-2.05 (2H, m, 22-CH_2), 2.15-2.21 (2H, m, 23-CH_2), 3.35 (1H, m, 3β-H), 3.51 (1H, m, 7α-H), 4.42 (1H, d, N$\underline{H}$-COOC(CH_3)$_3$), 5.48 (1H, d, NH).

24-amino-3α-tert-butyloxycarbonyl-7β-hydroxyl-5β-cholanoate (12)

To a solution of **(7)** (100 mg, 0.203 mmol) in dry DMF (10 ml) were added EDC (180 µl, 1.017 mmol) and HOBt·H_2O (0.138g, 1.017 mmol) at 0^{o}C under N_2 atmosphere for 3 h. When intermediate formed, 28% ammonia solution (11.88 µl, 0.305 mmol) was added drop-wise at 0^{o}C and then stirred to RT for overnight. Reaction completion was monitored by TLC using hexane: EtOAc=1:2 as the mobile phase, then the mixture was poured into 1 M HCl solution (50 ml) and extracted with EtOAc (3×50 ml). The organic phase was washed with water (2×50 ml) and brine (1×50 ml), dried over $MgSO_4$, filtered and the solvent was removed under reduced pressure. The crude product was purified by column chromatography using hexane: EtOAc=1:2 as the mobile phase to yield the product as white foam (80 mg, 0.1630 mmol, 80.3%).

^{1}H-NMR δ ($CDCl_3$): 0.65 (3H, s, 18-CH_3), 0.91 (3H, s, 19-CH_3), 0.93 (3H, d, J = 6.2 Hz, 21-CH_3), 1.01-1.23 (4H, m, 8-CH, 9-CH, 14-CH, 17-CH), 1.24-1.29 (3H, m, 1-CH_2, 20-CH), 1.31-1.39 (10H, m, 2-CH_2, 4-CH_2, 6-CH_2, 7-CH_2, 11-CH_2), 1.41 (9H, s, COOC($C\underline{H}_3$)$_3$), 1.67-1.79 (4H, m, 15-CH_2, 16-CH_2), 1.81-1.90 (2H, m, 22-CH_2), 2.05-2.12 (2H, m, 22-CH_2), 2.24-2.30 (2H, m, 23-CH_2), 3.50 (1H, m, 3β-H), 3.52 (1H, m, 7α-H), 4.46 (1H, d, N$\underline{H}$-Boc), 5.63 (2H, d, NH_2).

^{13}C-NMR ppm ($CDCl_3$): 12.1 (18-C, CH_3), 14.2 (19-C, CH_3), 18.5 (21-C, CH_3), 21.1 (11-C, CH_2), 23.5 (15-C, CH_2), 26.9 (16-C, CH_2), 28.4 (O-C-($\underline{C}H_3$)$_3$), 28.7 (2-C, CH), 31.7 (22-C, CH_2), 32.9 (20-C, CH), 34.1 (10-C, CH), 35.0 (4-C, CH_2), 35.4 (23-C, CH_2), 35.6 (6-C, CH_2), 36.8 (1-C, CH_2), 39.3 (5-C, CH), 40.0 (8-C, CH), 40.2 (12-C, CH_2), 42.9 (9-C, CH), 43.7 (13-C, CH), 50.0 (14-C, CH), 55.0 (3-C, CH), 55.8 (17-C, CH), 71.3 (7-C, CH), 80.0 (O-$\underline{C}$-(CH_3)$_3$), 155.0

(NH-CO-O-C-(CH_3)$_3$), 176.2 (24-C, COOH).

24-cyclopropylamino-3α-tert-butyloxycarbonyl-7β-hydroxyl-5β-cholanoate (13)

To a solution of **(7)** (100 mg, 0.203 mmol) in dry DMF (10 ml) were added EDC (180 µl, 1.017 mmol) and HOBt·H_2O (0.138g, 1.017 mmol) at 0°C under N_2 atmosphere for 3 h. When intermediate formed, cyclopropylamine (21.4 µl, 0.305 mmol) was added drop-wise at 0°C and then stirred to RT for overnight. Reaction completion was monitored by TLC using hexane:EtOAc=1:2 as the mobile phase, then the mixture was poured into 1 M HCl solution (50 ml) and extracted with EtOAc (3×50 ml). The organic phase was washed with water (2×50 ml) and brine (1×50 ml), dried over $MgSO_4$, filtered and the solvent was removed under reduced pressure. The crude product was purified by column chromatography using hexane: EtOAc=1:2 as the mobile phase to yield the product as white foam (102 mg, 0.187 mmol, 92.1%).

^{1}H-NMR δ ($CDCl_3$): 0.64 (3H, s, 18-CH_3), 0.89 (3H, s, 19-CH_3), 0.92 (3H, d, J = 6.2 Hz, 21-CH_3), 1.04-1.23 (4H, m, 8-CH, 9-CH, 14-CH, 17-CH), 1.24-1.30 (3H, m, 1-CH_2, 20-CH), 1.31-1.40 (10H, m, 2-CH_2, 4-CH_2, 6-CH_2, 7-CH_2, 11-CH_2), 1.41 (9H, s, COOC(CH_3)$_3$), 1.65-1.78 (4H, m, 15-CH_2, 16-CH_2), 1.79-1.86 (2H, m, 22-CH_2), 1.95-2.05 (2H, m, 22-CH_2), 2.18-2.24 (2H, m, 23-CH_2), 3.35 (1H, m, 3β-H), 3.51 (1H, m, 7α-H), 4.43 (1H, d, NH-COOC(CH_3)$_3$), 6.08 (1H, d, NH).

24-butylamino-3α-methanesulfonamido-7β-hydroxyl-5β-cholanoate (14)

Compound **(8)** (100 mg, 0.183 mmol) was dissolved in 25% TFA/dry DCM (5 ml) and stirred for 30 min under N_2 atmosphere at RT (followed by TLC analysis using hexane: EtOAc=1:2 as mobile phase) and then the solvent was removed under reduced pressure. The mixture was extracted with EtOAc (2×50 ml) and then the solvent was evaporated. The crude product (80 mg, 0.179 mmol) was dissolved in anhydrous DCM (8 ml) and then the mixture was cooled to 0°C. The solution of methanesulfonyl chloride (13.9 µl, 0.179 mmol)

and Et_3N (27.5 µl, 0.197 mmol) in dry DCM (2 ml) was added drop-wise to the mixture and stirred overnight at RT. When all the starting material was reacted, the crude product was purified by column chromatography using hexane: EtOAc=1:2 as the mobile phase to yield the product as white foam (70 mg, 0.133 mmol, 72.9%).

^{1}H-NMR δ ($CDCl_3$): 0.66 (3H, s, 18-CH_3), 0.91 (3H, s, 19-CH_3), 0.94 (3H, d, J = 6.2 Hz, 21-CH_3), 1.12-1.18 (4H, m, 8-CH, 9-CH, 14-CH, 17-CH), 1.25-1.38 (3H, m, 1-CH_2, 20-CH), 1.39-1.56 (10H, m, 2-CH_2, 4-CH_2, 6-CH_2, 7-CH_2, 11-CH_2), 1.72-1.79 (4H, m, 15-CH_2, 16-CH_2), 1.80-1.89 (2H, m, 22-CH_2), 1.97-2.07 (2H, m, 22-CH_2), 2.18-2.24 (2H, m, 23-CH_2), 2.95 (3H, s, S-C<u>H</u>$_3$), 3.22 (2H, q, HN-C<u>H</u>$_2$), 3.26 (1H, m, 3β-H), 3.53 (1H, m, 7α-H), 3.98 (1H, d, N<u>H</u>), 5.38 (1H, t, N<u>H</u>). ^{13}C-NMR ppm ($CDCl_3$): 12.1 (18-C, CH_3), 14.2 (19-C, CH_3), 18.6 (21-C, CH_3), 21.0 (11-C, CH_2), 23.5 (15-C, CH_2), 26.8 (2-C, CH), 28.6 (16-C, CH_2), 29.0 (20-C, CH), 30.9 (NH-CH_2-<u>C</u>H_2), 31.1 (23-C, CH_2), 33.9 (4-C, CH_2), 35.3 (20-C, CH), 35.4 (10-C, CH), 35.7 (6-C, CH_2), 36.7 (1-C, CH_2), 39.2 (5-C, CH), 39.3 (NH-<u>C</u>H_2-CH_2), 40.1 (9-C, CH), 42.1 (12-C, CH_2), 43.7 (S-<u>C</u>H_3), 45.5 (13-C, CH), 46.7 (3-C, CH), 53.8 (14-C, CH), 55.8 (17-C, CH), 66.6 (7-C, CH), 177.8 (24-C, COOH). HRMS: Found: $(M+H)^+$ = 524.3652, calculated $C_{29}H_{52}N_2O_4S^+$ =524.3648. IRvmax (ATR): 2930, 2864, 1736, 1698, 1382 cm^{-1}.

24-butylamino-3α-ethanesulfonamido-7β-hydroxyl-5β-cholanoate (15)

Compound **(8)** (100 mg, 0.183 mmol) was dissolved in 25% TFA/dry DCM (5 ml) and stirred for 30 min under N_2 atmosphere at RT (followed by TLC analysis using hexane:EtOAc=1:2 as mobile phase) and then the solvent was removed under reduced pressure. The mixture was extracted with EtOAc (2×50 ml) and then the solvent was evaporated. The crude product (80 mg, 0.179 mmol) was dissolved in anhydrous DCM (8 ml) and then the mixture was cooled to 0^{o}C. The solution of ethanesulfonyl chloride (17 µl, 0.179 mmol) and Et_3N (27.5 µl, 0.197 mmol) in dry DCM (2 ml) was added drop-wise to the mixture and stirred overnight at RT. When all the starting material was reacted,

the crude product was purified by column chromatography using hexane: EtOAc=1:2 as the mobile phase to yield the product as white foam (65 mg, 0.121 mmol, 66%).

^{1}H-NMR δ ($CDCl_3$): 0.66 (3H, s, 18-CH_3), 0.91 (3H, s, 19-CH_3), 0.94 (3H, d, J = 6.2 Hz, 21-CH_3), 1.12-1.22 (4H, m, 8-CH, 9-CH, 14-CH, 17-CH), 1.25-1.38 (3H, m, 1-CH_2, 20-CH), 1.39-1.56 (10H, m, 2-CH_2, 4-CH_2, 6-CH_2, 7-CH_2, 11-CH_2), 1.72-1.79 (4H, m, 15-CH_2, 16-CH_2), 1.80-1.90 (2H, m, 22-CH_2), 1.97-2.07 (2H, m, 22-CH_2), 2.18-2.24 (2H, m, 23-CH_2), 3.02 (2H, m, S-C<u>H</u>$_2$-CH3), 3.22 (2H, q, HN-C<u>H</u>$_2$), 3.26 (1H, m, 3β-H), 3.53 (1H, m, 7α-H), 3.98 (1H, d, N<u>H</u>), 5.38 (1H, t, N<u>H</u>). ^{13}C-NMR ppm ($CDCl_3$): 2.2 (S-CH_2-<u>C</u>H_3), 12.6 (18-C, CH_3), 14.0 (19-C, CH_3), 15.1 (NH-CH_2-CH_2-CH_2-<u>C</u>H_2), 18.4 (21-C, CH_3), 23.0 (11-C, CH_2), 23.6 (15-C, CH_2), 25.0 (2-C, CH), 27.5 (16-C, CH_2), 30.9 (22-C, CH_2), 31.0 (NH-CH_2-<u>C</u>H_2-CH_2-CH_2), 34.0 (23-C, CH_2), 34.2 (4-C, CH_2), 34.3 (20-C, CH), 35.2 (10-C, CH), 36.2 (6-C, CH_2), 37.1 (1-C, CH_2), 39.3 (5-C, CH), 39.7 (NH-<u>C</u>H_2-CH_2), 40.5 (8-C, CH), 40.6 (12-C, CH_2), 42.5 (9-C, CH), 43.7 (13-C, CH), 47.2 (3-C, CH), 53.6 (14-C, CH), 55.0 (S-<u>C</u>H_3), 55.8 (17-C, CH), 66.7 (7-C, CH), 172.7 (24-C, COOH). HRMS: Found: $(M+H)^+$ =538.3808, calculated $C_{30}H_{54}N_2O_4S^+$ =538.3804. IRvmax (ATR): 2932, 2866, 1737, 1703, 1382 cm^{-1}.

24-butylamino-3α-propanesulfonamido-7β-hydroxyl-5β-cholanoate (16)

Compound **(8)** (100 mg, 0.183 mmol) was dissolved in 25% TFA/dry DCM (5 ml) and stirred for 30 min under N_2 atmosphere at RT (followed by TLC analysis using hexane: EtOAc=1:2 as mobile phase) and then the solvent was removed under reduced pressure. The mixture was extracted with EtOAc (2×50 ml) and then the solvent was evaporated. The crude product (80 mg, 0.179 mmol) was dissolved in anhydrous DCM (8 ml) and then the mixture was cooled to 0^{o}C. The solution of propanesulfonyl chloride (20 µl, 0.179 mmol) and Et_3N (27.5 µl, 0.197 mmol) in dry DCM (2 ml) was added drop-wise to the mixture and stirred overnight at RT. When all the starting material was reacted,

the crude product was purified by column chromatography using hexane: EtOAc=1:2 as the mobile phase to yield the product as white foam (75 mg, 0.136 mmol, 74.2%).

^{1}H-NMR δ ($CDCl_3$): 0.66 (3H, s, 18-CH_3), 0.91 (3H, s, 19-CH_3), 0.94 (3H, d, J = 6.2 Hz, 21-CH_3), 1.14-1.23 (4H, m, 8-CH, 9-CH, 14-CH, 17-CH), 1.26-1.38 (3H, m, 1-CH_2, 20-CH), 1.39-1.52(10H, m, 2-CH_2, 4-CH_2, 6-CH_2, 7-CH_2, 11-CH_2), 1.71-1.78 (4H, m, 15-CH_2, 16-CH_2), 1.79-1.84 (2H, m, 22-CH_2), 1.97-2.07 (2H, m, 22-CH_2), 2.16-2.21 (2H, m, 23-CH_2), 2.96 (2H, m, S-C$\underline{H}_2$), 3.22 (2H, q, HN-C$\underline{H}_2$-CH_2), 3.26 (1H, m, 3β-H), 3.53 (1H, m, 7α-H), 3.93 (1H, d, N$\underline{H}$), 5.37 (1H, t, N$\underline{H}$). ^{13}C-NMR ppm ($CDCl_3$): 11.0 (S-CH_2-CH_2-$\underline{C}H_3$), 12.2 (S-CH_2-$\underline{C}H_2$-CH_3), 12.6 (18-C, CH_3), 14.2 (19-C, CH_3), 17.2 (NH-CH_2-CH_2-CH_2-$\underline{C}H_2$), 18.5 (NH-CH_2-CH_2-$\underline{C}H_2$-CH_2), 18.6 (21-C, CH_3), 23.0 (11-C, CH_2), 25.9 (15-C, CH_2), 26.8 (2-C, CH), 28.3 (16-C, CH_2), 30.7 (20-C, CH), 31.0 (NH-CH_2-$\underline{C}H_2$-CH_2-CH_2), 33.4 (23-C, CH_2), 33.8 (4-C, CH_2), 34.1 (20-C, CH), 34.7 (10-C, CH), 35.6 (6-C, CH_2), 35.8 (1-C, CH_2), 38.4 (5-C, CH), 39.3 (NH-$\underline{C}H_2$-CH_2-CH_2-CH_2), 41.8 (8-C, CH), 42.5 (12-C, CH_2), 43.3 (9-C, CH), 45.4 (13-C, CH), 47.2 (3-C, CH), 51.5 (14-C, CH), 55.1 (17-C, CH), 63.4(S-$\underline{C}H_2$-CH_2-CH_3), 67.5 (7-C, CH), 176.2 (24-C, COOH). HRMS: Found: $(M+H)^+$ =522.3965, calculated $C_{31}H_{56}N_2O_4S^+$ =552.3961. IRvmax (ATR): 2932, 2867, 1737, 1708, 1306 cm^{-1}.

24-butylamino-3α-benzenesulfonamido-7β-hydroxyl-5β-cholanoate (17)

Compound **(8)** (100 mg, 0.183 mmol) was dissolved in 25% TFA/dry DCM (5 ml) and stirred for 30 min under N_2 atmosphere at RT (followed by TLC analysis using hexane:EtOAc=1:2 as mobile phase) and then the solvent was removed under reduced pressure. The mixture was extracted with EtOAc (2×50 ml) and then the solvent was evaporated. The crude product (80 mg, 0.179 mmol) was dissolved in anhydrous DCM (8 ml) and then the mixture was cooled to 0^{o}C. The solution of benzenesulfonyl chloride (23 µl, 0.179 mmol) and Et_3N (27.5 µl, 0.197 mmol) in dry DCM (2 ml) was added drop-wise to the

mixture and stirred overnight at RT. When all the starting material was reacted, the crude product was purified by column chromatography using hexane: EtOAc=1:2 as the mobile phase to yield the product as white foam (60 mg, 0.102 mmol, 56%).

^{1}H-NMR δ ($CDCl_3$): 0.63 (3H, s, 18-CH_3), 0.88 (3H, s, 19-CH_3), 0.90 (3H, d, J = 6.2 Hz, 21-CH_3), 1.05-1.23 (4H, m, 8-CH, 9-CH, 14-CH, 17-CH), 1.26-1.39 (3H, m, 1-CH_2, 20-CH), 1.40-1.49(10H, m, 2-CH_2, 4-CH_2, 6-CH_2, 7-CH_2, 11-CH_2), 1.71-1.77 (4H, m, 15-CH_2, 16-CH_2), 1.79-1.92 (2H, m, 22-CH_2), 1.98-2.08 (2H, m, 22-CH_2), 2.17-2.25 (2H, m, 23-CH_2), 3.07 (1H, m, 3β-H), 3.23 (2H, q, N-C<u>H</u>$_2$), 3.45 (1H, m, 7α-H), 4.76 (1H, d, N<u>H</u>), 5.59 (1H, t, N<u>H</u>), 7.48 (2H, m, meta aromatic-H), 7.55 (1H, t, para aromatic-H), 7.84(2H, t, ortho aromatic-H). ^{13}C-NMR ppm ($CDCl_3$): 12.2 (18-C, CH_3), 14.6 (19-C, CH_3), 18.4 (21-C, CH_3), 21.1 (11-C, CH_2), 23.4 (15-C, CH_2), 26.1 (2-C, CH), 26.9 (16-C, CH_2), 31.8 (21-C, CH_3), 35.5 (23-C, CH_2), 35.5 (4-C, CH_2), 35.7 (10-C, CH), 35.8 (20-C, CH), 36.2 (6-C, CH_2), 36.4 (1-C, CH_2), 39.9 (NH-<u>C</u>H_2-CH_2-CH_2-CH_2), 40.4 (8-C, CH), 40.5 (12-C, CH_2), 43.5 (13-C, CH), 45.5 (3-C, CH), 53.7 (14-C, CH), 55.9 (17-C, CH), 66.7 (7-C, CH), 126.8 (aromatic-C, CH), 129.1 (aromatic-C, CH), 133.4 (aromatic-C), 141.9 (aromatic-C), 177.8 (24-C, <u>C</u>OOH). HRMS: Found: $(M+H)^+$ =586.3808, calculated $C_{34}H_{54}N_2O_4S^+$ =586.3804. IRvmax (ATR): 2932, 2868, 1737, 1704, 1616, 1382, 1306 cm^{-1}.

24-pyrrolidin-3α-methanesulfonamido-7β-hydroxyl-5β-cholanoate (18)

Compound **(9)** (100 mg, 0.184 mmol) was dissolved in 25% TFA/dry DCM (5 ml) and stirred for 30 min under N_2 atmosphere at RT (followed by TLC analysis using hexane:EtOAc=1:2 as mobile phase) and then the solvent was removed under reduced pressure. The mixture was extracted with EtOAc (2×50 ml) and then the solvent was evaporated. The crude product (75 mg, 0.169 mmol) was dissolved in anhydrous DCM (8 ml) and then the mixture was cooled to 0^{o}C. The solution of methanesulfonyl chloride (13 µl, 0.169 mmol) and Et_3N (26 µl, 0.186 mmol) in dry DCM (2 ml) was added drop-wise to the

mixture and stirred overnight at RT. When all the starting material was reacted, the crude product was purified by column chromatography using hexane: EtOAc=1:2 as the mobile phase to yield the product as white foam (68 mg, 0.13 mmol, 70.7%).

^{1}H-NMR δ ($CDCl_3$): 0.66 (3H, s, 18-CH_3), 0.92 (3H, s, 19-CH_3), 0.94 (3H, d, J = 6.2 Hz, 21-CH_3), 1.05-1.23 (4H, m, 8-CH, 9-CH, 14-CH, 17-CH), 1.26-1.38 (3H, m, 1-CH_2, 20-CH), 1.39-1.51 (10H, m, 2-CH_2, 4-CH_2, 6-CH_2, 7-CH_2, 11-CH_2), 1.75-1.80 (4H, m, 15-CH_2, 16-CH_2), 1.81-1.95 (2H, m, 22-CH_2), 2.10-2.19 (2H, m, 22-CH_2), 2.27-2.33 (2H, m, 23-CH_2), 2.95 (3H, s, S-C$\underline{H}_3$), 3.25 (1H, m, 3β-H), 3.40 (4H, m, N-C$\underline{H}_2$), 3.54 (1H, m, 7α-H), 4.20 (1H, d, N$\underline{H}$). ^{13}C-NMR ppm ($CDCl_3$): 12.2 (18-C, CH_3), 14.2 (19-C, CH_3), 18.4 (21-C, CH_3), 21.0 (11-C, CH_2), 21.2 (15-C, CH_2), 23.5 (N-CH_2-$\underline{C}H_2$), 26.9 (2-C, CH), 28.6 (16-C, CH_2), 30.9 (22-C, CH_2), 30.9 (23-C, CH_2), 31.1 (4-C, CH_2), 33.9 (20-C, CH), 35.3 (10-C, CH), 35.7 (6-C, CH_2), 36.7 (1-C, CH_2), 39.3 (5-C, CH), 40.1 (8-C, CH), 42.1 (12-C, CH_2), 43.6 (S-$\underline{C}H_3$), 44.8 (9-C, CH), 45.2 (13-C, CH), 45.4 (3-C, CH), 49.9 (N-$\underline{C}H_2$-CH_2), 53.6 (14-C, CH), 55.0 (17-C, CH), 66.7 (7-C, CH), 176.2 (24-C, COOH). HRMS: Found: $(M+H)^+$ =522.3495, calculated $C_{29}H_{50}N_2O_4S^+$ =522.3491. IRvmax (ATR): 2930, 2864, 1742, 1690, 1386 cm^{-1}.

24-pyrrolidin-3α-ethanesulfonamido-7β-hydroxyl-5β-cholanoate (19)

Compound **(9)** (100 mg, 0.184 mmol) was dissolved in 25% TFA/dry DCM (5 ml) and stirred for 30 min under N_2 atmosphere at RT (followed by TLC analysis using hexane: EtOAc=1:2 as mobile phase) and then the solvent was removed under reduced pressure. The mixture was extracted with EtOAc (2×50 ml) and then the solvent was evaporated. The crude product (75 mg, 0.169 mmol) was dissolved in anhydrous DCM (8 ml) and then the mixture was cooled to 0^{o}C. The solution of ethanesulfonyl chloride (16 µl, 0.169 mmol) and Et_3N (26 µl, 0.186 mmol) in dry DCM (2 ml) was added drop-wise to the mixture and stirred overnight at RT. When all the starting material was reacted, the crude product was purified by column chromatography using hexane:

EtOAc=1:2 as the mobile phase to yield the product as white foam (60 mg, 0.112 mmol, 60.8%).

^{1}H-NMR δ ($CDCl_3$): 0.67 (3H, s, 18-CH_3), 0.94 (3H, s, 19-CH_3), 0.97 (3H, d, J = 6.2 Hz, 21-CH_3), 1.07-1.26 (4H, m, 8-CH, 9-CH, 14-CH, 17-CH), 1.28-1.38 (3H, m, 1-CH_2, 20-CH), 1.39-1.57 (10H, m, 2-CH_2, 4-CH_2, 6-CH_2, 7-CH_2, 11-CH_2), 1.76-1.80 (4H, m, 15-CH_2, 16-CH_2), 1.81-1.96 (2H, m, 22-CH_2), 1.96-2.02 (2H, m, 22-CH_2), 2.17-2.22 (2H, m, 23-CH_2), 3.00 (2H, m, S-C$\underline{H}_2$), 3.24 (1H, m, 3β-H), 3.40 (4H, m, N-C$\underline{H}_2$), 3.54 (1H, m, 7α-H), 3.96 (1H, d, N$\underline{H}$). ^{13}C-NMR ppm ($CDCl_3$): 8.60 (S-CH_2-$\underline{C}H_3$), 12.1 (18-C, CH_3), 14.2 (19-C, CH_3), 18.4 (21-C, CH_3), 21.0 (11-C, CH_2), 23.3 (15-C, CH_2), 26.2 (N-CH_2-$\underline{C}H_2$), 28.6 (2-C, CH), 30.1 (16-C, CH_2), 30.8 (22-C, CH_2), 30.9 (23-C, CH_2), 33.8 (4-C, CH_2), 34.0 (20-C, CH), 35.1 (10-C, CH), 36.6 (6-C, CH_2), 37.1 (1-C, CH_2), 39.8 (5-C, CH), 40.2 (8-C, CH), 41.6 (12-C, CH_2), 41.8 (9-C, CH), 43.3 (13-C, CH), 43.8 (3-C, CH), 47.2 (N-$\underline{C}H_2$-CH_2), 51.5 (14-C, CH), 55.6 (17-C, CH), 60.4 (S-$\underline{C}H_2$-CH_3), 66.6 (7-C, CH), 171.2 (24-C, COOH). HRMS: Found: $(M+H)^+$ 536.3653, calculated $C_{30}H_{52}N_2O_4S^+$ =536.3648. IRvmax (ATR): 2932, 2866, 1740, 1700, 1380 cm^{-1}.

24-pyrrolidin-3α-propanesulfonamido-7β-hydroxyl-5β-cholanoate (20)

Compound **(9)** (100 mg, 0.184 mmol) was dissolved in 25% TFA/dry DCM (5 ml) and stirred for 30 min under N_2 atmosphere at RT (followed by TLC analysis using hexane: EtOAc=1:2 as mobile phase) and then the solvent was removed under reduced pressure. The mixture was extracted with EtOAc (2×50 ml) and then the solvent was evaporated. The crude product (75 mg, 0.169 mmol) was dissolved in anhydrous DCM (8 ml) and then the mixture was cooled to 0^{o}C. The solution of propanesulfonyl chloride (19 µl, 0.169 mmol) and Et_3N (26 µl, 0.186 mmol) in dry DCM (2 ml) was added drop-wise to the mixture and stirred overnight at RT. When all the starting material was reacted, the crude product was purified by column chromatography using hexane: EtOAc=1:3 as the mobile phase to yield the product as white foam (70 mg,

0.126 mmol, 68.6%).

^{1}H-NMR δ ($CDCl_3$): 0.66 (3H, s, 18-CH_3), 0.92 (3H, s, 19-CH_3), 0.94 (3H, d, J = 6.2 Hz, 21-CH_3), 1.02-1.22 (4H, m, 8-CH, 9-CH, 14-CH, 17-CH), 1.28-1.40 (3H, m, 1-CH_2, 20-CH), 1.41-1.64 (10H, m, 2-CH_2, 4-CH_2, 6-CH_2, 7-CH_2, 11-CH_2), 1.66-1.79 (4H, m, 15-CH_2, 16-CH_2), 1.80-1.87 (2H, m, 22-CH_2), 2.13-2.19 (2H, m, 22-CH_2), 2.29-2.34 (2H, m, 23-CH_2), 2.96 (2H, t, S-C$\underline{H}_2$), 3.21 (1H, m, 3β-H), 3.40 (4H, m, N-C$\underline{H}_2$), 3.54 (1H, m, 7α-H), 3.99 (1H, d, N$\underline{H}$). ^{13}C-NMR ppm ($CDCl_3$): 11.97 (S-CH_2-CH_2-$\underline{C}H_3$), 12.1 (18-C, CH_3), 14.4 (19-C, CH_3), 17.2 (S-CH_2-$\underline{C}H_2$-CH_3), 18.5 (21-C, CH_3), 23.0 (11-C, CH_2), 23.5 (15-C, CH_2), 26.9 (N-CH_2-$\underline{C}H_2$), 27.6 (2-C, CH), 28.6 (16-C, CH_2), 30.9 (22-C, CH_2), 31.0 (23-C, CH_2), 33.4 (4-C, CH_2), 33.8 (20-C, CH), 35.2 (10-C, CH), 34.6 (6-C, CH_2), 35.8 (1-C, CH_2), 38.4 (5-C, CH), 41.8 (8-C, CH), 42.5 (12-C, CH_2), 43.3 (9-C, CH), 45.4 (13-C, CH), 47.2 (3-C, CH), 49.2 (N-$\underline{C}H_2$-CH_2), 51.4 (14-C, CH), 55.6 (17-C, CH), 63.0 (S-$\underline{C}H_2$-CH_2-CH_3), 67.5 (7-C, CH), 179.2 (24-C, COOH). HRMS: Found: $(M+H)^+$ =550.3808, calculated $C_{31}H_{54}N_2O_4S^+$ =550.3804. IRvmax(ATR): 2932, 2868, 1737, 1702, 1310 cm^{-1}.

24-pyrrolidin-3α-benzenesulfonamido-7β-hydroxyl-5β-cholanoate (21)

Compound **(9)** (100 mg, 0.184 mmol) was dissolved in 25% TFA/dry DCM (5 ml) and stirred for 30 min under N_2 atmosphere at RT (followed by TLC analysis using hexane: EtOAc=1:2 as mobile phase) and then the solvent was removed under reduced pressure. The mixture was extracted with EtOAc (2×50 ml) and then the solvent was evaporated. The crude product (75 mg, 0.169 mmol) was dissolved in anhydrous DCM (8 ml) and then the mixture was cooled to 0^{o}C. The solution of benzenesulfonyl chloride (21.5 µl, 0.169 mmol) and Et_3N (26 µl, 0.186 mmol) in dry DCM (2 ml) was added drop-wise to the mixture and stirred overnight at RT. When all the starting material was reacted, the crude product was purified by column chromatography using hexane: EtOAc=1:3 as the mobile phase to yield the product as white foam (75 mg, 0.128 mmol, 69.7%).

^{1}H-NMR δ ($CDCl_3$): 0.63 (3H, s, 18-CH_3), 0.88 (3H, s, 19-CH_3), 0.92 (3H, d, J = 6.2 Hz, 21-CH_3), 1.05-1.22 (4H, m, 8-CH, 9-CH, 14-CH, 17-CH), 1.25-1.37 (3H, m, 1-CH_2, 20-CH), 1.38-1.64 (10H, m, 2-CH_2, 4-CH_2, 6-CH_2, 7-CH_2, 11-CH_2), 1.66-1.90 (4H, m, 15-CH_2, 16-CH_2), 1.91-1.96 (2H, m, 22-CH_2), 2.10-2.17 (2H, m, 22-CH_2), 2.31-2.34 (2H, m, 23-CH_2), 3.06 (1H, m, 3β-H), 3.39 (4H, m, N-C<u>H</u>$_2$), 3.45 (1H, m, 7α-H), 4.66 (1H, d, N<u>H</u>), 7.48 (2H, m, meta aromatic-H), 7.55 (1H, t, para aromatic-H), 7.84 (2H, t, ortho aromatic-H). ^{13}C-NMR ppm ($CDCl_3$): 12.1 (18-C, CH_3), 14.4 (19-C, CH_3), 18.6 (21-C, CH_3), 21.1 (11-C, CH_2), 23.4 (15-C, CH_2), 26.1 (N-CH_2-<u>C</u>H_2), 26.9 (2-C, CH), 28.6 (16-C, CH_2), 31.2 (22-C, CH_2), 31.8 (23-C, CH_2), 35.5 (4-C, CH_2), 35.4 (20-C, CH), 36.2 (10-C, CH), 36.4 (6-C, CH_2), 38.4 (1-C, CH_2), 39.9 (5-C, CH), 40.5 (8-C, CH), 43.6 (12-C, CH_2), 45.5 (9-C, CH), 45.7 (13-C, CH), 46.7 (3-C, CH), 49.6 (N-<u>C</u>H_2-CH_2), 50.5 (14-C, CH), 55.1 (17-C, CH), 67.5 (S-<u>C</u>H_2-CH_2-CH_3), 71.1 (7-C, CH), 126.8 (aromatic-C, CH), 129.1 (aromatic-C, CH), 132.5 (aromatic-C), 141.9 (aromatic-C), 216.6 (24-C, COOH). HRMS: Found: $(M+H)^+$ =584.3653, calculated $C_{34}H_{52}N_2O_4S^+$ =584.3648. IRvmax (ATR): 2932, 2868, 1740, 1702, 1618, 1382, 1310 cm^{-1}.

24-cyclopentylamino-3α-methanesulfonamido-7β-hydroxyl-5β-cholanoate (22)

Compound **(10)** (100 mg, 0.179 mmol) was dissolved in 25% TFA/dry DCM (5 ml) and stirred for 30 min under N_2 atmosphere at RT (followed by TLC analysis using hexane: EtOAc=1:2 as mobile phase) and then the solvent was removed under reduced pressure. The mixture was extracted with EtOAc (2×50 ml) and then the solvent was evaporated. The crude product (80 mg, 0.174 mmol) was dissolved in anhydrous DCM (8 ml) and then the mixture was cooled to 0^{o}C. The solution of methanesulfonyl chloride (13.5 µl, 0.174 mmol) and Et_3N (26.7 µl, 0.192 mmol) in dry DCM (2 ml) was added drop-wise to the mixture and stirred overnight at RT. When all the starting material was reacted, the crude product was purified by column chromatography using hexane:

EtOAc=1:2 as the mobile phase to yield the product as white foam (68 mg, 0.126 mmol, 70.6%).

^{1}H-NMR δ ($CDCl_3$): 0.65 (3H, s, 18-CH_3), 0.92 (3H, s, 19-CH_3), 0.94 (3H, d, J = 6.2 Hz, 21-CH_3), 1.03-1.22 (4H, m, 8-CH, 9-CH, 14-CH, 17-CH), 1.23-1.38 (3H, m, 1-CH_2, 20-CH), 1.40-1.67 (10H, m, 2-CH_2, 4-CH_2, 6-CH_2, 7-CH_2, 11-CH_2), 1.72-1.82 (4H, m, 15-CH_2, 16-CH_2), 1.83-1.92 (2H, m, 22-CH_2), 1.95-2.02 (2H, m, 22-CH_2), 2.15-2.19 (2H, m, 23-CH_2), 2.95 (3H, s, S-C$\underline{H}_3$), 3.24 (1H, m, 3β-H), 3.52 (1H, m, 7α-H), 3.55 (1H, m, NH-$\underline{C}$H-CH_2), 4.26 (1H, d, NH), 5.39 (1H, d, NH). ^{13}C-NMR ppm ($CDCl_3$): 12.1 (18-C, CH_3), 14.2 (19-C, CH_3), 18.4 (21-C, CH_3), 21.1 (11-C, CH_2), 23.9 (NH-CH-CH_2-$\underline{C}H_2$), 26.9 (15-C, CH_2), 27.8 (2-C, CH), 28.6 (16-C, CH_2), 30.6 (22-C, CH_2), 30.8 (NH-CH-$\underline{C}H_2$-CH_2), 34.5 (23-C, CH_2), 34.6 (4-C, CH_2) 35.2 (20-C, CH), 35.3 (10-C, CH), 36.4 (6-C, CH_2), 37.2 (1-C, CH_2), 38.6 (5-C, CH), 40.0 (9-C, CH), 40.2 (12-C, CH_2), 42.9 (13-C, CH), 43.7 (S-$\underline{C}H_3$), 43.8 (3-C, CH), 51.5 (14-C, CH), 55.0 (17-C, CH), 55.9 (NH-$\underline{C}$H-CH_2-CH_2), 67.5 (7-C, CH), 172.3 (24-C, COOH). HRMS: Found: $(M+H)^+$ =536.3653, calculated $C_{30}H_{52}N_2O_4S^+$ =536.3648. IRvmax (ATR): 2930, 2864, 1742, 1700, 1382 cm^{-1}.

24-cyclopentylamino-3α-ethanesulfonamid-7β-hydroxyl-5β-cholanoate (23)

Compound **(10)** (100 mg, 0.179 mmol) was dissolved in 25% TFA/dry DCM (5 ml) and stirred for 30 min under N_2 atmosphere at RT (followed by TLC analysis using hexane:EtOAc=1:2 as mobile phase) and then the solvent was removed under reduced pressure. The mixture was extracted with EtOAc (2×50 ml) and then the solvent was evaporated. The crude product (80 mg, 0.174 mmol) was dissolved in anhydrous DCM (8 ml) and then the mixture was cooled to 0^{o}C. The solution of ethanesulfonyl chloride (16.5 µl, 0.174 mmol) and Et_3N (26.7 µl, 0.192 mmol) in dry DCM (2 ml) was added drop-wise to the mixture and stirred overnight at RT. When all the starting material was reacted, the crude product was purified by column chromatography using hexane:

EtOAc=1:2 as the mobile phase to yield the product as white foam (68 mg, 0.123 mmol, 68.8%).

^{1}H-NMR δ ($CDCl_3$): 0.66 (3H, s, 18-CH_3), 0.93 (3H, s, 19-CH_3), 0.99 (3H, d, J = 6.2 Hz, 21-CH_3), 1.03-1.22 (4H, m, 8-CH, 9-CH, 14-CH, 17-CH), 1.26-1.38 (3H, m, 1-CH_2, 20-CH), 1.39-1.62 (10H, m, 2-CH_2, 4-CH_2, 6-CH_2, 7-CH_2, 11-CH_2), 1.74-1.83 (4H, m, 15-CH_2, 16-CH_2), 1.84-1.90 (2H, m, 22-CH_2), 2.21-2.29 (2H, m, 22-CH_2), 2.35-2.41 (2H, m, 23-CH_2), 3.06 (2H, m, S-C<u>H</u>$_2$-CH_3), 3.36 (1H, m, NH-<u>C</u>H-CH_2), 3.78 (1H, m, 7α-H), 4.64 (1H, m, 3β-H), 6.12 (1H, d, NH). ^{13}C-NMR ppm ($CDCl_3$): 8.48 (S-CH_2-<u>C</u>H_3), 12.1 (18-C, CH_3), 14.2 (19-C, CH_3), 18.4 (21-C, CH_3), 21.0 (11-C, CH_2), 23.3 (NH-CH-CH_2-<u>C</u>H_2), 27.0 (15-C, CH_2), 28.6 (2-C, CH), 28.8 (16-C, CH_2), 30.1 (22-C, CH_2), 30.8 (NH-CH-<u>C</u>H_2-CH_2), 30.9 (23-C, CH_2), 31.1 (4-C, CH), 33.8 (20-C, CH), 35.1 (10-C, CH), 36.6 (6-C, CH_2), 37.1 (1-C, CH_2), 39.8 (5-C, CH), 40.2 (8-C, CH), 40.4 (12-C, CH_2), 41.6 (9-C, CH), 43.3 (13-C, CH) 43.7 (3-C, CH), 53.8 (14-C, CH), 54.8 (S-<u>C</u>H_2-CH_3), 55.1 (17-C, CH), 60.4 (NH-<u>C</u>H-CH_2-CH_2), 66.6 (7-C, CH), 172.3 (24-C, COOH). HRMS: Found: $(M+H)^+$ =550.3809, calculated $C_{31}H_{54}N_2O_4S^+$ =550.3804. IRvmax(ATR): 2932, 2868, 1738, 1701, 1386 cm^{-1}.

24-cyclopentylamino-3α-propanesulfonamido-7β-hydroxyl-5β-cholanoate (24)

Compound **(10)** (100 mg, 0.179 mmol) was dissolved in 25% TFA/dry DCM (5 ml) and stirred for 30 min under N_2 atmosphere at RT (followed by TLC analysis using hexane: EtOAc=1:2 as mobile phase) and then the solvent was removed under reduced pressure. The mixture was extracted with EtOAc (2×50 ml) and then the solvent was evaporated. The crude product (80 mg, 0.174 mmol) was dissolved in anhydrous DCM (8 ml) and then the mixture was cooled to 0^{o}C. The solution of propanesulfonyl chloride (19.6 µl, 0.174 mmol) and Et_3N (26.7 µl, 0.192 mmol) in dry DCM (2 ml) was added drop-wise to the mixture and stirred overnight at RT. When all the starting material was reacted, the crude product was purified by column chromatography using hexane:

EtOAc=1:1 as the mobile phase to yield the product as white foam (70 mg, 0.124 mmol, 69.1%).

^{1}H-NMR δ ($CDCl_3$): 0.65 (3H, s, 18-CH_3), 0.90 (3H, s, 19-CH_3), 0.93 (3H, d, J = 6.2 Hz, 21-CH_3), 1.02-1.22 (4H, m, 8-CH, 9-CH, 14-CH, 17-CH), 1.23-1.32 (3H, m, 1-CH_2, 20-CH), 1.33-1.59 (10H, m, 2-CH_2, 4-CH_2, 6-CH_2, 7-CH_2, 11-CH_2), 1.72-1.81 (4H, m, 15-CH_2, 16-CH_2), 1.82-1.88 (2H, m, 22-CH_2), 1.96-2.00 (2H, m, 22-CH_2), 2.17-2.19 (2H, m, 23-CH_2), 2.95 (2H, t, S-C<u>H</u>$_2$), 3.220 (1H, m, 3β-H), 3.53 (1H, m, 7α-H), 4.15 (1H, m, NH-<u>C</u>H-CH_2), 4.20 (1H, d, NH), 5.41 (1H, d, NH). ^{13}C-NMR ppm ($CDCl_3$): 11.9 (S-CH_2-CH_2-<u>C</u>H_3), 12.2 (S-CH_2-<u>C</u>H_2-CH_3), 12.6 (18-C, CH_3), 14.4 (19-C, CH_3), 18.5 (21-C, CH_3), 23.0 (11-C, CH_2), 25.9 (NH-CH-CH_2-<u>C</u>H_2), 26.8 (15-C, CH_2), 27.6 (2-C, CH), 28.3 (16-C, CH_2), 30.7 (22-C, CH_2), 31.0 (NH-CH-<u>C</u>H_2-CH_2), 33.4 (23-C, CH_2), 33.6 (4-C, CH), 33.8 (20-C, CH), 34.2 (10-C, CH), 34.6 (6-C, CH_2), 35.8 (1-C, CH_2), 38.4 (5-C, CH), 41.8 (8-C, CH), 43.3 (12-C, CH_2), 45.4 (9-C, CH), 47.2 (13-C, CH), 48.1 (3-C, CH), 51.5 (14-C, CH), 54.9 (17-C, CH), 55.6 (NH-<u>C</u>H-CH_2-CH_2), 63.0 (S-<u>C</u>H_2-CH_2-CH_3), 66.6 (7-C, CH), 178.7 (24-C, COOH). HRMS: Found: $(M+H)^+$ =564.3965, calculated $C_{32}H_{56}N_2O_4S^+$ =564.3961. IRvmax (ATR): 2932, 2867, 1738, 1702, 1310 cm^{-1}.

25-cyclopentylamino-3α-benzenesulfonamido-7β-hydroxyl-5β-cholanoate (25)

Compound **(10)** (100 mg, 0.179 mmol) was dissolved in 25% TFA/dry DCM (5 ml) and stirred for 30 min under N_2 atmosphere at RT (followed by TLC analysis using hexane: EtOAc=1:2 as mobile phase) then the solvent was removed under reduced pressure. The mixture was extracted with EtOAc (2×50 ml) and then the solvent was evaporated. The crude product (80 mg, 0.174 mmol) was dissolved in anhydrous DCM (8 ml) and then the mixture was cooled to 0^{o}C. The solution of benzenesulfonyl chloride (22.3 µl, 0.174 mmol) and Et_3N (26.7 µl, 0.192 mmol) in dry DCM (2 ml) was added drop-wise to the mixture and stirred overnight at RT. When all the starting material was reacted,

the crude product was purified by column chromatography using hexane: EtOAc=1:1 as the mobile phase to yield the product as white foam (80 mg, 0.133 mmol, 74.5%).

^{1}H-NMR δ ($CDCl_3$): 0.61 (3H, s, 18-CH_3), 0.88 (3H, s, 19-CH_3), 0.95 (3H, d, J = 6.2 Hz, 21-CH_3), 0.97-1.23 (4H, m, 8-CH, 9-CH, 14-CH, 17-CH), 1.25-1.32 (3H, m, 1-CH_2, 20-CH), 1.33-1.60 (10H, m, 2-CH_2, 4-CH_2, 6-CH_2, 7-CH_2, 11-CH_2), 1.63-1.81 (4H, m, 15-CH_2, 16-CH_2), 1.82-1.90 (2H, m, 22-CH_2), 1.96-2.06 (2H, m, 22-CH_2), 2.23-2.26 (2H, m, 23-CH_2), 3.09 (1H, m, 3β-H), 3.47 (1H, m, 7α-H), 4.15 (1H, m, NH-C̲H-CH_2), 4.74 (1H, d, NH), 5.54 (1H, d, NH), 7.49 (2H, m, meta aromatic-H), 7.54 (1H, t, para aromatic-H), 7.87 (2H, t, ortho aromatic-H).

^{13}C-NMR ppm ($CDCl_3$): 12.0 (18-C, CH_3), 17.2 (19-C, CH_3), 18.3 (21-C, CH_3), 21.1 (11-C, CH_2), 23.3 (NH-CH-CH_2-C̲H_2), 25.8 (15-C, CH_2), 28.3 (2-C, CH), 28.9 (16-C, CH_2), 30.9 (22-C, CH_2), 31.0 (NH-CH-C̲H_2-CH_2), 31.6 (23-C, CH_2), 32.8 (4-C, CH_2), 33.8 (20-C, CH), 35.1 (10-C, CH), 35.3 (6-C, CH_2), 39.3(1-C, CH_2), 39.8 (5-C, CH), 40.2 (8-C, CH), 40.3 (12-C, CH_2), 42.7 (9-C, CH), 43.5 (13-C, CH), 46.6 (3-C, CH), 51.5 (14-C, CH), 55.1 (17-C, CH), 55.8 (NH-C̲H-CH_2-CH_2), 67.5 (7-C, CH), 128.3 (aromatic-C, CH), 129.1 (aromatic-C, CH), 135.9 (aromatic-C), 144.3 (aromatic-C), 174.6 (24-C, COOH). HRMS: Found: $(M+H)^+$ =598.3805, calculated $C_{35}H_{54}N_2O_4S^+$ =598.3804. IRvmax (ATR): 2932, 2868, 1734, 1704, 1616, 1382, 1308 cm^{-1}.

24-amino-3α-ethanesulfonamido-7β-hydroxyl-5β-cholanoate (26)

Compound (12) (80 mg, 0.1630 mmol) was dissolved in 25% TFA/dry DCM (5 ml) and stirred for 30 min under N_2 atmosphere at RT (followed by TLC analysis using hexane: EtOAc=1:2 as mobile phase) and then the solvent was removed under reduced pressure. The mixture was extracted with EtOAc (2×50 ml) and then the solvent was evaporated. The crude product (80 mg, 0.2048 mmol) was dissolved in anhydrous DCM (8 ml) and then the mixture was cooled to 0^{o}C. The solution of ethanesulfonyl chloride (37.9 µl, 0.4096

mmol) and Et_3N (31.4 µl, 0.2253 mmol) in dry DCM (2 ml) was added drop-wise to the mixture and stirred overnight at RT. When all the starting material was reacted, the crude product was purified by column chromatography using DCM: MeOH=19:1 as the mobile phase to yield the product as white foam (70 mg, 0.415 mmol, 88.8%).

^{1}H-NMR δ ($CDCl_3$): 0.66 (3H, s, 18-CH_3), 0.92 (3H, s, 19-CH_3), 0.93 (3H, d, J = 6.2 Hz, 21-CH_3), 1.01-1.22 (4H, m, 8-CH, 9-CH, 14-CH, 17-CH), 1.24-1.31 (3H, m, 1-CH_2, 20-CH), 1.32-1.59 (10H, m, 2-CH_2, 4-CH_2, 6-CH_2, 7-CH_2, 11-CH_2), 1.68-1.78 (4H, m, 15-CH_2, 16-CH_2), 1.81-1.89 (2H, m, 22-CH_2), 2.06-2.13 (2H, m, 22-CH_2), 2.27-2.32 (2H, m, 23-CH_2), 2.99 (2H, q, S-C$\underline{H}_2$), 3.20 (1H, m, 3β-H), 3.53 (1H, m, 7α-H), 5.52 (2H, d, NH_2). ^{13}C-NMR ppm ($CDCl_3$): 8.5 (S-CH_2-$\underline{C}H_3$), 12.2 (18-C, CH_3), 14.4 (19-C, CH_3), 18.5 (21-C, CH_3), 21.2 (11-C, CH_2), 23.5 (15-C, CH_2), 26.9 (2-C, CH), 28.7 (16-C, CH_2), 30.9 (22-C, CH_2), 31.6 (2-C, CH), 33.9 (20-C, CH), 35.5 (10-C, CH), 35.6 (23-C, CH_2), 36.2 (6-C, CH_2), 36.4 (1-C, CH_2), 39.2 (5-C, CH), 40.1 (8-C, CH), 43.1 (12-C, CH_2), 43.7 (9-C, CH), 43.8 (13-C, CH), 48.3 (3-C, CH), 53.7 (14-C, CH), 55.1 (S-$\underline{C}H_2$-CH_3), 55.8 (17-C, CH), 71.2 (7-C, CH), 179.2 (24-C, COOH). HRMS: Found: $(M+H)^+$ =482.3179, calculated $C_{26}H_{46}N_2O_4S^+$ =482.3178. IRvmax (ATR): 2932, 2866, 1737, 1702, 1382 cm^{-1}.

24-cyclopropylamino-3α-ethanesulfonamido-7β-hydroxyl-5β-cholanoate (27)

Compound **(13)** (100 mg, 0.188 mmol) was dissolved in 25% TFA/dry DCM (5 ml) and stirred for 30 min under N_2 atmosphere at RT (followed by TLC analysis using hexane: EtOAc=1:2 as mobile phase) and then the solvent was removed under reduced pressure. The mixture was extracted with EtOAc (2×50 ml) and then the solvent was evaporated. The crude product (80 mg, 0.185 mmol) was dissolved in anhydrous DCM (8 ml) and then the mixture was cooled to 0^{o}C. The solution of ethanesulfonyl chloride (17.6 µl, 0.185 mmol) and Et_3N (28.4 µl, 0.204 mmol) in dry DCM (2 ml) was added drop-wise to the

mixture and stirred overnight at RT. When all the starting material was reacted, the crude product was purified by column chromatography using hexane: EtOAc=1:2 as the mobile phase to yield the product as white foam (88 mg, 0.168 mmol, 91.7%).

^{1}H-NMR δ ($CDCl_3$): 0.63 (3H, s, 18-CH_3), 0.88 (3H, s, 19-CH_3), 0.92 (3H, d, J = 6.2 Hz, 21-CH_3), 1.02-1.22 (4H, m, 8-CH, 9-CH, 14-CH, 17-CH), 1.32-1.35 (3H, m, 1-CH_2, 20-CH), 1.36-1.58 (10H, m, 2-CH_2, 4-CH_2, 6-CH_2, 7-CH_2, 11-CH_2), 1.66-1.80 (4H, m, 15-CH_2, 16-CH_2), 1.81-1.91 (2H, m, 22-CH_2), 1.95-2.03 (2H, m, 22-CH_2), 2.15-2.21 (2H, m, 23-CH_2), 2.67 (1H, q, NH-C<u>H</u>-CH_2), 2.98 (2H, q, S-C<u>H</u>$_2$), 3.18 (1H, m, 3β-H), 3.51 (1H, m, 7α-H), 4.55 (1H, d, N<u>H</u>), 5.84 (1H, d, N<u>H</u>). ^{13}C-NMR ppm ($CDCl_3$): 2.3 (S-CH_2-<u>C</u>H_3), 8.6 (HN-CH-<u>C</u>H_2), 12.2 (18-C, CH_3), 14.2 (19-C, CH_3), 18.4 (21-C, CH_3), 21.0 (11-C, CH_2), 23.3 (15-C, CH_2), 25.2 (HN-<u>C</u>H-CH_2), 26.8 (2-C, CH), 28.6 (16-C, CH_2), 30.1 (22-C, CH_2), 30.8 (23-C, CH_2), 30.9 (4-C, CH_2), 33.8 (20-C, CH), 35.1 (10-C, CH), 36.7 (6-C, CH_2), 37.1 (1-C, CH_2), 39.8 (5-C, CH), 40.0 (8-C, CH), 40.2 (12-C, CH_2), 41.8 (9-C, CH), 43.3 (13-C, CH), 43.7 (3-C, CH), 50.2 (14-C, CH), 53.8 (S-<u>C</u>H_2-CH_3), 55.1 (17-C, CH), 66.6 (7-C, CH), 174.7 (24-C, COOH). HRMS: Found: $(M+H)^+$ =522.3492, calculated $C_{29}H_{50}N_2O_4S^+$ =522.3491. IRvmax (ATR): 2928, 2870, 1740, 1700, 1380 cm^{-1}.

General procedure for the formation of 24-methyl ester-3α-ethanesulfonamide-7β-formyloxy-5β-cholanoate (protected 3α-ethanesulfonamide UDCA):

To a solution of (**6**) (240 mg, 0.450 mmol) in dry DCM, was added TFA/dry DCM (1:4) and stirred at RT for 40 min. When TLC showed the completion of the reaction, DCM was removed firstly. The residue was neutralized with 2M NaOH solution into pH=7 and was then extracted with EtOAc (3×75 ml). The combined organic layer was removed in vacuo. After high vacuum drying, the compound was put into dry DCM (10 ml) immediately without any purification. Et_3N (85 µl, 1.1 eqv.) and ethanesulfonyl chloride (105 µl, 2.0 eqv.) were added

at 0°C and then stirred to r.t. for overnight under N_2. The solvent was removed *in vacuo* and the residue was purified by flash column chromatography (hexane: EtOAc=2:1) to afford the protected 3α-ethanesulfonamide UDCA (185 mg, 0.352 mmol, 78.2%).

24-alcohol-3α-ethanesulfonamido-7β-hydroxyl-5β-cholanoate (28)

To a cold solution of protected 3α-ethanesulfonamide UDCA (100 mg, 0.1902 mmol) in a mixture of dry EtOH and dry THF (30 ml), was added sodium (900 mg) carefully. The ice bath was removed when the sodium all dissolved. The reaction was stirred under RT for 2 d. After workup, the residue was purified by flash column chromatography (DCM: MeOH=19:1) to afford the desired compound (68 mg, 0.1449 mmol, 76.18%).

^{1}H-NMR δ ($CDCl_3$): 0.68 (3H, s, 18-CH_3), 0.93 (3H, s, 19-CH_3), 0.95 (3H, d, J = 6.2 Hz, 21-CH_3), 1.03-1.24 (4H, m, 8-CH, 9-CH, 14-CH, 17-CH), 1.26-1.34 (3H, m, 1-CH_2, 20-CH), 1.35-1.54 (10H, m, 2-CH_2, 4-CH_2, 6-CH_2, 7-CH_2, 11-CH_2), 1.73-1.84 (4H, m, 15-CH_2, 16-CH_2), 1.86-1.92 (2H, m, 22-CH_2), 2.26-2.30 (2H, m, 22-CH_2), 2.36-2.42 (2H, m, 23-CH_2), 3.01 (2H, q, S-C$\underline{H}_2$-CH_3), 3.23 (1H, m, 3β-H), 3.55 (1H, m, 7α-H), 3.75 (2H, m, C$\underline{H}_2$OH), 4.41 (1H, d, NH). ^{13}C-NMR ppm ($CDCl_3$): 8.5 (S-CH_2-$\underline{C}H_3$), 12.1 (18-C, CH_3), 14.4 (19-C, CH_3), 18.4 (21-C, CH_3), 21.2 (11-C, CH_2), 23.5 (15-C, CH_2), 26.9 (2-C, CH), 28.7 (16-C, CH_2), 30.8 (22-C, CH_2), 30.9 (4-C, CH_2), 33.9 (10-C, CH), 35.3 (20-C, CH), 36.2 (6-C, CH_2), 36.5 (1-C, CH_2), 39.2 (5-C, CH), 40.1 (8-C, CH), 43.0 (12-C, CH_2), 43.7 (9-C, CH), 43.8 (13-C, CH), 48.4 (3-C, CH), 53.7 (14-C, CH), 55.0 (S-$\underline{C}H_2$-CH_3), 55.8 (17-C, CH), 63.5 ($\underline{C}H_2$OH), 71.2 (7-C, CH). HRMS: Found: $(M-H)^-$ =482.2935, calculated $C_{26}H_{44}NO_5S^-$ =482.2946. IRvmax (ATR): 2936, 2871, 1741, 1327, 1147 cm^{-1}.

<u>General procedure for the formation of 3-oxo bile acids:</u>

The synthesis of methyl ester **39** from DCA (1.00 g, 2.55 mmol) was carried

out in MeOH (50 ml) by adding half an equivalent of catalyst concentrated HCl at reflux for overnight. TLC analysis (hexane: EtOAc=1:4) showed the disappearance of starting material. The solvent was removed in vacuum and the residue dissolved in EtOAc (100 ml) and washed with water (2 x 50 ml) and brine (50 ml). The combined organic layer was dried over $MgSO_4$ and filtered. The solvent was removed in vacuum. The methyl ester **39** (1.26 g, 2.73 mmol) and 4-DMAP (0.066 g, 0.2 eq.) were dissolved in dry pyridine (5 ml) and acetic anhydride (7.74 ml, 30 eq.) was added to the solution at RT and stirred overnight. When TLC showed the completion of the reaction, the mixture was poured into 1 M HCl (100 ml) and was then extracted with EtOAc (3x75 ml). The mixture was washed with water (5x100 ml) and brine (100 ml). The organic layer was dried over $MgSO_4$ and filtered. The solvent was removed in vacuum and then purified by flash column chromatography (hexane: EtOAc=3:1) to yield product **40** (1.42 g, 88%) as white foam. To a solution of di-acetyl DCA (1.42 g, 2.89 mmol) in dry MeOH (20 ml) was added dropwise acetyl chloride (0.23 ml, 1.3 eq.) at 0^{o}C. The mixture was allowed to warm to RT with stirring for overnight. When TLC showed the disappearance of the starting material, saturated aq $NaHCO_3$ solution was added to pH to 10–12. The mixture was extracted with EtOAc (3×75 ml) and then combined organic layer was washed with water (2×100 ml). The solvent was removed in vacuum and then purified by flash column chromatography (hexane: EtOAc=2:1) to obtain compound **41** (0.91 g, 70%). Compound **41** (0.91 g, 2.023 mmol) was dissolved in DCM (30 ml) and PCC (1.09 g, 5.0575 mmol, 2.5 eq.) was added in 3 times over one hour at RT with stirring for about 4 h. TLC analysis (hexane: EtOAc=1:1) showed the disappearance of starting material. The solvent was then removed in vacuum and EtOAc (100 ml) was added to the mixture. The organic layer was washed with water (3×100 ml) and brine (100 ml) and was dried over $MgSO_4$ and filtered. The solvent was removed to yield compound **42** (0.885 g, 98%) as white foam**.**

General procedure for the formation of 3β-OH bile acids with $NaBH_4$

Compound **42** (0.885 g, 1.9825 mmol) was put into a round-bottom flask and sealed well and 15 ml MeOH and 15 ml dry THF were added. The flask was cooled in an ice bath and $NaBH_4$ (0.225 g, 3 eq.) wad added with stirring over 15 min. After addition of $NaBH_4$ completed, the ice bath was removed and the reaction was kept under RT for overnight. TLC analysis indicated the disappearance of the starting material and formation of two products: one with a lower R_f of 0.2 and one with a higher R_f of 0.28 (mobile phase EtOAc: hexane=1:1). 2.0 M aq. HCl solution was added to adjust the pH of mixture into 6 and the solvent was removed. The residue was then extracted with EtOAc (3×75 ml). The organic layer was then washed with brine (100 ml). The combined organic layer was dried over $MgSO_4$ and filtered. The solvent was removed in vacuum and the semi-solid residue was purified by flash column chromatography using hexane: EtOAc=1:1 to afford the compound **43** (0.222 g, 25%) and majority of the compound **41** (0.667 g, 75%).

General procedure for the formation of 3β-OH bile acids with L-selectride solution:

To a cooled solution of compound **42** (0.90 g, 2.015 mmol) in dry THF (15 ml) was dropwise added a solution of L-selectride (1.8 ml, 4 eq.) under N_2 condition and the mixture was stirred at -18^oC for over one hour and then allowed to warm to RT and stirred for overnight. TLC analysis showed formation of two products: one with a lower R_f of 0.2, and one with a higher R_f of 0.28 (mobile phase hexane: EtOAc=1:1). The mixture was quenched with a saturated ammonium chloride solution (100 ml) and then extracted with DCM (3×50 ml). The combined organic layer was washed with brine (100 ml) and was dried over $MgSO_4$ and filtered. The solvent was removed in vacuum and then purified by flash column chromatography (hexane: EtOAc=1:1) to yield majority of product **43** (0.82 g, 90.35%) and a small amount of product **41** (0.09

g, 9.65%).

3β, 7α, 12α-trihydroxy-5β-cholanoate (3β-OH CA) (44)

To a solution of protected 3β-OH CA (100 mg) in MeOH (16 ml) was added 2M aq. NaOH solution (5 ml) at reflux and stirred for 36 h. When TLC analysis (hexane: EtOAc=1:8) showed the disappearance of starting material, 2M aq. HCl solution (5 ml) was added to neutralize the pH into 7. The MeOH was removed and the residue was extracted with EtOAc (3×75 ml). The combined organic layer was washed with water (2×100 ml) and brine (100 ml) and it was dried over $MgSO_4$ and filtered. The solvent was removed to yield compound **44** as a white foam (77.42 mg, 96%).

mp 170–173°C; ^{1}H-NMR δ ($CDCl_3$): 0.69 (3H, s, 18-CH_3), 0.93 (3H, s, 19-CH_3), 0.98 (3H, d, J = 6.2 Hz, 21-CH_3), 1.13-1.24 (4H, m, 8-CH, 9-CH, 14-CH, 17-CH), 1.24-1.40 (3H, m, 1-CH_2, 20-CH), 1.40-1.56 (10H, m, 2-CH_2, 4-CH_2, 6-CH_2, 7-CH_2, 11-CH_2), 1.72-1.77 (4H, m, 15-CH_2, 16-CH_2), 1.80-1.88 (2H, m, 22-CH_2), 2.37-2.47 (2H, m, 23-CH_2), 3.85 (1H, d, 7β-H), 3.98 (1H, s, 12β-H), 4.06 (1H, s, 3α-H). ^{13}C-NMR ppm ($CDCl_3$): 12.1 (18-CH_3), 14.2 (19-CH_3), 18.4 (21-CH_3), 21.0 (15-C, CH_2), 23.5 (16-C, CH_2), 26.9 (9-C, CH), 28.6 (11-C, CH_2), 30.8 (2-C, CH_2), 30.9 (22-C, CH), 34.1 (23-C, CH_2), 34.2 (1-C, CH_2), 35.2 (20-C, CH), 37.2 (4-C & 6-C, CH_2), 39.4 (10-C, C-CH_3), 40.2 (8-C, CH), 43.8 (5-C, C-CH_3), 49.8 (14-C, CH), 55.0 (17-C,CH), 68.8 (7-C, CH), 71.4 (3-C, CH), 73.3 (12-C, CH), 179.2 (24-C, COOH). HRMS: Found: $(M+H)^+$ =408.2802, calculated $C_{24}H_{39}O_5^+$ =408.2803. IRvmax (ATR): 3408, 2922, 2161, 1706, 1377 cm^{-1}.

3β, 12α-dihydroxy-5β-cholanoate (3β-OH DCA) (45)

To a solution of protected 3β-OH DCA (100 mg) in MeOH (16 ml) was added 2M aq. NaOH solution (5 ml) at reflux and stirred for 24 h. When TLC analysis (hexane: EtOAc =1:1) showed the disappearance of starting material, 2M aq. HCl solution (5 ml) was added to neutralize the pH into 7. The MeOH was

removed and the residue was extracted with EtOAc (3×75 ml). The combined organic layer was washed with water (2×100 ml) and brine (100 ml) and it was dried over $MgSO_4$ and filtered. The solvent was removed to yield compound **45** as a white foam (85.5 mg, 98%).

mp 160–162°C; ^{1}H-NMR δ ($CDCl_3$): 0.67 (3H, s, 18-CH_3), 0.93 (3H, s, 19-CH_3), 0.95 (3H, d, J = 6.2 Hz, 21-CH_3), 1.04-1.16 (4H, m, 8-CH, 9-CH, 14-CH, 17-CH), 1.23-1.33 (3H, m, 1-CH_2, 20-CH), 1.35-1.60 (10H, m, 2-CH_2, 4-CH_2, 6-CH_2, 7-CH_2, 11-CH_2), 1.61-1.76 (4H, m, 15-CH_2, 16-CH_2), 1.77-1.85 (2H, m, 22-CH_2), 2.22-2.38 (2H, m, 23-CH_2), 3.98 (1H,s, 12β-H), 4.09 (1H, s, 3α-H). ^{13}C-NMR ppm ($CDCl_3$): 12.7 (18-C, CH_3), 17.3 (19-C, CH_3), 23.6 (21-C, CH_3), 25.9 (15-C, CH_2), 26.5 (16-C, CH_2), 27.4 (6-C, CH_2), 28.9 (11-C, CH_2), 30.7 (2-C, CH_2), 30.8 (22-C, CH_2), 32.8 (23-C, CH_2), 32.9 (7-C, CH_2), 35.0 (20-C, CH), 35.8 (1-C, CH_2), 35.9 (8-C, 9-C, CH), 36.3 (4-C, CH_2), 36.4 (5C-CH), 46.5 (13-C, C-CH_3), 47.3(17-C, CH), 48.3 (14-C, CH), 67.2 (3-C, CH), 73.3 (12-C, CH), 179.3 (24-C, COOH). HRMS: Found: $(M+H)^+$ = 392.2852, calculated $C_{24}H_{39}O_4^+$=392.2854. IRvmax (ATR): 2925, 1706, 1446, 1377 cm^{-1}.

3β, 7α-dihydroxy-5β-cholanoate (3β-OH CDCA) (46)

To a solution of protected 3β-OH CDCA (100 mg) in MeOH (16 ml) was added 2M aq. NaOH solution (5 ml) at reflux and stirred for 36 h. When TLC analysis (hexane: EtOAc=1:2) showed the disappearance of starting material, 2M aq. HCl solution (5 ml) was added to neutralize the pH into 7. The MeOH was removed and the residue was extracted with EtOAc (3×75 ml). The combined organic layer was washed with water (2×100 ml) and brine (100 ml) and it was dried over $MgSO_4$ and filtered. The solvent was removed to yield compound **46** as a white foam (84.7 mg, 97%).

mp 192–193°C;^{1}H-NMR δ ($CDCl_3$): 0.64 (3H, s, 18-CH_3), 0.93 (6H, m, 19-CH_3, 21-CH_3), 1.04-1.15 (4H, m, 8-CH, 9-CH, 14-CH, 17-CH), 1.21-1.32 (3H, m, 1-CH_2, 20-CH), 1.36-1.60 (10H, m, 2-CH_2, 4-CH_2, 6-CH_2, 7-CH_2, 11-CH_2), 1.61-1.74 (4H, m, 15-CH_2, 16-CH_2), 1.75-1.86 (2H, m, 22-CH_2), 2.20-2.43 (2H,

m, 23-CH_2), 3.85 (1H, d, 7β-H), 4.06 (1H, s, 3α-H). ^{13}C-NMR ppm ($CDCl_3$): 11.8 (18-C, CH_3), 18.3 (19-C, CH_3), 21.0 (21-C, CH_3), 21.6 (11-C, CH_2), 23.2 (15-C, CH_2), 28.0 (16-C, CH_2), 29.8 (2-C, CH_2), 30.8 (22-C, CH_2), 31.1 (23-C, CH_2), 35.7 (1-C, CH_2), 35.8 (20-C, CH), 36.0 (10-C, C-CH_3), 37.3 (4-C, CH_2), 39.0 (6-C, CH) 39.3 (8-C, CH), 39.7 (12-C, CH_2), 41.9 (5-C, CH), 42.8 (13-C, C-CH_3), 50.5 (14-C, CH), 55.7 (17-C, CH), 68.8 (7-C, CH), 71.7 (3-C, CH), 178.6 (24-C, COOH). HRMS: Found: $(M+H)^+$ = 392.2847, calculated $C_{24}H_{39}O_4^+$=392.2854. IRvmax (ATR): 3354, 3239, 2925, 2158, 1686, 1444, 1379 cm^{-1}.

3β-hydroxy-5β-cholanoate (3β-OH LCA) (47)

To a solution of protected 3β-OH LCA (100 mg) in MeOH (16 ml) was added 2M aq. NaOH solution (5 ml) at reflux and stirred for 4 h. When TLC analysis (hexane: EtOAc =1:1) showed the disappearance of starting material, 2M aq. HCl solution (5 ml) was added to neutralize the pH into 7. The MeOH was removed and the residue was extracted with EtOAc (3×75 ml). The combined organic layer was washed with water (2×100 ml) and brine (100 ml) and it was dried over $MgSO_4$ and filtered. The solvent was removed to yield compound **47** as a white foam (94.2 mg, 98%).

mp 176–177°C; ^{1}H-NMR δ ($CDCl_3$): 0.63 (3H, s, 18-CH_3), 0.90 (3H, d, J = 6.1 Hz, 21-CH_3), 0.94 (3H, s, 19-CH_3), 1.00-1.16 (4H, m, 8-CH, 9-CH, 14-CH, 17-CH), 1.24-1.32 (3H, m, 1-CH_2, 20-CH), 1.38-1.56 (10H, m, 2-CH_2, 4-CH_2, 6-CH_2, 7-CH_2, 11-CH_2), 1.67-1.78 (4H, m, 15-CH_2, 16-CH_2), 1.80-1.88 (2H, m, 22-CH_2), 2.22-2.40 (2H, m, 23-CH_2), 4.09 (1H, s, 3α-H). ^{13}C-NMR ppm ($CDCl_3$): 12.1 (18-C, CH_3), 18.2 (19-C, CH_3), 21.1 (21-C, CH_3), 24.2 (11-C, CH_2), 26.5 (15-C, CH_2), 27.4 (16-C, CH_2), 28.2 (6-C, CH_2), 30.7 (2-C, CH_2), 30.8 (22-C, CH_2), 32.8 (7-C, CH_2), 32.8 (23-C, CH_2), 32.9 (7-C, CH_2), 34.6 (20-C, CH), 35.1 (10-C, C-CH_3), 35.8 (1-C, CH_2), 35.9 (8-C, CH), 36.5 (4-C, CH_2), 46.5 (5-C, CH), 47.3 (12-C, CH_2), 48.3 (13-C, C-CH_3), 55.0 (9-C, CH), 55.9 (17-C, CH), 56.7 (14-C, CH), 67.2 (3-C, CH), 179.3 (24-C, COOH). HRMS: Found:

$(M+H)^+$ =376.2902, calculated $C_{24}H_{39}O_3^+$=376.2905. IRvmax (ATR): 2929, 1722, 1671, 1448, 1377 cm^{-1}.

3β, 7β-dihydroxyl-5β-cholanoate (3β-OH UDCA) (48)

To a solution of protected 3β-OH UDCA (100 mg) in MeOH (16 ml) was added 2M aq. NaOH solution (5 ml) at reflux and stirred for 36 h. When TLC analysis (hexane: EtOAc =1:2) showed the disappearance of starting material, 2M aq. HCl solution (5 ml) was added to neutralize the pH into 7. The MeOH was removed and the residue was extracted with EtOAc (3×75 ml). The combined organic layer was washed with water (2×100 ml) and brine (100 ml) and it was dried over $MgSO_4$ and filtered. The solvent was removed to yield compound **48** as a white foam (82.9 mg, 95%).

mp 166–167°C; ^{1}H-NMR δ ($CDCl_3$): 0.67 (3H, s, 18-CH_3), 0.93 (3H, d, J = 6.1 Hz, 21-CH_3), 0.97 (3H, s, 19-CH_3), 1.04-1.20 (4H, m, 8-CH, 9-CH, 14-CH, 17-CH), 1.24-1.43 (3H, m, 1-CH_2, 20-CH), 1.43-1.52 (10H, m, 2-CH_2, 4-CH_2, 6-CH_2, 7-CH_2, 11-CH_2), 1.74-1.78 (4H, m, 15-CH_2, 16-CH_2), 1.82-1.83 (2H, m, 22-CH_2), 2.35-2.39 (2H, m, 23-CH_2), 3.54 (1H, m, 7α-H), 4.06 (1H, s, 3α-H). ^{13}C-NMR ppm ($CDCl_3$): 12.2 (19-C, CH_3), 18.4 (18-C, CH_3), 21.5 (21-C, CH_3), 23.9 (11-C, CH_2), 26.9 (15-C, CH_2), 28.6 (6-C, CH_2), 30.6 (2-C, CH_2), 30.9 (22-C, CH_2), 34.5 (23-C, CH_2), 35.1 (20-C, CH), 35.2 (10-C, C-CH_3), 36.9 (1-C, CH_2), 37.2 (4-C & 6-C, CH_2), 38.6 (8-C, CH), 40.1 (5-C, CH), 40.2 (9-C, CH), 43.6 (12-C, CH_2), 43.8 (13-C, C-CH_3), 55.0 (14-C, CH), 55.9 (17-C, CH). 66.7 (7-C, CH), 71.5 (3-C, CH), 177.8 (24-C, COOH). HRMS: Found: $(M+H)^+$ =392.2848, calculated $C_{24}H_{39}O_4^+$=392.2854. IRvmax (ATR): 2926, 2158, 1717, 1445, 1383 cm^{-1}.

3α, 6α, 7α-trihydroxyl-5β-cholanoate (γ-muricholic acid) (55)

To a solution of protected γ-muricholic acid (20 mg, 0.036 mmol) in MeOH (16 ml) was added 2M aq. NaOH solution (16 ml) at reflux and stirred for 2 d. When TLC analysis (hexane: EtOAc =1:3) showed the disappearance of

starting material, 2M aq. HCl solution (5 ml) was added to neutralize the pH into 7. The MeOH was removed and the residue was extracted with EtOAc (3×75 ml). The combined organic layer was washed with water (2×100 ml) and brine (100 ml) and it was dried over $MgSO_4$ and filtered. The solvent was removed to yield compound **55** as a white foam (12 mg, 0.029 mmol, 81.6%). mp 224–226°C; ^{1}H-NMR δ ($CDCl_3$): 0.66 (3H, s, 18-CH_3), 0.90 (3H, s, 19-CH_3), 0.93 (3H, d, J = 6.1 Hz, 21-CH_3), 1.07-1.18 (4H, m, 8-CH, 9-CH, 14-CH, 17-CH), 1.26-1.43 (3H, m, 1-CH_2, 20-CH), 1.44-1.53 (10H, m, 2-CH_2, 4-CH_2, 6-CH_2, 7-CH_2, 11-CH_2), 1.72-1.79 (4H, m, 15-CH_2, 16-CH_2), 1.93-1.94 (2H, m, 22-CH_2), 2.32-2.38 (2H, m, 23-CH_2), 3.39 (1H, brm, 3α-H), 3.82 (1H, m, 6α-H), 3.85 (1H, m, 7α-H). ^{13}C-NMR ppm ($CDCl_3$): 11.7 (18-C, CH_3), 18.2 (21-C, CH_3), 20.5 (11-C, CH_2), 23.0 (15-C, CH_2),23.5 (19-C, CH_3), 28.1 (16-C, CH_2), 30.4 (2-C, CH_2), 30.9 (22-C, CH_2), 31.0 (23-C, CH_2), 32.5 (9-C, CH), 32.6 (4-C, CH_2), 35.2 (20-C, CH), 35.5 (1-C, CH_2), 35.9 (10-C, C-$\underline{C}H_3$), 38.6 (8-C, CH), 39.5 (12-C, CH), 42.8 (13-C, $\underline{C}$-CH_3), 47.8 (5C-CH), 50.1 (14-C, CH), 55.8 (17-C, CH), 69.6 (7-C, CH_2), 71.7 (3-C, CH), 71.9 (6-C, CH_2), 174.5 (24-C, COOH). HRMS: Found: $(M+H)^+$ =408.2800, calculated $C_{24}H_{39}O_5^+$ =408.2803. IRvmax (ATR): 3602, 2924, 2160, 1719, 1380 cm^{-1}.

3α, 6α, 7β-trihydroxyl-5β-cholanoate (ω-muricholic acid) (56)

To a solution of protected ω-muricholic acid (20 mg, 0.036 mmol) in MeOH (16 ml) was added 2M aq. NaOH solution (16 ml) at reflux and stirred for 2 d. When TLC analysis (hexane: EtOAc =1:3) showed the disappearance of starting material, 2M aq. HCl solution (5 ml) was added to neutralize the pH into 7. The MeOH was removed and the residue was extracted with EtOAc (3×75 ml). The combined organic layer was washed with water (2×100 ml) and brine (100 ml) and it was dried over $MgSO_4$ and filtered. The solvent was removed to yield compound **56** as a white foam (11.5 mg, 0.028 mmol, 78.2%). mp 226–228°C; ^{1}H-NMR δ ($CDCl_3$): 0.67 (3H, s, 18-CH_3), 0.92 (3H, d, J = 6.1 Hz, 21-CH_3), 0.95 (3H, s, 19-CH_3), 1.06-1.21 (4H, m, 8-CH, 9-CH, 14-CH,

17-CH), 1.25-1.40 (3H, m, 1-CH_2, 20-CH), 1.41-1.59 (10H, m, 2-CH_2, 4-CH_2, 6-CH_2, 7-CH_2, 11-CH_2), 1.75-1.80 (4H, m, 15-CH_2, 16-CH_2), 1.93-1.97 (2H, m, 22-CH_2), 2.31-2.38 (2H, m, 23-CH_2), 3.40 (1H, t, 7β-H), 3.58 (1H, m, 3α-H), 3.79 (1H, dd, 6α-H). ^{13}C-NMR ppm ($CDCl_3$): 12.2 (18-C, CH_3), 18.4 (21-C, CH_3), 21.2 (11-C, CH_2), 23.6 (19-C, CH_3), 26.7 (15-C, CH_2), 28.5 (16-C, CH_2), 29.9 (4-C, CH_2), 30.8 (2-C, CH_2), 31.0 (22-C, CH_2), 31.1 (23-C, CH_2), 35.2 (20-C, CH), 35.3 (1-C, CH_2), 35.3 (10-C, C-$\underline{C}H_3$), 39.2 (9-C, CH), 40.0 (12-C, CH), 41.7 (8-C, CH), 43.8 (13-C, $\underline{C}$-CH_3), 47.8 (5C-CH), 55.0 (14-C, CH), 55.8 (17-C, CH), 71.2 (3-C, CH), 72.9 (6-C, CH_2), 75.5 (7-C, CH_2), 174.5 (24-C, COOH). HRMS: Found: $(M+H)^+$ =408.2802, calculated $C_{24}H_{39}O_5^+$ =408.2803. IRvmax (ATR): 3408, 2924, 2158, 1707, 1380 cm^{-1}.

General procedure for the formation of protected 3α-dansyl bile acids:

3α-azido UDCA **5** (120 mg, 0.261 mmol) was poured into EtOAc (30 ml) and then the mixture was added to a pre-reduced Pd/C (0.15 g) in EtOAc (20 ml) and stirred under H_2 at r.t. for 1 d. The mixture was filtered through a cellite pad and the cellite was washed with EtOAc (3×20 ml). The solvent was removed *in vacuo* to yield amine intermediates. These were dissolved in dry DCM (10 ml) immediately without any purification, Et_3N (85 µl, 1.1 eqv.) and dansyl chloride (0.15 g, 1.0 eqv.) were added at 0^{o}C and then stirred to r.t. for overnight under N_2. The solvent was removed *in vacuo* and the residue was purified by flash column chromatography (hexane: EtOAc=3:1) to afford the protected 3α-dansyl UDCA (100 mg, 0.1499 mmol, 57.4%).

3α-((5-(dimethylamino) naphthalene)-1-sulfonamido))-7β-hydroxyl-5β-cholanoate (3α-dansyl UDCA) (57)

To a solution of protected 3α-dansyl UDCA (100 mg, 0.1499 mmol) in MeOH (10 ml) was added 2M aq. NaOH solution (5 ml) at reflux and stirred fo16 h. When TLC analysis (hexane: EtOAc =1:1) showed the disappearance of starting material, 2M aq. HCl solution (5 ml) was added to neutralize the pH

into 7. The MeOH was removed *in vacuo* and the residue was extracted with EtOAc (3×50 ml). The combined organic layer was washed with water (2×100 ml) and brine (100 ml) and it was dried over $MgSO_4$ and filtered. The solvent was removed to yield compound **49** as a white foam (84.0 mg, 89.8%).

mp 210–213°C; ^{1}H-NMR δ ($CDCl_3$): 0.62 (3H, s, 18-CH_3), 0.83 (3H, d, J = 6.1 Hz, 21-CH_3), 0.89 (3H, s, 19-CH_3), 0.99-1.08 (4H, m, 8-CH, 9-CH, 14-CH, 17-CH), 1.12-1.23 (3H, m, 1-CH_2, 20-CH), 1.24-1.40 (10H, m, 2-CH_2, 4-CH_2, 6-CH_2, 7-CH_2, 11-CH_2), 1.73-1.94 (4H, m, 15-CH_2, 16-CH_2), 2.22-2.28 (2H, m, 22-CH_2), 2.32-2.40 (2H, m, 23-CH_2), 2.88 (6H, s, 2×CH_3), 3.04 (1H, m, 3β-H), 3.40 (1H, m, 7α-H), 4.77 (1H, d, N<u>H</u>-SO_2), 7.18 (1H, d, naphthalene-H_4), 7.52 (2H, m, naphthalene-H_3&H_7), 8.23 (2H, m, naphthalene-H_2&H_8), 8.51 (1H, d, naphthalene-H_6). ^{13}C-NMR ppm ($CDCl_3$): 12.0 (19-C, CH_3), 12.1 (18-C, CH_3), 18.3 (21-C, CH_3), 21.0 (11-C, CH_2), 23.4 (15-C, CH_2), 28.5 (2-C, CH_2), 28.6 (16-C, CH_2), 30.9 (22-C, CH_2), 31.5 (23-C, CH_2), 33.8 (4-C, CH_2), 35.1 (20-C, CH), 35.2 (10-C, <u>C</u>-CH_3), 37.1 (6-C, CH_2), 37.5 (1-C, CH_2), 39.1(5-C, CH), 40.0 (C-8, CH), 40.2 (12-C, CH_2), 42.9 (9-C, CH), 43.6 (13-C, <u>C</u>-CH_3), 45.5 (N-<u>C</u>H_3), 46.0 (3-C, CH), 53.8 (14-C, CH), 55.6 (17-C, CH), 71.1 (7-C, CH), 117.6 (naphthalene-C_4), 119.9 (naphthalene-C_q), 123.7 (naphthalene-C_2), 124.9 (naphthalene-C_8), 126.3 (naphthalene-C_7), 127.9 (naphthalene-C_3), 128.3 (naphthalene-C_6), 133.0 (naphthalene-C_q), 143.3 (naphthalene-C_1), 151.3 (naphthalene-C_5), 174.1 (24-C, COOH). HRMS: Found: $(M+H)^+$ =624.3588, calculated $C_{36}H_{52}N_2O_5S^+$ =624.3597. IRvmax (ATR): 2932, 2866, 1706, 1576, 1453, 1409 cm^{-1}.

24-taurine-3α-((5-(dimethylamino) naphthalene)-1-sulfonamido))-7β-hydroxyl-5β-cholanoate (taurine conjugated of 3α-dansyl UDCA) (58)

To a solution of 3α-dansyl UDCA **49** (10 mg, 0.016 mmol) in dry DMF (5 ml), COMU (0.0041 g, 0.016 mmol) was added and taurine (0.004 g, 0.032 mmol) was added after 5 min. The reaction was stirred for overnight to yield a white

solid (5.6 mg, 47.8%) after purification by flash column chromatography (DCM: MeOH=1:19).

mp 153–157°C; ^{1}H-NMR δ ($CDCl_3$): 0.59 (3H, s, 18-CH_3), 0.81 (3H, d, J = 6.1 Hz, 21-CH_3), 0.87 (3H, s, 19-CH_3), 1.00-1.08 (4H, m, 8-CH, 9-CH, 14-CH, 17-CH), 1.11-1.20 (3H, m, 1-CH_2, 20-CH), 1.22-1.40 (10H, m, 2-CH_2, 4-CH_2, 6-CH_2, 7-CH_2, 11-CH_2), 1.58-1.78 (4H, m, 15-CH_2, 16-CH_2), 1.81-1.91 (2H, m, 26-CH_2), 2.15-2.24 (2H, m, 22-CH_2), 2.32-2.35 (2H, m, 23-CH_2), 2.86 (6H, s, 2×CH_3), 3.01 (1H, m, 3β-H), 3.22 (2H, t, 27-CH_2), 3.37 (1H, m, 7α-H), 3.66 (2H, m, 25-CH_2), 4.35 (1H, t, N<u>H</u>-CH_2), 5.15 (1H, d, N<u>H</u>-SO_2), 7.14 (1H, d, naphthalene-H_4), 7.48 (2H, m, naphthalene-H_3&H_7), 8.23 (2H, m, naphthalene-H_2&H_8), 8.51 (1H, d, naphthalene-H_6). ^{13}C-NMR ppm ($CDCl_3$): 12.1 (19-C, CH_3), 14.0 (18-C, CH_3), 18.3 (21-C, CH_3), 21.0 (11-C, CH_2), 23.4 (15-C, CH_2), 26.8 (2-C, CH_2), 28.6 (16-C, CH_2), 30.9 (22-C, CH_2), 31.1 (23-C, CH_2), 33.7 (4-C, CH_2), 35.3 (20-C, CH), 35.4 (10-C, <u>C</u>-CH_3), 36.5 (6-C, CH_2), 38.5 (1-C, CH_2), 39.1 (NH-<u>C</u>H_2-CH_2-SO_2OH), 39.2 (5-C, CH), 39.9 (8-C, CH), 40.0 (12-C, CH_2), 42.6 (9-C, CH), 43.5 (13-C, <u>C</u>-CH_3), 43.7 (N-<u>C</u>H_3), 45.4 (3-C, CH), 47.2 (NH-CH_2-<u>C</u>H_2-SO_2OH), 53.8 (14-C, CH), 55.6 (17-C, CH), 66.6 (7-C, CH), 115.1 (naphthalene-C_4), 118.9 (naphthalene-C_q), 123.2 (naphthalene-C_2), 128.2 (naphthalene-C_8), 129.2 (naphthalene-C_7), 129.6 (naphthalene-C_3), 129.8 (naphthalene-C_6), 130.2 (naphthalene-C_q), 135.9 (naphthalene-C_1), 151.8 (naphthalene-C_5), 178.8 (24-C, <u>C</u>OOH). HRMS: Found: $(M+H)^+$ =731.3629, calculated $C_{38}H_{57}N_3O_7S_2^+$ =731.3638. IRvmax (ATR): 2931,1706, 1575, 1501,1453, 1399 cm^{-1}.

3α-((5-(dimethylamino) naphthalene)-1-sulfonamido)-12α-hydroxyl-5β-cholanoate (3α-dansyl DCA) (59)

To a solution of protected 3α-dansyl DCA (100 mg, 0.1499 mmol) in MeOH (10 ml) was added 2M aq. NaOH solution (5 ml) at reflux and stirred fo16 h. When TLC analysis (hexane: EtOAc =1:1) showed the disappearance of starting

material, 2M aq. HCl solution (5 ml) was added to neutralize the pH into 7. The MeOH was removed *in vacuo* and the residue was extracted with EtOAc (3×50 ml). The combined organic layer was washed with water (2×100 ml) and brine (100 ml) and it was dried over $MgSO_4$ and filtered. The solvent was removed to yield compound **49** as a white foam (84.5 mg, 90.3%).

mp 215–218°C; ^{1}H-NMR δ ($CDCl_3$): 0.62 (3H, s, 18-CH_3), 0.80 (3H, d, J = 6.1 Hz, 21-CH_3), 0.95 (3H, s, 19-CH_3), 0.99-1.09 (4H, m, 8-CH, 9-CH, 14-CH, 17-CH), 1.13-1.20 (3H, m, 1-CH_2, 20-CH), 1.24-1.39 (10H, m, 2-CH_2, 4-CH_2, 6-CH_2, 7-CH_2, 11-CH_2), 1.74-1.86 (4H, m, 15-CH_2, 16-CH_2), 2.21-2.29 (2H, m, 22-CH_2), 2.35-2.43 (2H, m, 23-CH_2), 2.89 (6H, s, 2×CH_3), 3.10 (1H, m, 3β-H), 3.92 (1H, s, 12β-H), 4.65 (1H, d, N<u>H</u>-SO_2), 7.19 (1H, d, naphthalene-H_4), 7.54 (2H, m, naphthalene-H_3&H_7), 8.24 (2H, m, naphthalene-H_2&H_8), 8.53 (1H, d, naphthalene-H_6). ^{13}C-NMR ppm ($CDCl_3$): 12.7 (19-C, CH_3), 14.7 (18-C, CH_3), 17.2 (21-C, CH_3), 21.0 (15-C, CH_2), 23.1 (2-C, CH_2), 27.4 (6-C, CH_2), 28.5 (16-C, CH_2), 28.6 (11-C, CH_2), 30.6 (22-C, CH_2), 30.9 (23-C, CH_2), 32.0 (7-C, CH_2), 33.5 (4-C, CH_2), 33.8 (20-C, CH), 35.0 (10-C, <u>C</u>-CH_3), 37.2 (C-8, CH), 37.5 (1-C, CH_2), 38.3 (9-C, CH), 45.5 (5-C, CH), 46.2 (N-<u>C</u>H_3), 46.6 (3-C, CH), 47.2 (13-C, <u>C</u>-CH_3), 47.5 (17-C, CH), 48.2 (14-C, CH), 67.6 (12-C, CH), 117.6 (naphthalene-C_4), 119.9 (naphthalene-C_q), 123.7 (naphthalene-C_2), 124.9 (naphthalene-C_8), 126.0 (naphthalene-C_7), 127.9 (naphthalene-C_3), 128.3 (naphthalene-C_6), 133.0 (naphthalene-C_q), 143.3 (naphthalene-C_1), 151.3 (naphthalene-C_5), 168.8 (24-C, COOH). HRMS: Found: $(M+H)^+$ =624.3589, calculated $C_{36}H_{52}N_2O_5S^+$ =624.3597. IRvmax (ATR): 3284, 2930, 1709, 1450, 1378 cm^{-1}.

24-taurine-3α-((5-(dimethylamino)naphthalene)-1-sulfonamido))-7β-hydroxyl-5β-cholanoate (taurine conjugated of 3α-dansyl DCA) (60)

To a solution of 3α-dansyl DCA **51** (10 mg, 0.016 mmol) in dry DMF (5 ml), COMU (0.0041 g, 0.016 mmol) was added and taurine (0.004 g, 0.032 mmol) was added after 5 min. The reaction was stirred for overnight to yield a white

solid (5.4 mg, 46.1%) after purification by flash column chromatography (DCM: MeOH=1:19).

mp 155–157°C; ^{1}H-NMR δ ($CDCl_3$): 0.60 (3H, s, 18-CH_3), 0.78 (3H, d, J = 6.1 Hz, 21-CH_3), 0.92 (3H, s, 19-CH_3), 1.01-1.06 (4H, m, 8-CH, 9-CH, 14-CH, 17-CH), 1.17-1.23 (3H, m, 1-CH_2, 20-CH), 1.24-1.60 (10H, m, 2-CH_2, 4-CH_2, 6-CH_2, 7-CH_2, 11-CH_2), 1.61-1.75 (4H, m, 15-CH_2, 16-CH_2), 1.77-1.80 (2H, m, 26-CH_2), 2.24-2.27 (2H, m, 22-CH_2), 2.33-2.37 (2H, m, 23-CH_2), 2.86 (6H, s, 2×CH_3), 3.08 (1H, m, 3β-H), 3.22 (2H, t, 27-CH_2), 3.67 (2H, m, 25-CH_2), 3.92 (1H, s, 12β-H), 4.37 (1H, t, N<u>H</u>-CH_2), 5.20 (1H, d, N<u>H</u>-SO_2), 7.15 (1H, d, naphthalene-H_4), 7.47 (2H, m, naphthalene-H_3&H_7), 8.24 (2H, m, naphthalene-H_2&H_8), 8.48 (1H, d, naphthalene-H_6). ^{13}C-NMR ppm ($CDCl_3$): 12.6 (19-C, CH_3), 14.1 (18-C, CH_3), 17.2 (21-C, CH_3), 23.0 (15-C, CH_2), 23.6 (2-C, CH_2), 25.9 (16-C, CH_2), 28.3 (6-C, CH_2), 29.7 (11-C, CH_2), 30.7 (22-C, CH_2), 31.0 (7-C, CH), 33.4 (23-C, CH_2), 33.4 (4-C, CH_2), 33.9 (20-C, CH), 34.5 (10-C, <u>C</u>-CH_3), 35.2 (8-C, CH), 35.8 (NH-<u>C</u>H_2-CH_2-SO_2OH), 35.9 (1-C, CH_2), 38.4 (10-C, <u>C</u>-CH_3), 42.5 (5-C, CH), 45.4 (N-<u>C</u>H_3), 46.2 (3-C, CH), 47.0 (13-C, <u>C</u>-CH_3), 47.2 (20-C, CH), 48.1 (14-C, CH), 54.0 (NH-CH_2-<u>C</u>H_2-SO_2OH), 73.3 (12-C, CH), 115.1 (naphthalene-C_4), 119.1 (naphthalene-C_q), 123.2 (naphthalene-C_2), 128.1 (naphthalene-C_8), 129.1 (naphthalene-C_7), 129.8 (naphthalene-C_3), 129.7 (naphthalene-C_6), 130.1 (naphthalene-C_q), 136.1 (naphthalene-C_1), 151.7 (naphthalene-C_5), 178.7 (24-C, <u>C</u>OOH). HRMS: Found: $(M+H)^+$ =731.3630, calculated $C_{38}H_{57}N_3O_7S_2^+$ =731.3638. IRvmax (ATR): 2930, 2863, 1706, 1576, 1448 cm^{-1}.

General procedure for the formation of protected 3α-chlorambucil bile acids:

3α-azido UDCA **5** (110 mg, 0.254 mmol) was poured into EtOAc (20 ml) and then the mixture was added to a pre-reduced Pd/C (0.12 g) in EtOAc (10 ml) and stirred under H_2 at r.t. for 1 d. The mixture was filtered through a cellite pad and the cellite was washed with EtOAc (3×20 ml). The solvent was removed *in*

vacuo to yield amine intermediates. These were dissolved in dry DMF (6 ml) immediately without any purification, chlorambucil (77 mg, 0.254 mmol, 1 eqv.), DCC (0.052 g, 0.254 mmol, 1 eqv.) and HOBt·H_2O (0.038 g, 0.279 mmol, 1.1 eqv.) were added at 0°C and then stirred to r.t. for overnight under N_2. The mixture was poured into water (100 ml) and extracted with EtOAc (3×75 ml). The organic layer was washed with water (2×100 ml) and brine (100 ml). The solvent was dried over Na_2SO_4 and then filtered. The solvent was removed in vacuo and the residue was purified by flash column chromatography (hexane: EtOAc=2:1) to afford the protected 3α-chlorambucil UDCA (120 mg, 0.17 mmol, 66.9%).

3α-(4-(4-(bis(2-chloroethyl)amino)phenyl)butanamido)-7β-hydroxyl-5β-cholanoate (3α-chlorambucil UDCA) (61)

To a solution of protected 3α-chlorambucil UDCA (120 mg, 0.17 mmol) in dry THF (15 ml) at 0°C, 2N LiOH solution (6 ml) was added. The reaction mixture was left stirring overnight at RT. When TLC (hexane: EtOAc=1:2) showed the formation of desired product R_f =0.11. The crude mixture was worked up and purified by flash column chromatography (hexane: EtOAc=1:2) to yield the product as white solid (105 mg, 0.158 mmol, 93.1%).

mp 161–165°C; ^{1}H-NMR δ ($CDCl_3$): 0.65 (3H, s, 18-CH_3), 0.90 (3H, d, J = 6.1 Hz, 21-CH_3), 0.92 (3H, s, 19-CH_3), 1.02-1.10 (4H, m, 8-CH, 9-CH, 14-CH, 17-CH), 1.11-1.22 (3H, m, 1-CH_2, 20-CH), 1.23-1.47 (10H, m, 2-CH_2, 4-CH_2, 6-CH_2, 7-CH_2, 11-CH_2), 1.61-1.66 (2H, m, CH_2-C$\underline{H_2}$-CH_2-CONH), 1.76-1.80 (4H, m, 15-CH_2, 16-CH_2), 2.08-2.20 (2H, t, CH_2-CH_2-C$\underline{H_2}$-CONH), 2.18-2.28 (2H, m, 22-CH_2), 2.31-2.42 (2H, m, 23-CH_2), 2.49-2.55 (2H, t, C$\underline{H_2}$-CH_2-CH_2-CONH), 3.44-3.55 (2H, m, 3β-H & 7α-H), 3.57-3.75 (8H, m, N-C$\underline{H_2}$-C$\underline{H_2}$-Cl), 5.41 (1H, d, N$\underline{H}$), 6.61 (2H, d, aromatic-$H_{ortho\ to\ N}$), 7.02 (2H, d, aromatic-$H_{para\ to\ N}$). ^{13}C-NMR ppm ($CDCl_3$): 10.7 (19-C, CH_3), 12.1 (18-C, CH_3), 18.4 (21-C, CH_3), 21.1 (11-C, CH_2), 23.5 (15-C, CH_2), 26.8 (CH_2-C$\underline{H_2}$-CH_2-CONH), 27.5 (16-C, CH_2), 28.6 (2-C, CH_2), 30.8 (22-C, CH_2),

30.9 (23-C, CH_2), 33.7 ($\underline{C}H_2$-CH_2-CH_2-CONH), 34.0 (20-C, CH), 35.2 (13-C, $\underline{C}$-CH_3) 35.3 (4-C, CH_2), 36.2 (CH_2-CH_2-$\underline{C}H_2$-CONH), 36.7 (6-C, CH_2), 37.2 (1-C, CH_2), 39.3 (5-C, CH), 40.2 (8-C, CH), 40.5 (12-C, CH_2), 42.5 (9-C, CH), 43.7 (13-C, $\underline{C}$-CH_3), 43.8 (N-CH_2-$\underline{C}H_2$-Cl), 49.2 (14-C, CH), 53.6 (3-C, CH), 55.0 (N-$\underline{C}H_2$-CH_2-Cl), 55.8 (17-C, CH), 66.9 (7-C, CH), 112.2 (aromatic-C), 129.6 (aromatic-C), 130.6 (aromatic-C), 144.3 (aromatic-C),172.3 ($\underline{C}$ONH), 178.7 (24-C, COOH). HRMS: Found: $(M+H)^+$ =676.3777, calculated $C_{38}H_{58}Cl_2N_2O_4^+$ =676.3774. IRvmax (ATR): 2928, 1707, 1616, 1518, 1450 cm^{-1}.

3α-(4-(4-(bis(2-chloroethyl)amino)phenyl)butanamido)-12α-hydroxyl-5β-cholanoate (3α-chlorambucil DCA) (63)

To a solution of protected 3α-chlorambucil UDCA (100 mg, 0.141 mmol) in dry THF (12 ml) at 0°C, 2N LiOH solution (6 ml) was added. The reaction mixture was left stirring overnight at RT. When TLC (hexane: EtOAc=1:2) showed the formation of desired product R_f=0.12. The crude mixture was worked up and purified by flash column chromatography (hexane: EtOAc=1:2) to yield the product as white solid (88 mg, 0.133 mmol, 94.0%).

mp 213–216°C; ^{1}H-NMR δ ($CDCl_3$): 0.71 (3H, s, 18-CH_3), 0.91 (3H, d, J = 6.1 Hz, 21-CH_3), 0.94 (3H, s, 19-CH_3), 1.02-1.10 (4H, m, 8-CH, 9-CH, 14-CH, 17-CH), 1.11-1.24 (3H, m, 1-CH_2, 20-CH), 1.25-1.49 (10H, m, 2-CH_2, 4-CH_2, 6-CH_2, 7-CH_2, 11-CH_2), 1.61-1.66 (2H, m, CH_2-$C\underline{H_2}$-CH_2-CONH), 1.77-1.80 (4H, m, 15-CH_2, 16-CH_2), 2.13-2.17 (2H, t, CH_2-CH_2-$C\underline{H_2}$-CONH), 2.24-2.35 (2H, m, 22-CH_2), 2.40-2.49 (2H, m, 23-CH_2), 2.56-2.60 (2H, t, $C\underline{H_2}$-CH_2-CH_2-CONH), 3.42-3.50 (1H, m, 12β-H), 3.63-3.68 (4H, m, N-CH_2-$C\underline{H_2}$-Cl), 3.69-3.76 (4H, m, N-$C\underline{H_2}$-CH_2-Cl), 4.03 (1H, s, 3β-H), 5.33 (1H, d, N$\underline{H}$), 6.69 (2H, d, aromatic-$H_{ortho\ to\ N}$), 7.09 (2H, d, aromatic-$H_{para\ to\ N}$). ^{13}C-NMR ppm ($CDCl_3$): 12.8 (19-C, CH_3), 12.9 (18-C, CH_3), 17.4 (21-C, CH_3), 21.0 (11-C, CH_2), 23.5 (15-C, CH_2), 26.9 (CH_2-$\underline{C}H_2$-CH_2-CONH), 27.5 (16-C, CH_2), 28.6 (2-C, CH_2), 30.7 (22-C, CH_2), 30.8 (23-C, CH_2), 33.5

(CH_2-CH_2-CH_2-CONH), 34.1 (20-C, CH), 35.5 (13-C, C-CH_3) 35.8 (4-C, CH_2), 36.0 (CH_2-CH_2-CH_2-CONH), 36.2 (6-C, CH_2), 37.2 (1-C, CH_2), 39.3 (5-C, CH), 40.2 (8-C, CH), 40.4 (12-C, CH_2), 42.3 (9-C, CH), 46.6 (13-C, C-CH_3), 47.4 (N-CH_2-CH_2-Cl), 49.2 (14-C, CH), 54.0 (3-C, CH), 55.0 (N-CH_2-CH_2-Cl), 55.8 (17-C, CH), 73.3 (12-C, CH), 113.0 (aromatic-C), 129.6 (aromatic-C), 134.0 (aromatic-C), 144.3 (aromatic-C), 157.4 (CONH), 172.0 (24-C, COOH). HRMS: Found: $(M+H)^+$ =676.3775, calculated $C_{38}H_{58}Cl_2N_2O_4^+$ =676.3774. IRvmax (ATR): 2927, 1707, 1625, 1518, 1448 cm^{-1}.

General procedure for the formation of 3-trifluoromethyl bile acids:

Compound **3** (1.53 g, 3.52 mmol) was dissolved in DCM (100 ml) and PCC (1.90 g, 8.800 mmol, 2.5 eq.) was added in 3 times over one hour at RT with stirring for about 4 h. TLC analysis (hexane: EtOAc=1:1) showed the disappearance of starting material. The solvent was then removed in vacuum and EtOAc (100 ml) was added to the mixture. The organic layer was washed with water (3×100 ml) and brine (100 ml) and was dried over $MgSO_4$ and filtered. The solvent was removed to yield compound 3-keto, 7β-formyloxy UDCA (1.50 g, 98.5%) as white foam**.** To a solution of 3-keto, 7β-formyloxy UDCA (0.15 g, 0.347 mmol) in dry THF (5 ml), 2M TMS-CF_3 solution (600 µl, 1.206 mmol, 3.48 eq.) and CsF (0.075 g, 1.42 eq.) were added over N_2 balloon in ice bath. The reaction was then stirred to RT for overnight. TLC analysis (Hexane: EtOAc= 3:1) showed completion and the solvent was removed under reduced pressure and the product extracted with EtOAc (3 x 50 ml) and washed with water (2 x 100 ml). The organic layer was dried over $MgSO_4$ and filtered. The solvent was removed in vacuo and the residue purified by flash column chromatography (Hexane: EtOAc= 7:1) to afford the protected 3-trifluoromethyl UDCA intermediate.

3α-trifluoromethyl-12α-hydroxyl-5β-cholanoate (3α-trifluoromethyl DCA) (65)

To a solution of protected 3-trifluoromethyl DCA (20 mg, 0.040 mmol) in MeOH (16 ml) was added 2M aq. NaOH solution (5 ml) at reflux and stirred for 5 h. When TLC analysis (hexane: EtOAc =1:1) showed the disappearance of starting material, 2M aq. HCl solution (10 ml) was added to neutralize the pH into 7. The MeOH was removed and the residue was extracted with EtOAc (3×50 ml). The combined organic layer was washed with water (2×100 ml) and brine (100 ml) and it was dried over $MgSO_4$ and then filtered. The solvent was removed to yield compound **65** as a white foam (15.6 mg, 0.034 mmol, 84.7 %).

mp 128–130°C; ^{1}H-NMR δ ($CDCl_3$): 0.72 (3H, s, 18-CH_3), 0.98 (3H, d, J = 6.1 Hz, 21-CH_3), 1.01 (3H, s, 19-CH_3), 1.12-1.20 (4H, m, 8-CH, 9-CH, 14-CH, 17-CH), 1.28-1.31 (3H, m, 1-CH_2, 20-CH), 1.43-1.62 (10H, m, 2-CH_2, 4-CH_2, 6-CH_2, 7-CH_2, 11-CH_2), 1.63-1.78 (4H, m, 15-CH_2, 16-CH_2), 2.28-2.35 (2H, m, 22-CH_2), 2.42-2.48 (2H, m, 23-CH_2), 4.03 (1H, d, 12α-H). ^{13}C-NMR ppm ($CDCl_3$): 12.5 (18-C, CH_3), 17.0 (19-C, CH_3), 22.9 (21-C, CH_3), 23.5 (11-C, CH_2), 25.5 (15-C, CH_2), 26.3 (16-C, CH_2), 27.2 (2-C, CH_2), 28.8 (22-C, CH_2), 30.8 (23-C, CH_2), 30.9 (1-C, CH_2), 32.3 (20-C, CH), 33.2 (10-C, C-CH_3), 33.3 (4-C, CH_2), 33.7 (6-C, CH), 35.0 (5-C, CH), 35.5 (8-C, CH), 38.6 (12-C, CH_2), 40.1 (9-C, CH), 40.3 (13-C, C-CH_3), 46.0 (14-C, CH), 46.2 (17-C, CH), 47.5 (12-C, CH), 71.0 (3-C, CH), 175.0 (24-C, COOH). HRMS: Found: $(M+H)^+$ =459.2730, calculated $C_{25}H_{39}F_3O_4^+$ =459.2722. IRvmax (ATR): 2929, 1706, 1449, 1380 cm^{-1}.

3α-trifluoromethyl-7β-hydroxyl-5β-cholanoate (3α-trifluoromethyl UDCA) (66)

To a solution of protected 3-trifluoromethyl UDCA (20 mg, 0.040 mmol) in MeOH (16 ml) was added 2M aq. NaOH solution (5 ml) at reflux and stirred for 5 h. When TLC analysis (hexane: EtOAc =1:1) showed the disappearance of starting material, 2M aq. HCl solution (10 ml) was added to neutralize the pH into 7. The MeOH was removed and the residue was extracted with EtOAc

(3×50 ml). The combined organic layer was washed with water (2×100 ml) and brine (100 ml) and it was dried over $MgSO_4$ and then filtered. The solvent was removed to yield compound **66** as a white foam (16.0 mg, 0.035 mmol, 86.9 %).

^{1}H-NMR δ ($CDCl_3$): 0.73 (3H, s, 18-CH_3), 0.94 (3H, d, J = 6.1 Hz, 21-CH_3), 0.99 (3H, s, 19-CH_3), 1.11-1.17 (4H, m, 8-CH, 9-CH, 14-CH, 17-CH), 1.27-1.31 (3H, m, 1-CH_2, 20-CH), 1.43-1.56 (10H, m, 2-CH_2, 4-CH_2, 6-CH_2, 7-CH_2, 11-CH_2), 1.59-1.77 (4H, m, 15-CH_2, 16-CH_2), 2.25-2.31 (2H, m, 22-CH_2), 2.33-2.45 (2H, m, 23-CH_2), 4.09 (1H, d, 7β-H). ^{13}C-NMR ppm ($CDCl_3$): 12.5 (18-C, CH_3), 18.7 (19-C, CH_3), 21.5 (21-C, CH_3), 23.2 (11-C, CH_2), 27.0 (15-C, CH_2), 27.9 (16-C, CH_2), 28.6 (2-C, CH_2), 30.6 (22-C, CH_2), 30.8 (23-C, CH_2), 31.2 (1-C, CH_2), 32.4 (20-C, CH), 33.7 (10-C, C-CH_3), 34.8 (4-C, CH_2), 35.4 (6-C, CH), 37.4 (5-C, CH), 39.4 (8-C, CH), 39.6 (12-C, CH_2), 41.9 (9-C, CH), 42.8 (13-C, C-CH_3), 55.1 (14-C, CH), 56.2 (17-C, CH), 69.5 (7-C, CH), 71.8 (3-C, CH), 175.3 (24-C, COOH). HRMS: Found: $(M+H)^+$ =459.2732, calculated $C_{25}H_{39}F_3O_4^+$ =459.2722. IRvmax (ATR): IRvmax (ATR): 2926, 2156, 1716, 1449, 1381 cm^{-1}.

3α-trifluoromethyl-7α-hydroxyl-5β-cholanoate (3α-trifluoromethyl CDCA) (67)

To a solution of protected 3-trifluoromethyl UDCA (20 mg, 0.040 mmol) in MeOH (16 ml) was added 2M aq. NaOH solution (5 ml) at reflux and stirred for 5 h. When TLC analysis (hexane: EtOAc =1:1) showed the disappearance of starting material, 2M aq. HCl solution (10 ml) was added to neutralize the pH into 7. The MeOH was removed and the residue was extracted with EtOAc (3×50 ml). The combined organic layer was washed with water (2×100 ml) and brine (100 ml) and it was dried over $MgSO_4$ and then filtered. The solvent was removed to yield compound **67** as a white foam (15.2 mg, 0.033 mmol, 82.5 %).

^{1}H-NMR δ ($CDCl_3$): 0.70 (3H, s, 18-CH_3), 0.97 (3H, d, J = 6.1 Hz, 21-CH_3),

0.98 (3H, s, 19-CH_3), 1.15-1.23 (4H, m, 8-CH, 9-CH, 14-CH, 17-CH), 1.24-1.30 (3H, m, 1-CH_2, 20-CH), 1.35-1.58 (10H, m, 2-CH_2, 4-CH_2, 6-CH_2, 7-CH_2, 11-CH_2), 1.62-1.75 (4H, m, 15-CH_2, 16-CH_2), 2.27-2.32 (2H, m, 22-CH_2), 2.40-2.46 (2H, m, 23-CH_2), 2.50-2.55 (2H, t), 3.89 (1H, d, 7α-H). ^{13}C-NMR ppm ($CDCl_3$): 11.8 (18-C, CH_3), 18.2 (19-C, CH_3), 20.8 (21-C, CH_3), 22.2 (11-C, CH_2), 23.7 (15-C, CH_2), 27.4 (16-C, CH_2), 28.1 (2-C, CH_2), 30.6 (22-C, CH_2), 30.8 (23-C, CH_2), 33.7 (1-C, CH_2), 33.8 (20-C, CH), 34.5 (10-C, C-CH_3), 35.3 (4-C, CH_2), 36.7 (6-C, CH), 39.3 (5-C, CH), 39.4 (8-C, CH), 39.6 (12-C, CH_2), 41.9 (9-C, CH), 42.8 (13-C, C-CH_3), 50.3 (14-C, CH), 55.8 (17-C, CH), 68.4 (7-C, CH), 71.0 (3-C, CH), 177.6 (24-C, COOH). HRMS: Found: $(M+H)^+$ =459.2721, calculated $C_{25}H_{39}F_3O_4^+$ =459.2722. IRvmax (ATR): 2926, 2160, 1680, 1442, 1386 cm^{-1}.

6.1.2 Reverse phase thin layer chromatography (PRTLC)

The TLC experiments were carried out on pre-coated C18 reverse phase TLC (20cm×20cm, F254) plates (Merck, Darmstadt, Germany). The plates were spotted with solutes of each test compound dissolved in DCM (10 µl). Plates were developed in a closed container across a development distance of 15 cm. The mixture of methanol-water (v/v) was used as development solvents and solvent composition for mobile phase is chosen by trial and error method. The plates were dried for 10-15 min after development and then stained with a 5% ammonium molybdate solution, and followed by heating to visualize the blue spots. All the components of the mobile phases were of the analytical grade of purity. All experiments were proceeded at ambient temperature.

6.2 Cell culture

6.2.1 Bile acids

All bile acids and bile acid derivatives were synthesized based on the procedures shown above. Synthesized bile acid compounds for biological tests

were maintained in DMSO as 1 mM stock solutions. The compounds were diluted up to the specific concentration of 1% DMSO (high concentration of DMSO damages cells). This ensures solubility and uniformity of all biological tests.

6.2.2 Cell subculture

Cells in T-75 flask grown to high confluence (80–90% confluence) need to be subcultured into different T-75 flasks for further growth. The medium was discarded, followed by trypsinization (adding 3 ml of trypsin-EDTA mixture to the confluent cultures) in the incubator for 3–5 min with regular gentle shaking, which allowed the cells to full detached from the flask. The trypsinized cells were added into a universal tube containing fresh medium and then centrifuged for 5 min at the speed of 900 rpm. The supernatant was then removed and the cell pellet was suspended in new medium and aliquoted into different T-75 flasks to make a volume of 15 ml cell medium.

6.2.3 Cell counting

The biological assay needs a consistent number of cells to be cultured. Cell concentrations were calculated using a bright-line haemocytometer (Hausser Scientific, Horsham, P.A., USA). A volume of 10 µl of the mixed cell suspension was injected into the haemocytometer below the glass microscope slide. The number of cells per ml was determined as average cell/mm^3×10^5 (overall multiplication factor). Here, the average cell/mm^3 is determined by averaging the number of cells present in each counting zone.

Cells were brought to a concentration of 1×10^5 cells/ml for MTT and Alamar Blue assay and 6.2×10^5 cells/ml for FXR agonist assay. The resulting different cell suspensions were seeded into the flat-bottom 96-well plate and incubated at 37ºC with 5%CO_2.

6.2.4 Cell preservation and recovery

Following the operating protocol of cell subculture, once the cell pellet was obtained after removal of the supernatant, 3 ml of FBS with 5% DMSO was added dropwise. A volume of 1 ml of this cryoprotectant suspension was added into a sterile cryovial and all the cryovials were placed into a -80^{o}C freezer for 24 h and then into a liquid nitrogen tank for longer term storage.

To recover the cells the cryovials were removed from the liquid nitrogen tank and thawed at RT and then at 37^{o}C in a water bath. The cell suspension was slowly added to the warm medium to avoid damaging the cell membrane and the suspension was then centrifuged at the appropriate rotation speed and time, which depended on the cell type. After removal of the supernatant, the cell pellet was resuspended in fresh medium and then transferred to a T-25 cell culture flask with 5 ml volume.

6.2.5 Caco-2 cell line

Caco-2 cell line is the adherent and continuous cell line derived from human epithelial colorectal cancer cells. It was grown as a monolayer in T-75 cell culture flask in DMEM low glucose type (pH=7.4) supplemented with 20% sterile and inactivated FBS, 1% sodium pyruvate solution, 1% 2 mM L-glutamine and 1% penicillin-Streptomycin (pen/strep) antibiotic solution. Cells were maintained in a humidified incubator set at 37^{o}C, 5% CO_2. Cell medium was changed approximately every second or third day until cells reached around 80–90% confluence followed by normal cell subculture procedures. When confluent, cells were split into 3. Caco-2 cells were used up to a maximum passage number of 50 in the normal case.

6.2.6 Huh-7 cell line

Hepatocellular carcinoma (Huh-7) cell line is epithelial-like human liver cell

derived carcinoma cell line that is mainly obtained from ATCC. It was grown in DMEM media high glucose type with 10% sterile FBS, 1% sodium pyruvate solution and 1% Penicillin-Streptomycin (pen/strep) antibiotic solution. Cells were maintained in a 37^{o}C, 5% CO_2 incubator. When confluent, cells were split into 2. Cell medium was changed approximately every second or third day until cells reached around 80–90% confluence followed by normal cell subculture procedures. All assays using Huh-7 cell line were done independently in triplicate, using cell cultures at low passages.

6.2.7 FXR-UAS-bla HEK 293T cell line

The GeneBLAzer FXR-UAS-bla HEK 293T cells contain human FXR ligand binding domain and express FXR β-lactamase reporter gene. They were cultured in DMEM with GlutaMAX^{TM} media supplemented with 10% dialyzed FBS, 1% NEAA solution, 2.5% HEPES solution, 1% 100 U/ml Penicillin-Streptomycin (pen/strep) antibiotic solution and a small amount of 100 µg/mlHygromycin antibiotics. Cells were maintained in a 37^{o}C, 5% CO_2 incubator. When confluent, cells were split into 3. Cell medium was changed approximately every second day until cells reached 80–90% confluence followed by normal cell subculture procedures.

6.3 MTT assay

%Cell viability can be measured in 96-well plates, following exposure to specific drugs or reagents, where MTT (3-(4, 5-dimethylthiazol-2-yl)-2, 5-diphenyltetrazolium bromide, Thiazolyl blue tetrazolium bromide is widely used. The MTT assay is based on the ability of viable cells to produce fluorescent purple formazan (reduced form) from the cleavage of the tetrazolium salt in the mitochondria of viable cells. Cells were placed into 96 well plates at a concentration of 1×10^5 cells/ml for test cells in 100 µl appropriate FBS containing medium. The cells were incubated for 24 h to allow

for adherence before treatment. After 24 h, the medium is aspirated from the well and FBS free medium is added. The cells were treated with the drug solution at indicated concentration for the appropriate time. At the same time, some wells need to be vehicle controlled with 1% DMSO. Two hours before the end of treatment, 10 µl of 2.5 mg/ml MTT was added into the solution. At 24 h time point, the medium was gently removed and 100 µl DMSO was added into the wells. The plates were shaken for around 10 minutes to allow the dissolution of formazan crystals. The absorbance of each well can be read on a VERSA$_{max}$ Microplate Reader (Molecular Devices, Sunnyvale, CA, USA) at a wavelength of 570 nm. % cell viability was determined by calculating to the vehicle controlled.

$$\%\ \text{cell viability} = \frac{\text{Abs (compound tested well)-Abs (blank well)}}{\text{Abs (vehicle controlled well)-Abs (blank well)}} \times 100\%$$

Values represent the mean ± SEM (standard error of the mean) of three experiments performed in triplicate. Resultant concentration effect curves were transformed and analyzed using GraphPad Prism 5 (San Diego, CA, USA).

6.4 Alamar Blue assay

% Cell viability can also be measured using another fluorometric assay reagent called Alamar Blue (resazurin, oxidized form, 7-hydroxy-3H-phenoxazin-3-one-10-oxide). It is a water-soluble, cell permeable, stable, non-toxic and weakly fluorescent blue indicator dye but very sensitive to light. Resazurin undergoes colorimetric change based on cellular metabolic reduction by mitochondrial enzymes that carry diaphorase activity. Its reduced form (resorufin, 7-hydroxy-3H-phenoxazin-3-one) shows pink and is highly fluorescent. The intensity of fluorescence is direct proportion to the viable cells present. Cells were placed into 96-well plates at a concentration of 1×10^5 cells/ml for test cells in 100 µl appropriate FBS-containing medium. After incubating for 24 h, the medium is aspirated from the

well and FBS free medium is added. The cells were treated with the drug solution at indicated concentration for the appropriate time. At the same time, some wells need to be vehicle controlled with 1% DMSO. After another 24 h, Alamar Blue reagent (10% v/v, 10 µl) was added into the solution straight away (no need to replace culture medium before adding Alamar Blue reagent because dead or dying cells in the culture medium did not influence the overall fluorescence of reduced Alamar Blue reagent and the fluorescence fully depended on living cells attached to the well bottom) and then incubated for 2-4 h until color changes into pink from blue. The fluorescence absorbance of each well can be read on a VERSAmax Microplate Reader (Molecular Devices, Sunnyvale, CA, USA) at an excitation wavelength of 544 nm and an emission wavelength of 590 nm with bottom read mode. % cell viability was normalized to the vehicle controlled (wells without cells but with culture medium containing 10% v/v Alamar Blue reagent) with the same formula above and values represent the mean ± SEM (standard error of the mean) of three experiments performed in triplicate.

6.5 FXR agonist assay

Activation of FXR can be measured based on the fluorescence detected. Cells were placed into 384-well plates with black and clear bottom at a concentration of 6.2×10^5 cells/ml for FXR-UAS-bla HEK 293T cells in 32 µl appropriate FBS containing medium. After incubating for 4 h, the cells were treated with the bile acid drug solution at indicated concentration for the appropriate time. At the same time, some wells need to be vehicle controlled with 0.5% DMSO. After 16 h, 6X Substrate loading solution was added into each well. The fluorescence of each well was detected with specific plate reader at an excitation wavelength of 409 nm and an emission wavelength of 460 nm (Blue channel) or 530 nm (Green channel).

6.6 Analysis of chlorambucil by HPLC assay

Preparation of the biological samples: Huh-7 cells in a volume of 250 µl were plated into 24 well plate (cell density is 8×10^4 cells per well) and incubated for 24 h before treatments. The medium was removed then and 250 µl of chlorambucil and chlorambucil conjugates were added into the wells at 10 µM (prepared in supplement free medium containing 1% of DMSO) at 37°C. The mixture was then collected into Eppendorfs and the cells were quickly washed with chilled PBS. RIPA lysis buffer was then added into the cells and shaken for 15 min. The lysate was also collected into another Eppendorf and stored at -20°C for further measurements.

The measurement of chlorambucil samples were carried out at RT. The supernatant and the lysate were diluted 1 in 2 with acetonitrile HPLC grade (adding 250 µl ACN to make up the volume of the sample to 500 µl). The samples were centrifuged at 5000 rpm for 10 min to eliminate the cellular debris which might block the column. The chromatography was conducted on an X-bridge C-18 reverse phase column (4.6×250, 5 µm particle size). HPLC conditions were injection volume: 20 µl; flow rate: 1.5 ml/min; running time: 20 min for the drug chlorambucil and UDCA chlorambucil and 30 min for the DCA chlorambucil; Column temperature: 35°C; mobile phase: water: 1% formic acid in water/1% formic acid in acetonitrile=50:50; detection wavelength: 254 nm. Each compound was tested three times.

RIPA lysis buffer used: [20 mM Tris/HCl (at pH 8.0), 5 mM EDTA, 1 mM phenylmethyl-sulfonyl fluoride, 1.5 mg leupeptin, 137 mM NaCl, 10% (v/v) Glycerol, and protease inhibitor cocktail]

6.7 Statistical analysis

Statistical analysis and comparison of different groups were done using a one-sample t-test. Data were graphically represented as the mean ± SEM. All data were analyzed using GraphPad Prism5 software. A P-value lower than

0.05 was considered to be statistically significant.

References

[1]De Aguiar Vallim TQ, Tarling EJ, Edwards PA. Pleiotropic roles of bile acids in metabolism. Cell Metab. 2013; **17**(5): 657–669.

[2] Stroeve JH, Brufau G, Stellaard F, Gonzalez FJ, Staels B, Kuipers F. Intestinal FXR-mediated FGF15 production contributes to diurnal control of hepatic bile acid synthesis in mice. Lab Invest. 2010; **90**(10): 1457–1467.

[3] Hanafi NI, Mohamed AS, Sheikh Abdul Kadir SH, Othman MHD. Overview of Bile Acids Signaling and Perspective on the Signal of Ursodeoxycholic Acid, the Most Hydrophilic Bile Acid, in the Heart. Biomolecules. 2018; **8**(4): 159.

[4] Gilat T, Leikin-frenkel A, Goldiner I, Halpern Z, Konikoff FM. Administration of a Fatty Acid Bile Acid Conjugate. Hepatology. 2002; **35**(3): 597–600.

[5] Chiang JY. Bile acid regulation of gene expression: roles of nuclear hormone receptors. Endocr Rev. 2002; **23** :443–463.

[6] Hofmann AF, Sjövall J, Kurz G, et al. A proposed nomenclature for bile acids. J Lipid Res. 1992; **33**(4): 599–604.

[7] Šarenac TM, Mikov M. Bile Acid Synthesis: From Nature to the Chemical Modification and Synthesis and Their Applications as Drugs and Nutrients. Front Pharmacol. 2018; **9**: 939.

[8] Enhsen A, Kramer W, Wess G. Bile acids in drug discovery. Drug Discov Today. 1998; **3**(9): 409–418.

[9] Monte MJ, Marin JJ, Antelo A, Vazquez-Tato J. Bile acids: chemistry, physiology, and pathophysiology. World J Gastroenterol. 2009; **15**(7): 804–816.

[10] Sanyal AJ, Hirsch JI, Moore EW. Premicellar taurocholate enhances calcium uptake from all regions of rat small intestine. Gastroenterology. 1994; **106**(4): 866–874.

[11] Koop I, Schindler M, Bosshammer A, Scheibner J, Stange E, Koop H. Physiological control of cholecystokinin release and pancreatic enzyme secretion by intraduodenal bile acids. Gut. 1996; **39**(5): 661–667.

[12] Begley M, Gahan CG, Hill C. The interaction between bacteria and bile. FEMS Microbiol Rev. 2005; **29**(4): 625–651.

[13] Houten SM, Watanabe M, Auwerx J. Endocrine functions of bile acids. EMBO J. 2006; **25**(7): 1419–1425.

[14A] Kiriyama Y, Nochi H. The Biosynthesis, Signaling, and Neurological Functions of Bile Acids. Biomolecules. 2019; **9**(6): 232.

[14B] Rasmuson S, Andrew R, Näsman B, Seckl JR, Walker BR, Olsson T. Increased glucocorticoid production and altered cortisol metabolism in women with mild to moderate Alzheimer's disease. Biol Psychiatry. 2001; **49**(6): 547–552.

[14C] Kim S, Jeon BS, Heo C, et al. Alpha-synuclein induces apoptosis by altered expression in human peripheral lymphocyte in Parkinson's disease. FASEB J. 2004; **18**(13): 1615–1617.

[15] Attili AF, Angelico M, Cantafora A, Alvaro D, Capocaccia L. Bile acid-induced liver toxicity: relation to the hydrophobic-hydrophilic balance of bile acids. Med Hypotheses 1986; **19**(1): 57–69.

[16] Palmeira CM, Rolo AP. Mitochondrially-mediated toxicity of bile acids. Toxicology. 2004; **203**:1–15.

[17] Hofmann AF. Pharmacology of ursodeoxycholic acid, an enterohepatic drug. Scand. J Gastroenterol Suppl. 1994; **204**: 1–15.

[18] Hagey LR, Crombie, DL, Espinosa E, Carey MC, Igimi H, Hofmann AF. Ursodeoxycholic acid in the Ursidae: Biliary bile acids of bears, pandas, and related carnivores. J. Lipid. Res. 1993; **34**(11): 1911–1917.

[19] Guchi YI, Ogami NI, Amaguchi MY, Eraoka FT. Effects of Chemical Modification of Ursodeoxycholic Acid on TGR5 Activation. Biol Pharm Bull. 2011; **34**(1): 1–7.

[20] Hagey LR, Crombie DL, Espinosa E, Carey MC, Igimi H, Hofmann AF. Ursodeoxycholic acid in the Ursidae: biliary bile acids of bears, pandas, and related carnivores. J Lipid Res. 1993; **34**(11): 1911–1917.

[21] Podda, M. Zuin, M.Battezzati, P. M.; Ghezzi, C. De Fazio, C.Dioguardi, M. L. Gastroenterology. 1989; **96**: 222–229.

[22] Luis B. Agellon. Metabolism and function of bile acids. Biochemistry of

Lipids, Lipoproteins and Membranes (4th Edition). 2002; **36**: 433–448.

[23] Nair P and Turjman N. Role of bile acids and neutral sterols in familial cancer syndromes of the colon. Dis Colon Rectum. 1983; **26**(9): 629–632.

[24] Sinakos E, Marschall HU, Kowdley KV, Befeler A, Keac, J, Lindor K. Bile acid changes after high-dose ursodeoxycholic acid treatment in primary sclerosing cholangitis: Relation to disease progression. Hepatology. 2010; **52**(1): 197–203.

[25] Hempfling W, Er KD, Beuers U. Systematic review: ursodeoxycholic acid -adverse effects and drug interactions. Aliment Pharmacol Ther 2003;**18**: 963–972.

[26A] Kotb MA. Molecular Mechanisms of Ursodeoxycholic Acid Toxicity & Side Effects: Ursodeoxycholic Acid Freezes Regeneration & Induces Hibernation Mode. Int. J. Mol. Sci. 2012; **13**: 8882–8914.

[26B] Lindor KD, Kowdley KV, Luketic VA, Harrison ME, McCashland T, Befeler AS, Harnois D, Jorgensen R, Petz J, Keach J, Mooney J, Sargeant C, Braaten J, Bernard T, King D, Miceli E, Schmoll J, Hoskin T, Thapa P, Enders F. High-dose ursodeoxycholic acid for the treatment of primary sclerosing cholangitis. Hepatology. 2009; **50**(3): 808–814.

[27] Hofmann AF. The continuing importance of bile acids in liver and intestinal disease. Arch Intern Med. 1999; **159**(22): 2647–2258.

[28] Paumgartner G, Beuers U. Ursodeoxycholic acid in cholestatic liver disease: mechanisms of action and therapeutic use revisited. Hepatology. 2002; **36**(3): 525–531.

[29] Copaci I, Micu L, Iliescu L, Voiculescu M. New Therapeutical Indications of Ursodeoxycholic Acid. Rom J Gastroenterol. 2005;**14**(3):259–266.

[30] Strazzabosco M, Spirlí C, Okolicsanyi L. Pathophysiology of the intrahepatic biliary epithelium. J Gastroenterol Hepatol. 2000; **15**(3): 244–253.

[31] Gamboa A, Tian C, Massaad J, Reshamwala P, Cai Q. The Therapeutic Role of Ursodeoxycholic Acid in Digestive Diseases. Annals of Gastroenterology & Hepatology. 2011; **2**(1): 43–49.

[32] Paumgartner G, Beuers U. Ursodeoxycholic Acid in Cholestatic Liver Disease. Hepatology. 2002; **36**(3): 525–531.

[33] Rodrigues CM, Steer CJ. Mitochondrial membrane perturbations in cholestasis. J Hepatol. 2000; **32**(1): 135–141.

[34] Qiao L, Yacoub A, Studer E, et al. Inhibition of MAPK and PI3K pathways enhances UDCA-induced apoptosis in primary rodent hepatocytes. Hepatology 2002; **35**(4): 779–789.

[35] Rodrigues CM, Fan G, Ma X, Kren BT, Steer CJ. A novel role for ursodeoxycholic acid in inhibiting apoptosis by modulating mitochondrial membrane perturbation. J Clin Invest. 1998; **101**(12): 2790–2799.

[36] Benz C, Angermüller S, Otto G, Sauer P, Stremmel W, Stiehl A. Effect of tauroursodeoxycholic acid on bile acid induced apoptosis in primary human hepatocytes. Eur J Clin Invest. 2000; **30**(3): 203–209.

[37] Gamboa A, Tian C, Massaad J, Reshamwala P, Cai Q. The Therapeutic Role of Ursodeoxycholic Acid in Digestive Diseases. Annals of Gastroenterology & Hepatology. 2011; **2**(1): 43–49.

[38] Paumgartner G, Beuers U. Ursodeoxycholic Acid in Cholestatic Liver Disease. Hepatology. 2002; **36**(3): 525–531.

[39] Lazaridis KN, Gores GJ, Lindor KD. Ursodeoxycholic acid mechanisms of action and clinical use in hepatobiliary disorders'. Journal of Hepatology. 2001; **35**:134–146.

[40] Fickert P, Zollner G, Fuchsbichler A, Stumptner C, Pojer C, Zenz R, Lammert F, Stieger B, Meier PJ, Zatloukal K, Denk H, Trauner M. Effects of ursodeoxycholic and cholic acid feeding on hepatocellular transporter expression in mouse liver. Gastroenterology. 2001; **121**(1): 170–183.

[41] Zollner G, Fickert P, Fuchsbichler A, Silbert D, Wagner M, Arbeiter S, Gonzalez FJ, Marschall HU, Zatloukal K, Denk H, Trauner M. Role of nuclear bile acid receptor, FXR, in adaptive ABC transporter regulation by cholic and ursodeoxycholic acid in mouse liver, kidney and intestine. J Hepatol. 2003; **39**(4): 480–488.

[42] Zollner G, Wagner M, Moustafa T, Fickert P, Silbert D, Gumhold J, Fuchsbichler A, Halilbasic E, Denk H, Marschall HU, Trauner M. Coordinated induction of bile acid detoxification and alternative elimination in mice: role of FXR-regulated organic solute transporter-alpha/beta in the adaptive response to bile acids. Am J Physiol Gastrointest Liver Physiol. 2006; **290**(5): G923–G932.

[43] Fischler B, Bodin K, Stjernman H, et al. Cholestatic liver disease in adults may be due to an inherited defect in bile acid biosynthesis. J Intern Med. 2007; **262**(2): 254–262.

[44] Lipsett PA, Medicine JH, Pitt HA. Front Biosci. Acute cholangitis. 2003; **8**: 1229–1239.

[45] Hoffman C. Verschluss der gallenwege durch verdickung der wandungen. Arch Pathol Anat Physiol. 1867; **39**: 206–215.

[46] Gidwaney NG, Pawa S, Das KM. Pathogenesis and clinical spectrum of primary sclerosing cholangitis. World J Gastroenterol. 2017; **23**(14): 2459–2469.

[47] Hirschfield GM, Dyson JK, Alexander GJM, et al. The British Society of Gastroenterology/UK-PBC primary biliary cholangitis treatment and management guidelines. Hirschfield GM, et al. Gut 2018; **67**:1568–1594.

[48] Transplant Liver in India. 2021. Primary Biliary Cholangitis - Transplant Liver in India. [online] Available at: <http://www.transplantliverinindia.com/primary-biliary-cholangitis/> [Accessed 16 December 2021].

[49A] Zein CO, Lindor KD. Latest and emerging therapies for primary biliary cirrhosis and primary sclerosing cholangitis. Curr Gastroenterol Rep. 2010; **12**(1): 13–22.

[49B] Kaplan MM, Gershwin ME. Primary biliary cirrhosis. N Engl J Med. 2005; **353**(12): 1261–1273.

[50] Gulamhusein AF. Cholangitis for the Gastroenterologist. Gastroenterology & Hepatology. 2019; **15**(3): 145–154.

[51] Beuers U. Drug insight: Mechanisms and sites of action of ursodeoxycholic acid in cholestasis. Nat Clin Pract Gastroenterol Hepatol. 2006; **3**(6): 318–328.

[52] Poupon R. Ursodeoxycholic acid and bile-acid mimetics as therapeutic agents for cholestatic liver diseases: an overview of their mechanisms of action. Clin Res Hepatol Gastroenterol. 2012; **36**(Suppl 1): S3–12.

[53] Buryova H, Chalupsky K, Zbodakova O, Kanchev I, Jirouskova M, Gregor M, Sedlacek R. Liver protective effect of ursodeoxycholic acid includes regulation of ADAM17 activity. BMC Gastroenterol. 2013; **13**: 155.

[54] Di Ciaula A, Wang DQ, Molina-Molina E, Lunardi Baccetto R, Calamita G4, Palmieri VO, Portincasa P. Bile Acids and Cancer: Direct and Environmental-Dependent Effects. Ann Hepatol. 2017;**16**(s1): 87–105.

[55] Bernstein H, Bernstein C, Payne CM, Dvorakova K, Garewal H. Bile acids as carcinogens in human gastrointestinal cancers. Mutat Res. 2005; **589**: 47–65.

[56] Jazrawi RP, de Caestecker JS, Goggin PM, Britten AJ, Joseph AE, Maxwell JD, Northfield TC. Kinetics of hepatic bile acid handling in cholestatic liver disease: effect of ursodeoxycholic acid. Gastroenterology. 1994; **106**(1): 134–142.

[57] Corpechot C, Carrat F, Bonnand A, Poupon RE, Poupon R. The effect of ursodeoxycholic acid therapy on liver fibrosis progression in primary biliary cirrhosis. Hepatology. 2000; **32**(6): 1196–1199.

[58] Nishigaki Y, Ohnishi H, Moriwaki H, Muto Y. Ursodeoxycholic acid corrects defective natural killer activity by inhibiting prostaglandin E2 production in primary biliary cirrhosis. Dig Dis Sci. 1996; **41**(7): 1487–1493.

[59] Verma A, Jazrawi RP, Ahmed HA, Davis T, Bland JM, Benson M, Orchard RT, Theodossi A, Maxwell JD, Northfield TC. Optimum dose of ursodeoxycholic acid in primary biliary cirrhosis. Eur J Gastroenterol Hepatol. 1999; **11**(10): 1069–1076.

[60] Lindor KD, Therneau TM, Jorgensen RA, Malinchoc M, Dickson ER.

Effects of ursodeoxycholic acid on survival in patients with primary biliary cirrhosis. Gastroenterology. 1996; **110**(5): 1515–1518.

[61] Parsa N. Environmental Factors Inducing Human Cancers. Iranian J Publ Health. 2012; **41**(11): 1–9.

[62] Hanahan D, Weinberg RA. The Hallmarks of Cancer. Cell. 2000; **100**(1): 57–70.

[63] Watabe J, Bernstein H. The mutagenicity of bile acids using a fluctuation test. Mutat Res. 1985; **158**(1-2): 45–51.

[64] Lee WS, Jung JH, Panchanathan R, Yun JW, Kim DH, Kim HJ, Kim GS, et al. Ursodeoxycholic Acid Induces Death Receptor-mediated Apoptosis in Prostate Cancer Cells. J Cancer Prev. 2017; **22**(1): 16–21.

[65] Amaral JD, Viana RJ, Ramalho RM, Steer CJ, Rodrigues CM. Bile acids: regulation of apoptosis by ursodeoxycholic acid. J Lipid Res. 2009; **50**(9): 1721–1734.

[66] Incidence I, Collaborators P. Global, regional, and national incidence, prevalence, and years lived with disability for 310 diseases and injuries, 1990 -2015: a systematic analysis for the Global Burden of Disease Study 2015. Lancet. 2016; **388**: 1545–1602.

[67] Jenkins DJ, Wolever TM, Rao AV, Hegele RA, Mitchell SJ, Ransom TP, Boctor DL, Spadafora PJ, Jenkins AL, Mehling C. Effect on blood lipids of very high intakes of fiber in diets low in saturated fat and cholesterol. N Engl J Med. 1993; **329**(1): 21–26.

[68] Khandekar MJ, Cohen P, Spiegelman BM. Molecular mechanisms of cancer development in obesity. Nat Rev Cancer. 2011; **11**(12): 886–895.

[69] Crowley-Weber CL, Payne CM, Gleason-Guzman M, Watts GS, Futscher B, Waltmire CN, Crowley C, Dvorakova K, Bernstein C, Craven M, Garewal H, Bernstein H. Development and molecular characterization of HCT-116 cell lines resistant to the tumor promoter and multiple stress-inducer, deoxycholate. Carcinogenesis. 2002; **23**(12): 2063–2080.

[70] Chan AT, Giovannucci EL. Primary prevention of colorectal cancer.

Gastroenterology. 2010; **138**(6): 2029–2043.

[71] Platz EA, Willett WC, Colditz GA, Rimm EB, Spiegelman D, Giovannucci E. Proportion of colon cancer risk that might be preventable in a cohort of middle-aged US men. Cancer Causes Control. 2000; **11**(7): 579–588.

[72] Payne CM, Bernstein C, Dvorak K, Bernstein H. Hydrophobic bile acids, genomic instability, Darwinian selection, and colon carcinogenesis. Clin Exp Gastroenterol. 2008; **1**: 19–47.

[73] Im E, Martinez JD. Ursodeoxycholic acid(UDCA) can inhibit deoxycholic acid (DCA)-induced apoptosis via modulation of EGFR/Raf-1/ERK signaling in human colon cancer cells. J. Nutr. 2004; **134**(2): 483–486.

[74] Earnest DL, Holubec H, Wali RK, Jolley CS, Bissonette M, Bhattacharyya AK, Roy H, Khare S, Brasitus TA. Chemoprevention of azoxymethane-induced colonic carcinogenesis by supplemental dietary ursodeoxycholic acid. Cancer Res. 1994; **54**(19): 5071–5074.

[75] Kohno H, Suzuki R, Yasui Y, Miyamoto S, Wakabayashi K, Tanaka T. Ursodeoxycholic acid versus sulfasalazine in colitisrelated colon carcinogenesis in mice. Clin Cancer Res. 2007; **13**(8): 2519–2525.

[76] Kim EK, Cho JH, Kim E, Kim YJ. Ursodeoxycholic acid inhibits the proliferation of colon cancer cells by regulating oxidative stress and cancer stem-like cell growth. PLoS One. 2017; **12**(7): e0181183.

[77] González PM, Lagos CF, Ward WC, Polli JE. Structural requirements of the human sodium-dependent bile acid transporter (hASBT): Role of 3- and 7-OH moieties on binding and translocation of bile acids. Mol Pharm. 2014; **11**(2): 588–598.

[78] Hofmann AF, Hagey LR. Key discoveries in bile acid chemistry and biology and their clinical applications: history of the last eight decades. J Lipid Res. 2014; **55**(8): 1553–1595.

[79] Devlin AS, Fischbach MA, Sciences T, Biosciences Q, Francisco S, Francisco S. A biosynthetic pathway for a prominent class of microbiota-derived bile acids. 2016; **11**(9): 685–690.

[80] Duane WC, Javitt NB. 27-hydroxycholesterol: production rates in normal human subjects. J Lipid Res. 1999; **40**(7): 1194–1199.

[81] Gupta S, Stravitz RT, Dent P, Hylemon PB. Down-regulation of Cholesterol 7α-Hydroxylase (CYP7A1) Gene Expression by Bile Acids in Primary Rat Hepatocytes is Mediated by the c-Jun N-terminal Kinase Pathway. J Biol Chem. 2001; **276**(19): 15816–15822.

[82] Ren S, Hylemon PB, Marques D, Gurley E, Bodhan P, Hall E, Redford K, Gil G, Pandak WM. Overexpression of cholesterol transporter StAR increases *in vivo* rates of bile acid synthesis in the rat and mouse. Hepatology. 2004; **40**(4): 910–917.

[83] Li T and Chiang, JY. Bile acid signaling in metabolic disease and drug therapy. Pharmacol. Pharmacol Rev. 2014; **66**(4): 948–983.

[84] Axelson M, Sjövall J. Potential bile acid precursors in plasma--possible indicators of biosynthetic pathways to cholic and chenodeoxycholic acids in man. J Steroid Biochem. 1990; **36**(6): 631–640.

[85] Fiorucci S, Biagioli M, Zampella A, Distrutti E. Bile acids activated receptors regulate innate immunity. Front Immunol. 2018; **9**: 1–17.

[86] Hofmann AF, Hagey LR, Krasowski MD. Bile salts of vertebrates: structural variation and possible evolutionary significance. J Lipid Res. 2010; **51**(2): 226–246.

[86] John Y. L Chiang. Bile Acid Metabolism and Signaling. Compr Physiol. 2015; **3**(3): 1191–1212.

[88] Susan A Joyce, Fergus Shanahan, Colin Hill, and Cormac GM Gahan. Bacterial bile salt hydrolase in host metabolism: Potential for influencing gastrointestinal microbe-host crosstalk. Gut Microbes. 2014; **5**(5): 669–674.

[89] Ridlon JM, Harris SC, Bhowmik S, Kang DJ, Hylemon PB. Consequences of bile salt biotransformations by intestinal bacteria. Gut Microbes. 2016; **7**(1): 22–39.

[90] Batta AK, Salen G, Arora R, Shefer S, Batta M, Person A. Side chain conjugation prevents bacterial 7-dehydroxylation of bile acids. J Biol Chem.

1990; **265**(19): 10925–10928.

[91] Hofmann AF. Detoxification of lithocholic acid, a toxic bile acid: relevance to drug hepatotoxicity. Drug Metab Rev. 2004; **36**(3-4): 703–722.

[92] John Y. L. Chiang. Bile acids: regulation of synthesis. Journal of Lipid Research. 2009; **50**: 1955–1966.

[93] Sayin SI, Marschall H, Ba F. Review Intestinal Crosstalk between Bile Acids and Microbiota and Its Impact on Host Metabolism. Cell Metab. 2016; **24**(1): 41–50.

[94] Hirano S, Masuda N, Oda H, Mukai H. Transformation of bile acids by Clostridium perfringens. Appl Environ Microbiol. 1981; **42**(3): 394–399.

[95] Mythen SM, Devendran S, Méndez-García C, Cann I, Ridlon JM. Targeted Synthesis and Characterization of a Gene Cluster Encoding NAD(P)H-Dependent 3α-, 3β-, and 12α-Hydroxysteroid Dehydrogenases from Eggerthella CAG:298, a Gut Metagenomic Sequence. *Appl Environ Microbiol*. 2018; **84**(7): e02475–17.

[96] Hofmann AF, Roda A. Physicochemical properties of bile acids and their relationship to biological properties: an overview of the problem. J Lipid Res. 1984; **25**(13): 1477–1489.

[97] Batta AK, Salen G, Shefer S. Transformation of bile acids into iso-bile acids by Clostridium perfringens: possible transport of 3 beta-hydrogen via the coenzyme. Hepatology. 1985;**5**(6):1126–1131.

[98] Torchia EC, Cheema SK, Agellon LB. Coordinate regulation of bile acid biosynthetic and recovery pathways. Biochem Biophys Res Commun. 1996; **225**(1): 128–133.

[99] Redniger RN. The coming of age of our understanding of enterohepatic circulation of bile salts. American Journal of Surgery. 2003; **185**(2):168–172.

[100] Prabha V, Ohri M. Review: Bacterial transformations of bile acids. World J Microbiol Biotechnol. 2006; **22**(2): 191–196.

[101] Reddy BS, Narasawa T, Weisburger JH, Wynder EL. Promoting effect of sodium deoxycholate on colon adenocarcinomas in germfree rats. J. Natl.

Cancer Inst. 1976; **56**: 441–442.

[102] Bayerdorffer E, Mannes GA, Ochsenkuhn T, Dirschedl P, Wiebecke B, Paumgartner G. Unconjugated secondary bile acids in the serum of patients with colorectal adenomas. Gut. 1995; **36**(2): 268–273.

[103] Shefer S, Salen G, Hauser S, et al. Metabolism of iso-bile acids in the rat. J Biol Chem. 1982; **257**(3):1401–1406.

[104] Sayin SI, Marschall H, Ba F. Review Intestinal Crosstalk between Bile Acids and Microbiota and Its Impact on Host Metabolism. Cell Metab. 2016; **24**(1): 41–50.

[105] Makishima , M., T. T. Lu, W. Xie, G. K. Whitfield, H. Domoto, R. M. Evans, M. R. Haussler, and D. J. Mangelsdorf. Vitamin D receptor as an intestinal bile acid sensor. Science. 2002; **296**(5571): 1313–1316.

[106] Staudinger, J. L., B. Goodwin, S. A. Jones, D. Hawkins-Brown, K. I. MacKenzie, A. LaTour, Y. Liu, C. D. Klaassen, K. K. Brown, J. Reinhard, et al. The nuclear receptor PXR is a lithocholic acid sensor that protects against liver toxicity. Proc Natl Acad Sci USA. 2001; **98**(6): 3369–3374.

[107] John Y. L Chiang. Bile Acid Biology, Pathophysiology, and Therapeutics. Clinical liver diseases. 2020; **15**(3): 91–94.

[108] Qi Y, Jiang C, Cheng J, Krausz KW, Li T. Bile acid signaling in lipid metabolism: Metabolomic and lipidomic analysis of lipid and bile acid markers linked to anti-obesity and anti-diabetes in mice. Biochimica et Biophysica Acta. 2015; **1851**(1): 19–29.

[109] Baptissart M, Martinot E, Beaudoin C, Lobaccaro J, Volle DH. Molecular Aspects of Medicine. 2017; **56**: 2–9.

[110] Fiorucci S, Distrutti E. Bile Acid-Activated Receptors, Intestinal Microbiota, and the Treatment of Metabolic Disorders. Trends Mol Med. 2015; **21**(11): 702–714.

[111] Chiang JYL, Ferrell JM. Bile acid receptors FXR and TGR5 signaling in fatty liver diseases and therapy. Am J Physiol Gastrointest Liver Physiol. 2020; **318**(3): G554–G573.

[112] Sahin M, Kayadibi H. Importance of the bile acid receptors in different metabolisms. Integr Obesity Diabetes. 2017; **3**(6): 1–5.

[113] Forman BM, Goode E, Chen J, et al. Identification of a Nuclear Receptor That Is Activated by Farnesol Metabolites. Cell. 1995; **81**: 687–693.

[114] Buhaescu I, Izzedine H. Mevalonate pathway: A review of clinical and therapeutical implications. Clinical Biochemistry. 2007; **40**: 575–584.

[115] Forman BM, Goode E, Chen J, et al. Identification of a nuclear receptor that is activated by farnesol metabolites. Cell. 1995; **81**(5): 687–693.

[116] Wang Y, Chen W, Moore DD, Huang W. FXR: a metabolic regulator and cell protector. Cell Res. 2008: **18**(11): 1087–1095.

[117] Watanabe M, Houten SM, Wang L, et al. Bile acids lower triglyceride levels via a pathway involving FXR, SHP, and SREBP-1c. The Journal of clinical investigation. 2004; **113**(10): 1408–1418.

[118] Kullak-ublick GA. The Role of FXR in Disorders of Bile Acid Homeostasis. Physiology. 2008; **23**(5): 286–295.

[119] Denson LA, Sturm E, Echevarria W, Zimmerman TL, Makishima M, Mangelsdorf DJ, Karpen SJ. The orphan nuclear receptor, shp, mediates bile acid-induced inhibition of the rat bile acid transporter, ntcp. Gastroenterology. 2001; **121**(1):140–147.

[120] Meier, P. J., Stieger, B. Bile salt transporters. Annu. Rev. Physiol. Annu Rev Physiol. 2002; **64**: 635–661.

[121] Trauner, M., Boyer, JL. Bile salt transporters: molecular characterization, function, and regulation. Physiol Rev. 2003; **83**(2): 633–671.

[122] Tu H, Okamoto AY, Shan B. FXR, a Bile Acid Receptor and Biological Sensor. Trends Cardiovasc Med. 2000; **10**: 30–35.

[123] Ballatori N, Christian WV, Lee JY, Dawson PA, Soroka CJ, Boyer JL, Madejczyk MS, Li N. OSTalpha-OSTbeta: A major basolateral bile acid and steroid transporter in human intestinal, renal, and biliary epithelia. Hepatology. 2005; **42**(6):1270–1279.

[124] Frankenberg T, Rao A, Chen F, Haywood J, Shneider BL, Dawson PA.

Regulation of the mouse organic solute transporter alpha-beta, Ostalpha-Ostbeta, by bile acids. Am J Physiol Gastrointest Liver Physiol. 2006; **290**(5): G912–922.

[125] Ballatori N, Fang F, Christian WV, Li N, Hammond CL. Ostalpha-Ostbeta is required for bile acid and conjugated steroid disposition in the intestine, kidney, and liver. Am J Physiol Gastrointest Liver Physiol. 2008; **295**(1): G179–186.

[126] Fiorucci S, Mencarelli A, Palladino G, Cipriani S. Bile-acid-activated receptors: targeting TGR5 and farnesoid-X-receptor in lipid and glucose disorders. Trends Pharmacol Sci. 2009; **30**(11): 570–580.

[127] Fiorucci S, Cipriani S, Baldelli F, Mencarelli A. Bile acid-activated receptors in the treatment of dyslipidemia and related disorders. Prog Lipid Res. 2010; **49**(2): 171–185.

[128] Calkin AC, Tontonoz P. Transcriptional integration of metabolism by the nuclear sterol-activated receptors LXR and FXR. Nat Rev Mol Cell Biol. 2012; **13**(4): 213–224.

[129] Lefebvre P, Cariou B, Lien F, Kuipers F, Staels B. Role of bile acids and bile acid receptors in metabolic regulation. Physiol Rev. 2009; **89**(1): 147–191.

[130] Zhang Y, Edwards PA. FXR signaling in metabolic disease. FEBS Lett. 2008; **582**(1):10–18.

[131] Sinal CJ, Tohkin M, Miyata M, Ward JM, Lambert G, Gonzalez FJ. Targeted disruption of the nuclear receptor FXR/BAR impairs bile acid and lipid homeostasis. Cell. 2000; **102**(6): 731–744.

[132] Wang YD, Chen WD, Wang M, Yu D, Forman BM, Huang W. Farnesoid X receptor antagonizes nuclear factor kappaB in hepatic inflammatory response. Hepatology. 2008; **48**(5): 1632–1643.

[133] Zhang S, Wang J, Liu Q, Harnish DC. Farnesoid X receptor agonist WAY-362450 attenuates liver inflammation and fibrosis in murine model of non-alcoholic steatohepatitis. J Hepatol. 2009; **51**(2): 380–388.

[134] Interceptpharma, Building a Specialty Focused Business in Chronic Liver

and Intestinal Diseases with High Unmet Medical Need. 2014; 1–25.

[135] Modica S, Murzilli S, Salvatore L, Schmidt DR, Moschetta A. Nuclear Bile Acid Receptor FXR Protects against Intestinal Tumorigenesis. Cancer Res. 2008; **23**: 9589–9595.

[136] Maria R, Garcia-irigoyen O, Moschetta A. Molecular Aspects of Medicine Bile acids and colon cancer: Is FXR the solution of the conundrum? Mol Aspects Med. 2017; **56**: 66–74.

[137] McGarr SE, Ridlon JM, Hylemon PB. Diet, anaerobic bacterial metabolism, and colon cancer: a review of the literature. J Clin Gastroenterol. 2005; **39**(2):98–109.

[138] Bajor A, Gillberg PG, Abrahamsson H. Bile acids: short and long term effects in the intestine. Scand J Gastroenterol. 2010; **45**(6): 645–664.

[139] Ajouz H, Mukherji D, Shamseddine A. Secondary bile acids: an underrecognized cause of colon cancer. World J Surg Oncol. 2014; **12**(1): 1–5.

[140] Ding L, Yang L, Wang Z, Huang W. Bile acid nuclear receptor FXR and digestive system diseases. Acta Pharm Sin B. 2015; **5**(2):135–144.

[141] Huang W, Ma K, Zhang J, et al. Nuclear receptor-dependent bile acid signaling is required for normal liver regeneration. Science. 2006; **312**(5771): 233–236.

[142] Zhang L, Wang YD, Chen WD, et al. Promotion of liver regeneration/repair by farnesoid X receptor in both liver and intestine in mice. Hepatology. 2012; **56**(6): 2336–2343.

[143] Chen WD, Wang YD, Meng Z, Zhang L, Huang W. Nuclear bile acid receptor FXR in the hepatic regeneration. Biochim Biophys Acta. 2011; **1812**(8): 888–892.

[144] Zhang LS, Huang XF, Meng ZP, Dong BN, Shiah S, et al. Significance and mechanism of CYP7A1 gene regulation during the acute phase of liver regeneration. Mol Endocrinol. 2009; **23**(2): 137–45.

[145] Meng Z, Wang Y, Wang L, et al. FXR regulates liver repair after CCl4-induced toxic injury. Mol Endocrinol. 2010; **24**(5):886–897.

[146] Meng Z, Liu N, Fu X, Wang X, Wang YD, et al. Insufficient bile acid signaling impairs liver repair in CYP27(-/-) mice. J Hepatol. 2011; **55**(4): 885–895.

[147] Huang W, Ma K, Zhang J, et al. Nuclear receptor-dependent bile acid signaling is required for normal liver regeneration. Science. 2006; **312**(5771): 233–236.

[148] Deuschle U, Schuler J, Schulz A, Schluter T, Kinzel O, et al. FXR controls the tumor suppressor NDRG2 and FXR agonists reduce liver tumor growth and metastasis in an orthotopic mouse xenograft model. PLoS One. 2012; **7**(10): e43044.

[149] Su H, Ma C, Liu J, Li N, Gao M, et al. Downregulation of nuclear receptor FXR is associated with multiple malignant clinicopathological characteristics in human hepatocellular carcinoma. Am J Physiol Gastrointest Liver Physiol. 2012; **303**(11): G1245–1253.

[150] Wang X, Fu X, Van Ness C, Meng Z, Ma X, Huang W. Bile Acid Receptors and Liver Cancer. Curr Pathobiol Rep. 2013; **1**(1): 29–35.

[151] Lax S, Schauer G, Prein K, Kapitan M, Silbert D, Berghold A, Berger A, et al. Expression of the nuclear bile acid receptor/farnesoid X receptor is reduced in human colon carcinoma compared to nonneoplastic mucosa independent from site and may be associated with adverse prognosis. Int J Cancer. 2012; **130**(10): 2232–2239.

[152] Modica S, Murzilli S, Salvatore L, Schmidt DR, Moschetta A. Nuclear bile acid receptor FXR protects against intestinal tumorigenesis. Cancer Res. 2008; **68**(23): 9589–9594.

[153] Edwards PA, Kast HR, Anisfeld AM. BAREing it all: the adoption of LXR and FXR and their roles in lipid homeostasis. J Lipid Res. 2002; **43**(1): 2–12.

[154] Stanimirov B, Stankov K, Mikov M. Pleiotropic functions of bile acids mediated by the farnesoid X receptor. Acta Gastroenterol Belg. 2012; **75**(4): 389–398.

[155] Cai SY, Xiong L, Wray CG, Ballatori N, Boyer JL. The farnesoid X

receptor FXRalpha/NR1H4 acquired ligand specificity for bile salts late in vertebrate evolution. Am J Physiol Regul Integr Comp Physiol. 2007; **293**(3): R1400–1409.

[156] Fiorucci S, Rizzo G, Donini A, Distrutti E, Santucci L. Targeting farnesoid X receptor for liver and metabolic disorders. Trends Mol Med. 2007; **13**(7), 298–309.

[157] Song X, Chen Y, Valanejad L, et al. Mechanistic insights into isoform-dependent and species-specifi c regulation of bile salt export pump by farnesoid X receptor. J Lipid Res. 2013; **54**(11): 3030–3044.

[158] Goodwin B, Jones SA, Price RR, Watson MA, McKee DD, Moore LB, Galardi C, Wilson JG, Lewis MC, Roth ME, Maloney PR, Willson TM, Kliewer SA. A regulatory cascade of the nuclear receptors FXR, SHP-1, and LRH-1 represses bile acid biosynthesis. Mol Cell. 2000; **6**(3):517–526.

[159] Lu TT, Makishima M, Repa JJ, Schoonjans K, Kerr TA, Auwerx J, Mangelsdorf DJ. Molecular basis for feedback regulation of bile acid synthesis by nuclear receptors. Mol Cell. 2000; **6**(3): 507–515.

[160] Wang H, Chen J, Hollister K, Sowers LC, Forman BM. Endogenous bile acids are ligands for the nuclear receptor FXR/BAR. Mol Cell. 1999; **3**(5): 543–553.

[161] Zhang M, Chiang JY. Transcriptional regulation of the human sterol 12α-hydroxylase gene (CYP8B1): Roles of hepatocyte nuclear factor 4α (HNF4α) in mediating bile acid repression. J Biol Chem. 2001; **276**(45): 41690–41699.

[162] Song KH, Chiang JY. Chiang. Glucagon and cAMP inhibit cholesterol 7alpha-hydroxylase (CYP7A1) gene expression in human hepatocytes: discordant regulation of bile acid synthesis and gluconeogenesis. Hepatology. 2006; **43**(1): 117–125.

[163] Inoue Y, Yu AM, Inoue J, Gonzalez FJ. Hepatocyte nuclear factor 4alpha is a central regulator of bile acid conjugation. J Biol Chem. 2004; **279**(4): 2480–2489.

[164] Inoue Y, Yu AM, Yim SH, et al. Regulation of bile acid biosynthesis by hepatocyte nuclear factor 4alpha. J Lipid Res. 2006; **47**(1): 215–227.

[165] Hayhurst GP, Lee YH, Lambert G, Ward JM, Gonzalez FJ. Hepatocyte nuclear factor 4alpha (nuclear receptor 2A1) is essential for maintenance of hepatic gene expression and lipid homeostasis. Mol Cell Biol. 2001; **21**(4): 1393–1403.

[166] Shih DQ, Bussen M, Sehayek E, et al. Hepatocyte nuclear factor-1alpha is an essential regulator of bile acid and plasma cholesterol metabolism. Nat Genet. 2001; **27**(4): 375–382.

[167] Thomas C, Pellicciari R, Pruzanski M, Auwerx J, Schoonjans K. Targeting bile-acid signalling for metabolic diseases. Nat Rev Drug Discov. 2008; **7**(8): 678–693.

[168] Wang L, Lee YK, Bundman D, et al. Redundant pathways for negative feedback regulation of bile acid production. Dev Cell. 2002; **2**(6): 721–731.

[169] Sinal CJ, Tohkin M, Miyata M, Ward JM, Lambert G, Gonzalez FJ. Targeted disruption of the nuclear receptor FXR/BAR impairs bile acid and lipid homeostasis. Cell. 2000; **102**(6):731–744.

[170] Kim I, Morimura K, Shah Y, Yang Q, Ward JM, Gonzalez FJ. Spontaneous hepatocarcinogenesis in farnesoid X receptor-null mice. Carcinogenesis. 2007; **28**(5): 940–946.

[171] Zhu Y, Li F, Guo GL. Tissue-specific function of farnesoid X receptor in liver and intestine. Pharmacol Res. 2011; **63**(4): 259–265.

[172] Lefebvre P, Cariou B, Lien F, Kuipers F, Staels B. Role of Bile Acids and Bile Acid Receptors in Metabolic Regulation. Physiol. Rev. 2009; **89**: 147–191.

[173] Gupta, S., Stravitz, R. T., Dent, P., Hylemon, P. B. Down-regulation of cholesterol 7α-hydroxylase (CYP7A1) gene expression by bile acids in primary rat hepatocytes is mediated by the c-Jun N-terminal kinase pathway. J Biol Chem. 2001; **276**(19): 15816–15822.

[174] Holt JA, Luo G, Billin AN, Bisi J, McNeill YY, Kozarsky KF, Donahee M, Wang DY, Mansfield TA, Kliewer SA, Goodwin B, Jones SA. Definition of a

novel growth factor-dependent signal cascade for the suppression of bile acid biosynthesis. Genes Dev. 2003; **17**(13): 1581–1591.

[175] Gupta S, Natarajan R, Payne SG, Studer EJ, Spiegel S, Dent P, Hylemon PB. Deoxycholic Acid Activates the C-Jun N-Terminal Kinase Pathway Via FAS Receptor Activation in Primary Hepatocytes. Role of Acidic Sphingomyelinase-Mediated Ceramide Generation in FAS Receptor Activation. J Biol Chem. 2004; **279**(7): 5821–5828.

[176] Graf D, Kurz AK, Reinehr R, Fischer R, Kircheis G, Haussinger D. Prevention of Bile Acid-Induced Apoptosis by Betaine in Rat Liver. Hepatology. 2002; **36**(4 Pt 1): 829–839.

[177] Park EJ, Zhao YZ, Kim YC, Sohn DH. PF2401-SF, Standardized Fraction of Salvia Miltiorrhiza and Its Constituents, Tanshinone I, Tanshinone IIA, and Cryptotanshinone, Protect Primary Cultured Rat Hepatocytes From Bile Acid-Induced Apoptosis by Inhibiting JNK Phosphorylation. Food Chem Toxicol. 2007; **45**(10): 1891–1898.

[178] Qiao L, Han SI, Fang Y, Park JS, Gupta S, Gilfor D, Amorino G, Valerie K, Sealy L, Engelhardt JF, Grant S, Hylemon PB, Dent P. Bile Acid Regulation of C/EBPbeta, CREB, and C-Jun Function, Via the Extracellular Signal-Regulated Kinase and C-Jun NH2-Terminal Kinase Pathways, Modulates the Apoptotic Response of Hepatocytes. Mol Cell Biol. 2003; **23**(9): 3052–3066.

[179] Hohenester S, Gates A, Wimmer R, Beuers U, Anwer MS, Rust C, Webster CR. Phosphatidylinositol-3-Kinase P110γ Contributes to Bile Salt-Induced Apoptosis in Primary Rat Hepatocytes and Human Hepatoma Cells. J Hepatol. 2010; **53**(5): 918–926.

[180] Potthoff MJ, Boney-Montoya J, Choi M, He T, Sunny NE, Satapati S, et al. FGF15/19 regulates hepatic glucose metabolism by inhibiting the CREB-PGC-1α pathway. Cell Metab. 2011; **13**(6): 729–738.

[181] Bhatnagar S, Damron HA, Hillgartner FB. Fibroblast growth factor-19, a novel factor that inhibits hepatic fatty acid synthesis. J Biol Chem. 2009;

284(15): 10023–10033.

[182] Kir S, Beddow SA, Samuel VT, Miller P, Previs SF, Suino-Powell K, et al. FGF19 as a postprandial, insulin-independent activator of hepatic protein and glycogen synthesis. Science. 2011; **331**(6024): 1621–1624.

[183] Shapiro H, Kolodziejczyk AA, Halstuch D, Elinav E. Bile acids in glucose metabolism in health and disease. J. Exp. Med. 2018; **215**(2): 383–396.

[184] Qiao L, Yacoub A, Studer E, Gupta S, Pei XY, Grant S, Hylemon PB, Dent P. Inhibition of the MAPK and PI3K Pathways Enhances UDCA-Induced Apoptosis in Primary Rodent Hepatocytes. Hepatology. 2002; **35**(4): 779–789.

[185] Schliess F, Kurz AK, vom Dahl S, Haussinger D. Mitogen-Activated Protein Kinase Mediate the Stimulation of Bile Acid Secretion by Tauroursodeoxycholate in Rat Liver. Gastroenterology. 1997; **113**(4):1306–1313.

[186] Twisk J, Hoekman MF, Lehmann EM, Meijer P, Mager WH, Princen HM. Insulin suppresses bile acid synthesis in cultured rat hepatocytes by down-regulation of cholesterol 7 alpha-hydroxylase and sterol 27-hydroxylase gene transcription. Hepatology 1995; **21**(2): 501–510.

[187] Song Y, Xu C, Shao S, Liu J, Xing W, Xu J, Qin C, Li C, Hu B, Yi S, Xia X, Zhang H, Zhang X, Wang T, Pan W, Yu C, Wang Q, Lin X, Wang L, Gao L, Zhao J. Thyroid-stimulating hormone regulates hepatic bile acid homeostasis via SREBP-2/HNF-4α/CYP7A1 axis. J Hepatol. 2015; **62**(5): 1171–1179.

[188] Baker DM, Wang SL, Bell DJ, Drevon CA, Davis RA. One or more labile proteins regulate the stability of chimeric mRNAs containing the 3’-untranslated region of cholesterol -7alpha -hydroxylase mRNA. J Biol Chem. 2000; **275**(26): 19985–19991.

[189] Agellon LB, Cheema SK. The 3’-untranslated region of the mouse cholesterol 7α-hydroxylase mRNA contains elements responsive to post-transcriptional regulation by bile acids. Biochem J. 1997; **328**(Pt 2): 393–399.

[190] Russell DW. The enzymes, regulation, and genetics of bile acid synthesis.

Annu Rev Biochem. 2003; **72**: 137–174.

[191] Zheng W, Lu Y, Tian S, et al. Structural insights into the heterodimeric complex of the nuclear receptors FXR and RXR. J Biol Chem. 2018; **293**(32): 12535–12541.

[192] Carotti A. Beyond Bile Acids: Targeting Farnesoid X Receptor (FXR) with Natural and Synthetic Ligands. Curr Top Med Chem. 2014; **14**(19): 2129–2142.

[193] Ding L, Yang L, Wang Z, Huang W. Bile acid nuclear receptor FXR and digestive system diseases. Acta Pharm Sin B. 2015; **5**(2):135–144.

[194] Merk D. Medicinal chemistry of farnesoid X receptor ligands: from agonists and antagonists to modulators. Future Med Chem. 2012; **4**(8): 1015–1036.

[195] Wang H, Chen J, Hollister K, Sowers LC, Forman BM. Endogenous bile acids are ligands for the nuclear receptor FXR/BAR. Mol Cell. 1999; **3**(5): 543–553.

[196] Liu J, Lu H, Lu YF, et al. Potency of individual bile acids to regulate bile acid synthesis and transport genes in primary human hepatocyte cultures. Toxicol Sci. 2014; **141**(2): 538–546.

[197] Parks DJ, Blanchard SG, Bledsoe RK, et al. Bile acids: natural ligands for an orphan nuclear receptor. Science. 1999; **284**(5418): 1365–1368.

[198] Makishima M, Okamoto AY, Repa JJ, et al. Identification of a nuclear receptor for bile acids. Science. 1999; **284**(5418); 1362–1365.

[199] Pellicciari R, Fiorucci S, Camaioni E, et al. 6alpha-ethyl-chenodeoxycholic acid (6-ECDCA), a potent and selective FXR agonist endowed with anticholestatic activity. J Med Chem. 2002; **45**(17): 3569–3572.

[200] Pellicciari R, Costantino G, Camaioni E, Sadeghpour BM, Entrena A, Willson TM, Fiorucci S, Clerici C, Gioiello A. Bile acid derivatives as ligands of the farnesoid X receptor. Synthesis, evaluation, and structure-activity relationship of a series of body and side chain modified analogues of

chenodeoxycholic acid. J Med Chem. 2004; **47**(18): 4559–4569.

[201] Carotti A. Beyond Bile Acids: Targeting Farnesoid X Receptor (FXR) with Natural and Synthetic Ligands. Curr Top Med Chem. 2014; **14**(19): 2129–2142.

[202] Merk D. Medicinal chemistry of farnesoid X receptor ligands: from agonists and antagonists to modulators. Future Med Chem. 2012; **4**(8): 1015–1036.

[203] Fiorucci S, Cipriani S, Mencarelli A, Baldelli F, Bifulco G, Zampella A. Farnesoid X Receptor Agonist for the Treatment of Liver and Metabolic Disorders: Focus on 6-ethyl-CDCA. 2011; **11**: 753–762.

[204] Kowdley KV, Luketic V, Chapman R, et al. A randomized trial of obeticholic acid monotherapy in patients with primary biliary cholangitis. Hepatology. 2018; **67**(5): 1890–1902.

[205] Mudaliar S, Henry RR, Sanyal AJ, Morrow L, Marschall HU, Kipnes M, Adorini L, Sciacca CI, Clopton P, Castelloe E, Dillon P, Pruzanski M, Shapiro D. Efficacy and safety of the farnesoid X receptor agonist obeticholic acid in patients with type 2 diabetes and nonalcoholic fatty liver disease. Gastroenterology. 2013; **145**(3): 574–582.

[206] Gabler M, Kramer J, Schmidt J, et al. Allosteric modulation of the farnesoid X receptor by a small molecule. Scientific Reports. 2018; **8**(1): 6846.

[207] Neuschwander-Tetri BA, Loomba R, Sanyal AJ, Lavine JE, Van Natta ML, Abdelmalek MF, Chalasani N, Dasarathy S, Diehl AM, Hameed B, Kowdley KV, McCullough A, Terrault N, Clark JM, Tonascia J, Brunt EM, Kleiner DE, Doo E; NASH Clinical Research Network. Farnesoid X nuclear receptor ligand obeticholic acid for non-cirrhotic, non-alcoholic steatohepatitis (FLINT): a multicentre, randomised, placebo-controlled trial. Lancet. 2015; **385**(9972): 956–965.

[208] Hirschfield GM, Mason A, Luketic V, Lindor K, Gordon SC, Mayo M, Kowdley KV, Vincent C, Bodhenheimer HC Jr, Parés A, Trauner M, Marschall HU, Adorini L, Sciacca C, Beecher-Jones T, Castelloe E, Böhm O, Shapiro D.

Efficacy of obeticholic acid in patients with primary biliary cirrhosis and inadequate response to ursodeoxycholic acid. Gastroenterology. 2015; **148**(4): 751–761.

[209] Cipriani S, Renga B, D'Amore C, Simonetti M, De Tursi AA, Carino A, Monti MC, Sepe V, Zampella A, Fiorucci S. Impaired Itching Perception in Murine Models of Cholestasis Is Supported by Dysregulation of GPBAR1 Signaling. PLoS One. 2015; **10**(7): e0129866.

[210] Fiorucci S, Distrutti E, Ricci P, Giuliano V, Donini A, Baldelli F. Targeting FXR in cholestasis: hype or hope. Expert Opin Ther Targets. 2014; **18**(12): 1449–1459.

[211] Pencek R, Marmon T, Roth JD, Liberman A, Hooshmand-Rad R, Young MA. Effects of obeticholic acid on lipoprotein metabolism in healthy volunteers. Diabetes Obes Metab. 2016; **18**(9): 936–940.

[212] Maloney, P. R. et al. Identification of a chemical tool for the orphan nuclear receptor FXR. J. Med. Chem. 2000; **43**(16): 2971–2974.

[213] Liu Y, Binz J, Numerick MJ, Dennis S, Luo G, Desai B, MacKenzie KI, Mansfield TA, Kliewer SA, Goodwin B, Jones SA. Hepatoprotection by the farnesoid X receptor agonist GW4064 in rat models of intra and extrahepatic cholestasis. J Clin Invest. 2003; **112**(11): 1678–1687.

[214] Moschetta A, Bookout AL, Mangelsdorf DJ. Prevention of cholesterol gallstone disease by FXR agonists in a mouse model. Nat Med. 2004; **10**(12): 1352–1358.

[215] Wang Y, Chen W, Wang M, Yu D, Forman BM. Hepatology. 2008; **48**(5): 1632–1643.

[216] Sepe V, Distrutti E, Limongelli V, Fiorucci S, Zampella A. Steroidal scaffolds as FXR and GPBAR1 ligands: from chemistry to therapeutical application. Future Med Chem. 2015; **7**(9):1109–1135.

[217] Fang S, Suh JM, Reilly SM, Yu E, Osborn O, Lackey D, Yoshihara E, Perino A, Jacinto S, Lukasheva Y, Atkins AR, Khvat A, Schnabl B, Yu RT, Brenner DA, Coulter S, Liddle C, Schoonjans K, Olefsky JM, Saltiel AR,

Downes M, Evans RM. Intestinal FXR agonism promotes adipose tissue browning and reduces obesity and insulin resistance. Nat Med. 2015; **21**(2): 159–165.

[218] Naoumov N V, Global N, Development D. 25 FXR-non-steroidal agonists. 2017; **452**: 28–29.

[219] Porez G, Prawitt J, Gross B, Staels B. Bile Acid Receptors as Targets for the Treatment of Dyslipidemia and Cardiovascular Disease. J Lipid Res. 2012; **53**(9): 1723–1737.

[220] Fujino T, Une M, Imanaka T, Inoue K, Nishimaki-mogami T. Structure-activity relationship of bile acids and bile acid analogs in regard to FXR activation. J Lipid Res. 2004; **45**(1): 132–138.

[221] Reschly EJ, Ai N, Ekins S, et al. Evolution of the bile salt nuclear receptor FXR in vertebrates. J Lipid Res. 2008; **49**(7): 1577–1587.

[222] Inagaki T, Moschetta A, Lee YK, Peng L, Zhao G, Downes M et al. Regulation of antibacterial defense in the small intestine by the nuclear bile acid receptor. Proc Natl Acad Sci USA. 2006; **103**(10): 3920–3925.

[223] Kainuma M, Makishima M, Hashimoto Y, Miyachi H. Design, synthesis, and evaluation of non-steroidal farnesoid X receptor (FXR) antagonist. Bioorg Med Chem. 2007; **15**(7): 2587–2600.

[224] Massafra V, Pellicciari R, Gioiello A, Mil SWC Van. Pharmacology & Therapeutics Progress and challenges of selective Farnesoid X Receptor modulation. Pharmacol Ther. 2018; **191**: 162–177.

[225] Singh RB, Niaz MA, Ghosh S. Hypolipidemic and antioxidant effects of Commiphora mukul as an adjunct to dietary therapy in patients with hypercholesterolemia. Cardiovasc Drugs Ther. 1994; **8**(4): 659–664.

[226] Urizar NL, Liverman AB, Dodds DT, Silva FV, Ordentlich P, Yan Y, Gonzalez FJ, Heyman RA, Mangelsdorf DJ, Moore DD. A natural product that lowers cholesterol as an antagonist ligand for FXR. Science. 2002; **296**(5573):1703–1706.

[227] Wu J, Xia C, Meier J, Li S, Hu X, Lala DS. The hypolipidemic natural product guggulsterone acts as an antagonist of the bile acid receptor. Mol Endocrinol. 2002; **16**(7): 1590–1597.

[228] Cui J, Huang L, Zhao A, et al. Guggulsterone Is a Farnesoid X Receptor Antagonist in Coactivator Association Assays but Acts to Enhance Transcription of Bile Salt Export Pump. J Biol Chem. 2003; **278**(12): 10214–10220.

[229] Owsley E, Chiang JY. Guggulsterone antagonizes farnesoid X receptor induction of bile salt export pump but activates pregnane X receptor to inhibit cholesterol 7α-hydroxylase gene. Biochem Biophys Res Commun. 2003; **304**(1): 191–195.

[230] Urizar NL, Moore DD. GUGULIPID: a natural cholesterol-lowering agent. Annu Rev Nutr. 2003; **23**: 303–313.

[231] Sepe V, Bifulco G, Renga B, et al. Discovery of Sulfated Sterols from Marine Invertebrates as a New Class of Marine Natural Antagonists of Farnesoid-X-Receptor. J. Med. Chem. 2011; **54**(5): 1314–1320.

[232] Maruyama T, Miyamoto Y, Nakamura T, et al. Identification of membrane-type receptor for bile acids (M-BAR). Biochem Biophys Res Commun. 2002; **298**(5): 714–719.

[233] Kawamata Y, Fujii R, Hosoya M, et al. A G protein-coupled receptor responsive to bile acids. J Biol Chem. 2003; **278**(11): 9435–9440.

[234] Guo C, Chen W, Wang Y, Wang Y, Chen W. TGR5 , Not Only a Metabolic Regulator. Front.Physiol. 2016; **7**: 646.

[235] Watanabe M, Houten SM, Mataki C, Christoffolete MA, Kim BW, Sato H, Messaddeq N, Harney JW, Ezaki O, Kodama T, Schoonjans K, Bianco AC, Auwerx J. Bile acids induce energy expenditure by promoting intracellular thyroid hormone activation. Nature. 2006; **439**(7075): 484–489.

[236] Vassileva G, et al. Targeted deletion of Gpbar1 protects mice from cholesterol gallstone formation. Biochem. J. 2006; **398**(3): 423–430.

[237] Keitel V, Reinehr R, Gatsios P, et al. The G-protein coupled bile salt

receptor TGR5 is expressed in liver sinusoidal endothelial cells. Hepatology. 2007; **45**(3): 695–704.

[238] Keitel V, Cupisti K, Ullmer C, Knoefel WT, Kubitz R, Häussinger D. The membrane-bound bile acid receptor TGR5 is localized in the epithelium of human gallbladders. Hepatology. 2009; **50**(3): 861–870.

[239] Fiorucci S, Mencarelli A, Palladino G, Cipriani S. Bile-acid-activated receptors: targeting TGR5 and farnesoid-X-receptor in lipid and glucose disorders. Trends Pharmacol Sci. 2009; **30**(11): 570–580.

[240] Sato H, Genet C, Strehle A, Thomas C, Lobstein A, et al. Anti-hyperglycemic activity of a TGR5 agonist isolated from olea europaea. Biochem Biophys Res Commun. 2007; **362**(4): 793–798.

[241] Schaap FG, Trauner M, Jansen PLM. development. Bile acid receptors as targets for drug development. Nat Rev Gastroenterol Hepatol. 2014; **11**(1): 55–67.

[242] Gertzen CG, Spomer L, Smits SH, Häussinger D, Keitel V, Gohlke H. Mutational mapping of the transmembrane binding site of the G-protein coupled receptor TGR5 and binding mode prediction of TGR5 agonists. Eur J Med Chem. 2015; **104**: 57–72.

[243] Sato, H. et al. Anti-hyperglycemic activity of a TGR5 agonist isolated from Olea Europea. Biochem. Biophys. Res. Commun. 2007; **362**: 793–798.

[244] Thomas C, Gioiello A, Noriega L, et al. TGR5-mediated bile acid sensing controls glucose homeostasis. Cell Metab. 2009; **10**(3):167–177.

[245] Wang YD, Chen WD, Yu D, Forman BM, Huang W. The G-Protein-coupled bile acid receptor, Gpbar1 (TGR5), negatively regulates hepatic inflammatory response through antagonizing nuclear factor kappa light-chain enhancer of activated B cells (NF-κB) in mice. Hepatology. 2011; **54**(4):1421–1432.

[246] Watanabe M, Houten SM, Mataki C, Christoffolete MA, Kim BW, Sato H, Messaddeq N, Harney JW, Ezaki O, Kodama T, Schoonjans K, Bianco AC, Auwerx J. Bile acids induce energy expenditure by promoting intracellular

thyroid hormone activation. Nature. 2006; **439**(7075): 484–489.

[247] Pols TWH, Noriega LG, Nomura M, Auwerx J. Europe PMC Funders Group The bile acid membrane receptor TGR5 as an emerging target in metabolism and inflammation. J Hepatol. 2011; **54**(6): 1263–1272.

[248] Comeglio P, Cellai I et al. INT-767 prevents NASH and promotes visceral fat brown adipogenesis and mitochondrial function. J Endocrinol. 2018; **238**(2): 107–127.

[249] Anfuso B., Tiribelli C., Adorini L., and Rosso N. Obeticholic acid and INT-767 modulate collagen deposition in a NASH *in vitro* model. Scientific Reports. 2020; **10**(1): 1699–1710.

[250] Rizzo G, Passeri D, De Franco F, et al. Functional characterization of the semisynthetic bile acid derivative INT-767, a dual farnesoid X receptor and TGR5 agonist. Mol Pharmacol. 2010; **78**(4): 617–630.

[251] Baghdasaryan A, Claudel T, Gumhold J, et al. Dual farnesoid X receptor/TGR5 agonist INT-767 reduces liver injury in the Mdr2-/- (Abcb4-/-) mouse cholangiopathy model by promoting biliary HCO_3^- output. Hepatology. 2011; **54**(4): 1303–1312.

[252] McMahan RH, Wang XX, Cheng LL, et al. Bile acid receptor activation modulates hepatic monocyte activity and improves nonalcoholic fatty liver disease. J Biol Chem. 2013; **288**(17): 11761–11770.

[253] Keitel V, Kubitz R, Häussinger D. Endocrine and paracrine role of bile acids. World J Gastroenterol. 2008; **14**(37): 5620–5629.

[254] Keitel V, Häussinger D. Perspective: TGR5 (Gpbar-1) in liver physiology and disease. Clin Res Hepatol Gastroenterol. 2012; **36**(5): 412–419.

[255] Dias JR, Ramachandra R. Synthetic Communications: Studies Directed toward Synthesis of Quassinoids. III. Selective Hydrolysis of the 3α-Acetate Functional Group of Cholic Acid Derivatives. Synthetic Communications. 1977; **7**(4): 293–297.

[256] Nudelman, A. Bechor, Y. Falb, E. Fischer, B. Wexler, B. A. Acetyl Chloride-Methanol as a Convenient Reagent for: A) Quantitative Formation of

Amine Hydrochlorides, B) Carboxylate Ester Formation, C) Mild removal of N-t-BOC- protective group. Synthetic Communications. 1998: **28**(3), 471–474.

[257] E. J. Corey, J. W. Suggs, Tetrahedron Lett., 1975, **16**, 2647–2650

[258] Zahra JP. Chemical shifts of bromomethine protons of constrained a-bromocyclohexanones, Temahedron. 1970; **26**: 15–26.

[259] Doi M, Matsui M, Shuto Y, Kinoshita Y. Biological Isomerization of Cyclohexanols by Aspergillus repens MA0197. Agric. Bioi. Chem. 1990; **54** (5): 1177–1181.

[260] E.F. Mooney. Annual Reports on NMR Spectroscopy, **3**：116.

[261] Suami Tetsuo, Ogawa Seiichiro, Synthesis and high resolution NMR analysis of 2,3-diaminocyclohexanol. Keio Science and Technology Reports. 1964; **17**(67): 101–110.

[262] F. A. L. ANET, the structure of strychnospermine evidence from double irradiation and variable temperature nmr. Canadian Journal of Chemistry. 1963; **41**(4): 883–888.

[263] Wigfield C. The chemistry of 2-methyltetrahydropyran-4-one: An L-Selectride reaction that gives predominantly the equatorial alcohol. Canadian Journal of Chemistry **56**(6):789–793.

[264] Cho BT. Recent development and improvement for boron hydride-based catalytic asymmetric reduction of unsymmetrical ketones. Chem. Soc. Rev. 2009; **38**: 443–452.

[265] Burkhardt ER, Matos K. Boron Reagents in Process Chemistry:Excellent Tools for Selective Reductions. Chem. Rev. 2006; **106**(7): 2617–2650.

[266] C.A. Brown. J. Am. Chem. Soc. 1973; **95**: 4101.

[267] K.E. McGhie and R.M. Paton. Tetrahydron Ltt. 1993, **34**, 2831.

[268] Hathaway BA. Reduction of 2,6-Dimethylcyclohexanone with Sodium Borohydride Revisited A Correction on the Structural Assignments of the Products, and the Discovery of a Solvent Effect. 1998; **75**(12): 1623–1624.

[269] George S. Zweifel, Michael H. Nantz, Peter Somfai. Modern Organic Synthesis: An Introduction, 2nd Edition. USA: John Wiley & Sons Inc, United

States (2017).

[270] Neufeldt SR, Jime G. A Twist on Facial Selectivity of Hydride Reductions of Cyclic Ketones: Twist-Boat Conformers in Cyclohexanone, Piperidone, and Tropinone Reactions. J Org Chem. 2014; **79**(23):11609–11618.

[271] Schmidt DR, Schmidt S, Holmstrom SR, et al. AKR1B7 Is Induced by the Farnesoid X Receptor and Metabolizes Bile Acids. 2011; **286**(4): 2425–2432.

[272] Sarbu C, Kuhajda K, Kevresan S. Evaluation of the lipophilicity of bile acids and their derivatives by thin-layer chromatography and principal component analysis. Journal of chromatography. 2001; **A917**(1-2): 361–366.

[273] Posa M, Kuhajda K. Hydrophobicity and haemolytic potential of oxo derivatives of cholic, deoxycholic and chenodeoxycholic acids.Steroids. 2010; **75**(6): 424–431.

[274] Meyer EE, Rosenberg KJ, Israelachvili J. Recent progress in understanding hydrophobic interactions. Proc. Nat. Acad. Sci. USA 2006; **103**(43): 15739–15746.

[275] Waring MJ. Lipophilicity in drug discovery. Expert Opin Drug Discov. 2010; **5**(3): 235–248.

[276] Lombardo F, Shalaeva MY, Tupper KA, Gao F, Abraham MH. ElogPoct: a tool for lipophilicity determination in drug discovery. J Med Chem. 2000; **43**(15): 2922–2928.

[277] Wenlock MC, Potter T, Barton P, Austin RP. A method for measuring the lipophilicity of compounds in mixtures of 10. J Biomol Screen. 2011; **16**(3): 348–355.

[278] Sharma R, Majer F, Kumar V, et al. Bile acid toxicity structure–activity relationship: Correlations between cell viability and lipophilicity in a panel of new and known bile acids using an oesophageal cell line (HET-1A). Bioorg Med Chem. 2010; **18**(18): 6886–6895.

[279] Clifford, R. D.; Deacon, C. A.; Holgate, E. M. Ann. Appl. Biol. 1969, 64, 131. Apud. Tomlinson, E. J. Chromatogr. 1975, **113**：1–45.

[280] Czyrski A, and Kupczyk B. The determination of partition coefficient of 6-mercaptopurine derivatives by thin layer chromatography. 2013; **2**(3): 1501–1506.

[281] Pyka A, Dołowy M. Lipophilicity of Selected Bile Acids as Determined by TLC. II. Investigations on RP18W Stationary Phase Lipophilicity of Selected Bile Acids as. 2007; **28**(2): 297–311.

[282] Rabtti EHMA, Vajs VE, et al. RP TLC-Based Lipophilicity Assessment of Some Natural and Synthetic Coumarins. 2012; **23**(3): 522–530.

[283] Posa M. Hydrophobicity and self-association of bile acids with a special emphasis on oxo derivatives of 5-βcholanic acid. Current Organic Chemistry, 2012; **16**(16)：1876–1904.

[284] L. Galantini, M. C. di Gregorio, M. Gubitosi, L. Travaglini, J. V. Tato, A. Jover, F. Meijide, V. H. Soto Tellini and N. V. Pavel, Curr. Opin. Bile salts and derivatives: Rigid unconventional amphiphiles as dispersants, carriers and superstructure building blocks. Colloid Interface Sci. 2015; **20**: 170–182.

[285] Poša M, Rašeta M, Kuhajda K. A contribution to the study of hydrophobicity (lipophilicity) of bile acids with an emphasis on oxo derivatives of 5β-cholanoic acid. Hem. Ind. 2011; **65**(2): 115–121.

[286] Carey MC. Measurement of the physical-chemical properties of bile salt solutions. Bile acids in Gastroenterology. Lancaster: MTP Press, 1983: 19–56.

[287] Billington D, Evans CE, Godfrey PP, Coleman R. Effects of bile salts on the plasma membranes of isolated rat hepatocytes. Biochem J. 1980; **188**(2): 321–327.

[288] Lindenburg L, Merkx M. Engineering Genetically Encoded FRET Sensors. Sensors (Basel). 2014; **14**(7): 11691–11713.

[289] Van de Wiel S, Merkx M, Van de Graaf S. Real Time Monitoring of Intracellular Bile Acid Dynamics Using a Genetically Encoded FRET-based Bile Acid Sensor. J Vis Exp. 2016; **107**: 53659.

[290] Velden LM Van Der, Golynskiy M V, Bijsmans ITGW, et al. Monitoring Bile Acid Transport in Single Living Cells Using a Genetically Encoded Forster

Resonance Energy Transfer Sensor. HEPATOLOGY. 2013; **57**(2): 740–752.

[291] Graaf SFJ Van De. Intestinal Farnesoid X Receptor Activation by Pharmacologic. Cell Mol Gastroenterol Hepatol. 2018; **5**(3): 223–237.

[292] Zaufel A, van de Wiel SMW, Yin L, Fauler G, Chien D, Dong X, Gilmer JF, Truong JK, Dawson P, van de Graaf SFJ, Fickert P, Moustafa T. Secondary (iso)BAs cooperate with endogenous ligands to activate FXR under physiological and pathological conditions. Biochimica et Biophysica Acta. 2021; **1867**(8): 166153.

[293] Qureshi SA. β-Lactamase: an ideal reporter system for monitoring gene expression in live eukaryotic cells Mini-Review. 2007; **42**(1):91–95.

[294] Knapp T, Hare E, Feng L, Zlokarnik G, Negulescu P. Detection of β-lactamase reporter gene expression by flow cytometry. 2003; **51**A(2): 68–78.

[295] Jones DM, Padilla-parra S. The β-Lactamase Assay: Harnessing a FRET Biosensor to Analyse Viral Fusion Mechanisms. Sensors (Basel). 2016; **16**(7):950.

[296] Lam VM, Beerepoot P, Angers S, Salahpour A. A Novel Assay for Measurement of Membrane-Protein Surface Expression using a β-lactamase Reporter. Traffic. 2013; **14**(7): 778–784.

[297] Hsu CA, Zhao J, Xia M. Transactivation and Coactivator Recruitment Assays for Measuring Farnesoid X Receptor Activity. High-Throughput Screening Assays in Toxicology. 2016; **1473**: 43–53.

[298] Hsu C, Hsieh J, Huang R, et al. Differential modulation of FXR activity by chlorophacinone and ivermectin analogs. Toxicol Appl Pharmacol. 2016; **313**: 138–148.

[299] F. Kuipers, V. W. Bloks and A. K. Groen. Beyond intestinal soap-bile acids in metabolic control. Nat Rev Endocrinol. 2014; **10**(8): 488–498.

[300] C. Thomas, R. Pellicciari, M. Pruzanski, J. Auwerx and K. Schoonjans. Targeting bile-acid signalling for metabolic diseases. Nat Rev Drug Discov. 2008; **7**(8): 678–693.

[301] Y. Alnouti. Bile Acid sulfation: a pathway of bile acid elimination and

detoxification. Toxicol Sci. 2009; **108**(2):225–246.

[302] Fujino T, Une M, Imanaka T, Inoue K, Nishimaki-Mogami T. Structure-activity relationship of bile acids and bile acid analogs in regard to FXR activation. J Lipid Res. 2004; **45**(1): 132–138.

[303] Schmidt DR, Schmidt S, Holmstrom SR, Makishima M, Yu RT, Cummins CL, Mangelsdorf DJ, Kliewer SA. AKR1B7 is induced by the farnesoid X receptor and metabolizes bile acids. J Biol Chem. 2011 Jan 28; **286**(4): 2425–2432.

[304] Mueller M, Thorell A, Claudel T, Jha P, Koefeler H, Lackner C, Hoesel B, Fauler G, Stojakovic T, Einarsson C, Marschall HU, Trauner M. Ursodeoxycholic acid exerts farnesoid X receptor-antagonistic effects on bile acid and lipid metabolism in morbid obesity. J Hepatol. 2015; **62**(6): 1398–1404.

[305] Wang H, Chen J, Hollister K, Sowers LC, Forman BM. Endogenous bile acids are ligands for the nuclear receptor FXR/BAR. Mol Cell. 1999; **3**(5): 543–553.

[306] Liston A, Whyte CE. Bile acids mediate signaling between microbiome and the immune system. Immunol Cell Biol. 2020; **98**(5): 349–350.

[307] Hsia SL, Elliott WH, Matschiner JT, Doisy EA Jr, Thayer SA, Doisy EA. Bile acids. XI. Structures of the isomeric 3 alpha, 6, 7-trihydroxycholanic acids. J Biol Chem. 1958; **233**(6): 1337–1339.

[308] Shaw R, Elliott WH. Bile acids LVII. Analysis of bile acids by high pressure liquid chromatography and mass spectrometry. Lipids. 1978; **13**(12): 971–975.

[309] Li J, Dawson PA. Animal models to study bile acid metabolism. Biochim Biophys Acta Mol Basis Dis. 2019; **1865**(5): 895–911.

[310] Eyssen H, Pauw GDE, Stragier J, Verhulst A. Cooperative Formation of ω-Muricholic Acid by Intestinal Microorganisms. Applied Environmental Microbiology. 1983; **45**(1):141–147.

[311] Eyssen HJ, De Pauw G, Van Eldere J. Formation of hyodeoxycholic acid

from muricholic acid and hyocholic acid by an unidentified gram-positive rod termed HDCA-1 isolated from rat intestinal microflora. Appl Environ Microbiol. 1999; **65**(7): 3158–3163.

[312] Bryda EC. The Mighty Mouse: the impact of rodents on advances in biomedical research. Mo Med. 2013; **110**(3): 207–211.

[313] Montet, J.-C., Parquet, M., Sacquet, E., Montet, A.-M., Infante, R., & Amic, J. β-Muricholic acid; potentiometric and cholesterol-dissolving properties. Biochimica et Biophysica Acta. 1987; **918**(1): 1–10.

[314] Francis MB, Allen CA, Sorg JA. Muricholic Acids Inhibit Clostridium difficile Spore Germination and Growth. PLoS ONE. 2013; **8**(9): e73653.

[315] Shah SA, Volkov Y, Arfin Q, Abdel-Latif MM, Kelleher D. Ursodeoxycholic acid inhibits interleukin 1 beta and deoxycholic acid-induced activation of NF-kappaB and AP-1 in human colon cancer cells. Int J Cancer; **118**(3): 532–539.

[316] Russell DW. The enzymes, regulation, and genetics of bile acid synthesis. Annu Rev Biochem. 2003; **72**: 137–174.

[317] Sun L, Pang Y, Wang X, Wu Q, Liu H, Liu B, Liu G, Ye M, Kong W, Jiang C. Ablation of gut microbiota alleviates obesity-induced hepatic steatosis and glucose intolerance by modulating bile acid metabolism in hamsters. Acta Pharm Sin B. 2019; **9**(4): 702–710.

[318] Zhang X, Deng R (2018). Dysregulation of Bile Acids in Patients with NAFLD, Nonalcoholic Fatty Liver Disease – An Update, Emad Hamdy Gad, IntechOpen, DOI: 10.5772/intechopen.81474.

[319] Spinelli V, Lalloyer F, Baud G, Osto E, Kouach M, Daoudi M, Vallez E, Raverdy V, Goossens JF, Descat A, Doytcheva P, Hubert T, Lutz TA, Lestavel S, Staels B, Pattou F, Tailleux A. Influence of Roux-en-Y gastric bypass on plasma bile acid profiles: a comparative study between rats, pigs and humans. Int J Obes (Lond). 2016; **40**(8): 1260–1267.

[320] Rudling M. Understanding mouse bile acid formation: Is it time to unwind why mice and rats make unique bile acids? J Lipid Res. 2016; **57**(12):

2097–2098.

[321] Wang DQ, Tazuma S. Effect of beta-muricholic acid on the prevention and dissolution of cholesterol gallstones in C57L/J mice. J Lipid Res. 2002; **43**(11): 1960–1968.

[322] Wang DQ, Tazuma S, Cohen DE, Carey MC. Feeding natural hydrophilic bile acids inhibits intestinal cholesterol absorption: studies in the gallstone-susceptible mouse. Am J Physiol Gastrointest Liver Physiol. 2003; **285**(3): G494–502.

[323] Sacquet EC, Raibaud PM, Mejean C, Riottot MJ, Leprince C, Leglise PC. Bacterial Formation of ω-Muricholic Acid in Rats. Applied Environmental Microbiology. 1979; **37**(6): 1127–1131.

[324] Sacquet E, Leprince C, Riottot M, Méjan C, Léglise P. Formation of omega-muricholic acid and fecal excretion of biliary acids in rats. C R Acad Hebd Seances Acad Sci D. 1977; **284**(7): 557–559.

[325] Joyce SA, Macsharry J, Casey PG, Kinsella M, Murphy EF, Shanahan F. Regulation of host weight gain and lipid metabolism by bacterial bile acid modification in the gut. PNAS. 2014; **111**(20): 7421–7426.

[326] Rosenthal N, Brown S. The mouse ascending: perspectives for human-disease models, Nat. Cell Biol. 2007; **9**(9): 993–999.

[327] Eppig JT. Mouse genome informatics (MGI) resource: genetic, genomic, and biological knowledgebase for the laboratory mouse. ILAR. 2017; **58**(1): 17–41.

[328] Turley SD, et al. Gender-related differences in bile acid and sterol metabolism in outbred CD-1 mice fed low- and high-cholesterol diets. Hepatology. 1998; **28**(4): 1088–1094.

[329] Dietschy JM, Turley SD. Control of cholesterol turnover in the mouse, J. Biol. Chem. 2002; **277**(6): 3801–3804.

[330] Chiang JYL. Bile acid metabolism and signaling in liver disease and therapy. Liver Res. 2017; **1**(1): 3–9.

[331] Goodwin B, Jones SA, Price RR, Watson MA, McKee DD, Moore LB,

Galardi C, Wilson JG, Lewis MC, Roth ME, Maloney PR, Willson TM, Kliewer SA. A regulatory cascade of the nuclear receptors FXR, SHP-1, and LRH-1 represses bile acid biosynthesis. Mol Cell. 2000; **6**(3): 517–526.

[332] Chiang JYL, Ferrell JM. Bile Acids as Metabolic Regulators and Nutrient Sensors. Annu Rev Nutr. 2019; **39**: 175–200.

[333] Chiang JYL, Ferrell JM. Bile Acid Metabolism in Liver Pathobiology. Gene Expr. 2018; **18**(2): 71–87.

[334] Takahashi S, Fukami T, Masuo Y, Brocker CN, Xie C, Krausz KW, Wolf CR, Henderson CJ, Gonzalez FJ. Cyp2c70 is responsible for the species difference in bile acid metabolism between mice and humans. J Lipid Res. 2016; **57**(12): 2130–2137.

[335] Lin Q, Tan X, Wang W, Zeng W, Gui L, Su M, Liu C, Jia W, Xu L, Lan K. Species Differences of Bile Acid Redox Metabolism: Tertiary Oxidation of Deoxycholate is Conserved in Preclinical Animals. Drug Metab Dispos. 2020; **48**(6): 499–507.

[336] Falany CN, et al. Glycine and taurine conjugation of bile acids by a single enzyme. Molecular cloning and expression of human liver bile acid CoA:amino acid N-acyltransferase, J. Biol. Chem. 1994; **269**(30): 19375–19379.

[337] Falany CN, et al. Cloning, expression, and chromosomal localization of mouse liver bile acid CoA:amino acid N-acyltransferase, J. Lipid Res. 1997; **38**(6): 1139–1148.

[338] Stephan ZF, Armstrong MJ, Hayes KC. Bile lipid alterations in taurine-depleted monkeys, Am. J. Clin. Nutr. 1981; **34**(2): 204–210.

[339] Wahlstrom A. Induction of farnesoid X receptor signaling in germ-free mice colonized with a human microbiota, J. Lipid Res. 2017; **58**(2): 412–419.

[340] Lida T, Momose T, Tamura T, Matsumoto T, Frederic C. Potential bile acid metabolites.14. Hyocholic and muricholic acid stereoisomers. Lipid Res. 1989; **30**: 1267–1279.

[341] Chiang JY. Recent advances in understanding bile acid homeostasis. F1000Res. 2017; **6**: 2029.

[342] Hu X, Bonde Y, Eggertsen G, Rudling M. Muricholic bile acids are potent regulators of bile acid synthesis via a positive feedback mechanism. J Intern Med. 2014; **275**(1): 27–38.

[343] Zhang Y, Klaassen CD. Effects of feeding bile acids and a bile acid sequestrant on hepatic bile acid composition in mice. J Lipid Res. 2010; **51**(11): 3230–3242.

[344] Sinha J, Chen F, Miloh T, Burns RC, Yu Z, Shneider BL. beta-Klotho and FGF-15/19 inhibit the apical sodium-dependent bile acid transporter in enterocytes and cholangiocytes. Am J Physiol Gastrointest Liver Physiol. 2008; **295**(5): G996–G1003.

[345] Jiménez E, Marín ML, Martín R, Odriozola JM, Olivares M, Xaus J, Fernández L, Rodríguez JM. Is meconium from healthy newborns actually sterile? Res Microbiol. 2008; **159**(3): 187–193.

[346] DiGiulio DB, Romero R, Amogan HP, Kusanovic JP, Bik EM, Gotsch F, Kim CJ, Erez O, Edwin S, Relman DA. Microbial prevalence, diversity and abundance in amniotic fluid during preterm labor: a molecular and culture-based investigation. PLoS One. 2008; **3**(8): e3056.

[347] Colombo C, Zuliani G, Ronchi M, Breidenstein J, Setchell KD. Biliary bile acid composition of the human fetus in early gestation. Pediatr Res. 1987; **21**(2): 197–200.

[348] Takahashi S, Fukami T, Masuo Y, Brocker CN, Xie C, Krausz KW, Wolf CR, Henderson CJ, Gonzalez FJ. Cyp2c70 is responsible for the species difference in bile acid metabolism between mice and humans. J Lipid Res. 2016; **57**(12): 2130–2137.

[349] Russell DW. The enzymes, regulation, and genetics of bile acid synthesis. Annu Rev Biochem. 2003; **72**: 137–174.

[350] Deo AK, Bandiera SM. Identification of human hepatic cytochrome p450 enzymes involved in the biotransformation of cholic and chenodeoxycholic acid. Drug Metab Dispos. 2008; **36**(10): 1983–1991.

[351] Ferrell JM, Boehme S, Li F, Chiang JY. Cholesterol

7α-hydroxylase-deficient mice are protected from high-fat/high-cholesterol diet-induced metabolic disorders. J Lipid Res. 2016; **57**(7): 1144–1154.

[352] Li T, Matozel M, Boehme S, Kong B, Nilsson LM, Guo G, Ellis E, Chiang JY. Overexpression of cholesterol 7α-hydroxylase promotes hepatic bile acid synthesis and secretion and maintains cholesterol homeostasis. Hepatology. 2011; **53**(3): 996–1006.

[353] Rudling M. Understanding mouse bile acid formation: Is it time to unwind why mice and rats make unique bile acids? J Lipid Res. 2016; **57**(12): 2097–2098.

[354] Chen J, Zheng M, Liu J, Luo Y, Yang W, Yang J, Liu J, Zhou J, Xu C, Zhao F, Su M, Zang S, Shi J; Ratio of Conjugated Chenodeoxycholic to Muricholic Acids is Associated with Severity of Nonalcoholic Steatohepatitis. Obesity (Silver Spring). 2019; **27**(12): 2055–2066.

[355] Takada S, Matsubara T, Fujii H, Sato-Matsubara M, Daikoku A, Odagiri N, Amano-Teranishi Y, Kawada N, Ikeda K. Stress can attenuate hepatic lipid accumulation via elevation of hepatic β-muricholic acid levels in mice with nonalcoholic steatohepatitis. Lab Invest. 2021; **101**(2):193–203.

[356] Goto J, Nambara T. Potential bile acid metabolites. 19. The epimeric 3α, 6 α, 7β-trihydroxy- and 3α, 6α, 7β, 12α-tetrahydroxy- 5a-cholanoic acids. Steroids. 1993; **58**(4):148–152.

[357] Lida T, Momose T, Tamura T, Matsumoto T, Frederic C. Potential bile acid metabolites.14. Hyocholic and muricholic acid stereoisomers. Lipid Res. 1989; **30**: 1267–1279.

[358] Bovara R et al. Enzymatic α/β Inversion of the C-7-Hydroxyl of Steroids. J. Org. Chem. 1993; **58**(2): 499–501.

[359] Lida T, Nishida S, Chang FC, Niwa T, Goto J, Nambara T. Potential bile acid metabolites. 19. The epimeric 3 alpha,6,7 beta-trihydroxy- and 3 alpha,6,7 beta,12 alpha-tetrahydroxy-5 alpha-cholanoic acids. Steroids. 1993; **58**(4): 148–152.

[360] Kang DW, and Luecke HF. Facile Synthetic Routes to Prepare

α-Muricholic Acid, Hyocholic Acid, and Their Taurine Conjugates. Bull. Korean Chem Soc. 2013; **34**(8): 2436–2440.

[361] Ken BY, Takeda I, Komeno T. Bile acids and steroids. The journal of biochemistry. 2018; **41**(3): 385–392.

[362] Barr, T., Heilbon, I. M., Jones, E. R. H., and Spring, F. S. J. J. Chem. Soc., 1938; 334–337.

[363] Schölmerich J, Becher MS, Schmidt K, Schubert R, Kremer B, Feldhaus S, Gerok W. Influence of hydroxylation and conjugation of bile salts on their membrane-damaging properties--studies on isolated hepatocytes and lipid membrane vesicles. Hepatology. 1984; **4**(4): 661–666.

[364] Güldütuna S, Zimmer G, Imhof M, Bhatti S, You T, Leuschner U. Molecular aspects of membrane stabilization by ursodeoxycholate [see comment]. Gastroenterology. 1993; **104**(6): 1736–1744.

[365] Invernizzi P, Salzman AL, Szabó C, Ueta I, O'Connor M, Setchell KD. Ursodeoxycholate inhibits induction of NOS in human intestinal epithelial cells and *in vivo*. Am J Physiol. 1997; **273**(1 Pt 1): G131–138.

[366] Araki Y, Andoh A, Bamba H, Yoshikawa K, Doi H, Komai Y, Higuchi A, Fujiyama Y. The cytotoxicity of hydrophobic bile acids is ameliorated by more hydrophilic bile acids in intestinal cell lines IEC-6 and Caco-2. Oncol Rep. 2003; **10**(6):1931–1936.

[367] Mello-vieira J, Sousa T, Coutinho A, et al. Biochimica et Biophysica Acta Cytotoxic bile acids, but not cytoprotective species, inhibit the ordering effect of cholesterol in model membranes at physiologically active concentrations. Biochimica et Biophysica Acta. 2013; **1828**(9): 2152–2163.

[368] Payne CM, Crowley-Skillicorn C, Bernstein C, Holubec H, Moyer MP, Bernstein H. Hydrophobic bile acid-induced mitotic perturbations and micronuclei formation: relevance to genomic instability in colon carcinogenesis. Nutr Cancer. 2011; **62**: 825–840

[369] Byrne, A.M., Foran, E., Sharma, R., Davies, A., Mahon, C., O'Sullivan, J., O'Donoghue, D., Kelleher, D. & Long, A., Bile acids modulate the Golgi

membrane fission process via a protein kinase Cη and protein kinase D-dependent pathway in colonic epithelial cells. Carcinogenesis. 2010; **31**(4): 737–744.

[370] Sousa T, Pokorna S, Castro R, Bernardes N. Towards and understanding of the role of Bax on bile acid-mediated cytoprotection. European Biophysics Journal. 2019; **48**: S177–S177.

[371] Ozcan U, Yilmaz E, Ozcan L, Furuhashi M, Vaillancourt E, Smith RO, Görgün CZ, Hotamisligil GS. Chemical chaperones reduce ER stress and restore glucose homeostasis in a mouse model of type 2 diabetes. Science. 2006; **313**(5790): 1137–1140.

[372] Engin F, Hotamisligil GS. Restoring endoplasmic reticulum function by chemical chaperones: an emerging therapeutic approach for metabolic diseases. Diabetes Obes Metab. 2010; **12**(Suppl 2):108–115.

[373] Issa M, Sedigheh Takhsha F, Chirumamilla CS, Pérez-Novo C, Vanden Berghe W, Cuendet M. Taurine-Conjugated Bile Acids Protect Expanding Hematopoietic Stem/Progenitor Cells from Unfolded Protein Stress As Natural Chaperones. Blood. 2014; **124**(21): 4318.

[374] Bell B. Tauroursodeoxycholate and Tauro-P-muricholate Exert Cytoprotection by Reducing Intrahepatocyte Taurochenodeoxycholate Content. Hepatology. 1993; **17**: 470–476.

[375] Mello-vieira J, Sousa T, Coutinho A, et al. Biochimica et Biophysica Acta Cytotoxic bile acids , but not cytoprotective species, inhibit the ordering effect of cholesterol in model membranes at physiologically active concentrations. Biochim Biophys Acta. 2013; **1828**(9): 2152–2163.

[376] Katagiri K, Nakai T, Hoshino M, Hayakawa T, Ohnishi H, Okayama Y, Yamada T, Ohiwa T, Miyaji M, Takeuchi T. Tauro-beta-muricholate preserves choleresis and prevents taurocholate-induced cholestasis in colchicine-treated rat liver. Gastroenterology. 1992; **102**(5): 1660–1667.

[377] Ohiwa T, Katagiri K, Hoshino M, Hayakawa T, Nakai T. Tauroursodeoxycholate and tauro-beta-muricholate exert cytoprotection by

reducing intrahepatocyte taurochenodeoxycholate content. Hepatology. 1993; **17**(3): 470–476.

[378] Ahmed SA, Gogal RM Jr and Walsh JE. A new rapid and simple non-radioactive assay to monitor and determine the proliferation of lymphocytes: an alternative to [3H]thymidine incorporation assay. J Immunol Methods. 1994; **170**(2): 211–224.

[379] Fields RD and Lancaster MV. Dual-attribute continuous monitoring of cell proliferation/cytotoxicity. Am Biotechnol Lab. 1993; **11**(4): 48–50.

[380] Takatsuki A, Kawamura K. The stucture of Tumicamycin. Agric Biol Chem. 1997; **41**(11): 2307–2309.

[381] Ettlinger C, Schindler J, Lehle L. Cell-cycle arrest of plant suspension cultures by tunicamycin. Planta .1986; **168**(1):101–105.

[382] Vai M, Popolo L, Alberghina L. Effect of tunicamycin on cell cycle progression in budding yeast. Exp. Cell Res. 1987; **171**(2): 448–459.

[383] Banerjee A, Lang JY, Hung MC, Sengupta K, Banerjee SK, Baksi K, Banerjee DK. Unfolded protein response is required in nu/nu mice microvasculature for treating breast tumor with tunicamycin. J Biol Chem. 2011; **286**(33): 29127–29138.

[384] Lebeaupin C, Proics E, de Bieville CH, Rousseau D, Bonnafous S, Patouraux S, Adam G, Lavallard VJ, Rovere C, Le Thuc O, Saint-Paul MC, Anty R, Schneck AS, Iannelli A, Gugenheim J, Tran A, Gual P, Bailly-Maitre B. ER stress induces NLRP3 inflammasome activation and hepatocyte death. Cell Death Dis. 2015; **6**(9): e1879.

[385] Nami B, Donmez H, Kocak N. Tunicamycin-induced endoplasmic reticulum stress reduces *in vitro* subpopulation and invasion of CD44+/CD24- phenotype breast cancer stem cells. Exp Toxicol Pathol. 2016; **68**(7): 419–426.

[386] McLean GW, Carragher NO, Avizienyte E, Evans J, Brunton VG, Frame MC. The role of focal-adhesion kinase in cancer – a new therapeutic opportunity. Nat Rev Cancer. 2005; **5**(7): 505–515.

[387] Das K and Roychoudhury A. Reactive oxygen species (ROS) and

response of antioxidants as ROS-scavengers during environmental stress in plants. 2014; **2**(53): 1–13.

[388] Dayem AA, Hossain MK, Lee S Bin, et al. The Role of Reactive Oxygen Species (ROS) in the Biological Activities of Metallic Nanoparticles. Int. J. Mol. Sci. 2017; **18**(1): 120.

[389] Wang J, Yi J. Cancer cell killing via ROS: to increase or decrease, that is the question. Cancer Biol Ther. 2008; **7**(12): 1875–1884.

[390] Trachootham D, Alexandre J, Huang P. Targeting cancer cells by ROS-mediated mechanisms: a radical therapeutic approach?. Nat Rev Drug Discov. 2009; **8**(7): 579–591.

[391] Perez MJ, Briz O. Bile-acid-induced cell injury and protection. World J Gastroenterol. 2009; **15**(14): 1677–1689.

[392] Phaniendra A, Babu D. Free Radicals: Properties, sources, targets, and their implication in Various Diseases. Indian J Clin Biochem. 2015; **30**(1): 11–26.

[393] Lin K, Xue J, Sun FF, Wong PY. Reactive Oxygen Species Participate in Peroxynitrite-Induced Apoptosis in HL-60 Cells. Biochem Biophys Res Commun. 1997; **119**(230): 115-–119.

[394] Marchi S, Giorgi C, Suski JM, et al. Mitochondria-ros crosstalk in the control of cell death and aging. J Signal Transduct. 2012; **2012**: 329635.

[395] Weiss JN, Korge P, Honda HM, Ping P. Role of the Mitochondrial Permeability Transition in Myocardial Disease. Circulation Research. 2003; **93**: 292–301.

[396] Eldmann RF, Aouzi DEH, Oreau ALM, Arie ANNE, Chneider DU, Ringuier ANB. Opening of the Mitochondrial Permeability Transition Pore Causes Matrix Expansion and Outer Membrane Rupture in Fas-Mediated Hepatic Apoptosis in Mice. Hepatology. 2000; **31**(3): 674–683.

[397] Higuchi H, Gores GJ. Bile Acid Regulation of Hepatic Physiology IV. Bile acids and death receptors. Am J Physiol Gastrointest Liver Physiol. 2003; **284**(5): 734–738.

[398] Luo X, Budihardjo I, Zou H, Slaughter C, Wang X. Bid, a Bcl2 interacting protein, mediates cytochrome c release from mitochondria in response to activation of cell surface death receptors. Cell. 1998; **94**(4): 481–490.

[399] Eskes R, Antonsson B, Osen-Sand A, et al. Bax-induced cytochrome C release from mitochondria is independent of the permeability transition pore but highly dependent on Mg2+ ions. *J Cell Biol*. 1998;**143**(1):217–224.

[400] Barrasa JI, Santiago-gómez A, Olmo N, Lizarbe MA, Turnay J. Biochimica et Biophysica Acta Resistance to butyrate impairs bile acid-induced apoptosis in human colon adenocarcinoma cells via up-regulation of Bcl-2 and inactivation of Bax. Biochimica et Biophysica Acta. 2012; **1823**(12): 2201–2209.

[401] Eskes R, Antonsson B, Osen-sand A, et al. Bax-induced Cytochrome C Release from Mitochondria Is Independent of the Permeability Transition Pore but Highly Dependent on Mg^{2+} Ions. The Journal of Cell Biology. 1998; **143**(1): 217–224.

[402] Palmeira CM, Rolo AP. Mitochondrially-mediated toxicity of bile acids. Toxicology. 2004; **203**: 1–15.

[403] Roda A, Minutello A, Angellotti MA, Fini A. Bile acid structure-activity relationship: evaluation of bile acid lipophilicity using 1-octanol/water partition coefficient and reverse phase HPLC. J Lipid Res. 1990; **31**(8):1433–1443.

[404] Brenner DA. Molecular pathogenesis of liver fibrosis. Trans Am Clin Climatol Assoc. 2009; **120**: 361–368.

[405] Hansell C, Nibbs R. Professional and part-time chemokine decoys in the resolution of inflammation. Sci STKE. 2007; **384**: e18.

[406] Reed JC. Apoptosis-based therapies. Nat Rev Drug Discov. 2002; **1**(2): 111–121.

[407] Higuchi H, Bronk SF, Takikawa Y, Werneburg N, Takimoto R, El-Deiry W, Gores GJ. The Bile Acid Glycochenodeoxycholate Induces TRAIL-Receptor 2/DR5 Expression and Apoptosis. J Biol Chem. 2001; **276**(42): 38610–38618.

[408] Higuchi H, Miyoshi H, Bronk SF, et al. Bid Antisense Attenuates Bile

Acid-Induced Apoptosis and Cholestatic Liver Injury. J Pharmacol Exp Ther. 2001; **299**(3): 866–873.

[409] Czabotar PE, Lessene G, Strasser A, Adams JM. Control of apoptosis by the BCL-2 protein family: implications for physiology and therapy. Nat Publ Gr. 2014; **15**(1): 49–63.

[410] Amaral JD, Viana RJS, Ramalho RM, Steer CJ, Rodrigues CMP. Bile acids: regulation of apoptosis by ursodeoxycholic acid. The Journal of Lipid Research. 2009; **50**：1721–1734.

[411] Ignacio J, Nieves B, Pe P, Lecona E, Turnay J, Lizarbe MA. Deoxycholic and chenodeoxycholic bile acids induce apoptosis via oxidative stress in human colon adenocarcinoma cells. Apoptosis. 2011; **16**(10): 1054–1067.

[412] Yerushalmi B, Dahl R, Devereaux MW, Gumpricht E, Sokol RJ. Bile acid-induced rat hepatocyte apoptosis is inhibited by antioxidants and blockers of the mitochondrial permeability transition. Hepatology. 2001; **33**(3): 616–626.

[413] Rodrigues CM, Fan G, Wong PY, Kren BT, Steer CJ. Ursodeoxycholic acid may inhibit deoxycholic acid-induced apoptosis by modulating mitochondrial transmembrane potential and reactive oxygen species production. Mol Med. 1998; **4**(3): 165–178.

[414] Rodrigues CM, Fan G, Ma X, Kren BT, Steer CJ. A novel role for ursodeoxycholic acid in inhibiting apoptosis by modulating mitochondrial membrane perturbation. J Clin Invest. 1998; **101**(12): 2790–2799.

[415] Youle RJ, Strasser A. The BCL-2 protein family: opposing activities that mediate cell death. Nat Rev Mol Cell Biol. 2008; **9**(1): 47–59.

[416] Renault TT, Floros KV, Chipuk JE. BAK/BAX activation and cytochrome c release assays using isolated mitochondria. Methods. 2013; **61**(2):146–155.

[417] Rodrigues CM, Ma X, Linehan-Stieers C, Fan G, Kren BT, Steer CJ. Ursodeoxycholic acid prevents cytochrome c release in apoptosis by inhibiting mitochondrial membrane depolarization and channel formation. Cell Death Differ. 1999; **6**(9): 842–854.

[418] Attili AF, Angelico M, Cantafora A, Alvaro D, Capocaccia L. Bile

acid-induced liver toxicity: relation to the hydrophobichydrophilic balance of bile acids. Med Hypotheses. 1986; **19**(1): 57–69.

[419] Qiao L, Studer E, Leach K, McKinstry R, Gupta S, Decker R, Kukreja R, Valerie K, Nagarkatti P, El Deiry W, Molkentin J, Schmidt-Ullrich R, Fisher PB, Grant S, Hylemon PB, Dent P. Deoxycholic acid (DCA) causes ligand-independent activation of epidermal growth factor receptor (EGFR) and FAS receptor in primary hepatocytes: inhibition of EGFR/mitogen-activated protein kinase-signaling module enhances DCA-induced apoptosis. Mol Biol Cell. 2001; **12**(9): 2629–2645.

[420] Ashkenazi A. Targeting death and decoy receptors of the tumour-necrosis factor superfamily. Nat Rev Cancer. 2002; **2**(6): 420–430.

[421] Krammer PH.CD95(APO-1/Fas)-mediated apoptosis: live and let die. Adv Immunol. 1999; **71**: 163–210.

[422] Katona BW, Anant S, Covey DF, Stenson WF. Characterization of enantiomeric bile acid-induced apoptosis in colon cancer cell lines. J Biol Chem. 2009; **284**(5): 3354–3364.

[423] Faubion WA, Guicciardi ME, Miyoshi H, et al. Toxic bile salts induce rodent hepatocyte apoptosis via direct activation of Fas. J. Clin. Invest. 1999; **103**(1): 137–145.

[424] Zhang G, Park MA, Mitchell C, Walker T, Hamed H, Studer E, Graf M, Rahmani M, Gupta S, Hylemon PB. Multiple cyclin kinase inhibitors promote bile acid-induced apoptosis and autophagy in primary hepatocytes via p53-CD95-dependent signaling. J Biol Chem. 2008; **283**(36): 24343–24358.

[425] Bennett M, Macdonald K, Chan SW, Luzio JP, Simari R and Weissberg P. Cell surface trafficking of Fas: a rapid mechanism of p53-mediated apoptosis. Science. 1998; **282**(5387): 290–293.

[426] Miyoshi H, Rust C, Roberts PJ, Burgart LJ, and Gores GJ. Hepatocyte apoptosis after bile duct ligation in the mouse involves Fas. Gastroenterology. 1999;**117**(3):669–677.

[427] Fischer R, Cariers A, Reinehr R, and Haussinger D. Caspase

9-dependent killing of hepatic stellate cells by activated Kupffer cells. Gastroenterology. 2002; **123**(3): 845–861.

[428] Villa-Morales M, Fernández-Piqueras J. Targeting the Fas/FasL signaling pathway in cancer therapy. Expert Opin Ther Targets. 2012; **16**(1): 85–101.

[429] Nakagawa T, Zhu H, Morishima N, et al. Caspase-12 mediates endoplasmic-reticulum-specific apoptosis and cytotoxicity by amyloid β. Nature. 2000; **403**(6765): 98–103.

[430] Rust C, Wild N, Bernt C, Vennegeerts T, Wimmer R, Beuers U. Bile acid-induced apoptosis in hepatocytes is caspase-6-dependent. J Biol Chem. 2009; **284**(5): 2908–2916.

[431] Tamaki N, Hatano E, Taura K, Tada M, Kodama Y, Nitta T, Iwaisako K, Seo S, Nakajima A, Ikai I, Uemoto S. CHOP deficiency attenuates cholestasis-induced liver fibrosis by reduction of hepatocyte injury. Am J Physiol Gastrointest Liver Physiol. 2008; **294**(2): G498–505.

[432] Navarro KAEE, Tong AW, Mehta JBR. Review article: therapeutic bile acids and the risks for hepatotoxicity. Pharmacology & Therapeutics. 2018; **47**(12): 1623–1638.

[433] Faubion WA, Guicciardi ME, Miyoshi H, Bronk SF, Roberts PJ, Svingen PA, Kaufmann SH and Gores GJ. Toxic bile salts induce rodent hepatocyte apoptosis via direct activation of Fas. J Clin Invest. 1999; **103**(1): 137–145.

[434] Rodrigues CM, Fan G, Wong PY, Kren BT and Steer CJ. Ursodeoxycholic acid may inhibit deoxycholic acid-induced apoptosis by modulating mitochondrial transmembrane potential and reactive oxygen species production. Mol Med. 1998; **4**(3):165–178.

[435] Yerushalmi B, Dahl R, Devereaux MW, Gumpricht E, and Sokol RJ. Bile acid-induced rat hepatocyte apoptosis is inhibited by antioxidants and blockers of the mitochondrial permeability transition. Hepatology. 2001; **33**(3): 616–626.

[436] Qiao D, Stratagouleas ED and Martinez JD. Activation and role of mitogen-activated protein kinases in deoxycholic acid-induced apoptosis. Carcinogenesis. 2001; **22**(1): 35–41.

[437] Powell AA, Akare S, Qi W, Herzer P, Jean-Louis S, Feldman RA, Martinez JD. Resistance to ursodeoxycholic acid-induced growth arrest can also result in resistance to deoxycholic acid-induced apoptosis and increased tumorgenicity. BMC Cancer. 2006; **6**(1): 219.

[438] Solá S, Aranha MM, Steer CJ, Rodrigues CM. Game and players: Mitochondrial apoptosis and the therapeutic potential of ursodeoxycholic acid. Curr Issues Mol Biol. 2007; **9**(2): 123–138.

[439] Martinez ID, Stratagoules ED, La Rue JM, Powell AA, Gause PR, Craven MT, Payne CM, Powell MB, Gerner EW and Earnest DL. Different bile acids exhibit distinct biological effects: the tumor promoter deoxycholic acid induces apoptosis and the chemopreventive agent ursodeoxycholic acid inhibits cell proliferation. Nutr Cancer. 1998; **31**(2): 111–118.

[440] Castro RE , Solá S, Steer C, and Rodrigues C. Bile acids as modulators of apoptosis. In Hepatotoxicity: From Genomics to *in vitro* and *in vivo* Models. 2007. S. Sahu, editor. John Wiley & Sons, West Sussex, UK. 391–419.

[441] Keene CD, Rodrigues CM, Eich T, et al. A bile acid protects against motor and cognitive deficits and reduces striatal degeneration in the 3-nitropropionic acid model of Huntington's disease. Exp Neurol. 2001; **171**(2): 351–360.

[442] Keely SJ, Steer CJ, Lajczak-McGinley NK. Ursodeoxycholic acid: a promising therapeutic target for inflammatory bowel diseases? Am J Physiol Gastrointest Liver Physiol. 2019; **317**(6): G872–G881.

[443] Heuman DM and Bajaj R. Ursodeoxycholate conjugates protect against disruption of cholesterol-rich membranes by bile salts. Gastorenterology. 1994; **106**(5): 1333–1341.

[444] Beuers U, Boyer JL, Paumgartner G. Ursodeoxycholic Acid in Cholestasis: Potential Mechanisms of Action and Therapeutic Applications. Hepatology. 1998; **28**(6): 1449–1453.

[445] Gouin, S and X.X. Zhu, Synthesis of 3 alpha- and 3 beta-dimers from selected bile acids. Steriods. 1996; **61**(11): 664–669.

[446] Lim SC, Han SI. Ursodeoxycholic acid effectively kills drug-resistant gastric cancer cells through induction of autophagic death. Oncol Rep. 2015; **34**(3): 1261–1268.

[447] Pérez-Holanda S, Rodrigo L, Viñas Salas J, Piñol Felis C. Efecto del ácido ursodeoxicólico en un modelo experimental de cáncer de colon [Effect of ursodeoxycholic acid in an experimental colon cancer model]. Rev Esp Enferm Dig. 2007; **99**(9): 491–496.

[448] Kim EK, Kim EJ, Cho JH, Park DK, Kwon KA, Chung JW, Kim KO and Kim YJ: The effects of ursodeoxycholic acid on cell cycle, reactive oxygen species, and proliferation of colon cancer cell. Gastroenterology. 2016; **150**(4): S955.

[449] Park Y, Kim J, Baek J. et al. Induction of apoptosis in HepG2 human hepatocellular carcinoma cells by a novel derivative of ursodeoxycholic acid (UDCA). Arch Pharm Res. 1997; **20**: 29–33.

[450] Park SE, Choi HJ, Yee SB, Chung HY, Suh H, Choi YH, Yoo YH, Kim ND. Synthetic bile acid derivatives inhibit cell proliferation and induce apoptosis in HT-29 human colon cancer cells. Int J Oncol. 2004; **25**(1): 231–236.

[451] Lee WS, Jung JH, Panchanathan R, et al. Ursodeoxycholic Acid Induces Death Receptor-mediated Apoptosis in Prostate Cancer Cells. J Cancer Prev. 2017; **22**(1): 16–21.

[452] Kumar HMS, Reddy BVS, Anjaneyulu S, Yadav JS. An Expedient and Highly Selective Conversion of Alcohols to Azides using a NaN_3/BF_3Et_2O System. Tetrahedron Letters. 1998; **39**(3087): 7385–7388.

[453] Rokhum L, Bez G. A practical one-pot synthesis of azides directly from alcohols. J. Chem. Sci. 2012; **124**(3): 687–691.

[454] Garegg PERJ. Conversion of hydroxyl groups into bromo groups in carbohydrates with inversion of configuration. J. Chem. 1981; **59**: 339–343.

[455] Liu, H, Qin, C. K, Han, G. Q.Xu, H. W, Ren, W. H and Qin, C. Y. Synthetic chenodeoxycholic acid derivative, HS-1200, induces apoptosis of human hepatoma cells via a mitochondrial pathway. Cancer Lett. 2008; **270**(2):

242–249.

[456] Choi, Y. H, Im, E. O, Suh, H, Jin, Y, Lee, W. H, Yoo, Y. H, Kim, K. W, Kim, N. D. Apoptotic activity of novel bile acid derivatives in human leukemic T cells through the activation of caspases.Int J Oncol. 2001; **18**(5): 979–984.

[457] El Kihel, L, Clement, M, Bazin, M. A, Descamps, G, Khalid, M and Rault, S. New lithocholic and chenodeoxycholic piperazinylcarboxamides with antiproliferative and pro-apoptotic effects on human cancer cell lines. Bioorg.Bioorg Med Chem. 2008; **16**(18): 8737–8744.

[458] Kim ND, Im E, Yoo YH, Choi YH. Modulation of the cell cycle and induction of apoptosis in human cancer cells by synthetic bile acids. Curr Cancer Drug Targets. 2006; **6**(8): 681–689.

[459] Geyer J, Wilke T, Petzinger E. The solute carrier family SLC10: more than a family of bile acid transporters regarding function and phylogenetic relationships. Naunyn Schmiedebergs Arch Pharmacol. 2006; **372**(6): 413–431.

[460] Lee WS, Jung JH, Panchanathan R, et al. Ursodeoxycholic Acid Induces Death Receptor-mediated Apoptosis in Prostate Cancer Cells. J Cancer Prev. 2017; **22**(1):16–21.

[461] Bronk SF, Werneburg N. The Bile Acid Glycochenodeoxycholate Induces TRAIL-Receptor 2 / DR5. J Biol Chem. 2001; **276**(42): 38610–38618.

[462] Song E, Chen J, Antus B, Wang M, Xie Y, Yao H, Exton MS. Interleukin-2 enhances susceptibility of colon cancer cells to FasR mediated apoptosis by up-regulating Fas receptor level and down-regulating FAP-1 expression. Int J Immunopathol Pharmacol. 2000; **13**(3):113–122.

[463] Hidalgo, I.J. and R.T. Borchardt, Transport of bile acids in a human intestinal epithelial cell line, Caco-2. Biochimica et Biophysica Acta (BBA)-General Subjects.1990; **1035**(1): 97–103.

[464] Rani V, Deep G, Singh RK, Palle K, Yadav UC. Oxidative stress and metabolic disorders: Pathogenesis and therapeutic strategies. Life Sci. 2016; **148**: 183–193.

[465] G.K.S. Prakash and F. Wang. Fluorine: the new kingpin of drug discovery. ChemInform. 2013; **30**(5): 30–36.

[466] Acen L, Zhu W, Wang J, et al. Recent advances in the trifluoromethylation methodology and new CF_3-containing drugs. Journal of Fluorine Chemistry. 2014; **167**: 37–54.

[467] Thayer AM. Having fluorine in life sciences molecules brings desirable benefits, but the trick is getting it in place and making sought-after building blocks. Chem. Eng. News 2006; **84**(23): 15–24.

[468] Liu X, Xu C, Wang M, Liu Q. Trifluoromethyltrimethylsilane: Nucleophilic Trifluoromethylation and Beyond. Chem. Rev. 2015; **115**: 683–730.

[469] Prakash, G. K. S.; Yudin, A. K. Chem. ReV. 1997; **97**: 757–786.

[470] Rubiales G, Alonso C, Marigorta EM De, Palacios F. Nucleophilic trifluoromethylation of carbonyl compounds and derivatives. ARKIVOC. 2014; **2014**(2): 362–405.

[471] G. K. S. Prakash, R. Krishnamurti, G. A. Olah. Fluoride-induced trifluoromethylation of carbonyl compounds with trifluoromethyltrimethylsilane (TMS-CF_3). A trifluoromethide equivalent. J. Am. Chem. Soc., 1989; **111:** 393–395.

[472] Sanhueza IA, Bonney KJ, Nielsen MC, Schoenebeck F. Trifluoromethylation of Ketones and Aldehydes with Bu_3SnCF_3. J. Org. Chem. 2013; **78**: 7749−7753.

[473] Yu, C., & Levy, G. C. Two-dimensional heteronuclear NOE (HOESY) experiments: investigation of dipolar interactions between heteronuclei and nearby protons. J. Am. Chem. Soc. 1984; **106**(22): 6533–6537.

[474] Leroux FR, Manteau B, Vors JP, Pazenok S. Trifluoromethyl ethers-synthesis and properties of an unusual substituent. Beilstein J Org Chem. 2008; **4**: 13.

[475] Q. A. Huchet, B. Kuhn, B. Wagner, H. Fischer, M. Kansy, D. Zimmerli, E. M. Carreira and K. Muller. On the polarity of partially fluorinated methyl groups J. Fluorine Chem. 2013; **152**: 119–128.

[476] V. Kubyshkin and N. Budisa. Hydrolysis, polarity, and conformational impact of C-terminal partially fluorinated ethyl esters in peptide models. Beilstein. J. Org. Chem. 2017; **13**: 2442–2457.

[477] Silva, A.J.C, Silva, J.G, Alves, S, Tonholo, J, Ribeiro, A.S. Dansyl-Based Fluorescent Films Prepared by Chemical and Electrochemical Methods: Cyclic Voltammetry, AFM and Spectrofluorimetry Characterization. J. Braz. Chem. Soc. 2011; **22**(9): 1808–1815.

[478] Heise C, Ehrentreich-F E, Bier FF. Dansyl, a fluorescent photoprotecting group for microarray applications. J Chem Technol Biotechnol. 2012; **87**(11): 1584–1592.

[479] Maeda K. New Method of Measurement of Epidermal Turnover in Humans. Cosmetics. 2017; **4**(4): 47–51.

[480] Muwal PK, Pandey S, Pandey PS. A novel dansyl-appended bile acid receptor for preferential recognition of Hg^{2+}. RSC Adv. 2014; **4**: 21531–21534.

[481] Gomez-mendoza M, Marin ML, Miranda MA. Dansyl Derivatives of Cholic Acid as Tools to Build Speciation Diagrams for Sodium Cholate Aggregation. The Journal of Physical Chemistry Letters. 2011; **2**(7): 782–785.

[482] Sarkar I, Mishra AK. Fluorophore tagged bio-molecules and their applications: A brief review. Applied Spectroscopy Reviews. 2018; **53**(7): 552–601.

[483] Rohacova, J., Marin, M. L., Martinez-Romero, A., O' Connor, J. E., Gomez-Lechon, M. J., Donato, M. T., Castell, J. V., and Miranda, M. A. Synthesis of new, UV-photoactive dansyl derivatives for flow cytometric studies on bile acid uptake. Org. Biomol. Chem. 2009; **7**: 4973–4980.

[484] Rohacova, J., Marin, M. L., and Miranda, M. A. Complexes between fluorescent cholic acid derivatives and human serum albumin. A photophysical approach to investigate the binding behavior. J. Phys. Chem. B 2010; **114**: 4710–4716.

[485] Gavin J, Quilty F, Majer F, et al. Bioorganic & Medicinal Chemistry Letters A fluorescent analogue of tauroursodeoxycholic acid reduces ER stress and is

cytoprotective. Bioorg Med Chem Lett. 2016; **26**(21): 5369–5372.

[486] El-Faham, A., et al., COMU: a safer and more effective replacement for benzotriazole-based uronium coupling reagents. Chemistry. 2009; **15**(37): 9404–9416.

[487] Chatterjee S, Bijsmans IT, van Mil SW, Augustijns P, Annaert P. Toxicity and intracellular accumulation of bile acids in sandwich-cultured rat hepatocytes: role of glycine conjugates. Toxicol In Vitro. 2014; **28**(2): 218–230.

[488] Kouloumenta A, Stephanou G, Demopoulos NA, Nikolaropoulos SS. Genetic effects caused by potent antileukemic steroidal esters of chlorambucil's active metabolite. Anticancer Drugs. 2005; **16**(1): 67–75.

[489] Carroll FI, Philip A, Blackwell JT, Taylor DJ, Wall ME. Antitumor and antileukemic effects of some steroids and other biologically interesting compounds containing an alkylating agent. J Med Chem. 1972; **15**(11): 1158–1161.

[490] Kasiotis KM, Magiatis P, Pratsinis H, Skaltsounis, AL, Abadji V, Charalambous A, Moutsatsou P, Haroutounian, SA. Synthesis and biological evaluation of novel daunorubicin-estrogen conjugates. Steroid. 2001; **66**(10): 785–791.

[491] [65] Baldwin RW. Monoclonal antibody targeting of anti-cancer agents: Mühlbock memorial lecture. European Journal of Cancer & Clinical Oncology. 1985; **21**(11): 1281–1285.

[492] Pastan I, FitzGerald D. Recombinant toxins for cancer treatment. Science. 1991; **254**(5035): 1173–1177.

[493] Singh V, Sairam MR, Bhargavi GN, Akhras RG. Hormonotoxins. Preparation and characterization of ovine luteinizing hormone-gelonin conjugate. J Biol Chem. 1989; **264**(6): 3089–3095.

[494] Bajusz S, Janaky T, Csernus VJ, Bokser L, Fekete M, Srkalovic G et al. Highly potent analogues of luteinizing hormone-releasing hormone containing D-phenylalanine nitrogen mustard in position 6. Proceedings of the National Academy of Sciences.1989; **86**(16): 6318–6322.

[495] Bajusz S, Janaky T, Csernus VJ, Bokser L, Fekete M, Srkalovic G, Redding TW, Schally AV. Highly potent metallopeptide analogues of luteinizing hormone-releasing hormone. Proc Natl Acad Sci U S A. 1989; **86**(16): 6313–3137.

[496] Janaky T, Juhasz A, Bajusz S, Csernus V, Srkalovic G, Bokser L et al. Analogues of luteinizing hormone-releasing hormone containing cytotoxic groups. Proceedings of the National Academy of Sciences. 1992; **89**(3): 972–976.

[497] Schally AV, Nagy A. Chemotherapy targeted to cancers through tumoral hormone receptors. Trends Endocrinol Metab. 2004; **15**(7): 300–310.

[498] Schein PS. Estramustine: historical background and preclinical trials. Semin Oncol. 1983; **10**(3 Suppl 3):1–2.

[499] Katzenellenbogen JA, Katzenellenbogen BS. Considerations in the design and evaluation of cytotoxic estrogens. Breast Cancer Res Tr 2. 1982; **2**: 347–353.

[500] Kreis W. Estramustine revisited. Cancer Treat Res. 1995; **78**:163–184.

[501] Keely NO, Meegan MJ. Targeting tumors using estrogen receptor ligand conjugates. Curr Cancer Drug Targets. 2009; **9**(3): 370–380.

[502] Faustino C, Serafim C, Rijo P, Reis CP. Bile acids and bile acid derivatives: use in drug delivery systems and as therapeutic agents. Expert Opin Drug Deliv. 2016; **13**(8): 1133–1148.

[503] Nurunnabi M, Khatun Z, Revuri V, Nafiujjaman M, Cha S, Cho S, Huh KM, Lee Y. Design and strategies for bile acid mediated therapy and imaging. RSC Advances. 2016; **78**(6): 73986–74002.

[504] Hurley LH. DNA and its associated processes as targets for cancer therapy. Nature Reviews Cancer. 2002; **2**: 188–200.

[505] Lawley PD. Alkylation of DNA and its aftermath. Bioessays. 1995; **17**(6): 561–568.

[506] Osborne MR, Wilman DE, Lawley PD. Alkylation of DNA by the nitrogen mustard bis(2-chloroethyl)methylamine. Chem Res Toxicol. 1995; **8**(2):

316–320.

[507] Brookes P, Lawley PD. The reaction of mono- and di-functional alkylating agents with nucleic acids. J Biochem. 1961; **80**(3): 496–503.

[508] Kohn KW, Hartley JA, Mattes WB. Mechanisms of DNA sequence selective alkylation of guanine-N7 positions by nitrogen mustards. Biochem Pharmacol. 1988; **37**(9): 1799–1800.

[509] Povirk LF and Shuker DE. DNA damage and mutagenesis induced by nitrogen mustards. Mutat Res. 1994; **318**(3): 205–226.

[510] Singh RK, Kumar S, Prasad DN, Bhardwaj TR. European Journal of Medicinal Chemistry Therapeutic journery of nitrogen mustard as alkylating anticancer agents: Historic to future perspectives. Eur J Med Chem. 2018; **151**: 401–433.

[511] Polavarapu A, Stillabower JA, Stubble SGW, Taylor WM, Baik M. The Mechanism of Guanine Alkylation by Nitrogen Mustards: A Computational Study. J. Org. Chem. 2012; **77**: 5914–5921.

[512] Kouloumenta A, Stephanou G, Demopoulos NA, Nikolaropoulos SS. Genetic effects caused by potent antileukemic steroidal esters of chlorambucil's active metabolite. Anticancer Drugs. 2005; **16**(1): 67–75.

[513] Carroll FI, Philip A, Blackwell JT, Taylor DJ, Wall ME. Antitumor and antileukemic effects of some steroids and other biologically interesting compounds containing an alkylating agent. J Med Chem. 1972; **15**(11): 1158–1161.

[514] Saha P, Debnath C, Bérubé G. Steroid-linked nitrogen mustards as potential anticancer therapeutics: A review. J Steroid Biochem Mol Biol. 2013; **137**: 271–300.

[515] Dacre JC, and Goldman M. Toxicology and pharmacology of the chemical warfare agent sulfur mustard. Pharmacol. Rev. 1996; **48**: 289–326.

[516] Omoomi FD. Molecular chlorambucil-methionine conjugate: novel anti-cancer agent against breast MCF-7 cell model. J Cancer Sci Ther. 2013; **5**(2): 75–84.

[517] Ruhland A, Fleer R, Brendel M. Genetic activity of chemicals in yeast: DNA alterations and mutations induced by alkylating anti-cancer agents. Mutation Res. 1978; **58**: 241–250.

[518] Qin X, Fang L, Chen F, Gou S. Conjugation of platinum (IV) complexes with chlorambucil to overcome cisplatin resistance via a 'joint action' mode toward DNA. Eur J Med Chem. 2017; **137**: 167–175.

[519] Catovsky, D Else M, Richards S. Chlorambucil still not bad: a reappraisal. Clin. Lymphoma Myeloma. 2011; **11** (Suppl 1): S2–6.

[520] Kaira K, Sunose Y, Ohshima Y, Ishioka NS, Arakawa K, Ogawa T, Sunaga N, Shimizu K, Tominaga H, Oriuchi N, Itoh H, Nagamori S, Kanai Y, Yamaguchi A, Segawa A, Ide M, Mori M, Oyama T, Takeyoshi I. Clinical significance of L-type amino acid transporter 1 expression as a prognostic marker and potential of new targeting therapy in biliary tract cancer. BMC Cancer. 2013 Oct; **13**: 482.

[521] Baringhaus KH, Matter H, Stengelin S, Kramer W. Substrate specificity of the ileal and the hepatic Na(+)/bile acid cotransporters of the rabbit. I. Transport studies with membrane vesicles and cell lines expressing the cloned transporters. J Lipid Res. 1999; **40**(9):1604–1617.

[522] Kramer, W., Wess, G., Schubert, G., Bickel, M., Girbig, F., Gutjahr, U., et al.
Liver-specific drug targeting by coupling to bile acids. J. Biol. Chem. 1992; **267**: 18598–18604.

[523] Kramersb W, Wesss G, Schuberts G, et al. Liver-specific Drug Targeting by Coupling to Bile Acids. The Journal of Biological Chemistry. 1992; **267**(26): 18598–18604.

[524] Kramer W, Wess G, Schubert G, Bickel M, Girbig F, Gutjahr U, Kowalewski S, Baringhaus K-H, Enhsen A, Glombik H, Muellner S, Neckermann G, Schulz S, Petzinger E. Liver-specifi drug targeting by coupling to bile acids. J Biol Chem 1992; **267**: 18598–18604.

[525] Kramer W, Wess G. Bile acid transport systems as pharmaceutical

targets. Eur J Clin Invest 1996; **26**: 715 –732.

[526] Enhsen A, Kramer W, Wess G. Bile acids in drug discovery. Drug discovery today. 1998; **3**(9): 409–418.

[527] Oswald M, Achim G, Ublick K, et al. Chlorambucil-taurocholate is transported by bile acid carriers expressed in human hepatocellular carcinomas. Gastroenterology. 1997; **113**(4): 1295–1305.

[528] Galmier M, Reux B, Madesclaire M, Madelmont J, Debiton E, Coudert P. Synthesis and cytotoxic properties of new fluorodeoxyglucose-coupled chlorambucil derivatives. Bioorg Med Chem. 2008; **16**(9): 5004–5020.

[529] Dayal B, Salen G, Toome B, Tint GS, Shefer S, Padia J. Lithium hydroxide/aqueous methanol: mild reagent for the hydrolysis of bile acid methyl esters. Steroids.1990; **55**: 233–237.

[530] Hill BT. Studies on the transport and cellular distribution of chlorambucil in the Yoshida ascites sarcoma. Biochem Pharmacol. 1972; **21**(4): 495–502.

[531] Oswald M, Achim G, Ublick K, et al. Chlorambucil-taurocholate is transported by bile acid carriers expressed in human hepatocellular carcinomas. Gastroenterology. 1997; **113**(4): 1295–1305.

[532] Aggarwal V, Tuli HS, Varol A, Thakral F, Yerer MB, Sak K, Varol M, Jain A, Khan MA, Sethi G. Role of Reactive Oxygen Species in Cancer Progression: Molecular Mechanisms and Recent Advancements. Biomolecules. 2019; **9**(11): 735.